1 Subregional Research Project – Task 4.1

Account Number: **20-5704-174**
Collaborators: **Amvrossios Bagtzoglou, Hannah M. Castellaw**

Objective: Investigate spatial distribution of recharge indices.

12/19/95 Create figures for Semi-Annual report.

SAS

Composite plots were recreated in a fancy format for inclusion into the semi-annual research report. The trace plots are from special runs with output every midnight each day in the decade.

Table 1-1: Plot Description (12/19/95)

Figure Name	Description
AAIAAP_sat_afdep.eps	A composite plot of three sets of infiltration sensitivities: alluvium properties, fracture properties, and climatic properties. Generated using **fancy_show_result.m** operating on **alluv_frac.result** and **alluv_frac_wea.result** in ***$BREATH3/RunFSens***.
s_vs_t_for_a_f_depth.eps	Traces of moisture content for a 4-month period starting December of the 8th year of simulated time (8.75 to 8.75 + 0.333 in the 10-year meteorological sequence). Alluvium depths for the simulations are 2, 5, 10, and 15 cm. Generated using **fancy_show_ndtrace.m** operating on the corresponding **ndtrace** files in ***$BREATH2/Subreg/RunFSens/ResultDir***.
q_vs_t_for_a_f_depth.eps	Same as **s_vs_t_for_a_f_depth.eps**, except infiltration fluxes traced. Generated using **fancy_show_eltrace.m** operating on the corresponding **eltrace** files in ***$BREATH2/Subreg/RunFSens/ResultDir***.

12/20/95 Import yesterday's figures into the notebook.

SAS

Import figures into the notebook. Quite a bit of style finagling required.

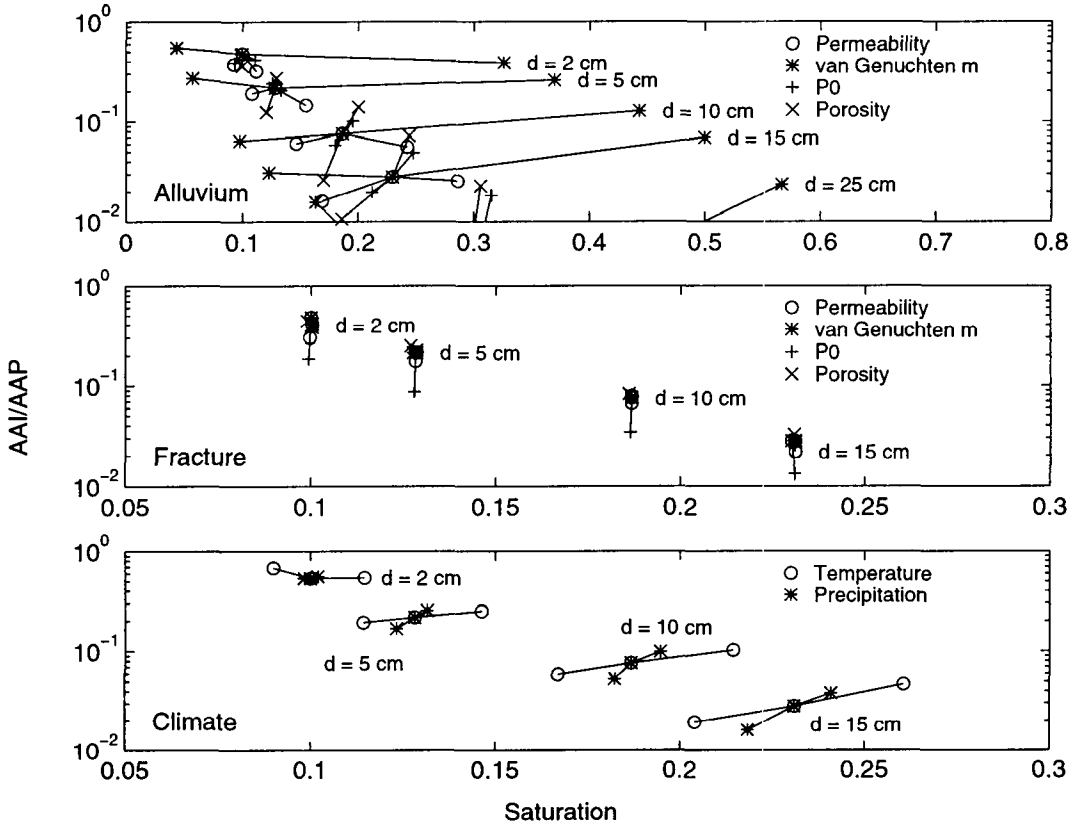

Figure 1-1: 12/20/95. AAIAAP_sat_afdep.eps. Sensitivities to alluvium properties, fracture properties, and climatic properties.

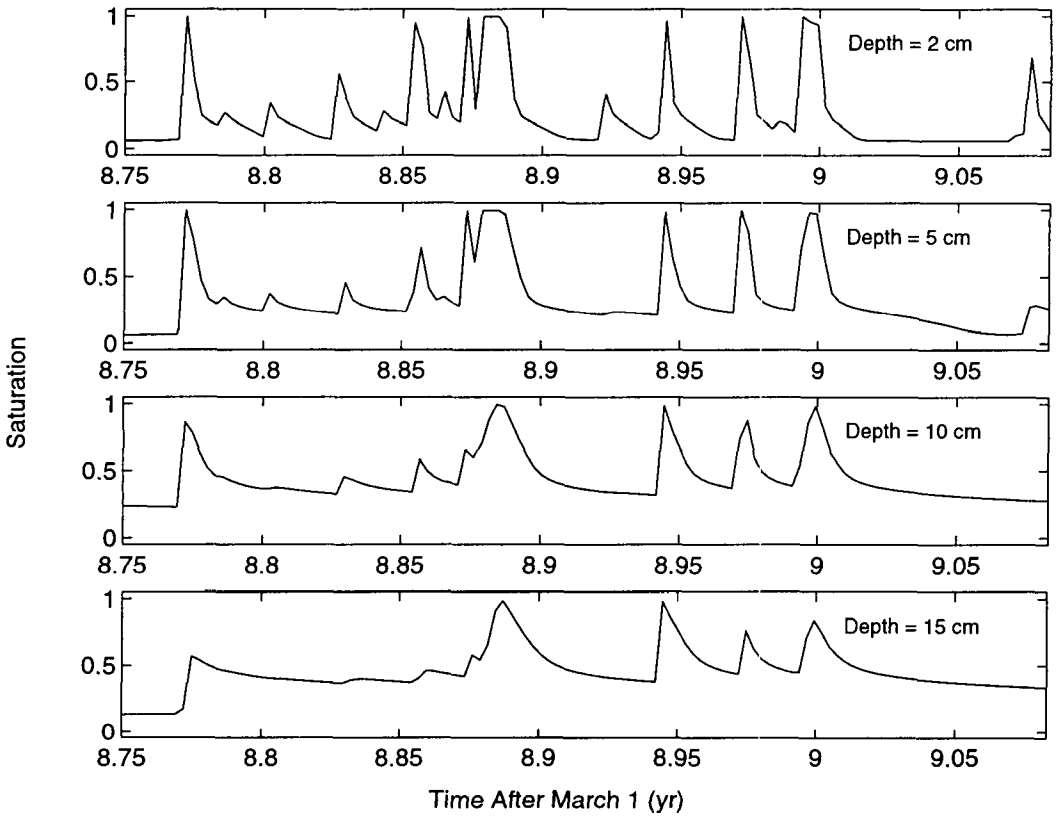

Figure 1-2: 12/20/95. s_vs_t_for_a_f_depth.eps. Traces of moisture content and infiltration flux for a 4-month period starting December of the 8th year of simulated time.

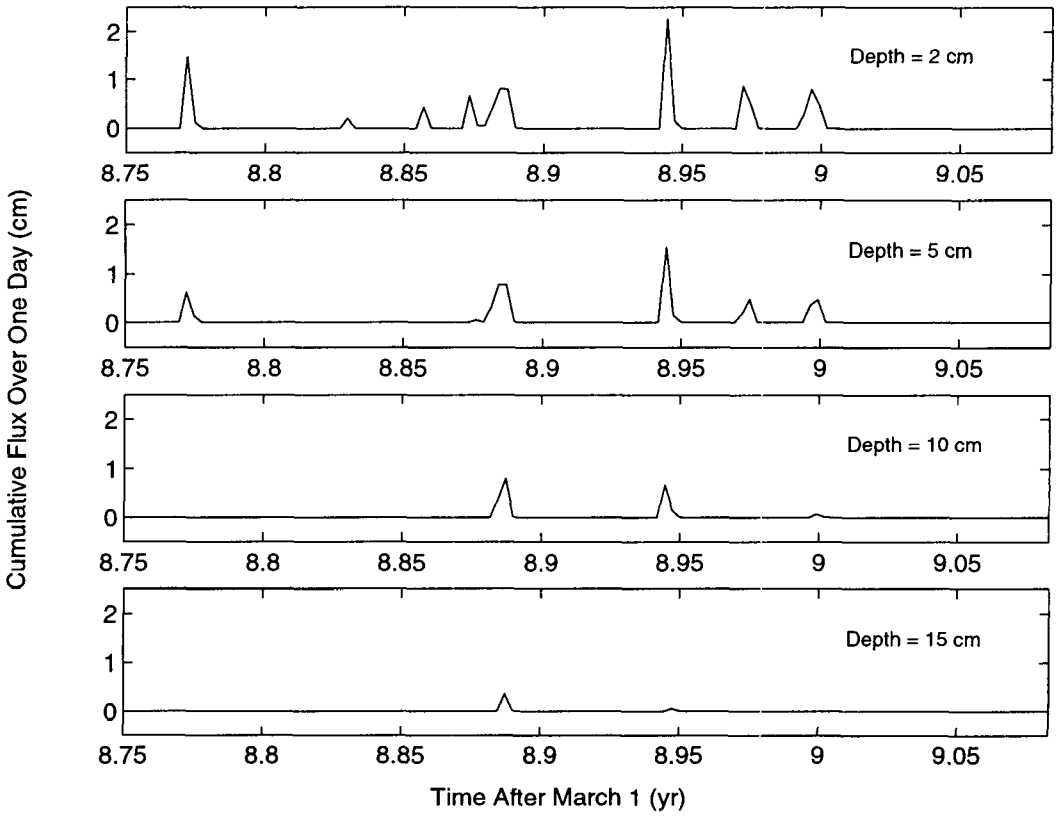

Figure 1-3: 12/20/95. q_vs_t_for_a_f_depth.eps. Traces of moisture content and infiltration flux for a 4-month period starting December of the 8th year of simulated time.

1/20/97 Final entry. SAS

This project has been closed out due to reorganization. The work is being continued under the Unsaturated and Saturated Flow in Isothermal Conditions KTI. This will be the final entry for this project in this notebook and the project will not show up in subsequent printouts.

2 Ambient Hydrology KTI – Infiltration

Account Number: **20-5708-861**
Collaborators: **Amvrossios Bagtzoglou, Gordon Wittmeyer**
Directories: **$SubRegBreath and as noted**

Objective: Perform detailed analysis of the spatial and temporal distribution of infiltration at Yucca Mountain (YM). A good deal of previous work is documented in the Scientific Notebook for the Subregional Flow and Transport Processes Research Project (subregional project) and various publications under the subregional project and the umbrella of the Iterative Performance Assessment and Performance Assessment Research projects. The research projects were closed out due to reorganization of the NRC and consequently CNWRA; infiltration work is largely being subsumed under the Ambient Hydrology KTI, with some applications possible under the Thermal Effects on Flow KTI in order to examine heating effects on infiltration. Initial efforts in the new project are to be directed towards documenting the work already completed in journal articles. Future work will depend very much on funding and time availability, but several avenues that may be explored include: (i) the impact of matrix-fracture interactions; (ii) watershed-scale modelling, with vegetation and lateral flow accounted for; (iii) geochemical tracer verification; and (iv) "shallow" diversion of infiltration due to the PTn layer.

1/26/96 Initial entry.

Work on infiltration under the subregional project and IPA is currently being documented in two journal articles. The first article deals with the impacts of hydraulic properties on 1D infiltration; the second looks at meteorology, documents the alluvium flow model, and estimates spatial and temporal distributions of infiltration. All simulations to date have been 1D; the first sets examined semi-infinite alluvium columns, with later sets looking at a shallow alluvium layer over a fracture continuum. It is quite clear that the fracture continuum will allow far more water to infiltrate than the alluvium columns; a relatively thin alluvium coating (less than 50 cm) will shut off fracture flow entirely, but sufficiently deep alluvium (greater than 5 m) will allow the flow to resume; hillslopes and ridgetops are the most important infiltration areas; micrometeorology is not a great factor, nor is the fracture description if there is enough fracture porosity; alluvium hydraulic properties have a significant influence, increasing with depth, but the depth of alluvium is the single most important parameter; detailed hourly description of meteorology is only important near precipitation events; and it is critical to use arithmetric averaging or upstream weighting for conductivities in the fracture

continuum.

In the process of creating traces of infiltration rates, it became apparent that several of the cases with very shallow alluvium covers (2 cm and 5 cm) spuriously created mass for one or more storms. Increasing the resolution in the top layer from roughly 1 cm per element to 1 mm per element fixed the problem for the simulations that were rerun this week (temperature and precipitation perturbations). Unfortunately, even though the new results show excellent self-consistency, there is significant deviation between the coarse and fine cases (roughly 50 percent less infiltration for 2-cm cases). A revised set were set off today for the hydraulic properties, but it takes roughly a day per simulation so it will be several weeks before all are completed.

1/30/96 Data Analysis.

Created *Matlab* files to analyze the lowest flux trace from a set of *breath* runs. The workhorse file, **stat_infil.m**, is in ***$HOME2/Matlab/BreathUtil***. Copies of the driver routine, **eval_all_stat.m**, must be put in the result directory of interest. Filled out a table for temporal behavior of infiltration in the paper on the spatial/temporal distribution of infiltration, aside from the 10-cm case which must be rerun due to accidental erasure of the trace files. The table is included here as Table 2-1. Also tracked down many of the figures to be included and rearranged the directory structure below ***$HOME2/Subreg*** to have better segregation of figures. New directories containing figures now are listed as ***FigureXxxx***, where ***Xxxx*** is one of ***Paper*** or ***YMElev***.

2/17/96 Error in viscosity units.

A persistent mistake was found in the specification of viscosity, dating from the earliest runs using *breath*. *breath* uses consistent units for all variables; however, the *Matlab* files used to create inputs for *breath* consistently uses viscosities three orders of magnitude too large. There is no net impact on the results when saturated conductivity is provided as data, as *breath* requires intrinsic permeability rather than saturated conductivity and intrinsic permeability is obtained by scaling hydraulic conductivity with the incorrect viscosity, which in turn is scaled back internally to *breath*. Accordingly, test problems based on saturated conductivity have been correctly calculated, since intrinsic permeability and viscosity are incorrect in compensating ways. Many other simulations are perfectly valid. Unfortunately, all sequences of infiltration experiments performed with alluvium and fractures have alluvium permeability specified (fracture saturated conductivity is specified), so that the reported permeabilities are actually off by three orders of magnitude. The *breath* code has

Table 2-1: Statistical behavior of net infiltration (AAI in mm/yr).

Depth (cm)	Multiple of AAP	°C Added to AAT	AAI	Wettest Year		Driest Year		Events	
				AAI	Events	AAI	Events	Max	Min
2	1.0	0	58.2	172.5	5	9.5	1	7 (1)	1 (1)
2	0.9	0	48.1	149.5	5	7.9	1	6 (2)	1 (1)
2	1.1	0	67.0	196.5	5	11.16	1	10 (1)	1 (1)
2	1.0	+3	50.6	158.2	5	8.79	1	6 (2)	1 (2)
2	1.0	−3	68.7	191.2	5	10.34	1	10 (1)	1 (1)
5	1.0	0	31.0	124.7	7	0.29	0	7 (1)	0 (1)
5	0.9	0	23.7	101.2	5	> 0.01	0	7 (1)	0 (2)
5	1.1	0	38.6	147.9	5	2.98	1	5 (2)	1 (3)
5	1.0	+3	25.3	108.3	5	0.59	0	5 (1)	0 (1)
5	1.0	−3	38.7	148.3	5	2.18	1	6 (1)	1 (3)
10	1.0	0	12.5	60.1	4	> 0.01	0	4 (1)	0 (3)
10	0.9	0	8.73	42.8	4	> 0.01	0	4 (1)	0 (5)
10	1.1	0	TBD	TBD	TBD	TBD	TBD	TBD	TBD
10	1.0	+3	9.68	49.9	4	> 0.01	0	4 (1)	0 (4)
10	1.0	−3	16.8	81.8	4	> 0.01	0	4 (1)	0 (3)
15	1.0	0	4.61	26.7	2	> 0.01	0	2 (2)	0 (7)
15	0.9	0	2.65	13.9	1	> 0.01	0	2 (1)	0 (8)
15	1.1	0	6.26	33.3	3	> 0.01	0	3 (1)	0 (6)
15	1.0	+3	3.18	17.3	2	> 0.01	0	2 (1)	0 (8)
15	1.0	−3	7.74	45.8	4	> 0.01	0	4 (1)	0 (7)

a temperature-dependent viscosity option, which I have not used; this option uses viscosities that are off by two orders of magnitude. I corrected this viscosity calculation in *breath* versions 1.1, 1.2, and 1.3 today.

The fix is to relabel all references to permeability to a value three orders of magnitude lower. The results are actually more comforting than the originally reported interpretations implied, since the actual range of permeabilities is in the range of silty sands through clean sands, rather than clean sands through gravels, and indeed are representative of the range of values reported for YM as was reported by various USGS papers. In fact, if my simulations were reported using saturated conductivities, the results would have been consistent and it is quite possible that the persistent error would not have been found. The simulations were incorrectly presented in Stothoff et al.

(1995), Stothoff and Bagtzoglou (1996), Bagtzoglou et al. (1995), Stothoff et al. (1996), and the poster used for both Stothoff and Bagtzoglou (1995) and the 1995 Kearney Conference. It may yet be possible to save the version of Stothoff and Bagtzoglou (1996) that will be widely distributed.

3/8/96 Update figures and results.

SAS

In preparing a series of slides for a Geological Society of America conference on 3/12/96, I am taking the opportunity to tabulate the results generated from a sequence of runs using a tight grid, as explained in the entry of 1/26/95. All hydraulic-property cases and the pressure and temperature cases were rerun for the 2-cm and 5-cm alluvium depths. The base case scenario was rerun for the 10-cm, 15-cm, 500-cm, and 1000-cm alluvium depths, as well as the semi-infinite alluvium case.

The results of the simulations are summarized in Table 2-2. The base-case weather is denoted by an "m"; perturbations in AAP and in AAT are denoted by "r" and "t", respectively. AAP is perturbed by multiplying all precipitation values by the noted perturbation; AAT is perturbed by adding (t+) or subtracting (t−) the noted perturbation. The alluvium and fracture codes both coalesce the permeability, porosity, and van Genuchten parameters into a 4-digit code. The codes are selected to allow one integer per parameter, and are translated in Table 2-3. The odd translation for fracture intrinsic permeability and van Genuchten scaling pressure are because saturated hydraulic conductivity and van Genuchten α created better codes. Note that the -3 factor in the intrinsic permeability codes is the correction for the improperly specified viscosity in earlier runs, so all runs are consistently labelled.

4/16/96 Update results and interpret.

SAS

Over the past month, I've been running simulations with fairly extreme climatic change in order to examine what would be expected at YM. So far, only 2-cm and 5-cm alluvium depths have been run, since the deeper cases take much longer. The climatic change is accomplished by multiplying all precipitation by a constant factor and/or adding a constant temperature. For both 2-cm and 5-cm cases, all combinations of rain and temperature have been completed with rain multiplied by 2/3, 1, or 3/2, and -5, 0, or $+5$ degrees C added to the temperature. A similar sequence is underway for rain multiplied by 1/2, 1, or 2, and -10, 0, or $+10$ degrees C added to the temperature. I should probably run a 15-cm and semi-infinite sequence as well for completeness, but these would take a *long* time. The results are summarized in **af_cli.result** in ***$HOME1/RunCliFrac*** *(correction (dated 12/7/96):* ***$BREATH1/RunCliFrac****).*

Table 2-2: Summary of tight-grid infiltration simulation results

Weather Code	Weather Perturbation	Alluvium Depth (cm)	Alluvium Code	Fracture Code	Moisture Content	Flux (cm/yr)
m	0	2	5223	2713	0.0331	5.82
m	0	2	5223	2712	0.0331	5.89
m	0	2	5223	2714	0.0328	3.29
m	0	2	5223	2703	0.0328	7.32
m	0	2	5223	2723	0.0331	5.75
m	0	2	5223	2613	0.0331	5.90
m	0	2	5223	2813	0.0331	5.77
m	0	2	5223	0713	0.0330	5.19
m	0	2	5223	4713	0.0331	5.86
m	0	2	5222	2713	0.0218	7.05
m	0	2	5225	2713	0.0548	4.43
m	0	2	5213	2713	0.0324	5.92
m	0	2	5253	2713	0.0352	5.87
m	0	2	5123	2713	0.1015	6.17
m	0	2	5323	2713	0.0151	6.51
m	0	2	4223	2713	0.0293	6.20
m	0	2	6223	2713	0.0397	5.43
m	0	5	5223	2713	0.0484	3.10
m	0	5	5223	2712	0.0486	3.18
m	0	5	5223	2714	0.0484	1.72
m	0	5	5223	2703	0.0483	3.32
m	0	5	5223	2723	0.0486	3.08
m	0	5	5223	2613	0.0485	3.15
m	0	5	5223	2813	0.0486	3.07
m	0	5	5223	0713	0.0485	2.69
m	0	5	5223	4713	0.0486	3.17
m	0	5	5222	2713	0.0331	4.30
m	0	5	5225	2713	0.0750	1.56
m	0	5	5213	2713	0.0505	3.22
m	0	5	5253	2713	0.0469	2.93
m	0	5	5123	2713	0.1219	3.69
m	0	5	5323	2713	0.0251	3.28
m	0	5	4223	2713	0.0380	3.37
m	0	5	6223	2713	0.0625	3.05
t−	3.0	2	5223	2713	0.0381	6.87
t+	3.0	2	5223	2713	0.0294	5.06
r*	0.9	2	5223	2713	0.0324	4.81
r*	1.1	2	5223	2713	0.0338	6.90
t−	3.0	5	5223	2713	0.0562	3.87
t+	3.0	5	5223	2713	0.0423	2.53
r*	0.9	5	5223	2713	0.0465	2.37
r*	1.1	5	5223	2713	0.0503	3.86

Table 2-3: Summary of alluvium ($abcd$) and fracture ($efgh$) parameter codes

Code	Parameter	Translation
a	Intrinsic permeability k (cm^2)	$k = 10^{-a-3}$
b	van Genuchten m	$m = b/10$
c	van Genuchten scaling pressure P_0 ($gm/cm\text{-}s^2$)	$P_0 = c \times 10^4$
d	Porosity ε	$\varepsilon = d/10$
e	Intrinsic permeability k (cm^2)	$k = 1.14694 \times 10^{-e-3}$
f	van Genuchten m	$m = f/10$
g	van Genuchten scaling pressure P_0 ($gm/cm\text{-}s^2$)	$P_0 = 980 \times 10^{-g}$
h	Porosity ε	$\varepsilon = 10^{-h}$

Doubling rain and subtracting 10 degrees C from the temperature yields the most infiltration of all cases considered. For the 2-cm case, a factor of 4.3 increase is generated; for the 5-cm case, a factor of 6.6 increase is generated. Overall, this suggests that roughly a factor of 5 to 6 increase should be expected for this climatic condition, taking into account the importance of shallow covers relative to deeper covers. This increase could be quantified better using the newly developed colluvium-balance model discussed in the Geomorphology chapter.

4/17/96 Thoughts on creating an infiltration PDF. SAS

The original motivation for examining shallow infiltration was to provide a PDF for the deep percolation fluxes past the repository. Ross and I planned to have my shallow infiltration fluxes feed into his deep percolation models. At the time, my idea was to construct a response surface for shallow infiltration as a function of whatever parameters were found to be important. It is now years later, but my work is reaching a point where construction of such a PDF is in sight.

An infiltration PDF is not a particularly well-defined concept. Ideally, one would construct many realizations of the entire mountain, from the surface to the water table, and pass in the appropriate boundary fluxes. The TSPA approach breaks the mountain into representative columns, each with its own infiltration flux. I believe that the PDF of interest is actually the PDF describing fluxes in each column, and presumably the fluxes in the columns are correlated. Accordingly, the shallow infiltration work can only be step one in the process, albeit a critical link between climate and deep percolation.

If the infiltration work is split into shallow and deep components, I believe that the best

that the shallow infiltration work can do is to pass off plausible realizations of shallow fluxes to the deep percolation model, which in turn uses realizations of the stratigraphy and hydraulic properties to calculate fluxes through the repository. If indeed the fluxes at the repository in the deep model are insensitive to the degree of spatial variability in the shallow distributions, as I suspect, the smoothest distributions yielding minimal deviation at the repository should be used. A grid of spatially averaged infiltrations would be appropriate, perhaps on a 10-pixel spacing.

Ross' deep percolation work (Bagtzoglou et al., 1995) suggests that the repository is rather insensitive to focused recharge. Another approach that might be taken is to calculate the average infiltration over the area "upstream" of the repository. Unfortunately, the upstream area would be different for each realization, so that some representative area would need to be designated. The entire DEM feels excessive, while the repository footprint is too small. Perhaps the channel in Solitario Canyon to east of the footprint, extending a total of twice the north-south extent of the footprint?

The response surface idea can come into play at a second level in the average-infiltration approach. The first level is the construction of infiltration at a pixel as a function of parameter values. The second level is the construction of the average upstream infiltration as a function of parameter values. The response surface would assume that a single value of each hydraulic property is sampled and applied to the entire domain. Alternatively, it is possible to randomly assign properties to each pixel from an appropriate distribution and generate many realizations, calculating the average infiltration for each realization. Both of the approaches should be performed, using corresponding property PDFs, in order to see if important differences appear. I suspect that the two approaches will give essentially identical PDFs for shallow infiltration (some sort of law of large numbers), even if correlation between parameters is present.

In my model, the spatio-temporal distribution of shallow infiltration can be captured with 8 parameters: (i) four alluvium hydraulic properties (K_{sat}, porosity, and two van Genuchten parameters); (ii) two alluvium-depth properties; and (iii) average temperature and precipitation. The alluvium hydraulic properties could easily be functions of space. The average temperature and precipitation may be available from the geologic and other records (e.g., the Devil's Hole data, packrat middens). The alluvium-depth properties, however, are big unknowns; I feel these should be constants for a realization. The YM field trip planned for the near future will aid in constraining the alluvium-depth properties.

Given that the alluvium-depth properties and the climatic properties are constants for a realization, there is no reason to suspect that the two average-infiltration approaches would yield a

different PDF unless there is some systematic bias for hydraulic properties as a function of colluvium depth. Consider the environment of deposition. Shallow covers tend to be cobbly, with outcrops of rock. There may be some trend towards low spatial-average porosity, high permeability, and coarser grains in the shallower cover. Are shallow covers coarser? Something to check on the field trip, but how? Perhaps portable grain-size distributions, timing infiltration rates. Upon second thought, such ideas are silly – it would be very difficult to find discernable trends in the 2-cm through 15-cm regimes. It doesn't matter once the depths are greater than 0.5 m, since there is no infiltration to speak of anyway for such cases.

Since the two average-infiltration approaches should yield consistent PDFs, it makes sense to construct the response surface. I suspect that a reasonably detailed 8-dimensional surface could be calculated in hours; setting up the software could take a day or two, since the software should take advantage of new information from additional simulations as they might become available. Enforcing consistency between various simulations with various degrees of reliability may be a headache, as I have migrated to tighter and tighter numerical standards over time.

One issue that should be addressed is the issue of climatic change. I've talked to Dave Turner and Mike Miklas about retrieving climatic records. The idea would be to generate a series of plausible climatic-change realizations based on available data and feed it through the response surface to generate plausible traces of average infiltration. The resultant trace could be compared to TSPA traces. The deep percolation model really needs to be flogged to get the response of the repository horizon to infiltration rates for this to be most useful, but a nice paper could come out of the work.

4/23/96 Watershed modelling. SAS

Dr. David Woolhiser will be consulting to CNWRA on the subject of watershed modelling. A number of discussions have taken place between Woolhiser, Gordon, Ross, and myself, with the intent of scoping out the work to be performed. After these discussions, we have decided to break out the work into several packages of roughly $10 k apiece. The first package will be simulation of a representative wash feeding into Solitario Canyon from the west, which would be a surrogate for wash-scale modelling of easterly of Yucca Crest. The first package will test the methodology and feasibility of future work. Further packages would include the full Solitario Canyon watershed, and perhaps some detailed side-slope simulations with lateral subsurface flow.

To date, we have sent Woolhiser relatively limited information on the site. He has requested

additional information including

- a large contour map of the Solitario Canyon watershed;
- a contour map of slopes in the Solitario Canyon watershed;
- available information on infiltration;
- available information on saturated conductivity;
- channel cross-sections; and
- photographs of the channel cross-sections (for roughness estimates).

A field trip to YM is being planned for the near future, at which time channel cross-sections and photographs can be obtained. In addition, I will obtain measurements of alluvium depths to compare with my geomorphology model, and perhaps some limited infiltration sampling using a falling-head permeameter can be performed as well. According to Woolhiser, a representative channel section or two midway between incoming washes would probably be sufficient for his needs, with 3 or 4 sections in representative washes. Photographs of each section should be taken, roughly 50 feet downstream.

Woolhiser has software available that should be able to generate the weather conditions at the resolution required for his model.

5/18/96 Summary of field trip observations.

This past week, Ross Bagtzoglou, Gordon Wittmeyer, and I went to Solitario Canyon to obtain field measurements and observations. Ross and Gordon concentrated on surveying wash cross-sections for the mid- to lower-canyon reaches, while I concentrated on walking the mid- to lower-canyon from rim to rim taking spot measurements of colluvium depths and trying to make observations useful for comparison with computational models. My field observations are documented in a field book, CNWRA Controlled Copy number 175.

The first field day, May 13, we spent basically getting together procedures and familiarizing ourselves with the site and equipment. Ross and Gordon wrestled with the surveying equipment and data logger all day, finally becoming comfortable with the equipment after successfully surveying a motel room that evening. During the day, they located well USW H-7 (on the other side of the road

from Plug Hill) as a benchmark and made one cross-section at a stream-gage station adjacent to Plug Hill. Additional cross-sections were stymied by a recalcitrant data logger, apparently confused by a mixup in coordinates input for the first two locations.

I spent part of the first field day making measurements of alluvium to the west and northwest of the USW H-7 pad, walking up a sideslope to the crest and returning down a small wash. Wherever I took alluvium depth measurements, I marked a nearby bush with surveyor's tape with the idea of having the points surveyed in subsequently. As it turned out, we did not get a chance to survey the points due to delays caused by unfamiliarity with the equipment.

In order to estimate shallow alluvium/colluvium depths, I brought a tile probe with the idea of poking a hole into the alluvium until further advances were rejected. The tile probe is a metal rod with a diameter of 1/2 in, with a metal tip 4 cm long and a padded handle. The base of the adapter attached to the handle is 124 cm from the tip. I brought a 10-lb hammer attachment to replace the handle, in order to help drive the tile probe. I scored the probe, creating very distinctive grooves at 10, 20, 30, 40, and 50 cm distances from the tip, for quick depth and length estimates.

Proceeding up the slope from the USW H-7 pad to the west crest, point measurements ranged up to 44 cm. At one representative mid-slope location, depths were 27, 36, and 42 cm within 2 m; at another, depths were 17, 21, and 37 cm. At the crest, depths were typically 2 to 4 cm in places, at others 6 to 8 cm. Just below the crest, pockets of 12 to 18 cm colluvium were found, increasing with distance below crest to at least 37 cm. Walking down the rill, the channel was found to consist of bare rock in places, particularly at narrow and/or steep reaches. As the channel flattened, the scoured zones disappeared. Judging from the walls of the channel in scoured zones, alluvium depths could be as much as 2 m in places, but it is difficult to tell for sure. Certainly ridges between subwashes are up to 2 m.

It quickly became obvious that the idea of the tile probe was not going to work in alluvium over a certain depth or in regions with numerous chunks of rock, since rejection due to rubble was so likely compared to rejection due to bedrock. Accordingly, I concentrated use of the probe in shallow zones generally less than 40 cm in depth. These zones are of the most interest for infiltration estimates anyway.

The second part of the first day, I walked north along the bottom of Solitario Canyon further than well USW H-6. The stream channel morphology is rather confused in the entire stretch I walked north from Plug Hill. It appears that there are typically two channels, one for the eastern side of Solitario Canyon and one for the western side, but the channels are not strongly distinct and tend to braid. The bottom of the channel is not uniform, with patches of similar materials ranging from

very fine through gravel. There is brush in most of the channel, with somewhat less brush in the most active portions of the channel. There is a great deal of variability at a scale less than the 30 m x 30 m resolution provided by the DEMs we've been using, so that the cross-sections are essential. Unfortunately, in order to fully capture the stream channels, cross-sections would be required at a much higher density (every 20 to 50 m, I estimate) than Gordon and Ross set out to perform. Gordon and Ross were going by Woolhiser's estimates of one cross-section per side wash.

The second field day, I walked or crossed each of the washes in the watershed draining to the north of the USW H-7 pad. The watershed consists of 6 or 7 washes to the north and west of the pad. Proceeding to the north, I walked the Boomerang Point crestline, crossed to near the Jet Ridge crestline, and dropped back into the USW H-6 watershed. This day, I used Global Position System (GPS) pack to provide approximate latitude and longitude at selected locations. The GPS equipment is supposed to place one within 100 m of the correct location; if a second station is used, differential methods are supposed to yield sub-meter accuracy. Our original intent was to use a reference station and a rover station; however, we found that the supplied batteries were only good for 4-1/2 to 5 hours and we did not have four batteries to cover the full day. Upon return, I hear that motorcycle batteries might do the trick for a reference station.

The third field day, I was in Las Vegas and received a NTS badge and GET training.

The fourth (and my last) field day, I walked up the east part of Solitario Canyon to Yucca Crest, arriving not far from USW-UZ6. Again I used the GPS equipment without a reference station. I started at a trench apparently dug to expose the Solitario Canyon fault, and passed some terracing exposing the upper half of the PTn outcrop. Once at the Crest, I proceeded down the wash north of Highway Ridge to the first of two sets of trenches scraping away the alluvium cover from bedrock. The trenches extend from ridgetop to ridgetop. Due to time constraints, I only examined the southerly trench closely. This trench shows very little alluvial cover at the channel bottom, increasing to 1 or 1.5 m within 10 m of the bottom, and gradually thins to less than 10 cm at the top. Returning to the crest on the southern side of the roadway, I was able to observe the wash to the south as well. I returned to Solitario Canyon slightly north of USW H-3. Upon my return, judging from aerial photographs I was able to observe terrain typical of the western and central portions of the repository footprint; further to the east, the wash channels become wider and have little in the way of scouring in the channel bottoms.

During the four field days, Gordon and Ross completed on the order of 15 cross-sections, extending up Solitario Canyon most of the way from Plug Hill to USW H-6. The original plans to survey the entire canyon channel were discarded due to the messy nature of the channel above this

point and due to time constraints. The day after I left, Gordon and Ross visited the ESF.

Based on the three days of walking around and poking colluvium, it is clear that there are some problems with the colluvium model hooked together with the infiltration response surface, although the basic approach is sound. In general, even on ridgetops there are very few places that have less than 3 or 4 cm colluvium cover, and these places are usually exfoliation shards overlying bedrock. TC caprock boulders are generally massive and unfractured. Along crestlines, TC caprock exposures cover 50 to 90 percent of the surface (visually estimated). Moving downhill easterly from the crests, TC caprock boulders on the order of meters in length appear, get smaller and sparser, then disappear. In the cracks between TC caprock outcrops at the crestlines, it is typical for fine sand through loess to be present with depths at least 3 cm and less than 6 cm. Depths increase with distance from the crestline, averaging 10 cm or so between the larger boulders and increasing to 15 to 20 cm as the boulders decrease in size. There are occasional pockets with deeper colluvium, typically less than twice the average depths for the area. I saw few washes cutting directly into the caprock, aside from the western portions of crestlines, although it was not uncommon for caprock boulders to be sliding along other TC units into washes to the east.

Most of the exposures east of crestlines are TC units. Generally these are not highly fractured near the caprock but increase with depth. Any TC units below the caprock do not appear distinctive to my admittedly untrained eye. Chunks of the lower TC tend to be much smaller than the TC caprock boulders, generally being less than 50 cm. In the steepest portions of washes cutting TC units, bare country rock may be exposed, particularly in wash channels and up to 10 m above the channels in places. The washes on the west of Solitario Canyon tend to be steeper and shorter than the washes on YM proper. The YM washes tend to develop long regular reaches with uniform sideslopes, very nice for modelling. Based on a trench north of Highway Ridge, maximum alluvium depth on sideslopes should not be much more than 1 to 2 m, near the channel bottom. It appears that the long regular slopes are steepened at the base, due to removal of colluvium due to stream action during rainfall. It may be possible to estimate the depth of alluvium by projecting sideslopes out to midchannel in the upper portions of the washes.

All along the steep portions to the west of Yucca Crest, pockets may be as much as 40 cm, but generally are in the 5 to 15 cm range. A considerable amount of bare outcrop is present, as much as 50 percent or more of the surface area. Even partway down the flatter slopes, depths may not be more than 50 to 100 cm.

There are distinctive stripes of dark, highly varnished scree alternating with light, clean scree on many of the wash slopes. Stripes may be as little as 1 to 2 m on center and may be tens

of meters on center. Invariably the dark scree is raised relative to the clean scree, suggesting that runoff is focused on the clean scree and washes it. It may be safe to assume that the darker the scree, the higher it is relative to the adjacent light scree.

Two difficulties arise when comparing the infiltration conceptual model work with field observations. The first difficulty is in treating the regions near the crestlines. Although colluvium depths, where present, are generally greater than I've been assuming, the areal average might not be too bad. However, the flow modelling assumes that there is uniform depths of colluvium everywhere, while the actual situation is patchier and deeper. An obvious way of treating the actual situation is to decrease the porosity to account for the proportion of surficial area that is impermeable boulder. It may be that reducing porosity is essentially equivalent to reducing depth, since the volume available for flow is reduced by either approach. If so, accounting for boulder size and area may not be tremendously important in the colluvium model.

The second difficulty is in treatment of wash channels. The colluvium model breaks down when factors other than gravity become important, such as overland water flow. It should not be difficult to include a factor increasing colluvium fluxes due to streamflow, which will get rid of the (arbitrary) 20 m depths in upper channels. Unfortunately, all of the action is on a scale that is subgrid compared to the DEM measurements. The channels are only 1 to 2 m wide where the rock is bare, yet the grid is 30 m on a side. It may be necessary to overlay a refined grid on wash bottoms to properly capture infiltration, at least in upper portions of the washes. As the channel bottoms are relatively narrow, there may not be a great deal of infiltration relative to ridgetops.

5/28/96 Summary of second field trip observations.

As an adjunct to a Technical Exchange on the NRC audit of the DOE TSPA-95 performance assessment document, which was held in Las Vegas, a group of 8 NRC/CNWRA/consultant personnel took a tour of the ESF at YM (myself, C. Glenn, B. Behlke, M. Bell, A. Campbell, R. Manteufel, J. Walton, G. Stirewalt). The tour took place May 24, 1996. The tour was led by Alan ? of the DOE mapping team and hydrologic input was provided by Alan Flint of the USGS.

One of the more important observations that Alan Flint made regards lateral diversion in and near the PTn bedded tuffs. Previous TSPA analyses have assumed that lateral diversion may be strongly impacted by a very low permeability unfractured layer just below the PTn. However, the ESF borehole exposes a section of PTn that appears to be rather frequently, on the order of every 10 to 20 m by my observation, punctuated by small-offset faults. The offsets tend to be

less than a meter, and may easily have been missed in boreholes. The following day, I took a walk up from Solitario Canyon to Yucca Crest and noticed some small (10 to 20 cm) offsets at one PTn exposure. Alan Flint's observation is that lateral diversion is probably not going to be very significant, because the frequent offsets in the low-permeability unit should minimize the most significant source of lateral flow.

Along the way in the ESF tour, various chlorine-36 sampling locations were pointed out by A. Flint and A. Campbell from the Fabryka-Martin et al. (1996a) draft report. We also saw the heavily fractured zone, 1 km in length and still being encountered by the TBM. The fractures seemed to alternate between zones of fracture spacings less than 10 cm to zones where the spacing is more on the order of 30 to 40 cm.

As it rained (fairly heavily in spots) on May 24, I was inspired to take another walking tour of YM on May 25. Based on wetting front observations, which penetrated roughly 3.5 to 6.5 cm in various representative areas, and on water in exposed lithophysae, I estimate 1 to 2 cm of rain took place. I noticed that on Yucca Crest, enhanced wetting took place in the gaps between outcrops (10 cm and larger in spots), while under rubble scree on sideslopes less wetting took place (dry soil was not uncommon). While walking about, a storm cell drifted overhead and roughly a half hour of rain occurred. A total of no more than 5 minutes of reasonably heavy rain occurred, with most of the interval light to nearly non-existent. Exposed rubble faces were definitely wet; however, vertical sides tended to be dry with wetting fronts occurring at the top of perhaps 1 to 3 cm. Fifteen minutes after rain ceased, little or no trace of the event could be detected.

I also examined four of the trenches that are exposed in what I think is Split Wash or the next wash north (the wash with the Ghost Dance pavement and the wash immediately north of this wash). Each of these are sufficiently downstream that the wash bottom is at least 10 m wide. In this region, what I believe Alan Flint refers to as channel terraces are exposed. It appears that currently active wash channels are cutting into the terraces. Depth to bedrock at the deepest point in the trenches ranged from 2.5 to 4 m, as best as I could estimate. However, once the slope of the ground increased from the relatively flat terrace to side slope, cover decreased to the more typical 10 to 50 cm. It should be possible to identify these deeper zones simply by the slope or break in slope.

I also had the opportunity to talk with Alan Flint about his site-scale modelling work. He demonstrated time-traces of moisture content in various neutron-probe boreholes. In one channel terrace probe, lateral subsurface flow was clearly evident. He is currently using a 3-event (upgrading to 5-event) Markov-chain model to generate daily precipitation and daily mean temperature read-

ings. Each rainfall event is redistributed to essentially perch on the colluvium/bedrock interface at the end of the day, where it infiltrates according to matrix and fracture properties. Each Scott and Bonk (1984) layer has matrix properties assigned, either from direct measurement or from analog. Fractures are grouped into 3 size classes, and further subdivided into filled/unfilled areal fractions. Pixel size is 90 m on a side; no lateral diversion is considered. Evapotranspiration is a part of the model.

Pondering the site visit, it seems that the DEM is somewhat unwieldy for colluvium-flow calculations, as it completely misses meter-scale features such as wash channels. Ideas of quasi-1D flow-tube analyses occurred to me as being particularly appropriate for YM. Each flow tube would carry along local information on topography, width, depth, shape, vegetation, etc., in the form of integer categories or classes. Accordingly, the information could be encoded very compactly in the form of bit substrings within a few integers. Vegetation is another tricky topic inspired by discussions with Alan Flint, which it would be very nice to have a better handle on.

8/27/96 Pondering questions relevant to performance.

In brief, work to date has focused on

- 1D simulations
- bare soil (no vegetation)
- no matrix-fracture interaction
- instantaneous lateral redistribution
- long-term average impacts due to
  - hydraulic properties
  - meteorologic input
- spatial distribution of surface cover
- spatial distribution of AAI
- to a minor extent, response to climatic change

Most of the work is documented in a journal article currently in preparation. The text and figures for the article will be included in this notebook upon submission to the journal and internally documented.

After the completion of work to date, it is my opinion that numerical modelling can give reasonable estimates of spatial distributions for relative AAI, the relative response of AAI to climatic change, but not absolute magnitudes for AAI. Since almost all precipitation ends up returning to the atmosphere, small errors in evaporation estimates may yield large errors in AAI estimates. Thus, the large area of interest with associated high heterogeneity levels and complex physical behavior preclude more than bounding estimates for AAI.

A number of future investigation directions can be considered.

- The validity and conservativism of the 1D approach could be examined using 3D simulations with discrete fractures on the grid-block scale for the DEM (roughly 30 m x 30 m). A 2D or 3D code would need to be assembled, presumably with the additional processes of vegetation and snow considered. Studies on the grid-block scale would be aimed at ascertaining the impact of heterogeneity and fracture spacings.
- Hillslope- and watershed-scale studies can be examined to see if lateral redistribution would significantly alter the predicted spatial distributions for AAI. Again a 2D or 3D code would need to be assembled, similar or identical to the code for the grid-block-scale simulations.
- Detailed process-level simulations, on the scale of a single fracture, could be undertaken to see how the matrix might affect infiltration magnitudes and timings. Code development is required.
- Additional 1D simulations could be undertaken to see how vegetation and snow might affect infiltration magnitudes and timings. Code development is required.
- The simulations performed to date can be squeezed to obtain the most information possible. Perhaps the most important additional information regards the timing and magnitude of infiltration pulses. The weekly trace of fluxes for each simulation can be examined relative to the rainfall input to determine the pulse description as a function of precipitation description. Perhaps comparison to the bucket approach would be in order. Analysis and *Matlab* code development required.
- Given infiltration-pulse information, the spatial distribution and timings of fluxes through the PTn can be estimated. The important question is what time-scale pulses through the PTn

have and how uniform the distribution of fluxes at the bottom of the PTn would end up being, so that the representativeness of quasi-steady-state approaches can perhaps be assessed. A logical first step might be 1D simulations using the output from one or more of the 10-yr shallow simulations. Again, some sort of 3D simulator may be in order. Predictions of travel times through the PTn could be made prior to tests in the ESF.

A key point in nearly all of these future directions is the common thread of required code development. Even in 1D, additional refinements to *breath* are necessary, while 3D codes are not available at CNWRA that have the proper capabilities.

8/28/96 Data bibliography.

As discussed above, my studies examining the spatial distribution of AAI may be extended to below the PTn layer. If this is the case, it is extremely useful to collect all data pertaining to ambient unsaturated-zone hydrology at YM. I started collecting this type of information last month, as I needed to verify some of the information regarding alluvium depths measured in boreholes and trenches collected by Hannah Castellaw almost a year previously in order to double-check predictions of depths from DEM slopes. It took some time to find her sources, and in the interim I located additional information nestled in the CNWRA library. The current entry summarizes some of the information available.

Flint and Flint (1995) provide a summary of 99 neutron-probe boreholes, including locations, elevations, classifications, dates, alluvium depths, and lithology, as well as some analysis of the data. The entire moisture-content data set for all boreholes has been ordered from the DOE and should be arriving within the week, on tape. Attempts to email the data set were stymied due to the CNWRA inability to receive email greater than 1 Mb in size (the data set consists of two files of 12+ and 14.5+ Mb, respectively). The DOE system manager was not available to set up an anonymous ftp site.

The Flint and Flint (1995) neutron-probe locations are provided in Nevada State Plane (NSP) coordinates, not the CNWRA standard of Universal Transverse Mercator (UTM). Information on the locations and elevations of most of the YM boreholes are also specified in a data file obtained from the DOE in January, 1994, with specifications for 243 boreholes. Alluvium depths are not specified, although various other sources of information are available including Fernandez et al. (1994), Schenker et al. (1995), and numerous drilling log reports and summaries. Some of the most recent boreholes are not in the DOE tape and locations are available from other sources

and are only specified in NSP coordinates. I have collected the available information in directory ***$HOME2/Matlab/3Ddata***, with **neutron_hole.dat** containing the most complete information.

Flint and Flint (1990) provide data from 73 samples in 9 boreholes, all in nonwelded and bedded tuffs (i.e., PTn, Calico Hills). Each sample is precisely located within the respective borehole. The emphasis is on studying data-determination methods in relatively permeable and porous YM cores, presumably because these are faster to analyse. Porosity, grain density, bulk density, intrinsic permeability (measured 4 ways), relative permeability versus saturation (measured 2 ways), and potential versus water content (measured 3 ways) are tabulated. Some analysis comparing the measurement techniques for the intrinsic permeability values is performed. No attempt to estimate van Genuchten parameters is made, and it seems to me that the data is not of sufficiently high quality to make the attempt.

Rautman et al. (1995) provide data obtained from a sampling grid along 1.4 km of the PTn outcrop in Solitario Canyon, with a total of about 330 core samples obtained from 26 vertical transects. Bulk properties (porosity, bulk density, and particle density) are presented for all samples; sorptivity and saturated hydraulic conductivity are presented for almost all samples (except where handling damaged the sample). Locations of vertical (upslope) transects are specified as a northward offset to a transect reported by Flint et al. (1996b), with core samples located relative to the base of the sampled sequence. Distinct vertical trends in the properties are shown in plots, and high r^2 values ($r^2 > 0.824$) were obtained between the 4 bulk properties.

Flint et al. (1996b) provide data obtained from 5 vertical and 3 horizontal sampling transects, with a total of 656 core samples. Bulk properties (porosity, bulk density, and particle density) are presented for all samples; either measured or estimated saturated hydraulic conductivity is presented for most samples; and sorptivity is presented for some samples for two horizontal transects. In addition, moisture retention information is obtained for 41 of the samples, with estimated van Genuchten and Brooks-Corey parameters. Relative-permeability information was not determined. Regression equations are presented for properties as a function of porosity. Arguments were made that porosity values can be used to estimate van Genuchten parameters; perhaps additional information can be gleaned from the sorptivity information. The report appears to be the best current source for property data suitable for modelling.

The five vertical transects presented by Flint et al. (1996b) are further analyzed by McKenna and Rautman (1995) to examine correlation information. The correlation structure appears to be nonstationary horizontally. Appropriate downhole sampling strategies are suggested.

Schenker et al. (1995) collect and reference a large number of data sets and impose PDF

descriptions on them. Most of the data are from cores extracted from boreholes; transect sampling information from Rautman et al. (1995) and Flint et al. (1996b) does not appear. Porosity and bulk density have 1234 and 2173 measurements, respectively. There are 257 saturated hydraulic conductivity values from 8 boreholes. The matrix van Genuchten parameters are reportedly determined from the original pressure/saturation data sets by the authors, yielding 211 property estimates; however, the set of estimates is not directly available. Fracture properties are estimated using fracture spacing and orientation data from four boreholes (G-1, G-4, a #1, and GU-3), saturated bulk conductivity data from the saturated zone in 7 boreholes (G-4, H-1, H-3, H-4, b #1, p #1, and J-13) and bulk gas permeabilities from barometric fluctuations observed in 2 boreholes (UZ-1 and a #4). Lots of extrapolation is required due to the sparseness of the fracture data.

10/5/96 ACNW, change in PI.

SAS

I attended the ACNW meeting in Las Vegas on September 26 and 27, 1996. My impressions are discussed in the trip report. However, there are a few important issues in particular that should be examined.

- Five independent estimates of infiltration (surface modeling by A. Flint, isotopic tracers, fracture coatings, thermal profiles, and core-sample moisture contents and pressures) all point to fluxes on the order of 1 to 10 mm/yr.
- Fault zones are considered highly permeable (1000 Darcy) horizontally, but less so vertically.
- In general, gas bulk permeabilities are on the order of 2 to 10 Darcy.
- Inverse modeling pulls the TSw matrix permeabilities up 1 or 2 orders of magnitude above core information.
- First-cut drift-scale 2D heterogenous-matrix simulations are underway with dripping requiring a transient pulse of 280 mm/yr.
- G. Bodvarsson claims that the ECM and the dual-permeability models must be identical at steady state. *Note: I think this is not correct and may explain the shift in TSw permeabilities he is obtaining.*

Last week, I became PI for the Unsaturated and Saturated Flow under Isothermal Conditions (USFIC) KTI, as I have the most hours allocated and Gordon has relatively few hours. Upcoming duties include a presentation on the USFIC KTI work at the Annual Program Review on November

13, 1996, and on December 5, 1996. The first (45 min + 15 min) presentation is to focus on technical and programmatic aspects, with subtopics including

- Status of subissue(s) resolution
- Integration with other KTIs
- Analysis of infiltration/percolation
- Results of sensitivity analyses
- Work priorities for 1997-98

The second (60 min) presentation is to focus on technical, programmatic, and managerial aspects, with subtopics including

- Infiltration/percolation rates
- Preferred conceptual model for fracture-matrix flow
- Future climate scenario and formation of perched water
- Relationship to total system performance
- Strategy for review of viability analysis

Issues involving infiltration and percolation should be straightforward to discuss. The two technical issues that will be difficult to discuss will be the preferred conceptual model for fracture-matrix flow and the future climate scenario related to the formation of perched water. I take these topics as spurs to perform some quick calculations and have discussions with Ross and others. In particular, testing Bodvarsson's opinion on the steady-state equivalence of the ECM and dual-permeability approaches is in order, as is coming up with a contour plot of areal AAI as a function of precipitation and temperature.

10/16/96 Start of alluvium/bedrock simulations.

The approach that Alan Flint is taking to estimating shallow infiltration, as he has described it to me, essentially fills the alluvium pore space with as much water as will fit and runs off the excess (i.e., infinite alluvium conductivity), then using evapotranspiration to mine water back to the

atmosphere. A perched-water system is assumed to exist above the bedrock due to the infiltration events. Water moves into the bedrock assuming gravity drainage within the bedrock. Three classes of fracture sizes, fractions of filled and unfilled fractures, and matrix permeability are combined to yield an equivalent conductivity for the 7 classes. In contrast, I have completely neglected the matrix, filled fractures, and transpiration, and have used highly resolved simulations to capture the dynamics of flow in detail.

I have observed that in simulations with bedrock exposed (i.e., alluvium with permeability less than 10^{-8} cm^2), essentially no infiltration occurs. I have not considered the case of alluvium overlying bedrock, however. I hypothesize that little or no infiltration will occur until several meters of alluvium cover the bedrock. When the alluvium/matrix interface is below the active zone, flow should be essentially steady through the bedrock at the bedrock K_{sat} or the semi-infinite infiltration rate for the alluvium, whichever is smaller. When the active zone interacts with the matrix/bedrock interface, I suspect that the low-permeability bedrock will prevent significant infiltration. As verification of this hypothesis, I am setting up several simulations to probe the behavior of alluvium overlying unfractured bedrock.

The Tiva Canyon tuff microstratigraphy is of primary interest. According to Flint et al. (1996b), the shardy base has a mean K_{sat} of 1.6×10^{-6} m/s ($k = 1.6\times10^{-9}$ cm^2= 5.0×10^{4} mm/yr), while the remaining Tiva Canyon layers have K_{sat} ranging from 3.1×10^{-9} to 3.0×10^{-12} m/s (k ranges from 3.1×10^{-12} to 3.0×10^{-15} cm^2, or 98 to 0.95 mm/yr). None of these should exhibit bare-soil infiltration if the low-permeability matrix-only results can be extrapolated.

To test the hypothesis, the base-case colluvium over three material cases will be examined: (i) shardy base, (ii) caprock, and (iii) upper lithophysal. These cases are representative of the range of k and are of interest in their own right. Samples BT26Hs, PW19s, and TPC52s will be used to determine van Genuchten properties, using the 2-parameter estimates. A summary of properties is shown in Table 2-4, with the colluvium and base-case fracture properties shown for reference. Initially, a 10-cm and a 25-cm depth-of-cover case will be run for each, as representative cases. Further examination may suggest additional cases.

10/19/96 First results for alluvium/bedrock simulations. SAS

Four of the six runs have completed 3 cycles of boundary conditions: both shardy-base cases, the 10-cm caprock case, and the 25-cm upper-lithophysal case. Each of the cases erroneously used colluvium permeabilities 1000 times larger than desired, due to incompletely correcting the

Table 2-4: Summary of colluvium and matrix properties used in simulations.

Material	K_{sat} m/s	ε	θ_r	van Genuchten α MPa^{-1}	van Genuchten m	van Genuchten P_0 $(\times 10^6)$ gm $cm^{-1}s^{-2}$
Colluvium	9.8×10^{-6}	0.300	0.000	50.0[1]	0.200	0.2[2]
Caprock	3.1×10^{-9}	0.105	0.002	5.00	0.301	2.0
Upper lithophysal	8.9×10^{-12}	0.108	0.001	2.90	0.310	3.4
Shardy base	1.6×10^{-6}	0.235	0.035	3.01	0.237	3.3
Fracture	0.011	0.001	0.000	10^5	0.700	9.8×10^{-5}

[1] Correct value is 500 (2/26/97) SAS

[2] Correct value is 0.02 (2/26/97) SAS

viscosity value in the new input-file generation routine **ingen_am.m** in ***$BREATH2/Subreg/-MakekmpoKmao***. The input and output cases are renamed correctly to reflect this error, and **ingen_am.m** was corrected. The matrix properties are correct.

None of the cases are particularly near cyclic steady state, but some conclusions can already be drawn from the first results. The shardy base is permeable enough that significant infiltration can occur, perhaps 10 mm/yr or more. Interestingly, there are indications that deeper cover provides more infiltration for the shardy base, opposite to the alluvium/fracture case. The caprock case shows some indications of infiltration as well, perhaps on the order of 1 mm/yr. The upper lithophysal case is drying out from the initial condition of 0.25 mm/yr.

Based on this rather limited set of runs, a few conclusions are presenting themselves to me:

- The capillary barrier effect is turned around for the case of matrix underlying alluvium, so that water is preferentially drawn into the matrix.
- The conclusions regarding alluvium cases that allow and disallow infiltration may not be far off for a shallow cover over bedrock.
- There may be some additional infiltration due to cover protection.
- Materials as permeable as the caprock are probably dominated by fracture flow for shallow covers and matrix flow for deeper covers.
- As the permeability increases from the caprock, matrix flow dominates.

- As the permeability decreases from the caprock, fracture flow dominates.

The only microstratigraphic layers more permeable than the caprock, according to Flint et al. (1996b), are located in the sequence including the Tiva Canyon shardy base through the nonwelded units of the Yucca Mountain and Pah Canyon Tuffs to above the Topopah Spring upper lithophysal zone. These microstratigraphic layers are essentially the PTn layer addressed in my previous analyses, perhaps a little larger, which only is about 5 percent of the total subregional outcrop area. Accordingly, I expect that the alluvium/fracture results considered before would not be significantly modified for most of the subregional area.

A much more definitive modeling approach can be conceived with some modification to *breath*. The idea is to have multiple interacting continua throughout the bedrock, all with a common pressure in the alluvium. The multiple-continuum approach will allow partitioning between the fractures and matrix to be examined, particularly since separate continua can be defined for various fracture-aperature size classes. The approach is also essential for considering deep-percolation processes.

12/7/96 Updated results for alluvium/bedrock simulations.

A new file was created in ***$BREATH1/RunTightAM*** entitled **am_all.result** to document the results of alluvium/matrix simulations. The file follows a generic standard with many entries not used. The columns of the result file are, in order:

- Depth of soil (cm),
- Alluvium code (see Table 2-3),
- Bedrock code (Table 2-4 for properties),
- Perturbation code

  b0 Base case (precipitation and temperature may vary),

  e0 Longwave radiation is scaled,

  s0 Shortwave radiation is scaled,

  v0 Vapor density is scaled,

  w0 Windspeed is scaled,

  ge Solar aspect is rotated east (perturbation in degrees),

gw Solar aspect is rotated west (perturbation in degrees),

gn Solar aspect is rotated north (perturbation in degrees),

gs Solar aspect is rotated south (perturbation in degrees),

- Perturbation,
- Precipitation multiplier,
- Temperature shift,
- Average soil moisture content at the interface, and
- Average net infiltration (cm/yr).

Most of the values in the file should be viewed as order of magnitude results rather than fully converged, as more cycles are required for full convergence in almost all cases. The runs are primarily useful for screening where fracture flow would dominate. From the runs, it appears that significant matrix infiltration can occur for the Tiva Canyon caprock and shardy units, while fracture flow should dominate in Tiva Canyon upper lithophysal and Topopah Springs lower nonlithophysal units.

The shardy unit is considered part of the PTn, has large infiltration, and is the most permeable unit of any of the microstratigraphic layers considered. The 10-cm case has AAI approximately 24 percent of AAP, while the 25-cm case has AAI approximately 16 percent of AAP. The remainder of the PTn should have smaller AAI. Assuming that the PTn as a whole yields AAI roughly equivalent to 10 to 20 percent of AAP is probably justified based on these simulations. Note that in the FY96 Annual Progress Report (Bagtzoglou et al., 1997), my assumption was that 10 percent of AAP enters the PTn, and I found that the overall sensitivity to the PTn unit is quite low.

The Tiva Canyon caprock matrix shows behavior unlike any other unit considered, as AAI *increases* with soil depth for the two soil depths considered. Experience from early semi-infinite experiments suggests that essentially no infiltration should occur for exposed materials with this permeability. A cover of soil appears to provide a permeable zone to allow water to penetrate the subsurface while protecting caprock from evaporative processes, and the difference in bubbling pressure between soil and caprock preferentially sucks water into the bedrock. The caprock is laterally extensive over the repository, primarily in regions where my colluvium/fracture models predict high AAI, so revisiting this material with *breath* modified to consider both bedrock and fractures simultaneously would be appropriate. Note that one would expect that the caprock should never have much more than 50 cm of cover.

Today I tried to finalize the table of atmospheric influences on infiltration for a colluvium/fracture system. The table is in ***$BREATH1/RunCliFrac*** and is called **af_egsvw.result**, abstracting the results of simulations run over the period from July through November. The simulations do not consider changes in precipitation or temperature. The columns of the result file are, in order:

- Depth of soil (cm),
- Alluvium code (see Table 2-3),
- Fracture code (see Table 2-3),
- Perturbation code

  b0 Base case (precipitation and temperature do not vary),

  e0 Longwave radiation is scaled,

  s0 Shortwave radiation is scaled,

  v0 Vapor density is scaled,

  w0 Windspeed is scaled,

  ge Solar aspect is rotated east (perturbation in degrees),

  gw Solar aspect is rotated west (perturbation in degrees),

  gn Solar aspect is rotated north (perturbation in degrees),

  gs Solar aspect is rotated south (perturbation in degrees),

- Perturbation,
- Average soil moisture content at the interface, and
- Average net infiltration (cm/yr).

The values in the file have reliably reached cyclic steady state.

An important observation was made during the finalization process. The final simulations in the colluvium/fracture set of simulations overlapped the first soil/bedrock simulations. I had previously noticed that there are cases where the combination of soil and underlying material require such small time steps during a large infiltration event that a simulated hour may not complete within the 10000-time-step limit. For the last simulation, I imposed a 50000-time-step limit for each hour; during large infiltration events even this limit might be reached before the

hour was up, but more than half of the events exceeding 10000 time steps completed before 50000 time steps were finished. For the case with the larger limit on the number of time steps, larger net infiltration was obtained than would have been expected (5.5 mm/yr rather than roughly 1 mm/yr). The implication is that my estimates of AAI are too low in some (but not all) cases. I suspect that the error is generally additive, on the order of several mm/yr, rather than being a multiplicative error. Unfortunately, it is not possible to untangle which simulations yield underpredictions without rerunning the simulations. I believe that sensitivity predictions may be relatively unaffected, but there is some question regarding the appropriate decay in infiltration with soil depth.

12/8/96 Estimating regression relationships for AAI.

As part of estimating regression relationships between hydraulic properties, climatic variables, and AAI, I fit the data to predicted values using a least-squares fit. Say, for example, that the relationship is

$$\log_{10}\left(\frac{AAI}{AAP}k^{1/2}\right) = \alpha_0 + \alpha_1\left[\left(\frac{m}{m_0}\right)^2 - 1\right] + \alpha_2\left[\left(\frac{P_0}{P}\right)^{1/2} - 1\right] + \alpha_3\left[\left(\frac{\varepsilon}{\varepsilon_0}\right) - 1\right], \qquad (2\text{-}1)$$

where k is intrinsic permeability, m is van Genuchten $m = 1 - 1/n$, P is bubbling pressure (the reciprocal of van Genuchten α in the units used here), ε is porosity, a subscript 0 represents a reference value for the parameter, and the α values are hydraulic-parameter sensitivity constants.

For any particular simulation, the only unknowns in the relationship are the α values. Thus, for a simulation, one can write the equation as

$$C_0 = \alpha_0 + \alpha_1 C_1 + \alpha_2 C_2 + \alpha_3 C_3, \qquad (2\text{-}2)$$

where the C values result from evaluating the hydraulic-property functions. Combining all simulations results in the matrix relationships

$$\left[\mathbf{C}_1\ \mathbf{C}_2\ \mathbf{C}_3\right]\{\alpha\} = \{\mathbf{C}_0\}, \qquad (2\text{-}3)$$

where bold-face represents a vector. When provided with linear equations having a matrix that is not square, *Matlab* solves the equations using least squares (exactly the appropriate behavior). Any reported regressions are coded using *Matlab* to take advantage of this feature.

1/7/97 Documenting plots for ANS-1997 submission.

Budhi was invited to give an invited talk at the American Nuclear Society (ANS) convention in June, 1997. A summary of the talk is required for the conference, consisting of 450 to 900 words.

The summary presents the methodology for creating infiltration maps and sensitivity maps, in an extremely schematic fashion. Included in the summary are two plots, one of my latest base infiltration map and a newly created sensitivity plot for sensitivity of infiltration to soil depth.

The plots were generated with a master *Matlab* driver called **do_sens_eval.m**, which in turn calls a number of other routines. The current versions of required files and concommitant input were stored in a subdirectory of ***$HOME2/Matlab/YMInfil*** entitled ***ANS96***. The directory was stored in a tar file entitled **ANS96_plotgen_tar**, which was in turn compressed using the gzip command (appending ".gz" to the file name).

Sensitivity S_k of areal-average AAI to generic parameter α_k can be calculated using normalized sensitivity coefficients (Sykes et al., 1985)

$$S_k = \frac{\alpha_k}{AAI}\frac{\mathrm{d}AAI}{\mathrm{d}\alpha_k} \tag{2-4}$$

$$S_k = \alpha_k \frac{\mathrm{d}\ln AAI}{\mathrm{d}\alpha_k} \tag{2-5}$$

The sensitivity coefficients are calculated by using first-order derivatives between a high and low perturbation, normalized by a reference value. In general, sensitivity coefficients will change as the set of base input values change. For the example problem, the base-case soil depth was uniformly multiplied by 0.9 and 1.1 to provide perturbations. Values of S_k less than or equal to 0 were arbitrarily set to 10^{-32} for plotting purposes (the most-negative value was on the order of -10^{-16}). Note that sensitivities are largest on sideslopes and are zero wherever depth does not change infiltration (e.g., deep soil, PTn outcrops under current modeling shortcuts).

1/8/97 Documenting 1996 annual report work. SAS

An archive file was created in both ***$HOME2/Matlab/YMInfil*** and in ***$HOME2/Matlab/-ColluvWaste*** documenting the input files and limited output files used to generate figure 10-4 and tables 10-1 and 10-2 in chapter 10 of the NRC High-Level Radioactive Waste Program Annual Progress Report, Fiscal Year 1996. Both archive files are called **AnnRep96_tar**; both are compressed. The file in ***$HOME2/Matlab/YMInfil*** includes all of the files from ***$HOME2/Matlab/ColluvWaste***, for completeness, and is submitted to QA as formal documentation of the results. A couple of files were added or fixed up for readability and reproducibility of results. Description of the process is in a ReadMe file in the archive.

1/13/97 Documenting alluvium regression.

SAS

Alluvium depths are not well captured by the equilibrium mass-wasting scheme in areas of deep alluvium, partly due to the irregular topography of the washes. In order to have a reasonable representation for deep alluvium, in August, 1995, Ross Bagtzoglou developed a regression for alluvium depth b as a function of slope s:

$$b = 47\exp(-0.32s). \tag{2-6}$$

The regression was based on borehole information for b and the nearest-neighbor values from the DEM for s. No borehole classification was performed, and ad-hoc data censoring was used for the regression. Due to time constraints, the work was performed very quickly.

I revisited the regression expression last summer, and decided that it is probably better to use an expression of the form

$$\ln(b) = a + b\ln(s). \tag{2-7}$$

I pulled together as much available information on alluvium depths as I could find and sorted it into a file called **neutron_hole.dat** in ***$HOME2/Matlab/3Ddata***. Neutron-borehole data is reported by Flint and Flint (1995); other data sources are noted in **neutron_hole.dat**. I pulled neutron-borehole data from channels and terraces into separate files (**chan.dat**, and **st.dat**, respectively); other boreholes with reported alluvium depths were pulled into file **well.dat**. A total of 110 boreholes are included in these three classes; an additional 64 boreholes are not considered.

Boreholes with shallow covers (i.e., ridgetops, sideslopes) are not considered further, as I feel that alluvium depths for these boreholes are not reported with sufficient accuracy and are in a range of depth that should be handled by the mass-wasting approach anyway.

For the regression, each of the boreholes was assigned the slope of the nearest-neighbor pixel in the DEM. An additional censoring process eliminated all boreholes with unreported soil depths or having soil depths less than 1 m, leaving a total of 37 boreholes, conveniently grouped as 9 channel boreholes and 28 deep-alluvium boreholes. The data points and regression lines are shown in Figure 2-1, manually generated by regressing all data using **regress_set.m** and further processing with the **show_regress.m** routine. I feel that it is questionable whether the overall regression should use the channel data, as the pixels are larger than the channel width. Even if the channel data is included, the regression line is not tremendously changed. As a note, the correlation coefficient with the original formulation is 0.59 and 0.58 for the channel and terrace, respectively; using the new formulation the correlation coefficient is 0.66 and 0.69, respectively.

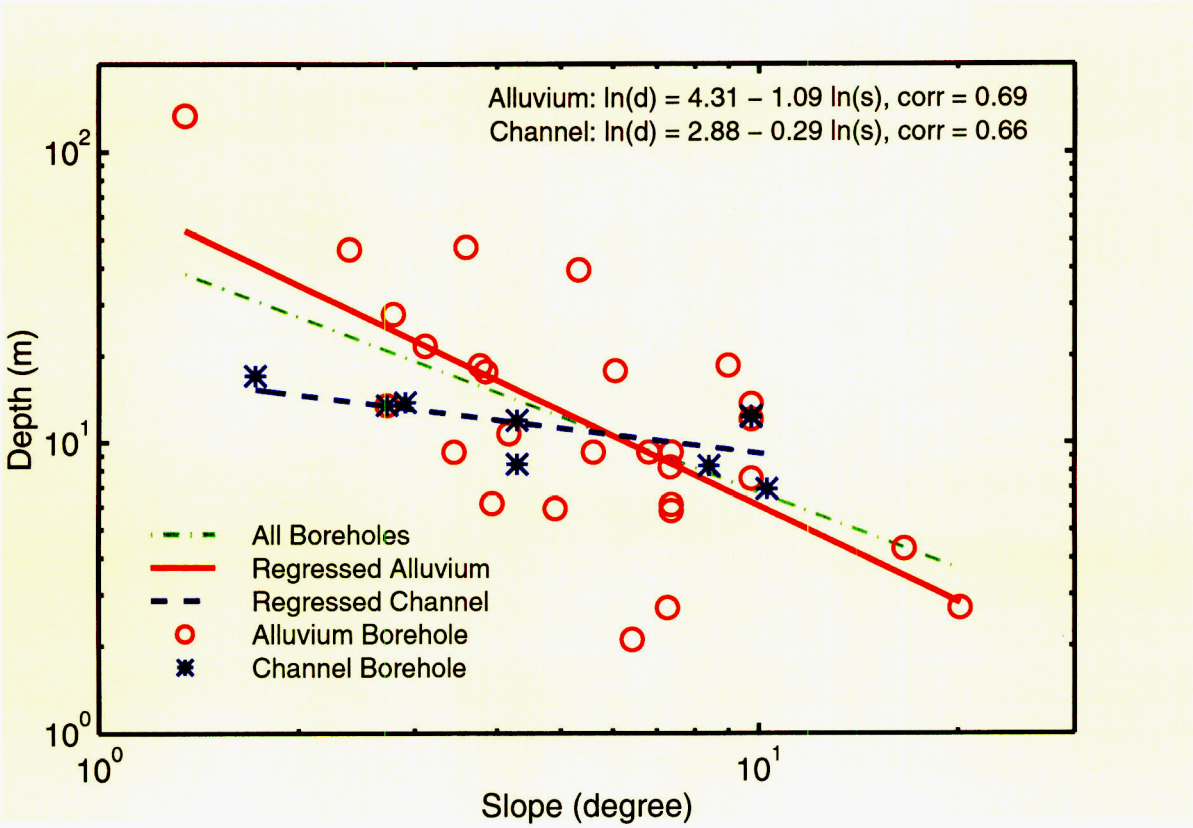

Figure 2-1: 1/13/97. Regression of borehole alluvium depths with nearest-neighbor DEM slopes.

1/15/97 Documenting infiltration abstractions.

In ***$HOME2/Matlab/YMInfil/SubregSpaceDist***, abstractions for AAI as a function of material and meteorologic properties are examined using **find_best_regress.m**. Abstractions for AAI as a function of material properties were originally developed in the summer of 1996. The abstractions were developed "by eye" and are more formally documented here.

The deep-alluvium abstraction originally developed is in the form

$$\log_{10}\left(\frac{AAI}{AAP}k^{1/2}\right) = \alpha_0 + \alpha_1\left[\left(\frac{m}{m_0}\right)^2 - 1\right] + \alpha_2\left[\left(\frac{P_0}{P}\right)^{1/2} - 1\right] + \alpha_3\left[\left(\frac{\varepsilon}{\varepsilon_0}\right) - 1\right], \qquad (2\text{-}8)$$

where

k is intrinsic permeability,
m is van Genuchten $m = 1 - 1/n$,
P is bubbling pressure (the reciprocal of van Genuchten α in the units used here), and
ε is porosity.

A subscript 0 represents a reference value for the parameter ($m_0 = 0.2$, $P_0 = 2000$ Pa, and $\varepsilon_0 = 0.3$), and the α values are hydraulic-parameter sensitivity constants. Equation 2-8 was originally reported by Bagtzoglou et al. (1997).

Using **find_best_regress.m** and **f_deep_hyd_fit.m**, a best-fit exponent was determined using the 28 material-property-variation simulations in **alluv.result** that have non-negative infiltration. Also, the impact of assuming a $\log_{10}$ relationship instead of a scaling relationship can be determined. These are performed by flipping switches at the top of **find_best_regress.m**.

Using the more formal abstraction process, a better regression is

$$\log_{10}\left[\frac{AAI}{AAP}\left(\frac{k}{k_0}\right)^{1/2}\right] = \alpha_0 + \alpha_1\left[\left(\frac{m}{m_0}\right)^{\beta_1} - 1\right] + \alpha_2\left[\left(\frac{P}{P_0}\right)^{\beta_2} - 1\right] + \alpha_3\left[\left(\frac{\varepsilon}{\varepsilon_0}\right)^{\beta_3} - 1\right], \quad (2\text{-}9)$$

where k_0 is 10^{-8} cm^2 and the β values are fitting exponents. A plot of the least-squares fit for the exponents is shown in Figure 2-2, where the fit for each curve only uses simulations with the parameter varying. Note that there is more noise in the value for P than in the other parameters.

The best-fit coefficients are shown in Table 2-5. The least-squares fit is also shown for the counterpart of the formal abstraction equation using logarithms,

$$\log_{10}\left[\frac{AAI}{AAP}\left(\frac{k}{k_0}\right)^{1/2}\right] = \alpha_0 + \alpha_1\log_{10}\left(\frac{m}{m_0}\right) + \alpha_2\log_{10}\left(\frac{P}{P_0}\right) + \alpha_3\log_{10}\left(\frac{\varepsilon}{\varepsilon_0}\right). \quad (2\text{-}10)$$

The best scaling fit is better than the logarithm fit for each parameter. If the logarithm of k is examined, however, the associated α coefficient is -0.495 and associated logarithm fit is 0.258, strongly supporting pulling k into the left-hand side as is done in Equation 2-9.

1/20/97 Documenting infiltration abstractions.

SAS

In ***$HOME2/Matlab/YMInfil/SubregSpaceDist***, abstractions for AAI as a function of material and meteorologic properties are examined using **find_best_regress.m**. Abstractions for AAI as a function of material properties were originally developed in the summer of 1996. The abstractions were developed "by eye" and are more formally documented here.

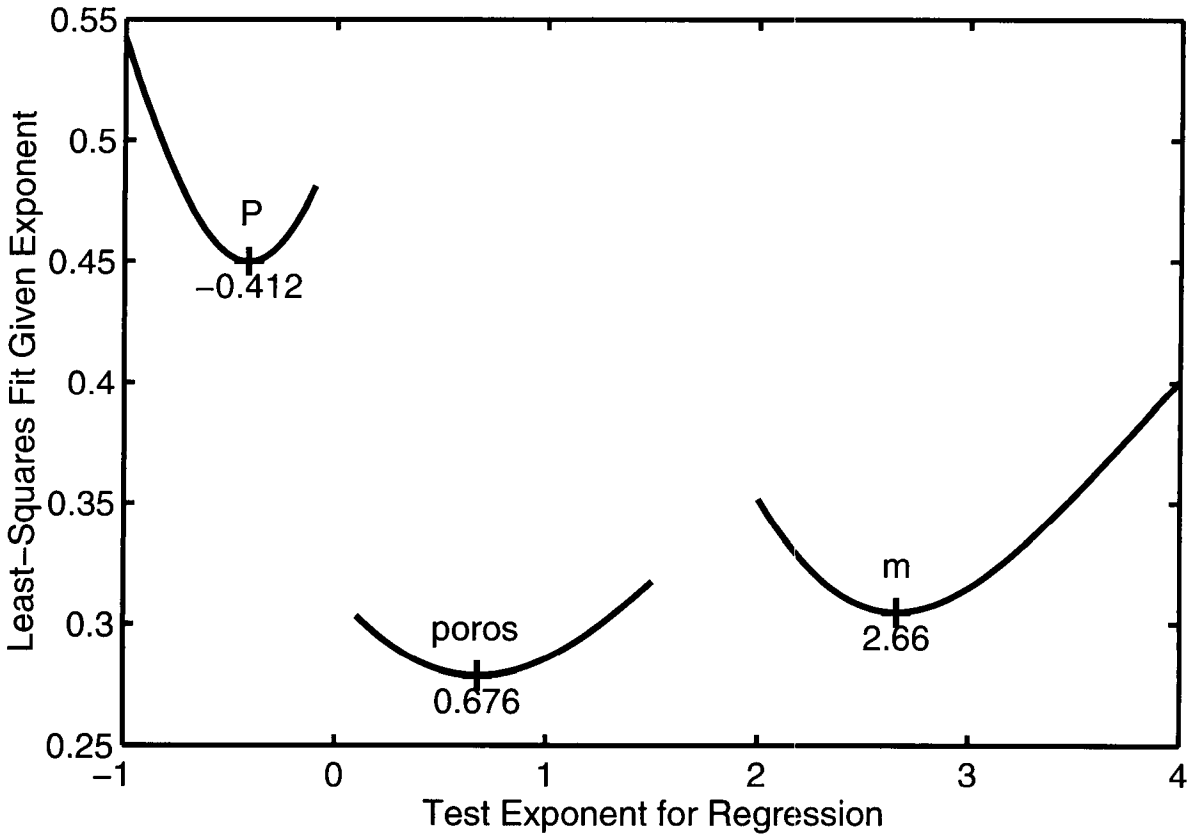

Figure 2-2: 1/15/97. Least-squares fit of simulation prediction to abstraction prediction for various exponents in Equation 2-9.

Table 2-5: Best-fit abstractions to material properties in deep alluvium.

Parameter	α	β	Fit	Log Fit
Scaling Constant	-1.38165	—	0.587745	1.09475
van Genuchten m	0.42505	2.6576	0.304383	0.821475
P	2.05672	-0.41248	0.449886	0.50599
ε	-1.39944	0.67568	0.278631	0.633175

Table 2-6: Regression values for deep-alluvium meteorologic abstraction.

Parameter	Exponent	Scale Fit	Curvature	Log Fit
AAL	-0.03723	0.308036	0.0284408	0.289575
AAP	-0.2889	0.419721	0.486325	0.440836
AAT	-15.96	0.648594	0.000370696	0.700391
AAV	2.075	0.323644	0.0174236	0.357603
AAW	0.2412	0.304608	0.0112994	0.28684

A routine called **f_deep_met_fit.m** was developed to check out the appropriateness of abstractions in the form of a scaling or a logarithmic representation, identical to the approach followed for material properties. Some trial-and-error runs were followed to pick reasonable base values for exponents, varying one parameter at a time. The value of the sought exponent was observed to shift about, depending on the values of the remaining exponents. Accordingly, the *Matlab* routine **fmins** was used to perform a global minimization for all meteorologic-variable exponents simultaneously. A modified version of **f_deep_met_fit.m** entitled **f_deep_met_reg.m** was created to follow the format required by **fmins**.

Two sets of regression results are presented in Table 2-6, for simultaneously determined exponents and for logarithmic regression, labelled Scale Fit and Log Fit, respectively. Each reported fit only uses simulations where the variable of interest is perturbed (including the base value of the variable). The column entitled Curvature represents the second derivative of the scale fit with respect to the variable, and is a measure of sensitivity; the larger the value of curvature, the better the exponent is determined. The logarithmic fit does not admit this measure. The best fit is to AAP; the worst fit is to AAT. The exponent for AAL, AAV, and AAW is roughly within a value of ± 1; the exponent for AAP is better determined and the exponent for AAT is much more poorly determined.

Based on comparing the fits reported in Table 2-6, it can be concluded that a logarithmic representation should be used for AAL and AAW and a scaled representation should be used for the remaining variables. The best-fit coefficients for this representation are shown in Table 2-7. The parameters without a reported value for exponent are represented using a logarithmic representation.

Table 2-7: Regression coefficients for deep-alluvium meteorologic abstraction. *Correction dated 1/23/97: Two curvature numbers were incorrectly transcribed. Correct numbers are italicized in the table.* SAS

Parameter	Exponent	Coefficient	Fit	Curvature
AAL	—	-1.52051	0.312029	—
AAP	-0.2416	-5.56806	0.420087	0.4858
AAT	-16.67	0.945489	0.649914	0.700391 *0.000366185*
AAV	2.138	0.281891	0.326738	0.357603 *0.0171413*
AAW	—	-0.321916	0.307231	—

1/22/97 Documentation of USGS data acquisition. SAS

I set up ***$HOME2/AmbientKTI/3Ddata*** as an archive for site-specific data acquired from or reported by DOE or subcontractors, such as core-sample data. Today A. Ramos typed in the moisture-retention data from Appendix II of Flint et al. (1996b). He double-checked his typing and I confirmed each number. I noticed that the original report is missing a number for sample TPC27s and for sample TPC15s. The original wordperfect file is called **usgs_ofr95-280_app2.wp** and an ASCII version is called **usgs_ofr95-280_app2.asc**. File **Sources** in the same directory documents this procedure.

Sources also documents previously obtained data residing in the same directory. The complete neutron-probe data discussed by Flint and Flint (1995) was obtained from the DOE office in September, 1996. Table 4 from Rautman et al. (1995) was obtained from C. Rautman on November 6, 1996, using email. Tables I-1 through I-8 from Flint et al. (1996b) were obtained directly from L. Flint on November 4, 1996, also by email.

1/24/97 Deep-alluvium meteorology regressions. SAS

I have noticed an increasing sensitivity of AAI to meteorologic properties as AAI decreases. Work to date has used the deep-alluvium regression equation the form

$$\log_{10}(H) = \alpha_0 + \sum_i \alpha_i U_i, \tag{2-11}$$

where $H = (AAI/AAP)U_k$, U_i represents a normalized value for parameter i, and the α values are constants. Two forms of U_i are considered, (i) the scaling fit (e.g., $U_{AAV} = [(AAV/AAV_0)^\beta - 1]$),

and (ii) the logarithmic fit (e.g., $U_{AAL} = \log_{10}(AAL/AAL_0)$). Note that both forms are zero for the base case of the parameter. Results for the two forms are discussed in the entry for 1/20/97, in which it was determined that AAL and AAW are probably better fit using the logarithmic form and AAP, AAT, and AAV are probably better fit using the scaling form.

In order to account for this sensitivity, I postulate that the deep-alluvium regression equation for meteorologic properties is in the form

$$\log_{10}(H) = \alpha_0 + \sum_i \alpha_i U_i + [a_0 + a_1 \log_{10}(H)] \sum_j \alpha_j U_j \tag{2-12}$$

$$= \frac{\alpha_0 + \sum_i \alpha_i U_i + a_0 \sum_j \alpha_j U_j}{(1 - a_1) \sum_j \alpha_j U_j}, \tag{2-13}$$

where index i represents a parameter that is insensitive to H and index j represents a parameter that is sensitive to H. Note that a_0 is arbitrarily set to 1 if there are no parameters considered insensitive to H. Again using *Matlab* routine fmins, I created a file to evaluate the least-squares fit of the simulation data to the regression equation with **f_deep_met_eval.m**. Although thousands of iterations are required to reach convergence, the new formulation significantly improves the data fit. For example, overall least-square-fits from 1/20/97 for simultaneous fits of AAP, AAT, and AAV are about 1.5 times larger than the new formulation provides. The form in Equation 2-13 is more general than a similar equation that uses $[a_0 + a_1 U_(k)]$ as the scale, although the latter form should work as well.

Hint for the future: the solution procedure appears to really benefit from periodic restarts. Perhaps the solution steps get too small and the restart enlarges them.

2/14/97 Daily-averaged meteorology.

Insofar as A. Flint typically uses daily meteorologic values when simulating infiltration, and I have been using hourly values in the vicinity of rainfall events and monthly values otherwise, and as daily simulations run faster than hourly simulations, I'm starting a few test cases to check on whether it actually makes a significant difference. I had looked at this years ago and found that averaging makes a relatively small difference, most important near precipitation events, and precipitation is the most important variable to capture. The simulations used 2-cm grids rather than the 1-mm grids I currently am using, so perhaps the conclusion may be altered.

Met files are generated in ***$HOME2/AuxRain/Climate***. A meteorology file with daily inputs averaged from the Desert Rock data, **dr_0d0d_24as.met**, was generated using **make_-**

ave_metseq('dr_0d0d_24as.met', 24). The met file was created by averaging all fair-day met values in a window of 30 days around each day, then overwriting the days with precipitation with the original, unaveraged, values for those days. It is possible to change the size of the window for averaging and the window for not averaging by changing hard-coded numbers in the call to **move_metave.m**.

The met file was copied to ***$SubRegBreath/RunTightAM*** and a sequence of simulations was started with 50 cm of alluvium over porous bedrock. These simulations took on the order of 3 days with hourly values.

2/27/97 Daily-averaged meteorology results and calcite.

Directory ***$SubRegBreath/RunTightAM/ResultDir*** holds the results of ten simulations of daily meteorology compared to hourly meteorology. The simulations are designated by **_ds** following both **reg07** and **reg08**. These designators represent bedrock cases 1 and 2, respectively, derived from regressed relationships by Flint et al. (1996b). The comparable cases with hourly meteorology are missing the **_ds** designator.

The *Matlab* routine **make_DH_Plot** was created to plot the results as shown in Figure 2-3. The plots show convergence over repeated input cycles to a constant value of decadal-average flux with depth; complete convergence occurs when the decadal-average flux is constant over all depths. Perturbations from the base meteorology are labeled $2/3P$, $3/2P$, $T+5$, and $T-5$, for multipliers in precipitation (P) and shifts of temperature (T) uniformly applied to all values.

Two items are of particular interest in Figure 2-3. First, although the two bedrocks have permeabilities different by an order of magnitude, AAI remains essentially unchanged. More importantly, there is significant difference between the hourly and daily meteorologic inputs, with the hourly values yielding significantly higher infiltration. With the current procedure for handling evaporation, I conclude that the simulator cannot be trusted to yield reliable results with daily inputs.

I have thus far examined the behavior of deep soil, soil overlying open fractures, and soil overlying bedrock. The one related case that remains to be investigated is the behavior of soil overlying fractures filled with calcite. It is reported by Flint et al. (1996a) that measured values for saturated hydraulic conductivity on fracture-fill materials averages 43.2 mm/day (5×10^{-7} m/s or approximately 5×10^{-10} cm^2). No van Genuchten properties are reported. The fracture-filling permeability is almost as large as the most permeable bedrock. After consulting with Gordon

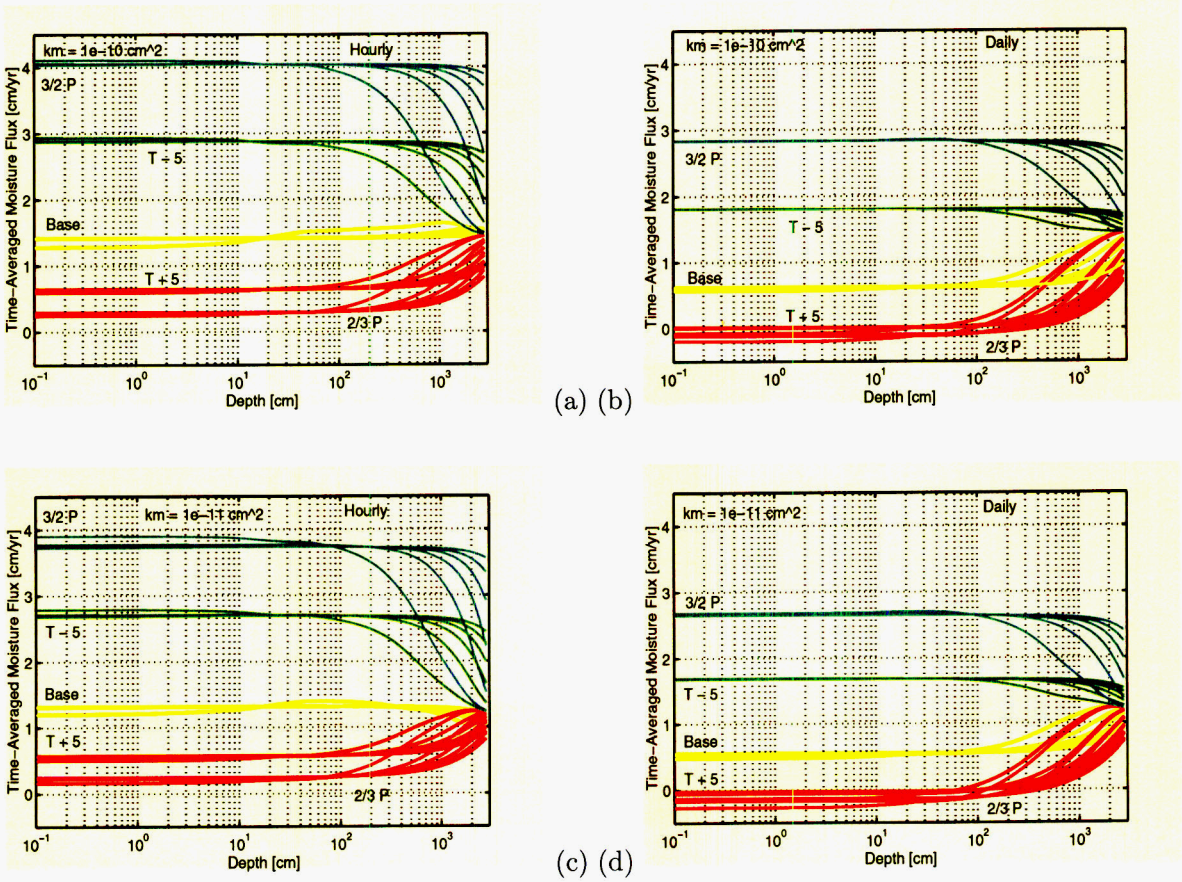

Figure 2-3: 2/27/97. Time history of decadal-average moisture flux after each of 6 decades, as a function of AAP and AAT, for (a) hourly meteorologic input and bedrock 1, (b) daily meteorologic input and bedrock 1, (c) hourly meteorologic input and bedrock 2, and (d) daily meteorologic input and bedrock 2.

Wittmeyer, it is probably not unreasonable to have fracture fillings with $\varepsilon = 0.1$, van Genuchten $\alpha = 100$ MPa^{-1}, and van Genuchten $n = 2$ (van Genuchten $m = 0.5$).

In ***$SubRegBreath/RunTightAM***, I am setting off a set of simulations assuming that the matrix is impermeable, fracture pore space is representative of the fracture classes in TCw as reported by Flint et al. (1996a), and the fracture-filling properties are as above. The three classes have reported fracture pore volume of 2.6×10^{-5}, 2.6×10^{-4}, and 2.6×10^{-3}, for 2.5 μm, 25 μm, and 250 μm fractures, respectively. Since porosity must also account for fracture pore space, filling porosity will be 2.6×10^{-4} (rounded to 10^{-4}). Precasting behavior suggests that infiltration will

increase with increasing soil depth (to the order of 1 m), due to the capillary attraction that calcite has relative to soil, but infiltration should be relatively small due to the rather small net porosity. Files with **cal3**, **cal4**, and **cal5** for fracture properties represent fracture pore volumes of 10^{-3}, 10^{-4}, and 10^{-5}, respectively.

In conversations with L. Flint (USGS) today, she clarified the weighting schemes that were used by Flint et al. (1996a) assign the values of 0.09, 0.055, 0.005, 0.025, 0.8, and 0.025 as the weights for open 2.5 μm, open 25 μm, open 250 μm, filled 2.5 μm, filled 25 μm, and filled 250 μm fractures, respectively. She also will send me data packets with the full set measured values, Without having the data in front of her, Lorrie independently used the thinking that Gordon used to suggest how the filling properties would be different from matrix properties.

3/1/97 Preliminary calcite simulations.

Three simulations have completed, each with 10 cm of soil over fillings with total porosity of 10^{-4}, 10^{-5}, and 10^{-6}, respectively. Interestingly, the three porosity cases do not appear to yield total infiltrations that are significantly different. The fractures respond very quickly, due to the small pore volume and high permeability, so it is adequate to use 2 decades for simulations. Partial results for deeper soils show decreases in infiltration with depth, similar to open fractures. A sequence of simulations for **cal3** and **cal4** were fired with the standard set of climate variations (AAP and AAT). A similar set of simulations, varying filling properties, will be run subsequently.

An error was found in the UZFLOW module converting meters to feet. The error came directly from the *Matlab* routine that calculates AAP, AAT, and AAT on each pixel of a DEM. Accordingly, all previous reported predictions for AAI are slightly incorrect, and should be slightly increased. Over the range of YM elevations (1100 to 1500 m), corrected values of AAP are 8 to 13 mm/yr larger, AAT are 0.65 to 0.9 °C cooler, and AAT are 1.2×10^{-7} to 1.4×10^{-7} drier.

4/10/97 Trip report for Yucca Mountain fieldwork.

The remainder of this entry is adapted from the trip report for a two-day trip to Yucca Mountain to perform characterization field work. Field documentation for the trip is in CNWRA notebooks 175 (soils and vegetation) and 217 (Solitario Canyon measurements).

Persons Present

The trip to Yucca Mountain (YM), on March 26 to 28, 1997, was undertaken by S. Stothoff and J. Winterle (CNWRA), D. Groeneveld and J. Thompson (Natural Resources, Inc.), and D. Or (Utah State University).

Background and Purpose of Trip

CNWRA is working with D. Groeneveld, D. Or, and J. Thompson to aid in characterizing the impact of vegetation upon shallow infiltration. Transpiration is a process included in DOE models but not considered in CNWRA modeling efforts to date. The intent of the CNWRA work is to incorporate vegetation into infiltration-modeling efforts in a plausible and defensible manner, with appropriate modeling of soil-moisture uptake by plants of particular interest. The trip was inspired by the need for field-checking hypothesized relationships between vegetation and bedrock type, soil cover, slope, and solar loading. In a parallel effort, watershed-scale modeling is being performed by D. Woolhiser. Soil permeability in the wash channels is one of the critical parameters in the watershed-scale model. J. Winterle accompanied the group to obtain soil permeabilities in Solitario Canyon channels, which will be used in the watershed-scale model.

Summary of Activities

The field work was split into three activities: (i) a spot-check vegetation survey verifying the more-detailed TRW vegetation work and examining factors governing the distribution of individual species (D. Groeneveld and J. Thompson); (ii) a spot-check of soil-permeability measurements to verify more-detailed United States Geological Survey (USGS) work, as well as examination of plant rooting distributions (D. Or and S. Stothoff); and (iii) channel permeability measurements in Solitario Canyon (J. Winterle). The vegetation survey was conducted over four days while the remaining work was performed over two days. Prior to the main trip, D. Groeneveld flew a photographic airborne survey of plant distributions, augmenting a collection of coarser-scale photographs taken previously by EG&G.

Overall Impressions

The trip was extremely useful in orienting Or to the YM site and to identifying and refining hypotheses regarding the spatial distribution of plants and plant uptake patterns. Soil measurements taken during field activities will provide direct input into modeling activities. The trip was also useful in planning future activities with Groeneveld and Or.

Interpretations Based on Field Observations

Prior to the field excursion, aerial photographs were examined and it was noticed that linear vegetation features could be identified, particularly along Yucca Crest. As a working hypothesis, it was felt that these linear features represent fissures in the bedrock that the plants were able to take advantage of for water uptake. To verify this hypothesis, several pits were dug adjacent to flourishing plants. Two pits were dug along an apparent linear feature in the Tiva Canyon caprock. Bedrock was reached at a depth of approximately 30 to 40 cm under the plants and in both pits a fissure of approximately 5 to 15 cm was identified, aligned with the vegetation feature, that was densely populated with roots. In one of the pits, a carbonate layer was identified within the fissure at a depth of roughly 5 cm below soil/bedrock contact; in the other, no distinct carbonate layer was identified to a depth of about 20 to 30 cm but there did appear to be increasing carbonate concentrations in the soil with depth.

Plant roots were exposed at three additional sites with shallower soil. At one site, in caprock, both plants exposed had roots predominantly within fissures or extending to fissures. At the second site, in caprock, the plant selected was in the center of a pocket of soil several meters across, with bedrock cropping out on three sides and a soil depth of at least 30 to 40 cm directly under the plant. Although a fissure existed, the plant did not appear to take special advantage of the fissure but appeared to take advantage of runoff from the surrounding bedrock. Nearby plants in fissures between bedrock outcrops appeared more verdant. At the third site, on a side slope in the upper lithophysal unit of the Tiva Canyon formation, the plants were rooted in rubble with 30 cm of cover. For these locations, typical of ridgetops and side slopes, the use of unrestricted rooting systems reported in the literature is precluded due to the strong influence of bedrock.

In all locations examined, the soil cover was sandy loam to loam with bedrock fragments, and was rather permeable. The fine portion of the soil appears to be æolian in nature wherever it was examined. Although permeabilities and soil depths were only determined at a few locations,

soil samples were collected at scattered locations (including each vegetation transect). Roughly two dozen soil samples were obtained. The similarity of the samples suggests that it would be reasonable to assume that soils are reasonably similar over the entire mountainside (except perhaps in areas with sorting due to overland flow such as washes and wash channels), consistent with Flint et al. (1996a).

Four ponded-head permeameter measurements were made at three sites with relatively shallow slopes along Yucca Crest and Highway Ridge. Measured saturated conductivity values ranged from 1.2×10^{-3} to 4.9×10^{-3} cm/s. The smallest reading occurred at a site where a large rock was subsequently found to lie directly under the disk; the next-largest reading was 2.9×10^{-3} cm/s. For comparison, Flint et al. (1996a) reported soil conductivities in the YM area of 5.6×10^{-4} to 3.8×10^{-3} cm/s based on soil-texture analysis. Three tension-head measurements (two readings with different suctions at one site, one reading at another site) were also obtained, indicating consistent values. The measured values are remarkably similar.

Rock particles found in the soil ranged from small pebbles through cobble-sized blocks. In the pits and in trenches with bedrock exposed, the bedrock was considerably more irregular than the soil surface implying that vegetation may be preferentially located in locally deeper pockets of soil where water can be stored for longer periods after precipitation.

The welded Tiva Canyon units do not exhibit gullying along the side slopes of the washes over the proposed repository footprint, suggesting that erosional processes are not dominated by overland flow. The high permeability of the shallow soils and the dense carbonates existing in fractures exposed by trenches in the TCw units below the caprock further suggest that lateral flow is likely to be primarily along the soil/bedrock interface rather than as overland flow. The distribution of vegetation suggests that lateral flow may be significant; vegetation is relatively sparse at the top of slopes and relatively dense at points where slopes flatten. Note that the existence of subsurface lateral flow is also suggested by neutron-probe measurements.

Based on topography, soil depth, and bedrock materials, the ground surface over the repository footprint can be divided into four categories:

Tiva Canyon caprock on ridgetops. Slopes are generally moderate (less than 10 degrees) with shallow soils (0 to 40 cm with pockets greater than 60 cm). The bedrock is generally massive with fissures spaced sufficiently far apart in places to provide significant organization to vegetation. The fissures are typically 5 to 15 cm in aperture, and appear to form by æolian soils filling between boulders. Bedrock is irregular in topography, with at least 40 cm variation

possible within the space of 2 m. The bedrock is sufficiently permeable that moisture may interact significantly with it over periods of days to weeks. Soil fills the fissures to a depth of at least 5 to 30 cm, with carbonate fillings possible. Roots are common, almost ubiquitous, within fractures. Net infiltration may be quite significant due to shallow soils. Several vegetation transects were taken in this environment, 4 soil-permeability and 2 bedrock-permeability measurements were made, and 5 bedrock-exposure pits were dug.

Tiva Canyon welded units (i.e., lithophysal units) below the caprock. Slopes are generally moderate to steep (10 to 45 degrees). Scree exists where slopes are greater than roughly 40 degrees. Bedrock is irregular in topography, although perhaps less so than for the caprock. There is some evidence of stairstepping in the bedrock surface that is not echoed in the soil profile, which may provide localized pockets for vegetation. Fractures are typically narrow in aperture (less than 1 cm) but closely spaced. The fractures appear to be filled with carbonates as a rule, and generally not penetrated by roots except for perhaps a few localized zones with wider apertures. Vegetation is predominantly Great Basin on the north-facing slopes and Mojavian on the south-facing slopes, with vegetation densities about twice as large on the north-facing slopes. Vegetation increases in density downslope. Net infiltration may be significant due to shallow soils. Lateral redistribution along the soil/bedrock interface may also be significant. Several vegetation transects were taken in this environment, a pair of soil-permeability measurements were taken, and several trenches and pavements were examined in detail.

Alluvium-filled washes. Slopes are shallow and soils tend to be greater than 1 m in depth. Net infiltration may not be significant, due to the large storage capacity of the soils and the presence of vegetation. This environment was not examined in detail, aside from one or two vegetation transects.

The west face of Yucca Crest. Slopes are quite steep, as much as 50 degrees. Numerous strata are exposed, ranging from densely welded to nonwelded. Soil pockets exist of as much as 50 cm even in the steepest slopes. Vegetation is dominated by crack-dwelling species. Overland flow should be significant, as evidenced by gully formation. Of the four environments this environment is by far the most complex to model however, relatively little of the repository footprint is overlain by this category. The environment was not examined in detail, aside from daily hikes up and down to Yucca Crest.

Hydraulic Conductivity Measurements in Solitario Canyon

J. Winterle obtained 13 hydraulic conductivity measurements for the stream beds in Solitario Canyon and its side canyons. These measurements were obtained using a Guelph Permeameter which is used by augering a hole 20 to 40 cm deep into the sediments and measuring infiltration of water out of the bottom of this hole while a constant water level is maintained in the hole. There were problems with this technique involving difficulty in augering holes due to the presence of large cobbles, and a tendency for the holes to collapse due to the lack of cohesiveness of the sediments. Nevertheless, 13 measurements were obtained with hydraulic conductivities on the order of 10^{-3} to 10^{-1} cm/s. These values are consistent with published values for silty sands and gravels. It should be noted that 10^{-2} cm/s is the upper limit of the range of hydraulic conductivities for which the Guelph permeameter is designed, thus the values outside of this range may not be as accurate as the lower values; however, they do represent a good order-of-magnitude estimate. Samples of sediments were obtained from the auger holes and their hydraulic conductivities are currently being measured in the laboratory. Locations of each of the conductivity measurements was recorded using a GPS unit. The GPS measurements are accurate to the nearest 100 m. Table 2-8 summarizes the data collected.

Problems Encountered

The real-time differential GPS did not function properly, almost certainly due to operator error. Reported measurements are therefore only accurate to within 100 m.

4/27/97 Conversion of neutron-probe data to matlab format.

SAS

The complete set of neutron-probe readings from the 98 neutron-probe boreholes plus UZ-7 (described by Flint and Flint (1995)), obtained September, 1996, from the DOE office, were converted to *Matlab* format. An awk script (**reduce_neut.awk**) converted the ASCII file to a reduced format, and a *Matlab* script converted it to a binary format for fast reads. Two additional *Matlab* scripts were created to examine the plots as a time history, **plot_neut.m** and **plot_neut_set.m**. Borehole UZ-7 is designated as neutron-probe borehole number 99. The scripts are stored in ***$HOME2/AmbientKTI/3Ddata***.

The awk conversion uses the csh sequence "`zcat neutron_* | nawk -f reduce_neut.awk`

Table 2-8: Hydraulic conductivity measurements in Solitario Canyon on March 27 and 28, 1997.

Sample #	UTM (m) N	UTM (m) E	Hydraulic Conductivity (cm/s)	Notes
1	546637	4077467	0.04	silty coarse gravels; many large cobbles
2	546517	4077632	0.02	coarse gravel with fine silty sand
3	546794	4077389	0.07	sandy coarse gravel
4	546826	4077651	0.05	well-sorted, pea-sized gravel
5	546772	4077250	0.002	silty, sandy gravel; large cobbles
6	546667	4077103	0.007	silty, sandy gravel; a few large cobbles
7	546612	4076972	0.002	silty coarse gravel
8	546593	4076710	0.012	sandy gravel; a few large cobbles
9	546597	4076410	0.02	sandy gravel
10	547186	4079275	0.1	coarse sand and gravel
11	547135	4078848	0.04	well-sorted pea-gravel with coarse sand
12	547121	4078681	0.01	well-sorted pea-gravel with coarse sand
13	547021	4078283	0.002	silty overbank sediments stream channel well-sorted pea-gravel

> `neut.date_num_dep_mc`".

There appears to have been some adjustment of elevations in late 1985, judging from offsets in all boreholes with records that early.

5/9/97 Documentation of upper-bound infiltration estimates.

If the temperature and thermal conductivity profiles of a rock mass are known, one can calculate the energy flux due to conduction. If the actual energy flux through the rock mass differs from the conductive flux, it must be due to advection (i.e., energy transported through liquid or vapor fluxes). When a vertical column has smaller conductive fluxes than actual fluxes, it may be due to cool infiltrating water warming while moving to depth or upward vapor transport with an associated large latent-heat transport. In order to estimate infiltration fluxes when moisture movement is predominantly vertical, one can use an analytic solution or a numerical simulator accounting for both conductive and advective fluxes, and adjust the infiltration flux until the measured temperature profile is obtained. Lachenbruch and Sass (1977) presented a relationship that indicates that

the reduction in apparent heat flux is roughly proportional to the volume of infiltrating water, the thermal gradient, and the distance considered. Typically it is assumed that vapor flux is negligible, although this assumption is not necessary if the vapor flux can be accounted for. Implicit in the approach is the assumption that the liquid and rock remain in thermal equilibrium.

One of the advantages of the method is the lack of necessity for knowing details of how the liquid moves within the rock. On the other hand, it is necessary to have an independent estimate for the thermal flux, which can be difficult to obtain. It is also necessary to know thermal conductivities, but these are typically quite well constrained.

Estimates of thermal and liquid fluxes throughout the NTS are presented by Sass et al. (1980) and Sass and Lachenbruch (1982), with the results summarized by Sass et al. (1988). Sass et al. (1988) analyzed a set of boreholes in the YM area, with resulting estimates of conductive and total heat fluxes from the saturated zone (SZ) into the unsaturated zone (UZ) of 40 ± 9 and 49 ± 8 mW/m^2, respectively, with an average heat flux in the UZ of about 41 mW/m^2. Sass et al. (1988) contour conductive heat fluxes in the YM area (Figure 15 by Sass et al., 1988), which indicates that conductive fluxes are 70 to 74 mW/m^2 southeast through southwest of YM; roughly 60 mW/m^2 in the southwest part of Midway Valley; roughly 50 mW/m^2 in and near Fortymile Wash, Dune Wash, Yucca Wash, and Solitario Canyon (SC); and roughly 30 to 40 mW/m^2 over the repository footprint and north past Drillhole Wash. Sass et al. (1988) suggest that there may be an apparent reduction of heat flow from the SZ to the UZ of 5 to 10 mW/m^2, and calculate that this apparent reduction of heat flow could be achieved by 2 to 5 mm/yr net infiltration and about 8 mW/m^2 reduction would be achieved if 0.1 mm/yr of water were vaporized. Lateral flow in the shallow SZ is also considered a possible source of local anomalies. Sass et al. (1988) also note (without further comment) that apparent heat flux is negatively correlated with elevation; one might infer that lateral diversion to lower topographic areas may be occurring, although the study by Rousseau et al. (1996), discussed below, would suggest the opposite due to the insulating properties of alluvium.

An implication of the analysis by Sass et al. (1988) is that, at least locally over the repository block and Drillhole Wash, deficits in the apparent heat flux that occur in the UZ may be as much as 20 mW/m^2[assuming that 10 mW/m^2 is roughly equivalent to 5 mm/yr infiltration, as calculated by Sass et al. (1988)], so that locally about 10 mm/yr infiltration might be estimated. When estimating infiltration, it may be better to estimate the vertical heat flux from boreholes that are unlikely to have significant infiltration. Infiltration fluxes in deep alluvium and not close to channels are likely to be quite small, so that the boreholes in Midway Valley and south of YM in deep alluvium may be more representative of regional vertical heat flux. If so, vertical heat flux

could be as much as 60 to 75 mW/m^2 and local deficits at YM could be as much as 45 mW/m^2, implying that locally more than 20 mm/yr infiltration could be inferred from the thermal data. Assuming that the UZ heat flux is 60 mW/m^2, heat-flux deficits on the order of 15 to 30 mW/m^{2}in the area of the repository block and Drillhole Wash could be justified, implying that local infiltration rates may be 7 through 15 mm/yr in this area.

One significant advantage of the heat-flux method is that it can yield upper-bound estimates for infiltration rates. Assuming that the regional heat flux is 85 mW/m^2, neglecting all other sources of reduction in apparent heat flux such as lateral flow in the SZ and vapor fluxes, using a value of 35 mW/m^2 as the average apparent heat flux over the repository block, and using the rule-of-thumb that 10 mW/m^2 reduction in apparent flux is equivalent to 5 mm/yr infiltration, one finds that the maximum average infiltration over the repository block is about 25 mm/yr.

The chloride mass balance technique, as applied by Fabryka-Martin et al. (1996b), assumes that average Cl^- concentration multiplied by total flux is conserved, or

$$C_o P = CI, \tag{2-14}$$

where

- P is average precipitation rate,
- C_o is the Cl^- concentration corresponding to the average Cl^- deposition rate,
- C is the Cl^- concentration in a well-mixed reservoir at depth, and
- I is the net infiltration.

Knowing the average precipitation rate, Cl^- concentration corresponding to the average Cl^- deposition rate, and Cl^- concentration in a well-mixed reservoir at depth, the percolation flux at depth can be determined. Yang et al. (1996) report Cl^- concentrations in perched water of 4.1 to 15.5 mg/L, with 15 of the 17 reported values no greater than 8.3 mg/L and a Cl^- concentration of 7 mg/L at NRG-7a (the nearest borehole to UZ-4 and UZ-5 with a reported perched-water sample). Using the same precipitation rate (170 mm/yr) and Cl^- concentration (0.62 mg/L) as Fabryka-Martin et al. (1996b), and assuming that the perched water is well mixed with the matrix waters, calculated net infiltration is 25.7, 12.7, and 6.8 mm/yr for concentrations of 4.1, 8.3, and 15.5 mg/L, respectively.

An infiltration value of about 26 mm/yr would represent an upper bound based upon the perched-water chloride data; if the matrix waters do not mix completely with the perched water, infiltration values may be lower. The estimated infiltration values are more consistent with the shallow infiltration estimates than the estimates from the PTn, however, suggesting that a con-

siderable portion of the infiltrating water may bypass the PTn matrix. The upper-bound value obtained by chloride mass balance on perched water, 26 mm/yr, is remarkably consistent with the upper-bound value obtained by geothermal heat-flux calculations.

5/19/97 Revisiting alluvium regression.

SAS

Since the discussion of 1/13/97, additional information on alluvium depths, borehole location, and borehole geomorphic classification (e.g., channel, sideslope) has been gleaned from the literature and the data file obtained with the site atlas. I incorporated the new information to obtain regression coefficients.

As it turns out, I was not able to reproduce the original slopes calculated by Hannah Castellaw in August, 1995. Apparently she used the slope at the nearest neighbor of the DEM, with all calculations performed in ArcInfo. I tried to use: (i) the slope at the nearest neighbor, (ii) the interpolated slope from the slope at the four nearest neighbors, and (iii) the interpolated slope from the elevations at the four nearest neighbors. None of these matched the previous slopes, although some were close. Unfortunately, the regressions exhibit poorer fits than before, particularly for the channels (although the channels have many more points now). It may be that Hannah used a different DEM coordinate grid; she has not worked at CNWRA for a year or two, so it will be difficult or impossible to retrace the exact calculations. There does seem to be quite a bit of scatter.

I revised the set of files used to estimate regression coefficients in ***$HOME2/Matlab/-3Ddata***. New data files were created in the format that the load_well file expects, and the other load routines call load_well. The original data and *Matlab* files all have ".1" appended. The routine that calculates the slope at the borehole locations is called calc_pt_slope; internally there are switches to calculate the slope according to the three options mentioned above.

5/25/97 Results of 1D simulations.

SAS

Over the last several months, a series of *breath* version 1.2 simulations were run examining the impact of alluvium-filled fissures and calcite-filled fractures. These simulations used the same strategy as was used for the open fractures, in that the bedrock was assumed impermeable and the porosity of the filling was lowered to account for the fracture porosity. The alluvium simulations use kmpo5223_aKmao5222 as the base case, while the calcite simulations use kmpo5223_cKmao7554 as

Table 2-9: Summary of alluvium (*abcd*) and fracture (*efgh*) parameter codes

Code	Parameter	Translation
Soil cover (kmpo*abcd*_aKmao*efgh*)		
a	Intrinsic permeability k (cm^2)	$k = 10^{-a-3}$
b	van Genuchten m	$m = b/10$
c	van Genuchten scaling pressure P_0 (gm/cm-s^2)	$P_0 = c \times 10^4$
d	Porosity ε	$\varepsilon = d/10$
Soil-filled fissure (kmpo*abcd*_aKmao*efgh*)		
e	Intrinsic permeability k (cm^2)	$k = 10^{-a-3}$
f	van Genuchten m	$m = f/10$
g	van Genuchten scaling pressure P_0 (gm/cm-s^2)	$P_0 = c \times 10^4$
h	Porosity ε	$\varepsilon = 10^{-h}$
Calcite-filled fracture (kmpo*abcd*_cKmao*efgh*)		
e	Saturated hydraulic conductivity K_{sat} (cm^2)	$K_{sat} = 10^{-e}$
f	van Genuchten m	$m = f/10$
g	van Genuchten scaling pressure P_0 (gm/cm-s^2)	$P_0 = 10^g$
h	Porosity ε	$\varepsilon = 10^{-h}$

the base case. The alluvium simulations used soil depths of 10, 25, and 50 cm; the calcite simulations used soil depths of 10, 25, 50, 100, and 150 cm. The alluvium simulations used fracture-alluvium porosity values of 10^{-2}, 10^{-3}, and 10^{-4}. The calcite simulations had a nearly full suite of calcite perturbations for soil depths of 10, 25, 50, 100, and 150 cm (2 perturbations calcite permeability, and calcite van Genuchten m; 1 perturbation for calcite P_0 and porosity) and a full suite of 2 perturbations for all soil properties with a soil depth of 10, 25, or 50 cm. The codes for the output files are discussed in Table 2-9. Note that the code for alluvium-filled should have been kmpo*abcd*_akmpo*efgh* and the code for calcite-filled should have been kmpo*abcd*_cKmpo*efgh* for clarity.

The average flux over the second decade, averaged over the depths of 1 to 10 m, were extracted using extract_qstate.m (coded in *Matlab*) for all simulations. Similarly, the decadal average moisture content in the node above the soil/fracture interface was extracted for each case. All values were stored in **af_allcli.result** in ***$BREATH2/Subreg***. The net-infiltration results are summarized in Table 2-10.

Several conclusions can drawn from the simulation results. The alluvium results suggest that as the fracture aperture decreases, net infiltration increases. The effect decreases as the soil

Table 2-10: Net infiltration (mm/yr) for various cases with soil- and calcite-filled fractures

Code	10-cm	25-cm	50-cm
kmpo5223_aKmao5222	17.2	7.13	4.44
kmpo5223_aKmao5223	21.4	8.30	4.92
kmpo5223_aKmao5224	22.4	8.53	4.99
kmpo5223_cKmao7554	17.4	8.55	4.85
kmpo4223_cKmao7554	14.7	2.70	0.42
kmpo6223_cKmao7554	21.6	13.8	10.7
kmpo5123_cKmao7554	18.2	12.9	8.66
kmpo5323_cKmao7554	21.5	12.0	8.24
kmpo5213_cKmao7554	26.3	17.6	12.7
kmpo5253_cKmao7554	10.3	1.25	0.13
kmpo5222_cKmao7554	23.0	15.8	11.6
kmpo5225_cKmao7554	9.48	1.80	0.29
kmpo5223_cKmao6554	33.1	14.8	8.08
kmpo5223_cKmao8554	3.31	1.81	1.43
kmpo5223_cKmao7454	15.2	7.50	4.78
kmpo5223_cKmao7654	19.2	9.21	4.70
kmpo5223_cKmao7564	42.6	23.6	14.2
kmpo5223_cKmao7555	17.5	8.57	4.87

depth increases, and is not tremendously large in any case. The calcite results suggest that the alluvium properties are not important relative to calcite properties when soil is 10 cm, but dominate when soil is 50 cm. Variation in calcite properties yields largest change in net infiltration when soils are shallow and are muted somewhat when soils are deep. The calcite property having strongest impact on net infiltration appears to be P_0, followed by K_{sat}.

The capillary properties of alluvium and calcite may be the most important parameters for calculating bare-soil infiltration. It appears that the ratio of alluvium P_0 to calcite P_0 is a controlling factor on infiltration. As the ratio gets smaller (calcite has finer pores relative to alluvium) net infiltration increases. One can attribute this to the propensity of calcite to imbibe moisture and not release it back to the soil to satisfy evaporation.

The variation of moisture content with net infiltration for the bottom node of the soil follows the general patterns ascertained before. There is a clear trend for drier soil with increasing net infiltration when the fracture-filling properties are changed, however, whether the filling is calcite

or soil (note that only soil porosity was varied).

6/11/97 Documentation of soil sample analysis.

During the annual CNWRA QA audit, in which the USFIC KTI was audited, an issue of data collection was raised. During the YM field trip examining shallow infiltration processes in caprock, documented in the entry dated 4/10/97, 23 soil samples were collected and analyzed for electrical conductivity and percent hydrometer estimates of grain size and texture, by Utah State University Analytical Laboratories (Utah State University, Logan, UT 84322-4830, 801/797-2217). The reported analysis is dated 17 April, 1997; I have filed a copy of the results in my file cabinet. These samples were collected at various locations around YM at the suggestion of David Groeneveld and Dani Or (consultants hired for their expertise in characterizing shallow flow processes).

Typically our QA program requires that such analyses be planned prior to data collection and that verification of the analysis procedure be performed in order to be fully complient with QA requirements. I was made aware of their recommendation while we were in the field and did not realize that an external agency (albeit an agency at the same university that Dani Or is an employee of) was to perform the analyses. Note that the soil samples are only intended for qualitative verification of our observations that all of the fine materials at the site are remarkably similar and are not intended for numerical estimates or to provide data for regulatory positions. We will have to note that data was not collected under CNWRA QA procedures if and when we use the information.

6/30/97 Root growth simulations for caprock paper.

I am writing a paper documenting our investigations of hydrologic issues regarding the interaction of vegetation with fissures in TCw caprock environments with Dani Or and David Groeneveld (consultants). The paper consists of three major components: (i) a description of field observations, (ii) simulation of the impact of vegetation on hydrologic behavior in the presence of fissures, and (iii) simulation of root growth in the presence of fissures. David has been writing the description of the fieldwork. Dani has been performing 2D simulations of a vertical cross-section with 5 fissures overlain by soil using HYDRUS-2D, which is an enhancement of SWMS-2D (Šimůnek et al., 1992), in order to examine the hydrologic behavior component. I have been attempting to use Version 2.0 of a 3D code developed at UC-Davis by Jan Hopmans, Volker Clausnitzer, and Francesca Somma that explicitly models individual roots and distributes uptake to the surrounding nodes.

The root-growth code does not have a name; I will refer to it as Root-Growth Simulation Model (RootSim) from now on. RootSim is a research-level code, so it has a number of shortcomings that would not be expected in a production code and that make it difficult to use for our purposes. Some shortcomings include:

- Every element must be the same size and rectangular shape.
- Properties are defined by node rather than element.
- Boundary conditions are restricted to a mixture of:
  - one (time-varying) flux value (as many nodes as desired),
  - one (time-varying) head value (as many nodes as desired).
- Gravity drainage is not allowed.
- The code relies on a non-portable random-number generator.

The code was run through a FORTRAN static analyzer code, for_study (called fstudy on bashful), provided by Cobalt Blue. SPARC version 2.0.1 was used for the test. A number of errors and warnings were identified, either through compilation messages, fstudy, or tracking down errors in simulation behavior, including:

- 24 overlength lines
- a branch into a block
- variable *init* used before being initialized
- calling subroutine ChInit when chemistry is disabled (thereby changing *dtMaxC*)
- 9 unused common blocks in routines
- 13 changes in common blocks between routines (different variable names)
- 21 instances where precision was lost (real to integer or double precision to single precision)
- rand is system-dependent (and does not work for SGI)

The common-block and lost-precision messages were ignored; the remaining messages were fixed. The rand problem was accommodated by writing a short C routine to use the rand48 routine

provided as part of the SGI library. In addition, a modification was made so that the **outfem** output files also include *cAvg*, so that the output file can be reused as a restart file without modification. Modifications and suggested modifications are further documented in file **Errors** in ***$HOME2/AmbientKTI/Root.***

Several tests have been run trying to get appropriate simulations for the paper. The physical problem entails a shallow soil atop a soil-filled fissure next to a matrix block, with a plant starting either directly over the fissure or starting at some distance, with the idea being to compare some measure (e.g., total plant mass) at the end of the simulation. Dani set up the original input files based on the documentation, and some properties were not totally appropriate for YM. Some of the plant properties have never even been measured.

Through a process of trial and error, I've modified the problem from the original set up by Dani. Problem setup and changes include:

- A relatively small domain is being modeled (an 11x12x36 grid, 25 mm on an element side). This represents a tradeoff between computational speed and grid refinement.
- Soil depth is about 10 cm and the fissure is about 15 cm wide (only half is modeled). The "about" is due to the node-defined material properties.
- Bedrock material properties are TCw cuc, with retention parameters for sample PW19s, composite-sample caprock K_{sat} (Flint et al., 1996b).
- Soil retention parameters are for a loamy soil (Dani refers to a Carsel and Parrish, 1988) and K_{sat} is texture-estimated for YM soil (Schmidt, 1989).
- Soil strength has caused difficulties in simulations. Soil strength is defined in the code to be $(1-\theta)^3 S_{smax}$, where θ is effective saturation and S_{smax} is soil strength at residual saturation (with apparently arbitrary units). The **root.in** input file defines a soil strength at which growth ceases for each type of material. Dani changed the bedrock retention properties to artificially maintain very dry (very strong) conditions. I put realistic retention properties, and the roots acted as though the bedrock was clay. Changing the bedrock strength to an extremely large value (10^{32}) caused numerical problems (NaN for root-tip location), which I interpret as due to overenthusiastic adjustment to strength gradients, so I cut it back to 10^8 and gradually increased to 10^{11}. Results are not totally satisfactory due to the transition zone between nodes where properties change in an uncontrolled manner. I also had problems by making maximum soil strength too large (14) compared to the plant-growth cutoff at residual saturation (6), which I fixed by making the maximum soil strength 6 as well.

- Appropriate boundary and initial conditions are difficult to provide with the version of the code we have available. One can provide either a constant-head or constant-flux bottom condition and both tend to misrepresent the available water. Either a no-flow or specified-head (representing equilibrium with the atmosphere) top condition may work. I have been running into problems with balancing available water with rock availability. The latest solution is to provide wetting events every 15 or 30 days and have no-flow boundaries at the bottom. I initially used initial conditions at 50 cm suction head.
- The current conditions have been changed to 300 cm suction head in soil (field capacity of 0.3 bar) and 3000 cm (3 bar) suction head in the rock, redistributed with 15 days of evaporation (15 bar) at the top and no flow at the bottom. Rain (7.5 mm) is applied at 15, 30, 45, and 75 days, and evaporation continues throughout at 5 bar.
- When very wet conditions occur, the plant over bedrock develops more biomass than the plant over the fissure, even though the fissure plant has much greater penetration. The bedrock plant is apparently using the bedrock as an additional source of moisture and developing along the bedrock interface. I am not totally convinced that this is not an artifact of the slushy material-property zone, but the caprock *is* quite permeable.

7/8/97 Modification of Scott and Bonk electronic version.

An electronic ARC/INFO coverage of Scott and Bonk (1984) geology is one of the data sets included on the DOE tape discussed in the 3/23/97 entry. There are 118 polygons that do not have a lithologic attribute and one alluvium polygon that is mislabeled as ym. Jim Prikryl extracted the coverage in UTM format last week and I have started entering the missing coverages by visual inspection. All work is in ***$HOME2/Matlab/YMGeology***. The updated coverage information is listed as **scotbonu.wat**; the original coverage is stored in subdirectory ***Orig***.

7/11/97 Regression for TPA shallow infiltration.

It was brought to my attention that the UZFLOW module of the TPA3 code, which predicts infiltration on a pixel-by-pixel basis over YM, was predicting far more mean annual infiltration (MAI) than mean annual precipitation (MAP) under full glacial conditions. The regression formula features bicubics in both MAP and mean annual temperature (MAT), and apparently these cause problems outside the range of interpolation. The formulation is for soil over an open-fracture continuum.

I revisited the form of the regression equation and have come up with a more robust (and simpler) formulation that appears to work well even through 4× current MAP and -15 °C cooler than current MAT. The formulation fails for soil depths greater than 25 cm, but these depths should have negligible infiltration for the system considered and can be set to zero. For very shallow soils (< 10 cm) and extremely cool and wet conditions (beyond the range simulated), the formulation predicts MAI in excess of MAP. These cases should have MAI set to equal MAP.

The regression equation is intended to account for several facets of MAI behavior in this system: (i) MAI generally changes logarithmically with changing inputs; (ii) MAI is more sensitive to changing inputs when soil depths are larger; and (iii) MAI is more sensitive to changing inputs when MAI is small. The simplest form of an equation satisfying these conditions is

$$H = B^{b_1}[\sum_{i=1}^{N} a_i f_i(u_i)](1 + b_2 H), \tag{2-15}$$

where

- H is $\log_{10}(MAI/MAP)$
- a_i is a regressed constant
- b_i is a regressed constant
- u_i is a normalized regression variable (e.g., MAP, MAT)
- $f_i(u_i)$ is a regression relationship for variable u_i
- B is $(b\varepsilon)/(b_0\varepsilon_0)$
- b is soil depth
- b_0 is base-case soil depth
- ε is porosity
- ε_0 is base-case porosity

In ***$HOME2/Matlab/YMInfil/SubregSpaceDist*** I created two new *Matlab* routines, **run_sreg.m** and **f_regshal2.m**, that perform the regression using the formulation.

7/14/97 More regression for TPA shallow infiltration.

In ***$HOME2/Matlab/YMInfil/SubregSpaceDist*** I created a new *Matlab* routine, **eval_TPA_fun.m**, that evaluates the function in Equation 2-15 (with best-fit constants) for every pixel in the standard YM DEM with soil depths given in **basecaseDepth.mat**. The areal-average MAI resulting from the formula, both as MAI and as normalized, is shown in Figure 2-4(a) and (b), respectively.

Following up on the incentive to examine the results in detail, I collected the simulations

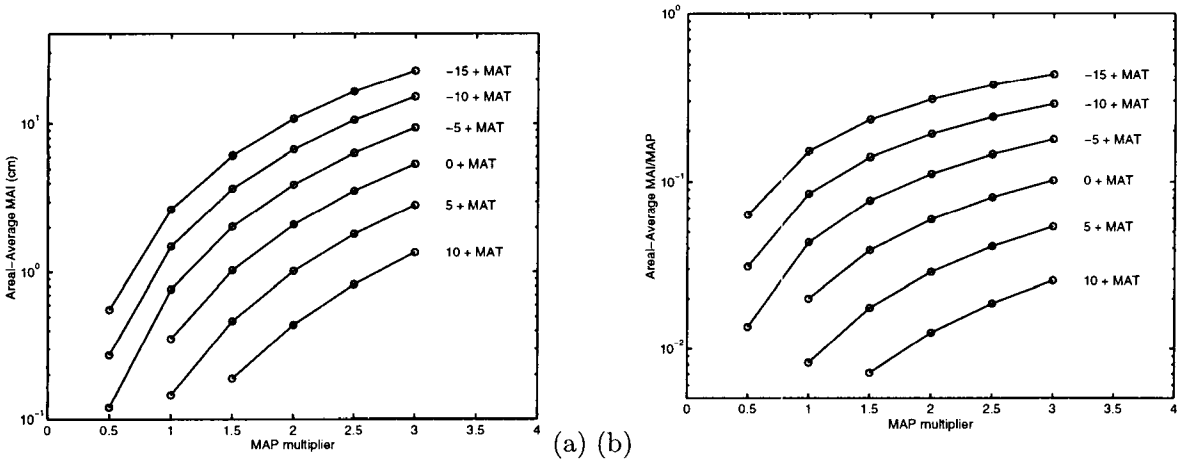

Figure 2-4: 7/14/97. Areal-average MAI for YM area, using regression formula based on soil/open-fracture system, (a) in dimensional form, and (b) in nondimensional form.

performed to date in **am_all.result** in ***$BREATH1/RunTightAM***. I modified the format of the file to include the date that the simulation was completed. I cursorily examined the soil-over-calcite simulations to check on the sensitivity to depth and climate. By plotting the simulations with the fracture code of **cal3** against the areal-average simulations, it appears that even though the calcite simulations do not span the same range as the soil-over-fracture simulations, the change in infiltration with climate should have similar trends. Overall infiltration may be greater with the calcite due to the lesser sensitivity to soil depth (e.g., 10 cm soil depth has 29 mm/yr while 50 cm soil depth has 7 mm/yr MAI). Fracture properties have a much greater impact on MAI for the calcite simulations than for the open-fracture simulations; permeability and bubbling pressure are the two big players, along with soil porosity.

A cursory check of simulations with base-case alluvium filling fissures with various soil depths and fissure porosities suggests that the falloff of MAI with soil depth has a characteristic slope, as the **cal3** simulations have about 1.5 times as much MAI for a given soil depth. Interestingly, MAI increases slightly as fissure porosity decreases.

10/10/97 Modification to scientific notebook.

Today I created a new chapter in this notebook, entitled "Ambient Hydrology KTI – Hydraulic Properties," and moved entries from this chapter to the new chapter. The entries include:

- 8/29/96,
- 9/21/96,
- 9/24/96,
- 3/23/97,
- All entries from 8/31 through 10/8/97.

The intention is to segregate entries into related groups, in order to improve clarity. No alterations were made to any entry (except for the move itself).

4/12/98 Documentation of future-climate analog trip.

The following is a nearly verbatim copy of a trip report discussing a visit to potential future-climate analog sites in southern Nevada. The trip took place April 5 through 8, 1998, and was reported by S. Stothoff.

Background and purpose of trip

The majority of work characterizing infiltration at YM has assumed that present-day conditions exist and relatively little work has been performed that addresses infiltration under future climatic conditions. The infiltration model used in the NRC's TPA3 exercises conservatively neglects transpiration. Under current climatic conditions, the atmospheric evaporation demand is so much larger than precipitation that neglecting transpiration provides infiltration estimates that are only moderately conservative. However, under the cooler and moister conditions that are anticipated to occur in future glacial cycles, neglecting transpiration is expected to have a much more significant impact on infiltration predictions.

An infiltration model incorporates transpiration by specifying total soil-water uptake and the distribution of that uptake with depth. In order to calibrate an infiltration model, it is necessary to identify the vegetation expected for the particular climate and geomorphic environment. Given the expected vegetation, it may be possible to estimate appropriate plant rooting depths and uptake patterns from the literature.

Analogs to YM under future climatic conditions, if found, will be used to calibrate the vegetative patterns used as input to the infiltration model. As information on the hydrologic behavior of the sideslopes at YM is least well characterized of all environments at YM, the washes are the primary analog environment that is sought. Analogs to the caprock environment are also sought, with secondary importance. Analog sites were identified within sight of YM in earlier fieldwork (i.e., the Prow, Shoshone Mountain), but the analogs are not sufficient to characterize the range of climatic and geomorphic environments encountered at YM under a glacial cycle. Additional potential analog locations were identified from topographic maps, geologic maps, and aerial surveys. These locations include Rainier Mesa, on the Nevada Test Site (NTS); Timber Mountain and the North Pahroc Range (both in Lincoln County); the Grapevine Range (near Beatty, NV); and the Montezuma Range (near Goldfield). The current trip assessed the viability of these potential sites for future field work, with particular regard to matching bedrock, soil, vegetation, slope, annual precipitation, and mean air temperature to expected future conditions at YM. It is expected that not all of these characteristics will be matched perfectly.

Summary of activities

The fieldwork was intended to quickly identify potential sites for subsequent follow-up studies in greater depth. It is difficult to characterize soil and bedrock characteristics from aerial surveys, so the primary emphasis for this trip was to identify appropriate soil and bedrock characteristics. A primary criterion was that elevations were generally in the range of 6,000 to 8,000 ft, providing precipitation and temperatures similar to anticipated future climates at YM. After elevation, the next criterion used in screening was to identify formations with densely welded tuffs, which are fairly rare. Appropriate slopes and soil depths were secondary criteria for matching.

Several good analog locations were identified, in the Grapevine Mountains, Timber Mountain, and Rainier Mesa. The North Pahroc Range was found less useful for analog work, while the Montezuma Range was not investigated due to time constraints.

The geomorphic characteristics of portions of lower Phinney Canyon, in the Grapevine Mountains, are strongly analogous to YM washes, featuring densely welded and quite fractured tuffs, north- and south-facing slopes, and thin soils with plentiful rock shards. The Phinney Canyon site may have slightly lower fracture densities and slightly thicker soils than YM. Ground access requires 4WD vehicles and nearly 1-1/2 hr driving from pavement; however, within the canyon access is equivalent to that obtained in YM washes. Air access is unlimited.

Timber Mountain, north of Hiko in Lincoln County, offers outcrops of moderately welded tuff, nonexistent to shallow soils, and general characteristics strongly reminiscent of the caprock at YM. The soils appear to be developing in situ, with perhaps less æolian component than apparent at YM. Ground access requires 4WD vehicles and 10 mi driving from pavement. The last 1/2 mi was hiked, due to mud and uncertain conditions; it should be possible to move closer later in the year. Moderate hiking (1/2 mi) may be required to visit prime sites. Air access is unlimited.

Rainier Mesa, approximately 1 hr drive north of Gate 100 in the NTS, is capped by moderately welded tuffs strongly reminiscent of Yucca Crest. Below the mesa top, sequences of densely welded to nonwelded tuffs form long slopes reminiscent of the west flank of YM. Soil thicknesses also appear to be similar to YM, although the soils appear to have much greater organic contents. Further, infiltration estimates are available, based on measurements of dripping into the N tunnel. Ground access is on pavement, perhaps with some dirt roads. Unlike the other sites, air access may be limited or unavailable due to NTS restrictions, and camping is not an option, requiring 1-1/2 hr drive to the nearest motel.

The North Pahroc Range, between Hiko and Caliente in Lincoln County, offers north- and south-facing sideslopes at angles similar to YM washes and soils generally similar to YM soils. However, the bedrock is not as densely welded as the Tiva Canyon welded units, thereby is less fractured. Also, the easily accessible slopes are generally at a lower elevation than the other sites, yielding an analog to a warmer and drier future climate than the other sites. Areas with what appears to be densely welded tuff are visible from the road, but access would require extensive hiking on steep terrain. Ground access requires 4WD vehicles, but is better than either Timber Mountain or Phinney Canyon. Air access is unlimited.

Impressions/conclusions

Overall impressions

The trip was useful in identifying analog sites. The trip successfully identified several good analogs for future work, although it is desirable to have additional reconnaissance from the air (particularly at Timber Mountain and Rainier Mesa). Fieldwork will not be possible for some time, however, as snow exists at higher elevations (up to 1 m thicknesses were observed) and soils are frozen.

Juniper and piñon pine are efficient at extracting soil moisture due to the large rooting systems for these plants. Packrat midden studies (Brown et al., 1997) indicate that juniper was

present at elevations below 500 m in the Great Basin during the last glacial period (significantly lower than the base of YM). During the visit to Nevada, juniper was found at elevations less than 6,000 ft in some locations but piñon/juniper associations were absent at significantly higher elevations in other locations along the periphery of the NTS and Nellis AFB. If the 6,000-ft elevation represents a representative future-climate analog, both cases with and lacking vegetation should be examined to ascertain whether YM would be expected to have these species present in future conditions.

The presence in April of significant amounts of snow and frozen soil, with snowdrifts of up to 1 m in depth, suggests that it may be important to consider snow when modeling infiltration under future climates. None of the YM infiltration modeling to date has considered snow, as snow is not important at YM under current climatic conditions. Under current conditions, most infiltration occurs during the winter; if the ground is frozen, however, infiltration would be expected to peak when the snow melts. It may be that larger infiltration pulses would occur under such conditions, if the total winter precipitation infiltrated over a few weeks.

Summary of field observations

Timber Mountain

Timber Mountain is located approximately 35 mi northwest of Caliente and 40 mi north of Alamo, in Lincoln County, Nevada. Timber Mountain is located far enough east to significantly attenuate the effects of the Sierra Nevada rain shadow. Ground access to the Timber Mountain site is via a 4WD dirt road proceeding 10 mi northwest from the White River Narrows. Air access is not restricted.

The Shingle Pass Tuff (Tsp) unit, identified as densely welded by du Bray et al. (1987), is of primary interest for analog studies. The Tsp unit, described as pinkish-gray to pale-red-purple by du Bray et al. (1987), is a crystal-rich tuff similar in welding and fracturing to the caprock at YM. The peak of Timber Mountain is 8,600 ft in elevation. Areas with Tsp outcrops range from 6,000 to 8,100 ft in elevation, with the most accessible areas (within 1/2 mi of the roadway) roughly 6,600 to 7,000 ft in elevation. Areas outside this range in elevation would require hiking several miles, although the hiking does not appear to be strenuous. A northeast-southwest trending ridge, at approximately latitude 37° 57'30" N and longitude 115° 5' W, appears to be a good analog site for the YM crest.

Soils in the Tsp outcrop areas are thin to nonexistent. Much of the soil appears to be forming in situ, and first impressions suggest that a smaller æolian component is present than at YM. Frost heave is evident in spots. Traces of overland sheet flow were also observed. Plentiful piñon and juniper are present.

North Pahroc Range (Boundary Wash)

The Pahroc area is also in Lincoln County. The North and South Pahroc Ranges are separated by US Route 93 approximately 25 mi west of Caliente. The primary ground access to higher elevations in the Pahroc ranges is through Boulder Wash Road, a 4WD road cutting through the North Pahroc Range from Dry Lake Valley to White River Narrows roughly 25 mi southwest of Timber Mountain. Accessible areas are all less than 7,000 ft in elevation, with the roadway less than 6,000 ft in elevation. Air access is unlimited.

Sideslopes north and east of the roadway feature moderately welded crystal-rich tuffs, and slopes that are generally shallower than the washes at YM. Two types of bedrock were observed within 1/4 mi of the road, a pale lavender tuff and a reddish-brown tuff, with the reddish-brown tuff appearing more welded and more suitable for future work. Fractures appear to be more widely spaced than the Tiva Canyon welded (TCw) unit at YM. Soils appear to be fairly comparable to those at YM. Appearing and disappearing streams where soil pinches out were observed, providing evidence of downslope lateral subsurface flow. Juniper were present, but much more sparsely than at Timber Mountain. Ground access to the base of the slopes is easy, but significant uphill hiking is required to reach higher elevations.

A bowl at higher elevations was noted south of Boundary Wash Road, with bedrock apparently more welded than the sideslopes northeast of the road. Snow was present, particularly on north-facing slopes at the bowl elevation. A hike to the bowl was abandoned partway due to time constraints, but portions of the hike were quite steep and strenuous and would be difficult to attempt with significant equipment. Other ridges south of the road might serve as an analog, but again would require significant effort to reach.

The Boundary Wash area is an adequate analog site, although other analog sites were identified with better characteristics. Unattractive features of the site include significant hiking, moderate welding, and low elevation. It may be worthwhile to consider limited study of the area as a supplemental analog for partial glaciation. Any studies would be likely be most practical if aerial analysis were the primary study mode, with limited ground confirmation.

Grapevine Mountains (Phinney Canyon)

Phinney Canyon, an east-draining canyon in the Grapevine Mountains, is located between Scotty's Castle (in Inyo County, California) and Beatty, Nevada. Phinney Canyon is in Nye County, several miles east of the junction between Inyo County, Esmeralda County (Nevada), and Nye County. The Grapevine Mountains are likely to feel significant effects of the Sierra Nevada rain shadow. Ground access to the Grapevine Mountain site is via a series of 4WD dirt road proceeding west from Rhyolite, north past Bullfrog Mountain to Sarcobatus Flat, and west to Phinney Canyon. Travel time from Beatty to Phinney Canyon is between 1-1/4 to 2 hr. Air access is not restricted.

Portions of the lower Phinney Canyon appear to be rather analogous to the washes at YM, especially two stretches of south-facing slope and at least one stretch of north-facing slope between the elevations of 6,000 and 6,600 ft. In these areas, the tuff is densely welded, with shards exhibiting the characteristic clinkstone clatter. Fracture patterns are quite reminiscent of densely welded TCw sideslopes, as best as can be ascertained from outcrop observations. Soils were also quite reminiscent of the YM washes, with similar sizes and percentages of rock shards, although the soils may be somewhat thicker.

A small snowmelt stream on the southfacing side of the canyon was located along a small fault, forming a waterfall. Under the waterfall, a cave was hollowed out to perhaps 2-m depth. Dripping from ceiling fractures was observed at numerous locations within the cave, apparently arising from stream infiltration several meters above.

The vegetation was somewhat anomalous in the lower portions of Phinney Canyon. Typically, juniper is observed at lower elevations than piñon, but in Phinney Canyon juniper was much sparser at the lower elevations than was piñon. Juniper was primarily observed on sideslopes, with thin soils. Piñonwas quite dense in the wash bottom, reaching several meters in height.

The roadway was impassable due to snow at roughly 6,200 ft elevation. Drifts were as deep as 1 m at higher elevations, although deep depressions in the snow cover were formed at the base of most plants.

The Phinney Canyon site appears to be an excellent analog to YM washes, certainly the best of any site examined. Fractures may be slightly further apart than at YM, and soils may be somewhat thicker, but overall the site is highly recommended.

Rainier Mesa

Rainier Mesa, in the north-central portion of the NTS, rises to an elevation of roughly 7,000 ft. Rainier Mesa is topped with a moderately welded tuff caprock quite reminiscent of Yucca Crest with more boulders. Estimates of fluxes into the N-tunnel drifts provide information on net infiltration at Rainier Mesa, which can be used to calibrate infiltration models. Access to Rainier Mesa is by paved road, although camping at the site is unlikely to be allowed so that roughly 3 hr of driving will be required each day. Also, air access is strictly controlled and it may not be possible to obtain the aerial photographs required to quantify vegetation densities.

A carpet of snow up to 1/2 m thick covered the top of Rainier Mesa, closing the road and limiting observational opportunity. It appears that soils are similar to Yucca Crest, albeit with much greater organic content. Piñon, juniper, and mountain oak were found on the mesa caprock.

Long slopes extend from the mesa caprock to the valleys below, featuring hundreds of meters of densely welded through nonwelded tuffs. These slopes are reminiscent of the portions of the western flank of YM that lie above the Paintbrush Tuff nonwelded (PTn) outcrop. Densely welded tuffs, visible in road cuts, appear to be almost identical to the densely welded portions of the TCw tuff. These slopes may serve as an analog to the Solitario Canyon side of YM, although the lack of gully formation limits the analogy to Topopah Spring welded (TSw) exposures at YM. The slopes may also serve as an analog to the washes, but may suffer from the lack of a wash bottom collecting water. Perhaps the contrast between Rainier Mesa slopes and Phinney Canyon slopes may provide insight into lateral flow processes in the washes.

Conditions are currently very moist on the NTS. Yucca Lake is currently full to beyond the playa dimensions, and the alluvium at various locations on the Test Site is essentially saturated.

Problems encountered

None.

Pending actions

None.

Recommendations

Use the Phinney Canyon site for an analog to the YM washes, concentrating resources into evaluating the relatively poorly characterized sideslope environments. The Phinney Canyon studies should receive the highest priority for fieldwork. Analysis of aerial photography should be the primary study tool for the remaining sites, with limited ground confirmation of aerial observations. As much use should be made of aerial observations as is possible, as data acquisition is relatively fast, informative, and inexpensive.

Attachments

Annotated photographs of the potential analog sites examined during the trip were attached to the trip report. These are not included here.

4/28/98 Observations of rainfall/temperature variability.

As I was replying to comments on the UZFLOW module of the TPA code, it occurred to me that the variability about the bulk climate actually should incorporate all variability above the decade scale. Probably several scales are of interest: (i) decade, (ii) century, and (iii) millenial. Perhaps incorporating fine-scale Milankovich cycles would take care of the longer-scale perturbations.

The Beatty data is the most readily available for quick analysis of decadal scale perturbations. The Beatty data extends from 1945 through 1995, with daily observations of precipitation, maximum temperature, and minimum temperature. Unfortunately, the data appears to have gaps, with between 7 and 17 years missing at least 5 days of observations (up to 3 months were missing) and one year appearing to have repeated observations (which are removed during the analysis). In addition, the weather station was moved once or twice, which Nichols (1987) suggests affected the readings significantly. Nevertheless, some useful information can be extracted from the data. As a quick and dirty estimate, all years (except the first and last) were used, even partial years. The values for variability derived from the data are biased too high because of the missing data and station relocation.

The decadal mean values for mean annual infiltration were extracted for each combination of ten years (35 combinations) and for consecutive decades (3 sets). The mean precipitation was

about 5 in., with a standard deviation of 2.3 in. for annual variability and 1 in. for decadal-averaged variability (both methods) The average of the maximum and minimum temperature was used for mean annual temperature, yielding a mean of about 15.2 °C and standard deviations of 1, 0.46, and 0.53 °C for the annual, 35-combination, and 3-decade sets, respectively. The correlation coefficient between MAP and MAT is -0.24, -0.89, and -0.92 for these three cases. Some of the correlation is likely due to weather-station relocation.

I would suspect that the coefficient of variation is more appropriate for the precipitation (CV = σ/μ), so that the projection to YM would give a rough decadal variability of 0.2 times MAP, or about 30 to 35 mm/yr (assuming 150 to 175 mm/yr). Temperature variability should be roughly equivalent, so that appropriate decadal variability is 0.45 to 0.55 °C.

The longer-term variability is likely to be intermediate in magnitude between the decadal variability and the glacial-maximum variability. I suspect that the higher values of effective moisture reported by paleoclimatologists may represent a muted bulk variability with relatively short-term fluctuations (centuries) imposed on the bulk signal. If a reasonable multiplier of current MAP for bulk MAP is 2 (sampled 1.5 to 2.5), then microglacial perturbations with a CV of 1.5 would give peak glacial maxima of 3 times current MAP. An improved perturbation model might consist of short-term MAP oscillations with CV of about 0.2 (sampling 0.1 to 0.3) and mid-term MAP oscillations with CV of about 1.5 (sampling about 1 to 2). Note that the exponential dependence of MAI on MAP will give a larger expected MAI when perturbations are considered.

Temperature effects might be reasonably handled with short-term oscillations sampled between 0.4 and 0.6 °C and mid-term oscillations sampled between 2 and 4, and full-glacial maximum change sampled between 4 and 7 °C.

5/21/98 Trip report. SAS

The following is an excerpt from my trip report to YM from the period of May 13 through 18, 1998, in which characterization fieldwork was performed. My field documentation for the trip is in CNWRA notebook 175.

Persons Present

The trip to Yucca Mountain (YM) and Phinney Canyon (PC) (a potential climate-analog site), on May 13 through 18, 1998, was undertaken by R. Fedors (CNWRA) and consultants S. Stothoff, D. Groeneveld, D. Or, D. Woolhiser, and O. Chadwick.

Background and Purpose of Trip

CNWRA is working with S. Stothoff to refine model estimates of mean annual infiltration (MAI) over the repository performance period. The modeling to date has considered one-dimensional (1D) simulations of coupled heat and moisture transport, with the results of the simulations abstracted to grid blocks covering the repository footprint. The approach is limited by neglect of lateral flow, transpiration, soil genesis, and snow dynamics. The other consultants were retained to help refine the infiltration model to incorporate these processes appropriately. O. Chadwick provides expertise in soil genesis processes. D. Groeneveld provides expertise in Great Basin plant ecology. D. Or provides expertise in soil physics and field-measurement techniques. D. Woolhiser provides expertise in watershed modeling in the arid southwest.

Split Wash is strategically located above the path that the east-west exploratory drift is following. D. Woolhiser will be performing watershed-scale modeling for the north branch of Split Wash, and D. Or will be performing hillslope-scale modeling. These newly initiated activities require data on soil depth and other factors affecting overland flow and interflow, and are intended to consider both current and potential future climatic conditions. Much of the data collected on the trip is intended to feed these activities.

S. Stothoff, D. Groeneveld, and D. Or are attempting to characterize the impact of vegetation upon MAI over the next glacial cycle. Transpiration is a process included in DOE models but not considered in CNWRA modeling efforts to date. The intent of the CNWRA work is to incorporate vegetation into infiltration-modeling efforts in a plausible and defensible manner. The trip was inspired by the need for field-checking hypothesized relationships between vegetation and bedrock type, soil cover, slope, and solar loading.

Soil depth and composition are significant factors influencing infiltration over the period of repository performance. Although soil depth and composition at YM are reasonably well understood under current conditions, significant changes in these factors may occur as climatic conditions

change. O. Chadwick was retained for his expertise in soil genesis, with the anticipation that he may be able to identify likely past and future soil conditions. The field trip served as Chadwick's orientation to YM, with the trip to PC serving as an orientation to a site with climatic conditions similar to postulated future conditions at YM.

Summary of Activities

The fieldwork at YM was split into the following activities, performed primarily within Split Wash: (i) vegetation transects verifying the more-detailed TRW vegetation work and examining factors governing the distribution of individual species (D. Groeneveld and S. Stothoff); (ii) permeability measurements to characterize bedrock-fracture and soil properties (D. Or and R. Fedors), (iii) channel-characteristic measurements for the upper portions of Split Wash (D. Or and S. Stothoff), (iv) alluvial-terrace measurements (D. Or, D. Groeneveld, and S. Stothoff), (v) soil depth and composition measurements (O. Chadwick and R. Fedors), and (vi) field identification of potential infiltration hotspots in upper washes (S. Stothoff).

The fieldwork during the one-day trip to PC was split into the following activities: (i) orientation to the site (new to all but Stothoff), (ii) identification of vegetation study locations, and (iii) examination of soil characteristics.

Overall Impressions

The trip was extremely useful in orienting Chadwick to the YM site and in identifying and refining hypotheses regarding the soil depths and genesis processes. Soil and vegetation measurements taken during field activities will provide direct input into modeling activities. The trip was also useful in planning future activities with Chadwick, Groeneveld, Or, Stothoff, and Woolhiser.

Soil Genesis Interpretations Based on Field Observations

Significant insight was gained into the depth and composition of soils that might be expected over a glacial cycle at YM, both based on observations at YM (primarily in Split Wash) and at PC. The selection of Split Wash as a study location was fortuitous, as Split Wash may have the best-preserved deep alluvial terraces of all washes above the repository footprint. The stream channel has cut the

terraces as much as 20 m to reach bedrock. In other washes, clearcut traces of deeper soils are not evident, having been nearly obliterated by erosion, but colluvial lobes along the sideslope toes are suggestive of soils that were deeper by up to 1 m. Similar erosional activities have been observed across the arid southwest that are dated to 8 to 15 ka, coincident with removal of vegetation as the climate became warmer and drier following the last peak in glaciation. The soils now present across YM are predominantly æolian in origin, and are relatively shallow and unweathered. At PC (roughly 700 m higher than Yucca Crest), on the other hand, soils are deeper, moister, more weathered, and have greater organic content.

Yucca Mountain soils are typically sandy loams in texture, while Phinney Canyon soils are more characteristic of silty loams. Simulations using the 1D BREATH code have been performed using properties similar to sandy loams and silty loams, allowing MAI to be roughly compared for YM and PC. The simulations predict that MAI may increase by 1 to 1.5 orders of magnitude as climatic change proceeds, if the soils are characteristic of those presently at YM. However, assuming that soil increases in depth from 25 to 50 cm, rock fragments decrease from 50 percent to 33 percent by volume, and the fine component changes from a sandy loam to a silty loam, predicted MAI is approximately 2.5 orders of magnitude smaller at PC for the current climatic conditions. Most of the decrease is due to the textural change of the soil. It would be expected that the PC soils are more sensitive to changing climate than the YM soils, but even so the predicted net effect would almost certainly be a reduction in MAI. The predicted decrease in MAI does not account for vegetation, lateral flow, or snow dynamics. Due to the colder winter temperatures, substantial snow cover may develop and the ground may freeze. These effects would dramatically change the dynamics of recharge during the winter and spring and would likely substantially increase MAI.

The potentially significant impact on MAI of changing soil texture and depth points out the importance of soil genesis characterization. Without observations of remnant soils similar to those at PC, however, the existence of soil change is arguable. Buried soils similar to those at PC were observed at three locations, once on the ridgetop separating the uppermost forks of the north branch of Split Wash and twice on the caprock upgradient of Split Wash. These soil-texture observations are extremely suggestive that textural changes might be expected over a glacial cycle at YM, and these textural changes would be expected to reduce MAI. The rapidity of the textural changes is open to question, as it takes extended periods of time to weather sands into clays.

The rapidity of soil depth changes is also quite uncertain. Erosive tendencies vary with available moisture, with erosion occurring slowly when little moisture is available. Erosion increases with available moisture, but so does vegetation, until a point is reached where the increased stabilizing presence of vegetation counteracts the destabilizing influence of erosion. One would expect

that changes in soil depth might respond exponentially to changes in climate, with rapid change decaying into a stable system. Soil texture also responds exponentially, but over a longer time span.

If the observations regarding soil depth and texture changes are correct, one might expect that MAI would increase relatively quickly as conditions become cooler and wetter, then would gradually decrease as transpiration increases, soil depths increase and soil textures become finer. As conditions become warmer and drier after the glacial maximum, one would expect that MAI might respond to shallower soils quickly but relatively slowly change due to textural change.

During the field work, enhancements to the existing CNWRA model for soil depth genesis were discussed. These enhancements would be intended to examine potential rates of soil depth and soil texture change at YM. The current model considers one generic soil in equilibrium with the environment, with soil generated through weathering and moving due to creep and ephemeral streamflow. Potential enhancements would include time stepping, several soil-particle sizes, an æolian source of dust, and chemical weathering.

Observations of Potential MAI Hotspots

The remnant channel terraces in Split Wash are not the only anomalous feature of the watershed. The northern branch of Split Wash terminates with a small channel fork. The southern of the two channels is choked with talus and alluvium, and there is no sign of stream activity for several hundred meters. Evidence of streamflow is present above the area choked with alluvium. The Tcpmn unit (middle nonlithophysal unit of the Tiva Canyon formation) crops out along the walls in areas with gaping fractures and talus. In this area, the rocks appear to be washed clean of dust and fractures tend not to have carbonate fillings. The vegetation in this area is particularly dense.

The combination of copious talus, nonexistent channel flow, gaping fractures, and dense vegetation are all factors suggesting that substantial infiltration may occur in this portion of the watershed. A total area of roughly 10^4 m^2 might be classified as a potential infiltration hot spot. Interestingly, the east-west drift currently under construction will pass close to this wash. If the drift passes under the wash, it would not be surprising to find that *in situ* water fluxes are much larger than elsewhere in the repository footprint.

The observation that this particular wash area appears to be an infiltration hot spot while nearby washes do not appear to have such overt infiltration potential engendered lively discussion

of the features that infiltration hotspots might exhibit. The existence of talus slopes is an obvious indicator, as evaporation is greatly reduced by talus. The presence of gaping fractures, particularly with minimal carbonate filling, is another indicator. Both talus and gaping fractures can be linked to the particular rock type cropping out. Densely welded units tend to form talus, as erosion removes blocks along fracture planes rather than removing grain by grain. The lithophysal units have fewer and finer fractures than nonlithophysal units, as the presence of lithophysae during cooling relieves some of the strain that forms cooling joints. Lithophysal units tend to spall, forming plate-like talus, while the nonlithophysal units tend to form bulkier talus. The lithophysal talus appears to be somewhat less resistant to further breakdown than the nonlithophysal units. Accordingly, locations with nonlithophysal units cropping out provide a heuristic indicator for both gaping fractures and talus, which are both strong indicators for high infiltration.

S. Stothoff examined eight of the sixteen upper-wash channels between Highway Ridge and Antler Ridge, all of which feature Tcpmn outcrops, to see if they also have other features indicative of high infiltration. Two of the washes, the Split Wash fork already mentioned and the north branch of WT-2 Wash (just south of Whaleback Ridge), appear to have notable high-infiltration areas while the remaining washes appear to be more typical. The WT-2 Wash area shares with Split Wash the characteristics of no recent runoff, copious talus, gaping fractures, dense vegetation, and minimal fracture fillings (at least near the bedrock surface). The nonlithophysal-unit outcrop areas in all of these washes appear to be generally more conducive to infiltration than the lithophysal areas, but the potential for infiltration is mitigated in many of the washes by limited outcrop area, shallow channel slopes, or shallow sideslopes.

In general, talus was more common on north-facing slopes and exposed bedrock fractures were more common on south-facing slopes. Densely welded nonlithophysal units in the examined washes rarely had exposed bedrock in the actual channel, while the lithophysal units often exposed channel bedrock for significant portions of the upper wash.

With the notion that deeper soils are indicators of reduced MAI, due to increased storage and opportunity for evapotranspiration, clues regarding soil depth during glacial periods were also sought during the infiltration hotspot survey. Many of the washes featured concave-down slopes to the channel, which indicates that the most recent activity has been degradational. Colluvial lobes are apparent along many of the washes, suggestive that deeper soils may have existed in the past. If these washes become aggradational in the future, it would be expected that the deeper covers would reduce MAI and thereby reduce the hotspot activity.

11/9/98 Summary of activities.

SAS

I have been quite active in working on infiltration issues for the last several months. Two documents have been essentially completed during this period. One is work related to the one-dimensional (1D) bare-soil infiltration simulations, abstracting the simulation results into three formulae for MAI (depending on the hydraulic properties of the system). The abstractions were exercised on heterogeneity issues. The second document was compiled by D. Groeneveld, and discusses the ecologic and hydrologic implications of weedy brome grasses invading the YM area. Both of these documents will be inserted into the notebook, with annotations, upon completion.

I am currently putting together an updated map of MAI, using the new abstractions with site-specific data. An ARC-INFO file of the detailed bedrock geology of the central block (Day et al., 1998), obtained from the Department of Energy (DOE) (with original copy maintained by R. Martin), is used to provide a base for the estimate. The geology polygons are transferred to a grid as needed. Bedrock and soil hydraulic properties can be obtained from Flint et al. (1996a), as are fracture intensities. Typical fracture apertures and typical fillings for the units were estimated from my personal fieldwork, as no guidance is provided by Flint et al. (1996a).

Soil properties are from Flint et al. (1996a) as well, with Typic Haplocambids, Typic Calciargids, and Lithic Haplocambids assigned to areas mapped as alluvium, colluvium, and everywhere else, respectively. These assignments are based on the soils in the vicinity of the repository footprint in the soil map presented by Flint et al. (1996a). Of the eight classified soils, the largest K_{sat} is 3.8×10^{-5} m/s and the smallest is 5.6×10^{-6} m/s. These values are all large enough to produce maximal values of MAI, so that capturing the exact soil classification is likely not important.

The 1D simulations only use one type of layer beneath the soil, which can be unfilled fractures, soil- or carbonate-filled fractures, or bedrock. The abstractions handle each case. However, the actual field situation likely has some of each case for any one area, each affecting the local pressure gradients. The pressure field most representative of field conditions is assumed to be the one yielding the greatest fluxes, so that the maximum of the four cases is used.

The resulting predictions of MAI in the central block are significantly larger than any field observations suggest, particularly in deep alluvium. This is largely due to the neglect of vegetation in the 1D simulations. An uptake efficiency factor may be defined to account for the additional water that vegetation can extract beyond bare-soil evaporation. It is assumed that no additional extraction occurs with zero soil thickness and, if the soil is sufficiently thick to allow a full rooting zone, only a small percentage of the bare-soil MAI (e.g., 1 percent) escapes the rooting zone.

For intermediate soil thicknesses, the impact of transpiration on MAI is assumed to increase exponentially with increasing soil thickness, with the form

$$MAI = MAI_{bs} \exp(-\eta b), \tag{2-16}$$

where MAI_{bs} is the bare-soil MAI [L/T], η is the extinction coefficient [1/L], and b is the minimum between soil thickness and maximum rooting depth [L]. Shrubs under current climatic conditions would typically have a rooting zone of about a meter, according to David Groeneveld. Under wetter climates and larger vegetation, the rooting zone may be deeper but the extinction coefficient smaller. Takeover of bromus would provide a shallower rooting depth (roughly 30 cm), but the extinction coefficient might not change. Both David Groeneveld and Dani Or concur that the correction procedure is reasonable and plausible.

The uptake efficiency factor should be qualitatively correct. Plants tend to have exponentially decreasing biomass with depth (except in the top of the soil column), suggesting that uptake may fall off exponentially with depth. There is some error associated with not accounting for roots in the fractures below the soil zone, which we have observed in the field. The exact values used for the lower rooting-zone thickness and the percentage of MAI allowed through the plant uptake are most important in deep soils, not in the shallow soils over the repository (except in the caprock region). Quantifying the reduction factor more precisely will require implementing transpiration into *breath* and performing a series of simulations.

11/10/98 Activities related to infiltration maps.

SAS

Putting together the MAI map has brought forth several observations. The most important observation is in regard to neglecting transpiration, with proposed treatment discussed above. Additional observations are discussed below.

Under current soil textures, the fracture classifications providing the most infiltration are, in order from largest to smallest, soil-filled, carbonate-filled, and unfilled. Even a small percentage of the fractures with soil filling yields greater values of MAI than a much greater percentage filled with relatively high-permeability carbonate, and with only a few centimeters of cover fillings yield larger MAI than provided by unfilled fractures. Note that the soil-filled fracture simulations are insensitive to fracture pore space even down to 10^{-4}, and unfilled fractures are minimally sensitive until fracture pore space gets below 10^{-3}. I suspect that adjacent soil-filled and carbonate-filled fractures in the field may be dominated by the capillarity in the carbonate fillings, so that carbonate-dominated areas may see little influence from a few soil-filled fractures. The capillarity in fracture

fillings may be somewhat independent of unfilled fractures, as unfilled fractures are only active under infrequent, short, extremely wet conditions.

In order to accommodate these observations in the MAI map, soil-filled fractures are assumed not to exist except in caprock-like units and nonlithophysal units. Carbonates are assumed to dominate welded units and are present at low values in the non- to moderately welded units, except for caprock (with large soil-filled fractures). Unfilled fractures are assumed not present in caprock, minimally present in welded units, and dominant in less-welded units. Note that in less-welded units, MAI for bedrock may be larger than MAI for fractures. Also note that, thankfully, the lack of sensitivity to fracture pore space makes precise allocation of fracture pore space unimportant (except for the presence/absence of soil-filled fractures).

The bedrock is not known under regions mapped as alluvium or colluvium. Such areas are arbitrarily assigned bedrock properties (including fracture properties) of the lithophysal units, as such units are typically below colluvium. Note that it makes no difference what is assigned with deep soils.

The nominal map of MAI, using best estimates for bedrock and fracture properties, is somewhat different from maps I've produced earlier and from maps produced by United States Geological Survey (USGS). Without the vegetation adjustment, the trends in the map are similar to other efforts for shallow soils, with highest rates on the caprock. However, MAI is quite large in deep soils (as much as 80 mm/yr). With the vegetation adjustment, the deep-soil MAI drops to small values as before. There is a significant drop in MAI in the caprock with vegetation, while there is little change on sideslopes or ridges, so that the ridges are predicted to provide relatively large MAI. There is also a prominant pair of high-MAI stripes on the west flank of YM, due to nonlithophysal-unit outcrops, and additional nonlithophysal hotspot areas increasing to the south of the footprint.

Each pixel can be classified according to what feature provides the largest MAI (i.e., deep soil, bedrock, unfilled fracture, carbonate-filled fracture, or soil-filled fracture). Very few areas have unfilled-fracture dominance. Bedrock dominance is generally along channels or on the west flank of YM. Soil-filled fractures dominate in almost all areas where they exist (caprock, nonlithophysal units), while carbonate-filled fractures dominate in the welded units.

The nominal map is based on a refined elevation digital elevation model (DEM), obtained by using a cubic interpolant (interp2 in *Matlab*) on the original grid with cells 30 m on a side. A reduced area is considered, 2 km by 5 km, centered on the main repository block. Each cell is refined into 16 cells, 7.5 m on a side. The soil thickness is calculated directly on the refined grid,

with a much smoother representation. The ephemeral channels are far better captured, although grid cells on the order of 0.5 m on a side would be required to fully resolve the channels (perhaps for Split Wash).

1/12/99 Final version of caprock paper.

The following document is identical in content to a document resubmitted to the Journal of Hydrology. The original document was submitted in March, 1998; two reviewers for the journal provided reviews that raised questions and requested clarification. The reviewer comments were addressed in this document. The document was reformatted to place figures and tables into the scientific notebook numbering scheme, in appropriate locations; no text was otherwise altered. Also, note that the references show up in the reference list at the end of the project section.

THE EFFECT OF VEGETATION ON INFILTRATION IN SHALLOW SOILS UNDERLAIN BY FISSURED BEDROCK

Stuart A. Stothoff, Stothoff Environmental Modeling, Houston, TX 77006, USA[1]
Dani Or, Department of Plants, Soils, and Biometeorology, Utah State University, Logan, UT 84322-4820, USA[2]
David P. Groeneveld, Resource Management, Inc., Telluride, CO 81435, USA[3]
Scott B. Jones, Department of Plants, Soils, and Biometeorology, Utah State University, Logan, UT 84322-4820, USA[4]

ACKNOWLEDGEMENTS

This paper was prepared to document work performed by the Center for Nuclear Waste Regulatory Analyses (CNWRA) for the Nuclear Regulatory Commission (NRC) under Contract No. NRC-02-93-005. The activities reported here were performed on behalf of the NRC Office of Nuclear Material Safety and Safeguards, Division of Waste Management. The paper is an independent product of the CNWRA and does not necessarily reflect the views or regulatory position of the NRC. The authors would like to acknowledge the suggestions and comments made by G. Wittmeyer, B. Sagar, D. Woolhiser, and two anonymous reviewers, which tremendously improved the quality of the paper.

CNWRA-generated data contained in this document have been documented according to quality assurance requirements described in the CNWRA Quality Assurance Manual. Sources for other data should be consulted for determining the level of quality for those data. Neither the HYDRUS-2D simulator nor the root-growth simulator is configured under the CNWRA's Software Configuration Procedure. At present, the CNWRA does not anticipate the use of either of these codes for regulatory reviews.

3/6/99 Documentation for shallow-soil MAI abstractions.

In the process of reviewing a paper on shallow-soil abstractions for MAI, R. Fedors requested that I provide

- The spreadsheet for estimating coefficients
- *breath* input files for a fracture fill and infinite-soil column to be able to verify some points
- *breath* input and output files for unfilled fractures
- Post-processing scripts

In response, I am collecting all of the results into a documentation CD-ROM, including relevant papers, notebook entries, etc. The CD-ROM will be placed in QA storage.

3/30/99 Error in shallow-soil MAI abstractions.

As I was testing a *Matlab* simulator that will be used to calculate MAI in the presence of plants, I discovered a flaw in my assignment of fracture properties. I had realized that the porosity of the

fracture fillings needed to be multiplied by the fraction of the cross-sectional area occupied by the fractures. I had not realized that the permeability of the fracture fillings also needs to be adjusted. This misconception should not affect the regression analysis at all, except perhaps the capillary-barrier regression has less of a range in permeability than I originally thought. The capillary-barrier regression should not be materially affected in the unfilled-fracture parameter subspace.

The primary impact of the misconception is on estimates of MAI, driving down the estimates. It appears that there may be relatively little impact under present-day climate and soil, but under future soils MAI in a soil-fracture system may be drastically smaller. With the revised concept, MAI is much more sensitive to the fracture cross-sectional area.

With the corrected method of estimating fracture permeability, I recalculated the areal-average MAI over the repository. Otherwise using the same assumptions as was used for the AGU poster last fall, revised repository-average MAI was 8.8, 80, and 29 mm/yr for current, early glacial, and late glacial conditions. The corresponding values of MAI were 15, 106, and 45 mm/yr before.

Earlier, I had to artificially put the fraction of fractures containing soil to zero in some units because MAI in these units was dominated by the small soil-filled fraction. Revising these units to have a small soil-filled fraction had little effect. Only three categories showed appreciable control: unfilled, deep-soil, and bedrock (soil-filled and carbonate-filled fractures had minimal to no incidences of control).

Re-examining the fracture descriptions used by USGS, my feeling is that the caprock and TCmnl units have under-represented fracture area. I suspect that the fractures used by USGS may not represent fractures in outcrops and shallowly covered cases. For example, I think the caprock should have a description with something like 5 to 15 percent fissure area, while the USGS has a description with 9.2 fractures per meter, averaging 250 μm (or 0.23 percent). Similarly, the fracture area of the middle nonlithophysal turns out to be about 0.026 percent; at the surface I think this should be about two orders of magnitude greater. Increasing these units into a more representative area only minimally increases MAI (from 8.8 to 9.1 mm/yr) but results in 1/4 of the repository area having fracture control.

9/21/99 Newly obtained meteorologic information.

In order to relate vegetation, soils, climate, and infiltration, several sets of data have been acquired. This entry documents the data and some of the analyses.

The National Weather Service maintains a set of weather stations across the United States. At least two levels of station are maintained. Stations with the widest distribution are called COOP (Cooperative) stations; these typically record daily summary values. The available summary values of primary interest include precipitation, snowfall, snow depth, minimum air temperature, and maximum air temperature. These records are available from the National Climatic Data Center (NCDC) on CD-ROM, in the form of (i) state-wide series for station establishment through 1993, (ii) all stations for 1994 through 1996, and (iii) all stations for 1997. In addition to the 1994-1996 and 1997 CD-ROMs, three pre-1994 state CD-ROMS were acquired this month

- California
- Arizona and Nevada
- Utah and New Mexico

These CD-ROMs include a station history file and a station observation file for each state. There is also an NCDC online file that describes the location of each of the COOP stations, including latitude, longitude, and elevation. Some of the stations were moved during the period of service. The time-averaged location was used for these stations. Several of the elevations reported in the CD-ROM data were missing, clearly incorrect, or misread, so a processing check was performed to replace the CD-ROM information with the online file when the two elevations disagreed by more than 30 m.

Some of the COOP stations, with WBAN numbers, also maintain a higher measurement degree. These stations record additional variables, such as wind speed, cloud cover, and dew point. In addition, the records are available at more frequent intervals, at least hourly and sometimes more frequently. Unfortunately, there are relatively few WBAN stations in the region of interest. The daily summaries for these stations are available from the NOAA web site. All WBAN stations are also COOP stations, but the WBAN daily summaries also report additional information beyond the COOP information such as atmospheric pressure and percent of solar radiation. Data from a total of 18 stations were acquired (15 in NV, 1 in CA, 2 in UT), of which 2 have unusably short records. Of the usable stations, 10 include atmospheric pressure and 5 include percent of solar radiation.

An hourly record of solar radiation is available for a 30-yr period (1961 through 1990) from the Solar and Meteorological Surface Observation Network (SAMSON). All observations in the US are available on a 3-CD-ROM set from the NCDC. Observed data include several different forms of solar radiation, temperature, relative humidity, wind speed and direction, atmospheric pressure,

and precipitation (although not all of these are necessarily available at each station). The CD-ROM with the western states was acquired. There are 8 stations that should be useful: Tonopah, Ely, McCarren, Reno, Elko, Winnemucca, Barstow, CA, and Cedar City, UT. Several other stations exist in Arizona, Utah, and Idaho that might be useful, although these are fairly far from YM.

Data is also available for download from the DOE Technical Library web site. Several sets of met stations are maintained by DOE and USGS. The DOE has nine stations, while USGS has at least five stations (five are in the DOE online database) plus a network of non-recording gauges. Summary information on precipitation, temperature, relative humidity, and solar flux was obtained for the period 1986 through 1997 for the nine DOE stations, as well as hourly precipitation records for each of the stations for parts of the period (1993, half of 1994, 3/4 of 1995, half of 1996, and 1997). The obtained files are all labeled starting with *MS*, for monitoring station, with the names also including station IDs, range of dates, and met data (precipitation is implied). The hourly readings for temperature, relative humidity, solar flux, and atmospheric pressure (among others) are also available for download covering the same period of time. but it would take roughly a day to download all of this information. Probably the best thing to do is to request a data packet from DOE if the information is required, since the missing records may be available as well as the records for 1986 through 1992.

Hourly readings of relative humidity, temperature, solar flux, and windspeed were obtained for the five USGS stations over the period 10/1/94 through 10/1/95. Each variable is downloaded in 18 files; these were concatenated, extraneous header and tail information were removed, and the resulting files collected in an Excel spreadsheet.

The network of nonrecording gauges available online includes the periods 1/1/90-9/30/91, 10/1/93-9/30/94, and 11/1/94-9/30/95. Various other area nonrecording gauges are available online for the periods 2/84-9/85 and 3/89-9/90. These data were collected at intervals (*e.g.*, weekly, monthly); some intervals may be several months. These five sequences were obtained; as with the DOE stations, it may be best to request them directly in order to obtain a complete sequence of data.

Precipitation data were also obtained for 17 Nevada Test Site locations covering the period 10/1/82 through 9/27/85. These data appear to be part of a longer sequence that would be useful to obtain. Longer sequences from these stations form part of the basis for some of the infiltration modeling work performed by the USGS.

Daily data from four weather stations maintained by the USGS (McKinley and Oliver, 1994; McKinley and Oliver, 1995) in the 3 Springs area were obtained. These stations are used to provide

estimates of recharge at future-climate analog sites (Lichty and McKinley, 1995). The data include precipitation, soil and air temperature, relative humidity, and solar flux. Some of the records in the html download file were obviously mislabeled (inconsistent location name, inconsistent month or year); these records were corrected and the data were extracted from the download file and collated into a *Matlab* binary file.

9/22/99 Analysis of mean climatic parameters.

Analysis of climatic parameters is motivated by two functions: (i) distribution of conditions affecting MAI to individual pixels, so that areal-average estimates can be obtained; and (ii) distribution of conditions affecting vegetation to analog sites, so that vegetative species and density can be estimated for given climatic conditions.

The primary variables influencing net infiltration are precipitation (water source) and temperature (evapotranspiration). Evapotranspiration also depends on atmospheric vapor density, windspeed, and both shortwave and longwave radiation. Vegetation density depends on all of these variables as well, although precipitation, temperature, and shortwave radiation should be the primary climatic indicators for vegetative species mix and density. Shortwave radiation should be well predicted if latitude and ground slope are known, as long as some indication of cloudiness patterns can be determined. Unless there are strong regional or elevational trends in cloudiness that can be explicitly accounted for, it should be sufficient to use estimates of radiation assuming clear-sky conditions when predicting vegetation quantities.

Numerical simulation of a water balance using *breath* requires precipitation, air temperature, atmospheric vapor density, wind speed, shortwave radiation, and longwave radiation. Future modifications to *breath* may also require atmospheric pressure. When using numerical simulation to predict MAI, experience has shown that it is adequate to use hourly variation for the days immediately preceeding, during, and immediately after precipitation, and monthly variation outside this window. The importance of the window is because potential evapotranspiration is reduced on these days, due to increased relative humidity, decreased solar radiation, and cooler temperatures. The reduced evapotranspiration enables deeper penetration of wetting fronts during the window than would otherwise have occurred, thereby increasing the fraction of water reaching below the ET trap.

Based on all of these considerations, the primary variables of interest for analysis are MAP and MAT. The approach followed by Hevesi et al. (1992) was to cokrige MAP and elevation,

using stations in the area of YM. As an alternative, I choose to use a much wider range of data locations, use a regional interpolation, and only then see how well the YM information fits into the regional picture. An advantage of this approach is that regional information is available for much longer time periods than local information and is better distributed spatially. The local information provides a reality check and information on local variability.

The COOP data is the workhorse data set for precipitation and temperature, as there are hundreds of stations in Nevada and surrounding states. For the analyses, data from all stations in NV, AZ, UT, and CA with actual observations attached to stations in the station history file were extracted from the CD-ROMs in a standard format. Some stations were listed in the station history but had no observations, while some observations in the data file referenced nonexistent COOPS (usually only a month per station). A procedure was adopted that compensates for missing values and mismatched record lengths. An array of 366 julian days was created for each variable type (*e.g.*, precipitation, temperature). Each data observation was added to the data array and a counter for the corresponding day was incremented. The mean value for the day is obtained by dividing the sum of values by the number of observations. The annual value is obtained by the average of the mean array (the 366th day is weighted by 0.25 in the average, since it only occurs once every four years). Maximum and minimum values for each day as well as frequencies of nonzero occurrence were also accumulated. Extraction from the CD-ROMs was performed for every AZ, CA, NV, and UT station. The complete extraction took several hours.

After complete extraction, a reduced set of stations was extracted from the complete set. The reduced extraction includes all NV stations, all UT stations west of longitude 113, all AZ stations west of longitude 113 and north of latitude 35, and all CA stations east of longitude 118.2 and north of latitude 34.5 (north of the San Gabriel mountains and east of the crest of the southern Sierra Nevadas). All stations in Inyo and Mono counties were also explicitly included. The boundaries were selected to include stations in more-or-less the same climatic regime with at least a 2-degree buffer on every side of YM. The Sierra Nevada and San Gabriel ranges make natural boundaries, while the northern and eastern boundaries are more diffuse.

Note that it may be advantageous to also extract statistics by precipitation categories, such as precipitation bins, day before, day after, and interstorm. This information could provide information useful for generating storm and meteorological sequences. It would probably be necessary to lump numerous stations to generate robust parameters, although it is not obvious whether statistics should also be stratified by elevation. Extraction of these parameters would likely take several hours, although only a fraction of the stations originally extracted should be examined. Some of this work would fit nicely with the work that David Woolhiser is doing.

Most of the variables of interest don't require a tremendously long period of observation to be reasonably well estimated. Seasonally, atmospheric variables tend to be quite repetitive from year to year. On the other hand, precipitation is highly variable from year to year and annual averages require decades of observations to estimate reliably in the semiarid Mojave and Great Basin. Thus, stations with shorter records can be used for analyses of atmospheric variables than for precipitation. In the following analyses, the effect of record length is examined. Generally speaking, inclusion of all stations with record lengths at least 10 yr is adequate to estimate regression parameters, although the less-sensitive parameters may vary in their significance as the minimum record lengths change. The record length in years is defined as the number of observations divided by 365.25.

The pieces of information attached to each station that can be used for regression include latitude, longitude, and elevation. In the region of interest, annual-average clear-sky shortwave radiation is almost linear with latitude, so that a significant regression with one will provide a significant regression with the other (say for temperature). Temperature also generally varies linearly with elevation in the atmosphere, so there should be a good regression between temperature and elevation. There are orographic effects that tend to increase precipitation with elevation, while particularly in summer rain can evaporate while falling (decreasing precipitation with lowering of elevation). Therefore elevation should play a role in precipitation, but may be more important during the summer. Also, it is generally accepted that the Sierra Nevada range provides a rain shadow that lessens from west to east, perhaps providing a longitudinal impact. A quick inspection shows an exponential increase in MAP with elevation, suggesting that the logarithm of MAP is more appropriate than MAP directly (consistent with the results of Hevesi et al. (1992)).

Several observations are quickly apparent in the data. The maximum-temperature data can be quite well predicted using elevation and latitude/shortwave radiation. The minimum-temperature data is less well predicted using these factors, and there does not appear to be a strong regional effect in the error. Thus, local effects are probably significant in minimum temperature. Minimum temperature can be impacted by drainage of dense, cold air downslope from local hills or mountains; additional work is required to examine this type of effect. A quick feel might be obtained by overlaying the prediction errors on a topo map or DEM. I've downloaded the set of USGS 1-250,000 scale DEMs for most of the area of interest (some of the CA areas are missing), and Center for Nuclear Waste Regulatory Analyses (CNWRA) has the USGS topo maps at the same scale.

Local maximum slope or local curvature might be a likely predictor for additional regression analysis, reasoning that slope is required for drainage but a bowl may be necessary to capture the

air. Actually a valley bottom would be good too. Using a DEM, the predictors should be the maximum of the 4 local slopes and the maximum of the 4 local curvatures (N-S, E-W, NW-SE, NE-SW). Perhaps the maximum of the 8 local slopes should be checked too.

The log-precipitation data is also most strongly dependent on elevation, with some regional effect showing up as slight dependence on latitude and longitude. There is quite a bit of scatter around the regressions. Spatial plots of error over the region suggest that there are regional effects that are not linearly dependent on latitude and longitude.

A systematic set of regressions were performed for MAP, MAT, mean annual maximum temperature, mean annual minimum temperature, mean winter precipitation (julian days 281 through 170), and mean summer precipitation (julian days 171 through 280). For each regression, each multiple of elevation, latitude, longitude (Z, Lt, Lg, ZLt, ZLg, $LtLg$, and $ZLtLg$) was considered a predictor. All possible combinations of predictors were examined (individual, pairwise, triplets, etc.). Statistics are reported for each combination.

9/27/99 Results of analysis.

SAS

The COOP data were run through a regression analysis to determine predictive relationships as a function of spatial location (*e.g.*, latitude, longitude, elevation). Solar radiation is also important in an energy balance, so potential solar radiation was used as a base variable as well. Potential solar radiation is almost linear with latitude in the area of interest. All four base variables were normalized to keep coefficients of the same order of magnitude. Elevation was converted to kilometers, with normalization between 34 and 42 degrees for latitude, 113 and 120 degrees for longitude, and 280 and 310 W/cm^2 for solar radiation. *Correction dated 9/29/99: This was corrected to units of J/cm^2/dy by multiplying by 3600/365.25, or normalization from 2750 to 3050 J/cm^2/dy.* SAS
The regression analysis was performed with a routine written in *Matlab* called analyze_fit_set.

In the analysis, regression variables were created from all possible multiplicative combinations of 1, 2, or 3 base variables (a total of 34 combined variables). For example, elevation (Z) is presented as Z, Z^2, and Z^3 as well as with all other combinations of the remaining 3 base variables. A regression was performed using one combined variable at a time to determine the best single-variable predictor. The analysis was repeated with each combination of combined-variable pairs to find the best predictor pair. Higher-order sets were also searched until the point of diminishing returns was reached. Note that computational burdens became significant if more than triplets were considered (more than 5×10^4 analyses for quads and more than 3×10^5 analyses for quintuplets).

Each of the COOP stations have different record lengths. It is desirable to include as many stations as possible, while restricting the stations to ones with valid record lengths. Using the R^2 criterion as a basis, experimentation suggests that temperature predictions improve with number of stations (more extreme elevations), while precipitation predictions improve with length of record (thereby using only stations with appropriate means). Balancing of these factors appears to be reasonably achieved by using stations with record lengths of greater than 20, 5, and 40 yr for precipitation, temperature, and snow precipitation, respectively. The complete set of best predictions for each number of predictor variables is shown in Table 2-17 (for precipitation), Table 2-18 (for winter and summer precipitation), and Table 2-19 (for temperature). Corresponding scatterplots of observed versus predicted values are shown in Figures 2-14 through 2-15.

For temperature and snow precipitation, improvement is minimal if more than pair-wise combinations are considered. For precipitation, there is still improvement from 5- to 6-way combinations. Interestingly, the mean annual values for precipitation are better predicted than either summer or winter precipitation, although winter prediction is significantly better than summer prediction. The slow but steady improvement as additional predictor variable are added suggested that another type of interpolation might provide better results. A set of radial basis functions were added to the base variables, replacing all of the combination variables. The basis function locations were selected to provide a regular grid in normalized latitude/longitude coordinates. Both radial [$r = (Nt^2 + Ng^2)^{1/2}$] and inverse-radial ($1/r$) bases were used, with radial bases appearing to provide slightly better results. Limiting the MAP prediction to 6 predictors in the original scheme provides a best R^2 of 0.793. Using 9 predictors in the inverse-radial scheme for a grid on the one-third markers (*i.e.*, 0, 1/3, 2/3, and 1) in both directions provides a best R^2 of 0.782 (0.763 for 6 predictors). Using 7 predictors in the radial scheme with the same grid provides a best R^2 of 0.802 (0.796 for 6 predictors). The radial scheme is nominally superior to the original scheme, and is considerably less computationally demanding to exhaustively examine than the original scheme, due to the fewer possible variables. In the numbering scheme, grid locations are called poles and are numbered consecutively from left to right, moving from the bottom left corner to the top right corner. The best 7-predictor radial scheme has a minimum and maximum ratios of observed to predicted MAP of 0.64 and 1.69, respectively. Despite the nominal improvement, the original formulation is easier to implement and less arbitrary in selection of pole locations. There is still at least one predictor variable missing from the formulation, based on the remaining scatter.

The precipitation and temperature values for the nine DOE met stations in the YM area over the period 1986 through 1997 are shown as crosses in the scatterplots. The data for these nine stations are shown as a function of elevation in Figure 2-16. These values were not used in the regressions. The met station values for precipitation are well within the scatter of predicted-versus-

Table 2-17: Best estimated fits to mean annual COOP precipitation meteorological data. All fits are to the base-10 logarithm of the data.

SSE	R^2	$\min(V_{obs} - V_{reg})$	$\max(V_{obs} - V_{reg})$	Variables
MAP: 171 stations with at least 20 yr record				
1.2	0.515	-0.329	0.333	Z
0.856	0.631	-0.279	0.343	Z NtNgSw
0.669	0.700	-0.282	0.316	Z NgSw SwSwSw
0.552	0.744	-0.234	0.266	Z NgSw NgNgSw SwSwSw
0.490	0.759	-0.219	0.269	Nt ZSw NgSw ZNtNt NgNgSw
0.420	0.793	-0.220	0.275	Z SwSw NtNtNg NtNgNg NgNgNg NgSwSw
MAP: Inverse-radial basis functions (choice of 16 poles)				
1.2	0.515	-0.329	0.333	Z
0.847	0.639	-0.259	0.286	Z P7
0.652	0.715	-0.265	0.233	Z P1 P7
0.558	0.739	-0.242	0.210	Z P1 P7 P11
0.494	0.754	-0.228	0.229	Z P1 P7 P9 P11
0.449	0.763	-0.237	0.224	Z Ng P1 P7 P9 P11
0.412	0.772	-0.249	0.236	Z Ng P1 P6 P7 P9 P11
0.383	0.779	-0.253	0.239	Z Ng P1 P6 P7 P9 P11 P12
0.360	0.782	-0.257	0.234	Z Ng P1 P6 P7 P9 P10 P11 P12
MAP: Radial basis functions (choice of 16 poles)				
1.2	0.515	-0.329	0.333	Z
0.814	0.667	-0.315	0.266	Z P7
0.631	0.733	-0.279	0.237	Z Nt P7
0.529	0.765	-0.214	0.234	Z P5 P7 P9
0.468	0.780	-0.207	0.251	Z P7 P13 P14 P16
0.417	0.796	-0.186	0.227	Z P4 P5 P7 P9 P14
0.384	0.802	-0.195	0.228	Z Ng P5 P7 P9 P14 P16
0.355	0.810	-0.196	0.212	Z Ng Sw P1 P5 P7 P15 P16
0.330	0.818	-0.200	0.231	Z Nt Sw P7 P9 P11 P12 P14 P15

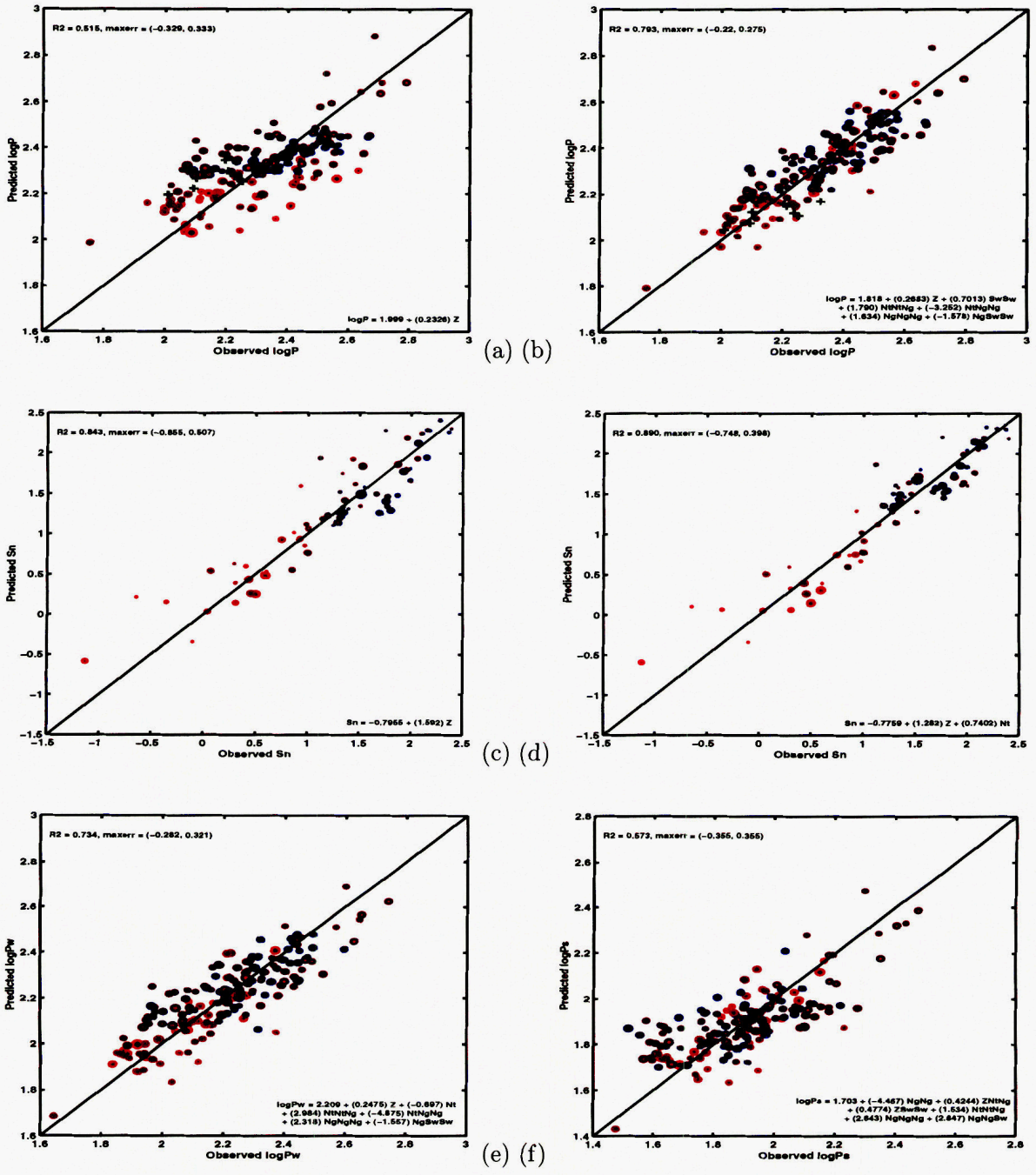

Figure 2-14: 9/27/99. Scatterplot of observed versus predicted mean annual log-10 precipitation, (a) 1 and (b) 6 predictors; log-10 snowfall, (c) 1 and (d) 2 predictors; and (e) winter (day 281 through 170) and (f) summer (day 171 through 280) precipitation, 6 predictors. Crosses represent DOE met stations in the YM area. Area of circles are proportional to length of record. Circle color changes from red to blue on west to east. Circle fill changes from red to blue on south to north.

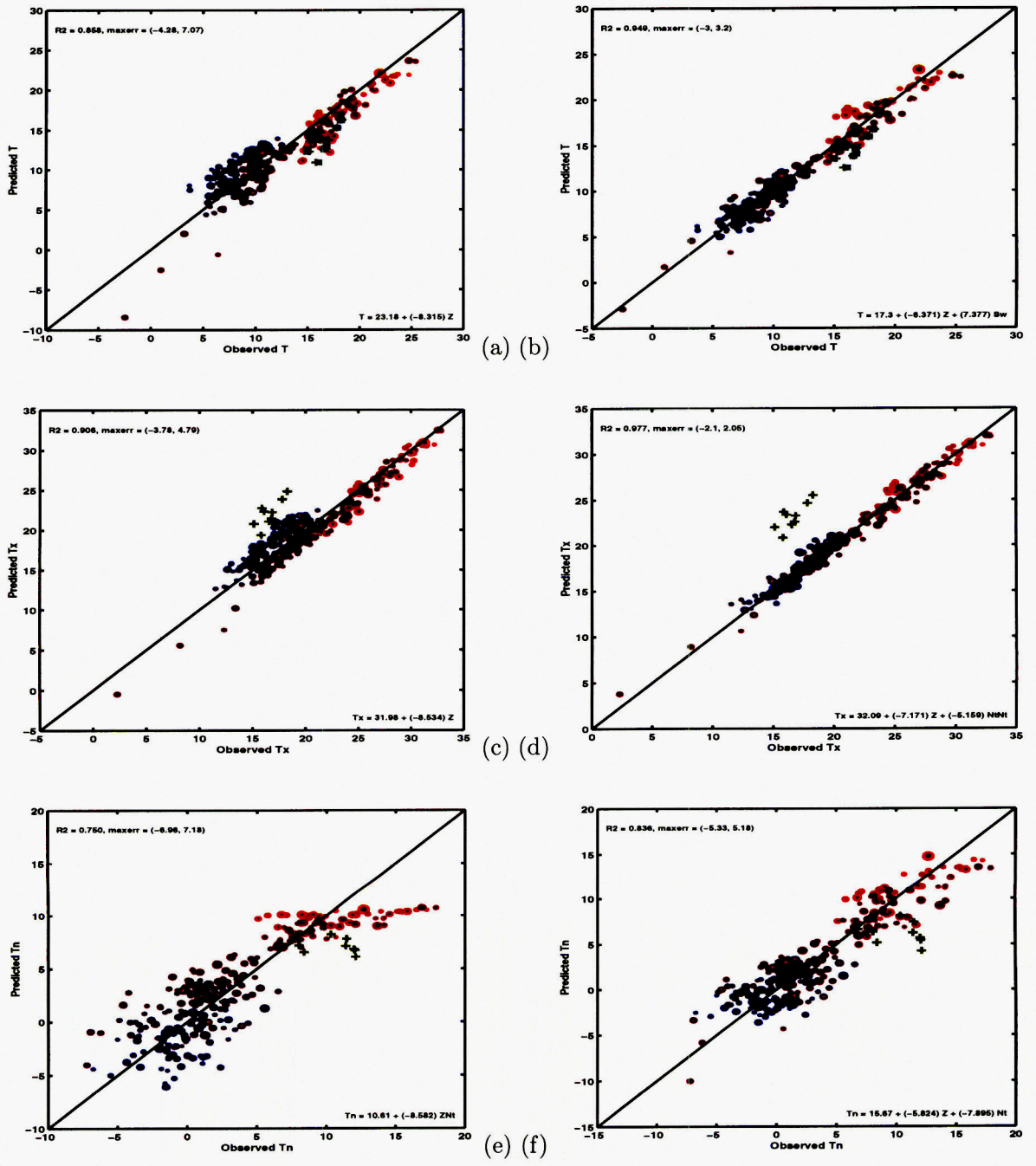

Figure 2-15: 9/27/99. Scatterplot of observed versus predicted mean annual temperature, (a) 1 and (b) 2 predictors; maximum temperature, (c) 1 and (d) 2 predictors; and minimum temperature, (e) 1 and (f) 2 predictors. Crosses represent DOE met stations in the YM area. Area of circles are proportional to length of record. Circle color changes from red to blue on west to east. Circle fill changes from red to blue on south to north.

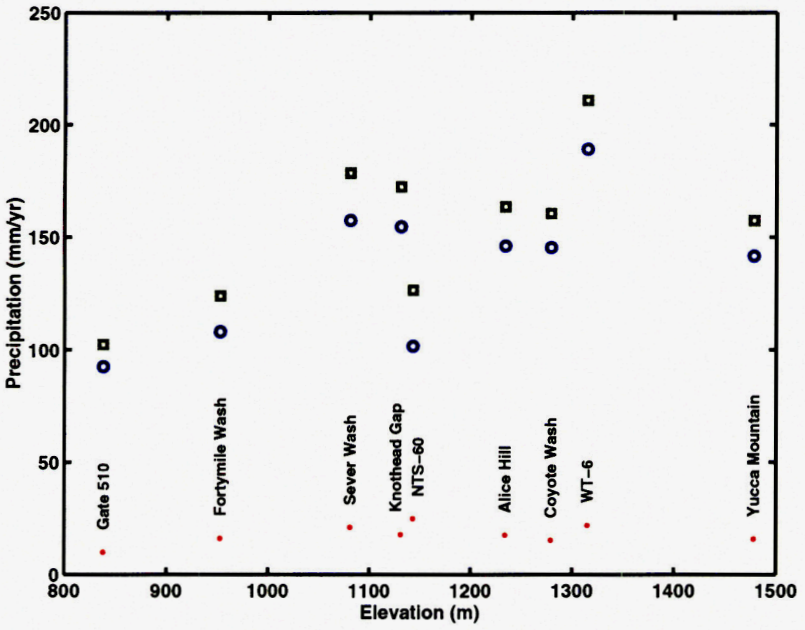

(a)

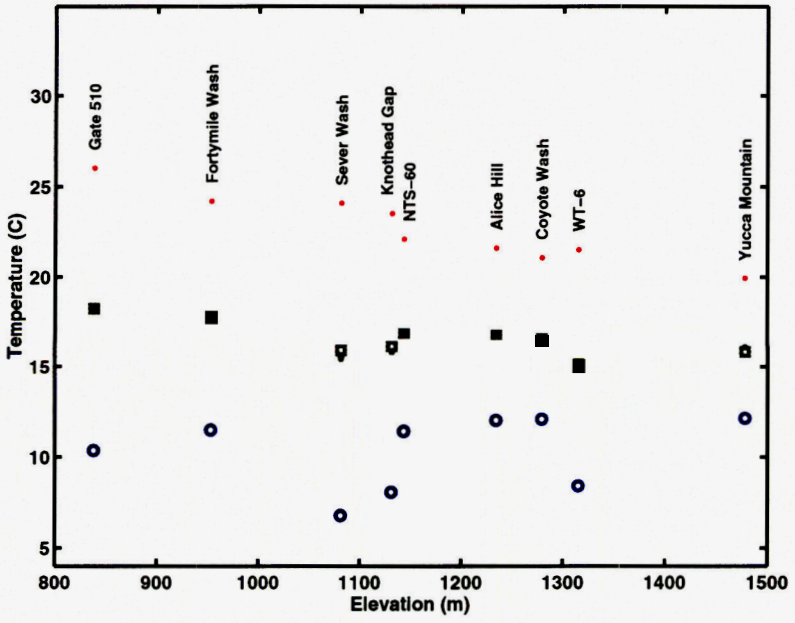

(b)

Figure 2-16: 9/27/99. Scatterplot of observed (a) mean summer (dot), winter (circle), and annual (square) precipitation; and (b) mean annual maximum (dot), minimum (circle), and average (square) temperature at DOE meteorologic stations. Crosses represent average of minimum and maximum temperatures.

Table 2-18: Best estimated fits to mean annual COOP precipitation (summer and winter) meteorological data, as well as snowfall depth. All fits are to the base-10 logarithm of the data.

SSE	R^2	$\min(V_{obs}-V_{reg})$	$\max(V_{obs}-V_{reg})$	Variables
Summer MAP: 171 stations with at least 20 yr record				
1.48	0.313	-0.347	0.388	ZZ
1.10	0.427	-0.328	0.405	Z NtNtSw
0.935	0.450	-0.335	0.380	ZSw SwSw ZNtNt
0.804	0.492	-0.329	0.339	Z NgNg NtNtSw
0.716	0.517	-0.388	0.373	ZSw NgNg NtNtNg NgNgNg NgNgSw
0.623	0.573	-0.355	0.355	NgNg ZNtNg ZSwSw NtNtNg NgNgNg NgNgSw
Winter MAP: 171 stations with at least 20 yr record				
1.25	0.520	-0.342	0.285	Z
0.938	0.596	-0.297	0.315	Z NtSw
0.786	0.622	-0.322	0.286	Z NtNgSw NgNgNg
0.667	0.660	-0.291	0.256	Z NtSw NgNg NgNgNg
0.584	0.686	-0.310	0.281	ZSw NgNg NtNtNg NgNgNg NgNgSw
0.498	0.734	-0.282	0.321	Z Nt NtNtNg NtNgNg NgNgNg NgSwSw
Snowfall: 73 stations with at least 40 yr record				
1.76	0.843	-0.855	0.507	Z
1.2	0.890	-0.748	0.398	Z Nt

observed points. The values for MAT are warmer than the regression equation by a few degrees Celsius, but are generally within the scatter of predicted-versus-observed points. Regionally, MAT decreases by about 6.37 °C with every kilometer of elevation, while the 9 DOE met stations have a shallower decrease of 4 to 5.5 °C/km. The regional decrease is shallower than the two-point Desert Rock/Kawitch slope (8.3 °C/km) I used in distributing MAT on DEMs for predictions of MAI, and the local YM decrease is shallower still. Predictions of MAI should be re-evaluated with the corrected values.

Interestingly, both the annual-average maximum and minimum temperature values are outside the scatter of coop points, especially the maximum temperature points. The maximum temperature points are significantly warmer than the regression while the minimum temperature points are significantly cooler than the regression, yet the difference between maximum and minimum temperature tends to be less than typical for coop stations by roughly 4 °C. The difference between

Table 2-19: Best estimated fits to mean annual COOP temperature data.

SSE	R^2	$\min(V_{obs} - V_{reg})$	$\max(V_{obs} - V_{reg})$	Variables
MAT: 262 stations with at least 5 yr record				
21.5	0.858	-4.28	7.07	Z
10.5	0.949	-3.00	3.2	Z Sw
T_{max}: 262 stations with at least 5 yr record				
17.4	0.906	-3.78	4.79	Z
7	0.977	-2.10	2.05	Z NtNt
T_{min}: 262 stations with at least 5 yr record				
30.2	0.75	-6.96	7.18	ZNt
19.9	0.836	-5.33	5.18	Z Nt
$T_{max} - T_{min}$: 262 stations with at least 5 yr record				
26.3	0.064	-6.26	5.23	ZZZ
20.7	0.132	-6.12	5.09	ZZZ NtNtSw

maximum and minimum temperature decreases with increasing elevation. These effects seem to be due to local effects. Maximum readings at and near the YM crest may be representative of warmer low-elevation air advected during the windy daylight hours. At night there appears to be drainage of cool air downslope and warm air upslope; minimum temperatures appear to increase with elevation, aside from 3 stations at the base of drainages that have anomalously cool minimum temperatures. I think that the relatively poorer prediction of regional mean annual minimum temperature is probably due to similar local drainage patterns. This conclusion is supported by the lack of regional trends in mean annual temperature difference in the coop dataset.

9/29/99 More results of analysis.

SAS

An error was made in the discussion and analysis regarding the units for shortwave radiation. In the original analyses, shortwave radiation was calculated without multiplying by the number of seconds in an hour, affecting the normalizing values for shortwave radiation. The shortwave radiation values were changed to mean daily shortwave radiation [J/cm^2] rather than annual radiation, so that the normalizing values reported above should be multiplied by 3600/365.25. Also, the 366th day of the year was given unit weight rather than 1/4 weight (leap year only) in calculating annual radiation. The modification of the leap year calculation results in regression coefficients that are different from the coefficients in the figures by a small amount, but the conclusions shouldn't be changed at all.

Table 2-20: Annual meteorological summary data from USGS analog sites.

MAP		MAT (°C)				Soil T		RH		Daily Solar	
mm/yr	Yr	Ave	Max	Min	Yr	°C	Yr	%	Yr	J/cm^2	Yr
3 Springs Basin - Kawich Peak Near Warm Springs											
369.13	4.00	6.37	9.62	1.00	3.95	5.62	4.00	44.20	2.00	1888	1.81
3 Springs Basin - 3 Springs Creek Near Warm Springs											
314.99	7.00	8.12	13.59	0.43	6.79	10.70	6.97	42.73	1.60	1820	6.92
East Stewart Basin - Veg Spring Near Ione											
524.89	6.00	6.71	9.19	-0.84	3.24	3.54	4.00	46.89	1.96	1375	1.81
East Stewart Basin - East Stewart Creek Near Ione											
476.63	6.92	4.66	8.13	-1.42	6.40	5.79	6.75	45.20	1.00	1651	6.66

A quick comparison was made to estimate the predictive power of the previously used relationships between MAP, MAT, and elevation. The R^2 value for the Hevesi et al. (1992) formula used for the 171 stations with at least 20 yr of data is 0.299 (the best elevation-only fit I came up with is 0.515 for the same data). The R^2 value for the 262 stations with at least 5 yr of data is 0.599 using the formula based on Desert Rock and 3 Springs, while the new elevation-only figure is 0.858.

I extracted annual summaries for the variables reported by McKinley and Oliver (1994) and McKinley and Oliver (1995). The data were obtained from the DOE Technical Library web site. These annual summaries are reported in Table 2-20.

Note that there are some odd things going on between mean air temperature and mean soil temperature; the soil temperature is inconsistently between 2.6°C warmer and 3.2°C cooler.

9/30/99 More results of analysis.

The USGS has operated a set of high-elevation precipitation gauges in southern and eastern Nevada. The sites range from 7760 through 10650 ft in elevation. David Groeneveld was able to obtain observations from these sites. The observations were made by emptying the gauges twice a year, in October and in May. The record length is from 1984 through 1998 for some and 1986 through 1998 for the others. David reports problems with missing or apparently incorrect values for some of the sites; one of the 12 sites had sufficient holes in the data record that David eliminated it from consideration. Both David Groeneveld and David Woolhiser think that winter snow may be

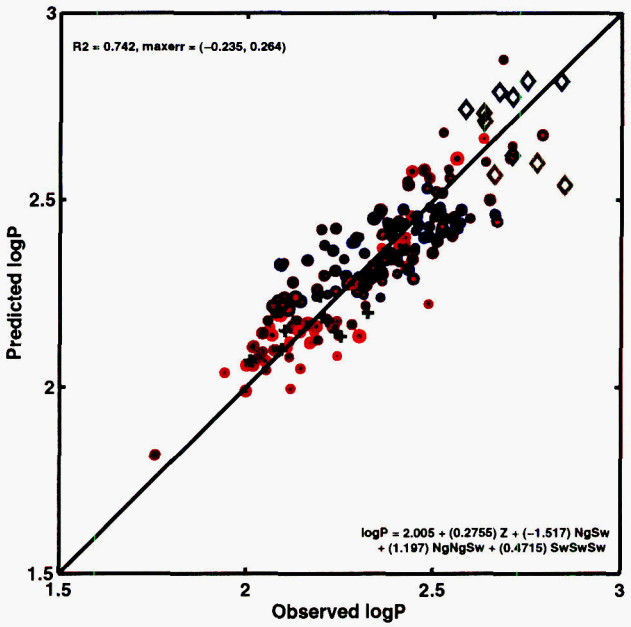

Figure 2-17: 9/30/99. Scatterplot of observed mean annual precipitation versus predicted. Crosses represent DOE met stations at YM. Dark cyan diamonds represent eastern NV stations and olive diamonds represent southern NV stations. Circles represent coop stations (only these were used for regression). Circle size is proportional to station record length. Circle color moves from red to blue as stations are located east to west. Circle fill moves from red to blue as stations are located south to north.

under-represented in the data set. David patched holes in the remaining records through regression techniques. This patching is documented in David's scientific notebook.

I plotted the high-elevation data on top of the scatterplots for the coop station regressions for comparison, in Figure 2-17 (for MAP) and Figure 2-18 (for summer and winter precipitation). The regressions use fewer predictors than the best-fit cases, but the fits are nearly as good and much faster to recreate.

The fit for MAP is quite good, and both the regression and the high-elevation data appear to be from the same population. Note that the coop points have at least 20 yr of observations, while the high-elevation points have at best 16 yr of observations.

The winter/summer data periods are somewhat different for the coop stations and for the

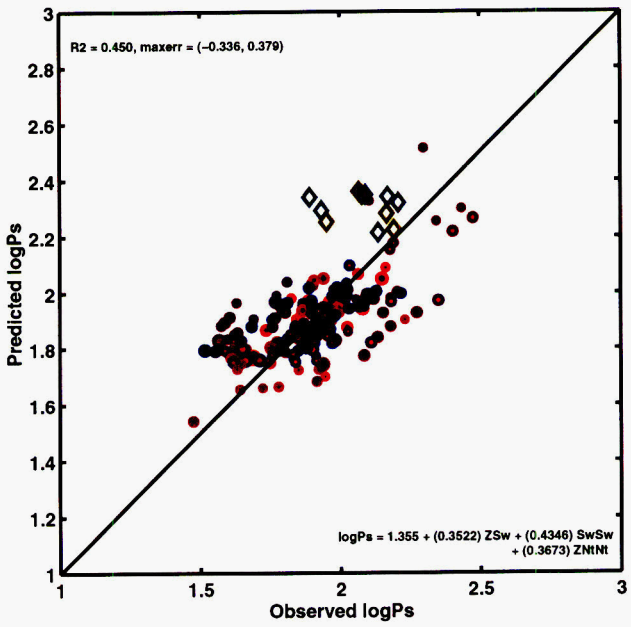

(a)

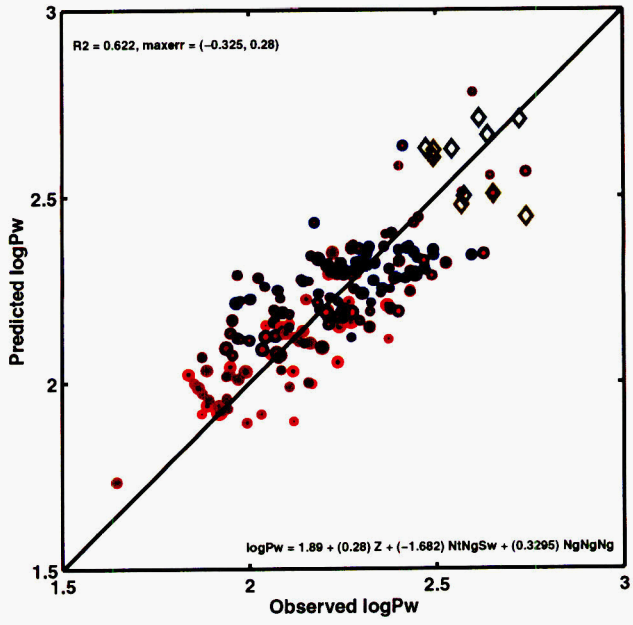

(b)

Figure 2-18: 9/30/99. Scatterplot of observed (a) mean summer and (b) mean winter precipitation. Data points use the same codes as in Figure 2-17.

high-elevation sites, with a shorter summer for coop stations (day 171 through 280) than for the high-elevation sites (roughly May through October). Thus, summer precipitation for the high-elevation sites is somewhat larger than it should be for perfect comparison with the coop data, and winter is somewhat smaller. The effect is more obvious in the summer data, since summer precipitation is smaller and the same absolute error will have a larger relative error in the set with the smaller average. Nevertheless, both summer and winter sets are also reasonably compatible. In summary, I think we have a pretty good representation for annual precipitation, temperature, and snowfall, good enough to publish.

It would be of great interest, for weather-generation purposes, to also examine the daily statistics (*e.g.*, fraction of wet days, fraction of wet days followed by wet, temperatures on wet versus dry days, etc.). Probably the statistics for temperature should be according to a bin based on precipitation. Typically these statistics are described by Fourier series. I would imagine that statistics would be much more robust if the same type of regression analysis as was performed for mean annual statistics were performed using all stations at the same time. In order to perform the analysis, the same type of extraction from the CD-ROMs would be required; however, the resulting output files would be considerably larger, since more information would be saved. The extraction would also be a little more complex, since strings of days would be examined rather than just single days and cross-comparisons of more than one data type would be required.

These coop statistics only address precipitation and temperature. Although these are the most important statistics, information required for generating the weather required for modeling infiltration also includes vapor density and incoming radiation. The SAMSON data should help out on these fronts.

10/2/99 Followup analysis of met data.

When the precipitation data were extracted from the coop CD-ROMs, I also extracted the frequency that rainfall occurred on each day. Every time a good data reading was obtained, a tally was incremented for that day of the year. Every time the good data reading was nonzero, another tally was incremented. The frequency is simply the ratio of the two tallies. The frequency is a noisy measure, especially since the record lengths are fairly short. However, choosing stations with longer records (*e.g.*, 20 yr) smooths out the noise to some extent. Using a time-averaged frequency smooths the record even more.

When a window of 30 dy on each side of each day is used (*i.e.*, averaging 61 consecutive

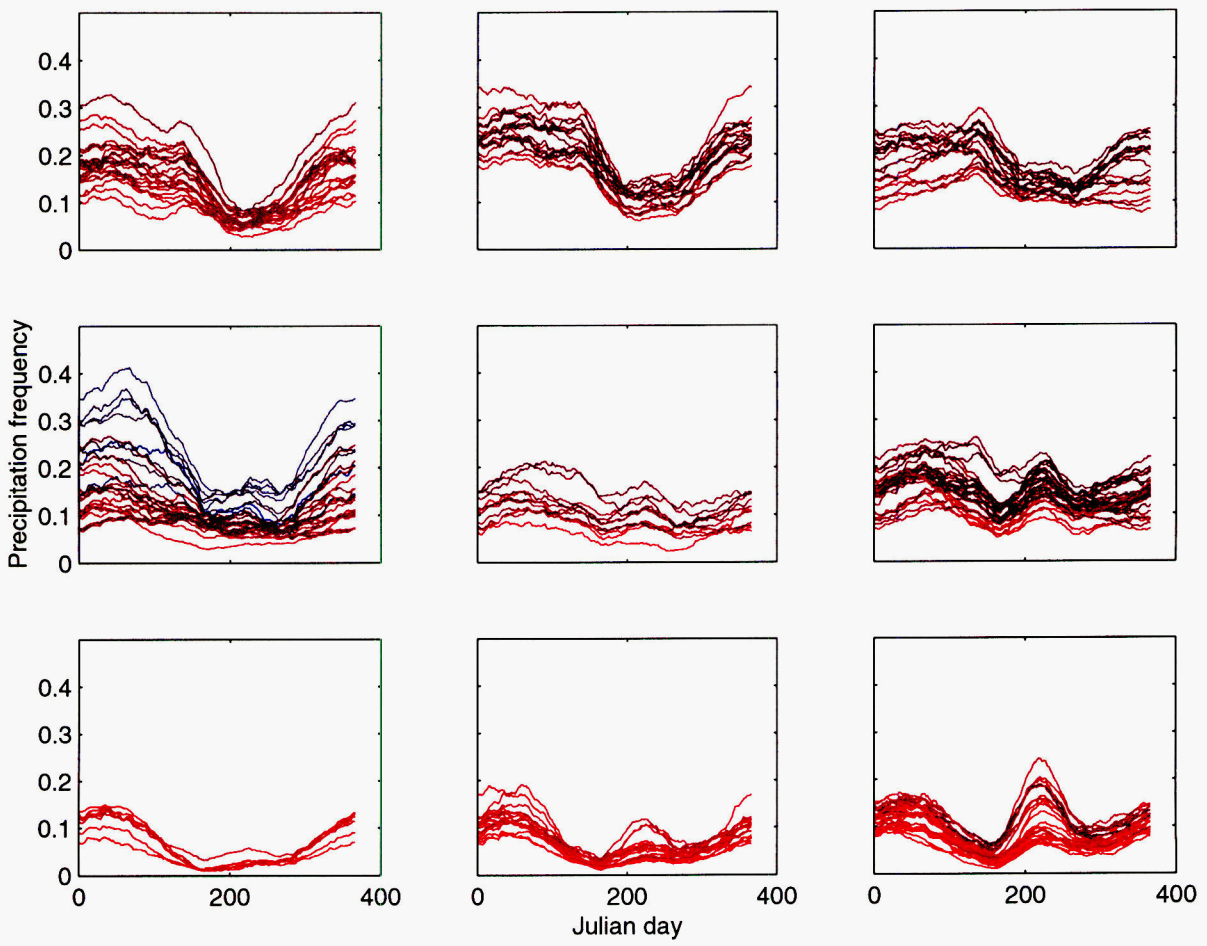

Figure 2-19: 10/2/99. Rainfall frequency for stations in 9 sectors of the study area. Traces are averaged over 61 days. Trace color moves from red to blue as stations increase in elevation.

readings), as shown in Figure 2-19, a reasonably smooth trace is obtained. A triangular weighting might be more appropriate, weighting closer days more than the more distant days. Nevertheless, the smoothed records are quite informative. All 171 stations with at least 20 yr of records were segregated into 9 sectors, and the smoothed trace for all stations within each sector were plotted in the same graph. Each trace was colored according to elevation. Rainfall frequencies increased with increasing elevation throughout the year, as might be expected. A very clear monsoonal pattern was evident in the SE sector, decaying to the north and west. Absolutely no monsoonal pattern is evident in the NW sector. The monsoonal strength, in terms of frequency of rainfall, appeared to increase with elevation. This factor was noticeable in the SE sector and not so obvious in the remaining sectors. Base on these observations, two fitting functions might be used for daily

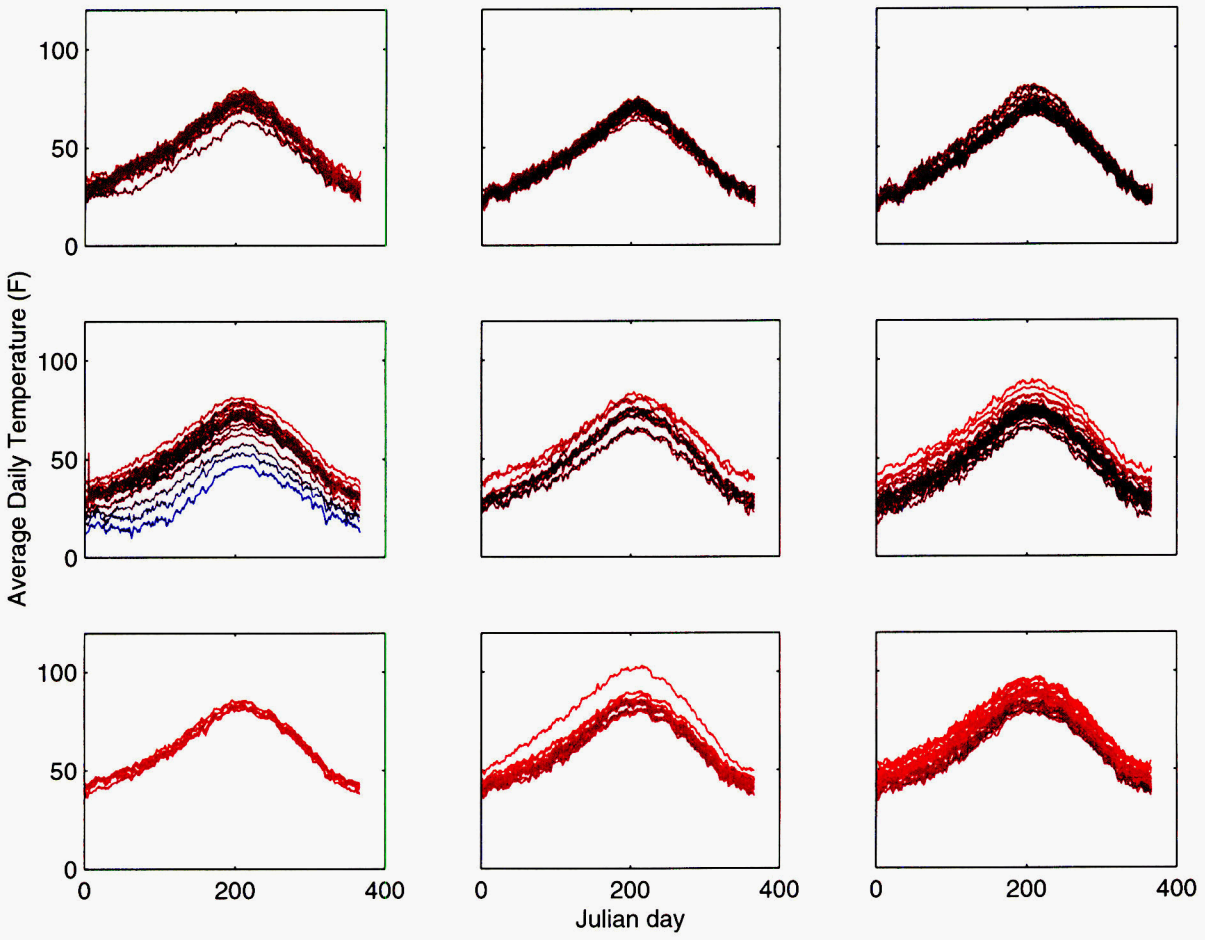

Figure 2-20: 10/2/99. Trace of mean daily temperature for stations in the 9 sectors of the study area. Trace color moves from red to blue as stations increase in elevation.

precipitation frequency: a frontal signature for the entire year (perhaps a sine or sine-squared function), and a monsoonal signature for the summer months (day 171 through roughly day 275). The monsoonal signature should be zero outside the summer and a sine or sine-squared during the summer (trough to trough period of 104 dy).

The temperature profiles also tend to consistently follow elevation, as shown in Figure 2-20. Note that the traces do not seem to follow a strictly sinusoidal pattern, instead almost a delayed triangular wave. These trace patterns are consistent with the Desert Rock patterns.

10/7/99 Ultimate analysis of met data. SAS

The set of coop data and the expanded met data sources at several stations provides an opportunity to perform some extended analyses. I envision a possible paper called *Simulated meteorologic sequences in the Great Basin and Mojave Deserts* or something along those lines. The idea would be to provide statistical analyses of the coop data to generate parameters for daily and hourly parameters. Ideas and approaches presented here are largely based on approaches used by Richardson and Wright (1984) and Curtis and Eagleson (1982), with extensions to account for sequences of wet/dry years. I think that the work would be quite useful outside of the YM community.

The theoretical framework for the analysis uses several levels of parameterization. The first level characterizes the statistics to be used for individual years. The second level characterizes the statistics to be used for days within a year. The finest level characterizes the distribution within a day.

Precipitation in the Great Basin follows cycles driven by the southern oscillation, with typically several years between peaks. An implication is that precipitation statistics are significantly different in wet years than in dry years. It may also be that other climatic variables also are different in wet years than in dry years, as air masses may have different trajectories and thus different states; this hypothesis would need to be looked at. Precipitation also occurs with two general sources: (i) frontal, or winter precipitation; and (ii) monsoonal, or summer precipitation. The frontal systems tend to move in from the Pacific, while the monsoonal systems tend to move in from the Gulf. Thus, the monsoonal signal is strongest in the southeast portion of the region of interest. It may make sense to examine frontal and monsoonal statistics separately, with an annual cycle for frontal precipitation and a superimposed cycle for monsoonal precipitation for a limited portion of the year (*e.g.*, day 171 through 275, approximately). Statistics for both of these cases would likely be described using sinusoids or powers of sinusoids. The frontal statistics would have an annual period while the monsoonal statistics would have a period of roughly 104 dy, with one trough-to-trough cycle considered (the period of the monsoon).

For those variables that are found to have different statistics in wet and dry years, it would make sense to have an index variable for the relative wetness strength. Extraction of the following statistics would then be performed for several wetness bins (very dry, dry, normal, wet, very wet) characterizing each year. Without having looked at the interannual variability yet, cutoffs for very dry and very wet bins might be half annual precipitation and twice annual precipitation.

Day-to-day precipitation statistics would be characterized in a two-step process: (i) calculate

whether or not the day receives precipitation, and (ii) calculate precipitation magnitude on the days that precipitation occurs. Two popular approaches to predicting days with precipitation are (i) to use transition probabilities in a Markov-chain calculation (*e.g.*, the probability of a wet day given that the preceding day is wet), calculating day-by-day whether the day is wet or not, and (ii) assume that the number of days between wet days is exponentially distributed and directly calculate the number of days. These are essentially equivalent procedures. In either case, given a wet day, precipitation magnitude is typically assumed to be exponentially distributed.

Non-precipitation parameters are continuous rather than episodic. Typical methods for predicting these use the idea of a Markov chain as well, with first-order correlations accounted for between the parameters (Matalas, 1967). Parameters required for evapotranspiration include temperature, atmospheric vapor density, incoming longwave and shortwave radiation, soil temperature, and windspeed. Longwave and shortwave radiation can be calculated from cloud cover. All of these vary during the day. Currently in *breath* these variables all combine to calculate evaporation based on the difference between soil and atmospheric vapor density multiplied by vapor conductance. My impression is that soil temperature and moisture are not strongly coupled over time periods longer than a few days at most. It may be adequate to estimate the conductance and soil temperature externally during *breath* simulations in cases where freezing is not an issue; or perhaps the soil temperature can be calculated without consideration of soil moisture, with temperature at several depths stored for interpolation. When snow is present, coupling may be necessary.

My *breath* simulations suggest that it should be quite adequate for infiltration simulations to use the mean profiles during the day. Even monthly averages are adequate on days away from precipitation (climate rather than weather), although temperature effects on vegetation were not considered. Based on this information, daily-summary statistics should be generated with disaggregation performed on days near precipitation, using the mean curve. Appropriate daily-summary statistics are mean and range for the variable. The daily responses should be tied to solar influences, so that disaggregation should be based on the solar day. For example, temperature typically has a minimum around sunrise and a maximum partway between noon and sunset. Cloud cover, vapor density, and windspeed also show typical trends based on the time of day relative to sunrise and sunset. The SAMSON database may provide these typical trends for a variety of stations – probably it would not be necessary for them to be restricted to the Great Basin.

It would be necessary to consider correlations between temperature, vapor density, and cloud cover; windspeed could likely be considered an independent variable. The day-to-day variation of atmospheric parameters is tied to whether it rains or not, and presumably the magnitude of precipitation as well. For example, it tends to be cooler and more humid on rainy days than on

sunny days. Accordingly, the statistics for each of the non-precipitation parameters are likely to respond to whether the day is wet or not. Previous work with the Desert Rock data suggests that the statistical descriptions exponentially decay from the wet-day to the dry-day parameters over a period of days to a week or more, and the perturbation in the statistical description is intensified by the magnitude of the precipitation. Hopefully the deviation from the dry-day patterns is responsive only to precipitation magnitude, so that seasonality does not need to be considered. Even more hopefully, deviations are not spatially dependent (elevation or latitude/longitude), so that all stations can be lumped together to estimate parameters. If the deviations are laterally dependent, local aggregations would be the best approach (*e.g.*, lump within the 9 sectors examined previously).

As a first step, the following actions should be performed for each coop station with at least 5 yr of both precipitation and temperature data:

- Extract the sequence of daily records for precipitation and min and max temperature
- Classify each year as wet, dry, or normal and perform the following analyses according to type of year
- For each day, extract the probabilities of a wet day and a wet day given that the previous day was wet
- For each day, estimate the mean and range of T by fitting an annual cycle
- For each day, save triplets of P, δT_{mean}, and δT_{ran} for lags from wet days of -5, -2, -1, 0, 1, 2, 5, 10, and 20 consecutive dry days following each wet day that occurs on the day of interest
- Explore relationships between P magnitude, seasonality, and spatial location.
- Explore relationships between P magnitude and rainy-day T descriptors through scatterplots. Check seasonal and spatial factors. Unless strong spatial relationships exist, lump all stations together to obtain statistics. Default assumptions are that there is a dip in T_{mean} proportional to $\log P$ and the change in T_{ran} is zero or proportional to $\log P$.
- Explore transition constant for dry-to-wet and wet-to-dry statistics

The reduced set of SAMSON observations should be mined for correlations between precipitation, temperature, vapor density, and cloud cover. All of these observations are hourly; unfortunately not all variables are observed at each station. An initial step should be performed that yields the mean variation pattern over a day. Daily mean and range should be extracted

for each of the parameters of interest. Similar analyses should be performed for the SAMSON observations as were performed for the coop data. One idea that might be checked is whether the deviation in non-precip met variables can be tied strictly to temperature deviations, which would simplify the analysis considerably.

I've noticed in the Desert Rock data that non-precip variables can respond as though precipitation is occurring even when no precipitation occurs. I expect that this is due to either fronts passing through or due to nearby precipitation. It may be interesting to see if there are distinct decay trends in such cases. If so, it may be of interest to try to capture such non-precip events and allow precipitation magnitude to have some negative component (ignored otherwise) but with other variables varying as though precipitation has occurred. Perhaps too complex.

10/8/99 Quick look at precipitation magnitude.

SAS

Based on yesterday's discussion, I took a crude quick look at the possibility that precipitation magnitude may vary spatially or temporally. I had already extracted the daily average precipitation and frequency information for each coop station, with moving-average frequencies plotted in Figure 2-19. In an analogous approach, I plotted (not shown) moving-average precipitation magnitude divided by moving-average frequency for each station with at least 40 yr of observations. It is necessary to use independent moving averages for both, since most records have days with no observations (forcing zero to be divided by zero). Elevation is indicated with color coding, and the same 9 sectors are used as previously. These curves are much noisier than the moving-average frequency curves shown in Figure 2-19.

Two observations can be drawn from the plots. Using relatively shorter windows for moving averages, it appears that the seasonality of precipitation magnitude variability may be relatively insignificant in the northern sectors. In the southwestern sector, winter precipitation magnitudes are large and summer precipitation magnitudes are small. In the southeastern sector, there is an additional bump corresponding to the monsoon, leading to a double-peaked precipitation magnitude pattern. These three patterns decay with distance. Somewhat surprisingly, there is no obvious link to elevation. These three patterns may correspond to frontal winter precipitation from the southwest, monsoonal summer precipitation from the southeast, and frontal jet-stream precipitation from the north or west.

The second observation arises when a relatively large window for averaging is used (*e.g.*, 3 months). This window size is enough to provide fairly smooth and temporally invariant curves.

Again there is no strong elevation dependence for precipitation magnitude, but there appears to be a small dependence on latitude. The average precipitation event appears to be somewhat less than 20 mm (*e.g.*, 16 to 18 mm) in the northern sectors, while the average precipitation event appears to be somewhat greater than 20 mm (*e.g.*, 22 to 24 mm) in the southern sectors. The central sectors have average events of roughly 20 mm. The scatter in any one sector is roughly comparable to the difference in mean between north and south. Thus, the south has relatively few but large events while the north has smaller, more frequent events.

In conclusion, the preliminary indication is that expected precipitation magnitude exhibits significant seasonality in the south but not in the north, and elevation is not a strong predictor for precipitation magnitude.

12/7/99 Quick calculation of wetting front results.

SAS

In order to make a presentation at AGU, I came up with the idea of examining consequences of bromus takeover. Two consequences are increased MAI and a delay to recharge.

I created a figure showing bare-soil MAI as a function of elevation for several climate scenarios. The previous regression work on COOP stations was used to make MAP and MAT functions at YM as a function of elevation. These functions are

$$\begin{aligned} \log_{10}(MAP) &= 1.999 + 0.2767Z - 1.535N_gS_w + 1.211N_gN_gS_w + 0.4991S_w^3 \\ &= 1.8346 + 0.2767Z \end{aligned} \tag{2-17}$$

$$\begin{aligned} MAT &= 56.8 - 6.063Z - 0.9534Lat \\ &= 21.68 - 6.063Z \end{aligned} \tag{2-18}$$

where the reduced formulas are for YM latitude and longitude (36°50′ N and 117°40′ W), Z is elevation (km), N_g is $(Lng - 113)/(120 - 113)$, S_w is $(MAR - 2750)/(3050 - 2750)$, Lat and Lng are latitude and longitude, respectively, and MAR is mean annual shortwave radiation (J/cm^2). The MAP relation uses the high-altitude data ($R^2 = 0.74$).

I tried using the soil/bedrock formula for MAI but the values came out alarmingly large, so I used the deep-alluvium formula instead with the sandy loam used in the WRR MAI-regression paper. The resulting predictions are shown in Figure 2-21.

A second figure attempts to predict how long it takes to impact the water table given a jump in steady flux boundary conditions. The first cut was to use *breath* for deep sandy loam, starting

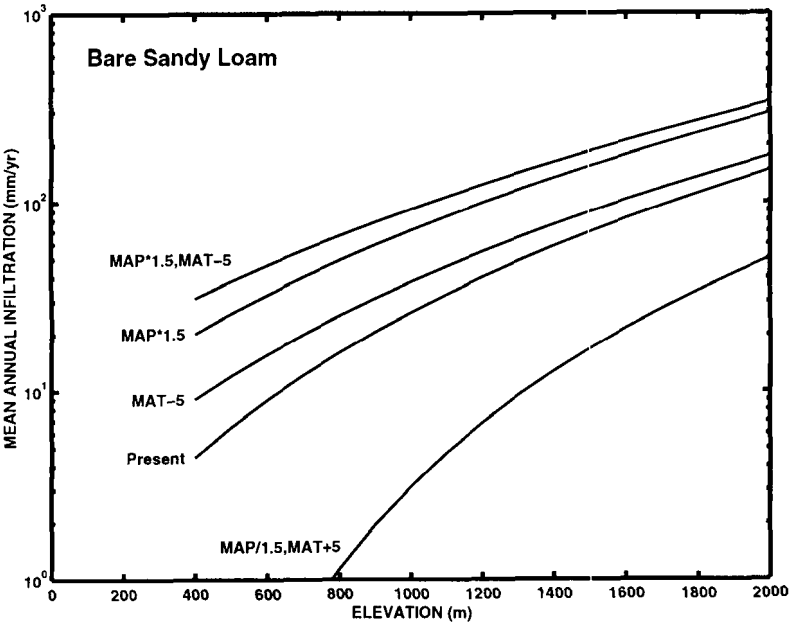

Figure 2-21: 12/7/99. Prediction of MAI as a function of climate and elevation for deep sandy loam.

with gravity drainage initial conditions and imposing a flux jump at the top. After running a couple of simulations, it occurred to me that I needed to calculate a velocity of the wetting front. The two *breath* runs both used 1 mm/yr gravity flux as initial conditions, with jumps to 10 and 100 mm/yr, respectively. These yielded velocities of approximately 0.45 and 1.86 m/yr.

Another approach uses sharp interface theory to calculate velocity. This is simply done using the formula

$$V = \frac{q_1 - q_0}{\varepsilon(\theta_1 - \theta_0)} \tag{2-19}$$

where V is velocity, q is flux, ε is porosity, θ is saturation, and subscripts 0 and 1 represent initial and final fluxes. The appropriate saturation values maintain a steady flux due strictly to gravity. I double-checked the formula against the two *breath* simulation results, obtaining velocities identical to within a few percent, so I conclude that the sharp interface approximation is quite adequate. The sharp interface results are shown in Table 2-21.

Table 2-21: Velocity of a wetting front in sandy loam assuming a jump in infiltration flux.

Initial Flux (mm/yr)	Jump Flux (mm/yr)	Velocity (m/yr)
0.1	1	0.07
0.1	10	0.29
0.1	30	0.63
0.1	100	1.48
1	10	0.43
1	30	0.83
1	100	1.82
5	10	0.68
5	30	1.17
5	100	2.32
10	30	1.42
10	100	2.68

8/3/00 Evaluation of future-climate simulations.

One of the sections of the report on infiltration processes summarizing work to date is to compare the effects of scaling Desert Rock climatic records to yield equivalent MAP and MAT and calculating MAI with the direct simulation of other sites. The motivation behind this exercise is to check on the DOE procedure of using analog records from Arizona and Washington.

I set up a set of simulations based on three meteorological data sets (Desert Rock, Tucson, and Spokane), three soil thicknesses (10, 25, and 50 cm), three soil/soil-filled fracture combinations (combo 1: K_{sat} is 10^{-9} cm^2, P_0 is 2×10^4 gm/cm-s^2, porosity is 0.3, and m is 0.2, with fracture volume fraction of 0.001; combo 2: same soil, but fracture volume fraction of 0.01; and combo 3: K_{sat} is 10^{-8} cm^2, P_0 is 5×10^4 gm/cm-s^2, porosity is 0.3, and m is 0.2, with fracture volume fraction of 0.01), and several scalings for each meteorological set.

The soil K_{sat} and P_0 are both multiplied by fracture volume fraction in the fracture zone. The first soil was examined in previous simulations, although the permeability in the fractures was incorrectly left unscaled. The second soil is coarser, representing something close to present conditions.

For each combination of meteorological data set and climate scaling, all 9 soil thickness/hydraulic

property combinations were run. The Tucson and Spokane data sets were based on the 1961-1990 SAMSON hourly data readings, with latitude artificially corrected to be identical to Desert Rock to reduce the effects of different solar flux. The Desert Rock data set is identical to the set used for the previous simulations reported in the WRR MAI paper. All met records used hourly values within 24 hr of a precipitation event and monthly values otherwise. The Desert Rock set consisted of 1 decade, repeated once, while the SAMSON sets used the 30 yr record without repeating.

My usual procedure for analyzing the records uses annual snapshot output from the simulations. I generally use the flux averaged over the bottom 5 m or so of the column to estimate MAI, and the average saturation just above the bedrock to get an estimate of mean annual saturation. For the purposes of the analysis I further examined the weekly trace of flux from several nodes within the domain. I was quite surprised to find that the wetting pulse had not reached the bottom of the column in many of the drier cases even after 30 yr. An alternate scheme uses the trace data from near the soil/bedrock interface to estimate MAI, since such shallow depths appear to reach equilibrium relatively quickly.

Using the trace data, I was able to disaggregate MAI into mean daily values by spreading the cumulative flux for each week to each of the days in the week, then averaging according to Julian day. Here again I had some surprises. Present-day Spokane infiltration appears to occur exclusively from November through February. Present-day Tucson infiltration is primarily during the summer monsoon, with a significant winter component as well. At Desert Rock, MAI appears to be primarily from 1 or 2 summer thunderstorms with only a small fraction from winter, exactly the opposite that I expected and opposite the indications from isotopes. As conditions become cooler and wetter, the winter component becomes more significant relative to summer.

The precipitation data does not follow the infiltration patterns. The Spokane data tends to be relatively uniform from month to month, especially the monthly averages over all 30 yr. The Tucson data has a definite summer peak, but winter precipitation seems to be overall larger. The Desert Rock data seems to indicate that winter precipitation is generally larger than summer.

I draw a tentative conclusion from these new simulations that a certain intensity of rainfall may be required to force infiltration deep enough to escape the evapotranspiration (ET) trap. Scaling the Desert Rock precipitation data may be adequate in winters but is probably unreasonable in summers, since the thunderstorms are already quite large.

Seasonality is quite different in the three cases. How will future climates change their seasons?

8/11/00 Future-climate simulation results.

SAS

Simulation results are shown in this section as a series of plots. Traces of cumulative moisture flux between volumes were saved on a weekly basis for all simulations. The average flux for each week is obtained by subtraction. For each simulation, a pair of plots are shown: (i) cumulative precipitation and flux from locations within the soil and fracture continuum, and (ii) mean daily precipitation and flux from the same locations. These present the same information in two different ways. In both sets of plots, the lines are color coded to distinguish between winter (blue, Julian days 305 through 74) and summer (red, Julian days 75 through 304). Winter corresponds to November 1 through March 15. Precipitation and infiltration are indicated on different axes, since infiltration is much smaller than precipitation. Precipitation is indicated with a thin line, moisture flux with thicker lines.

Coding schemes for the individual traces denote met data source location, soil case (the same order as in the previous entry), soil thickness (cm), observation depth (cm), MAP (mm/yr), and MAT (°C). Note that traces from high in the soil are much bouncier than traces from deep in the fracture, providing a way of quickly distinguishing the observation depth for the curves.

Deep wetting (responses at deep observation locations) does not occur unless MAI is at least 4 to 7 mm/yr. The minor fluxes recorded at depth are simply drainage from initial conditions. In many cases, there is a clear lag with depth before climatic conditions are felt, with 5 to 15 yr required for the first large pulse to reach tens of meters below the surface. Because of the lag, MAI estimates of less than 1 to 5 mm/yr should be read as < 1 or < 5 mm/yr. However, once the lower depths respond their cumulative fluxes seem to track the upper fluxes quite well. There can be a slower response to individual wetting events as well, sometimes taking a year or more for a pulse to pass.

A summary of MAI estimates from the cumulative flux plots are shown in Table 2-22. These estimates were obtained visually from the upper observation points. Only 33 of the 93 simulations have MAI greater than 1 mm/yr. Increasing soil thickness tends to decrease MAI, but some cases have greater MAI with 50 cm than with 25 cm thickness and one case has greater MAI with 50 cm than both 10 and 25 cm thicknesses.

Soil/fracture combos 1 and 2 tend to behave similarly, although usually similar climatic conditions yield larger MAI for the case with larger fractures (although certainly not by a factor of ten, more like a factor of 2 or 3). Soil/fracture combo 3 behaves significantly differently, being more sensitive to summer precipitation than the other combinations, although cooler and wetter

Table 2-22: Summary of MAI results from future-climate simulations. MAP and MAI are in mm/yr, MAT in °C.

MAP/MAT	Soil Combination 1			Soil Combination 2			Soil Combination 3		
Desert Rock meteorologic record									
167/16.7	< 1	< 1	< 1	< 1	< 1	< 1	4	< 1	< 1
251/11.7	3.5	< 1	< 1	2	1.2	2.3	40	8.5	0.9
334/9.7							60	27	18
Tucson meteorologic record									
305/17.1	0.9	< 1	< 1	< 1	< 1	< 1	21	5.5	0.9
305/12.1	6.6	< 1	< 1	16	14	1.2	34	12	2.4
153/17.1	< 1	< 1	< 1	< 1	< 1	< 1	1.6	< 1	< 1
153/12.1	2.3	< 1	< 1	3.5	< 1	< 1	8.5	< 1	< 1
Spokane meteorologic record									
419/8.5	7	0.6	0.9	9	3.6	4.5	40	3	1
419/13.5	< 1	< 1	< 1	1	< 1	< 1	5	< 1	< 1
210/8.5	< 1	< 1	< 1	0.85	< 1	< 1	1.2	< 1	< 1
210/13.5	< 1	< 1	< 1	< 1	< 1	< 1	< 1	< 1	< 1

conditions preferentially increase winter infiltration.

Based on these simulations, it appears that the Desert Rock and Tucson simulations may behave roughly comparably with meteorological scaling. In other words, scaling the Tucson record to match MAP and MAT targets should give roughly the same MAI as scaling the Desert Rock record to match the same targets. The Spokane simulations generally do not scale with the southwestern cases. I attribute this disparity to the intermittency patterns in precipitation. Spokane tends to have less variability than either Desert Rock or Tucson, as can be seen in Figures 2-22 through 2-24. Spokane storms are more frequent, smaller, and more uniform in magnitude than the southwestern storms. In particular, summer rainstorms are smaller than in the southwest. Since infiltration exponentially responds to precipitation, the different precipitation patterns result in different scalings. An implication is that decreasing variability will decrease MAI.

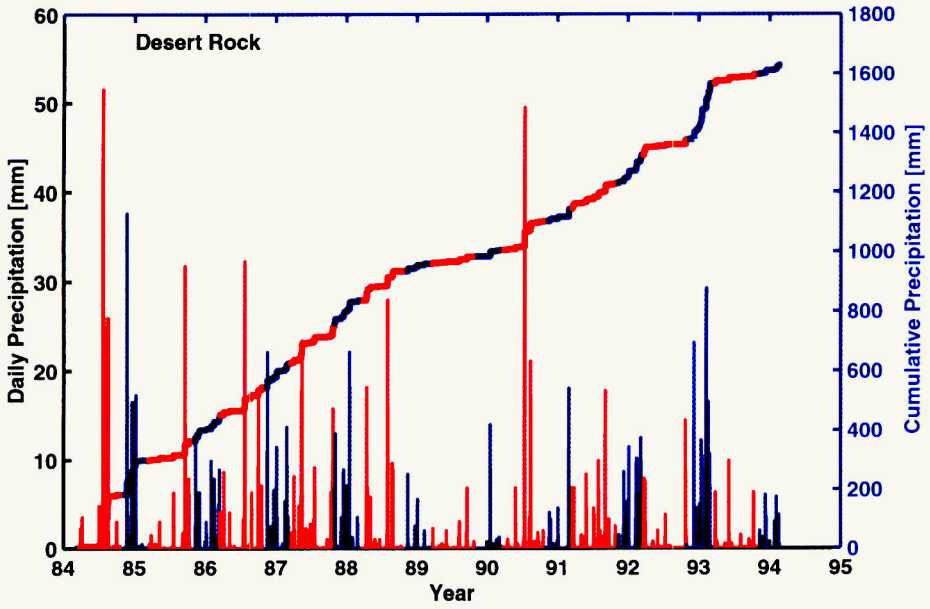

Figure 2-22: 8/11/00. Daily and cumulative precipitation for the Desert Rock meteorology.

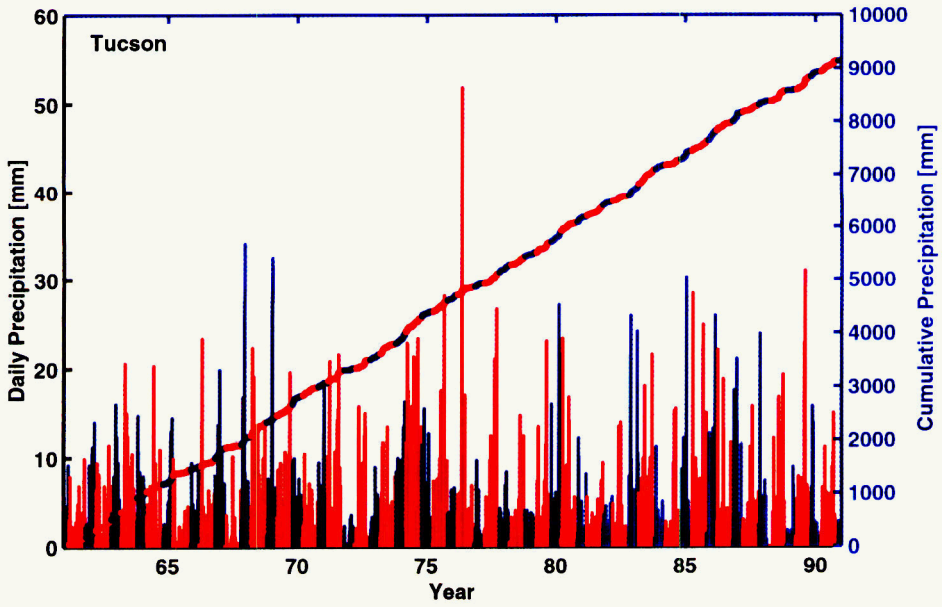

Figure 2-23: 8/11/00. Daily and cumulative precipitation for the Tucson meteorology.

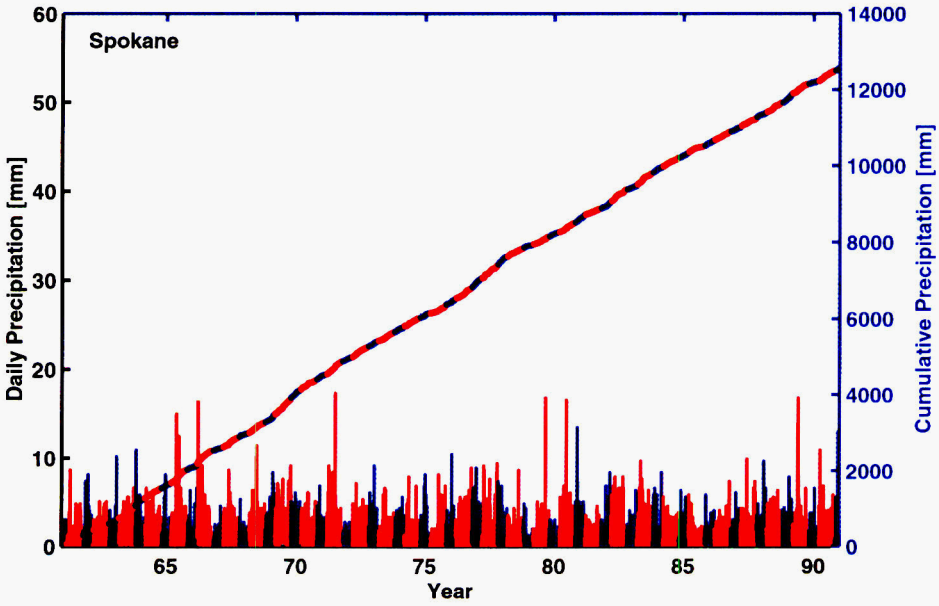

Figure 2-24: 8/11/00. Daily and cumulative precipitation for the Spokane meteorology.

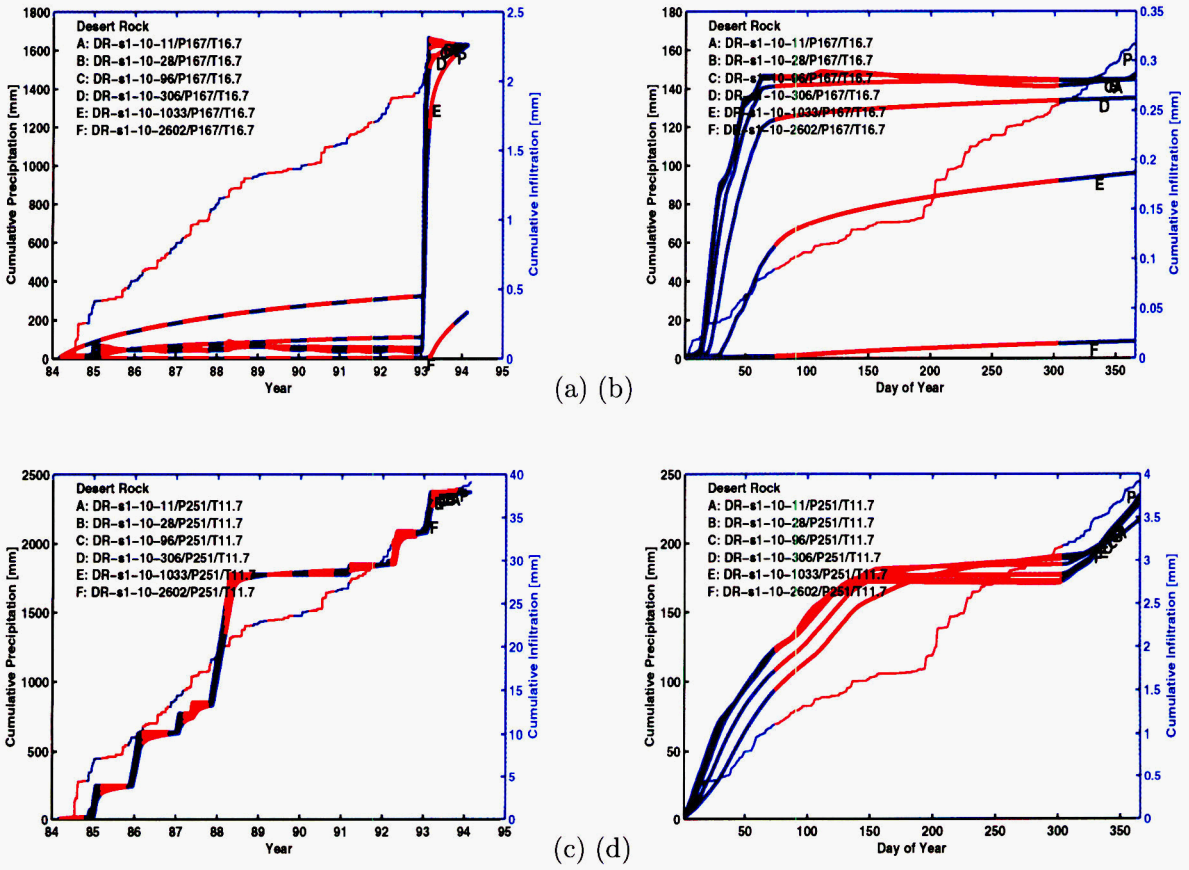

Figure 2-25: 8/11/00. Precipitation and moisture fluxes at 6 depths for 10 cm thickness of soil 1 using the Desert Rock meteorology. (a,c) Cumulative precipitation and moisture flux for different MAP and MAT scalings. (b,d) Corresponding mean daily values for the same simulations.

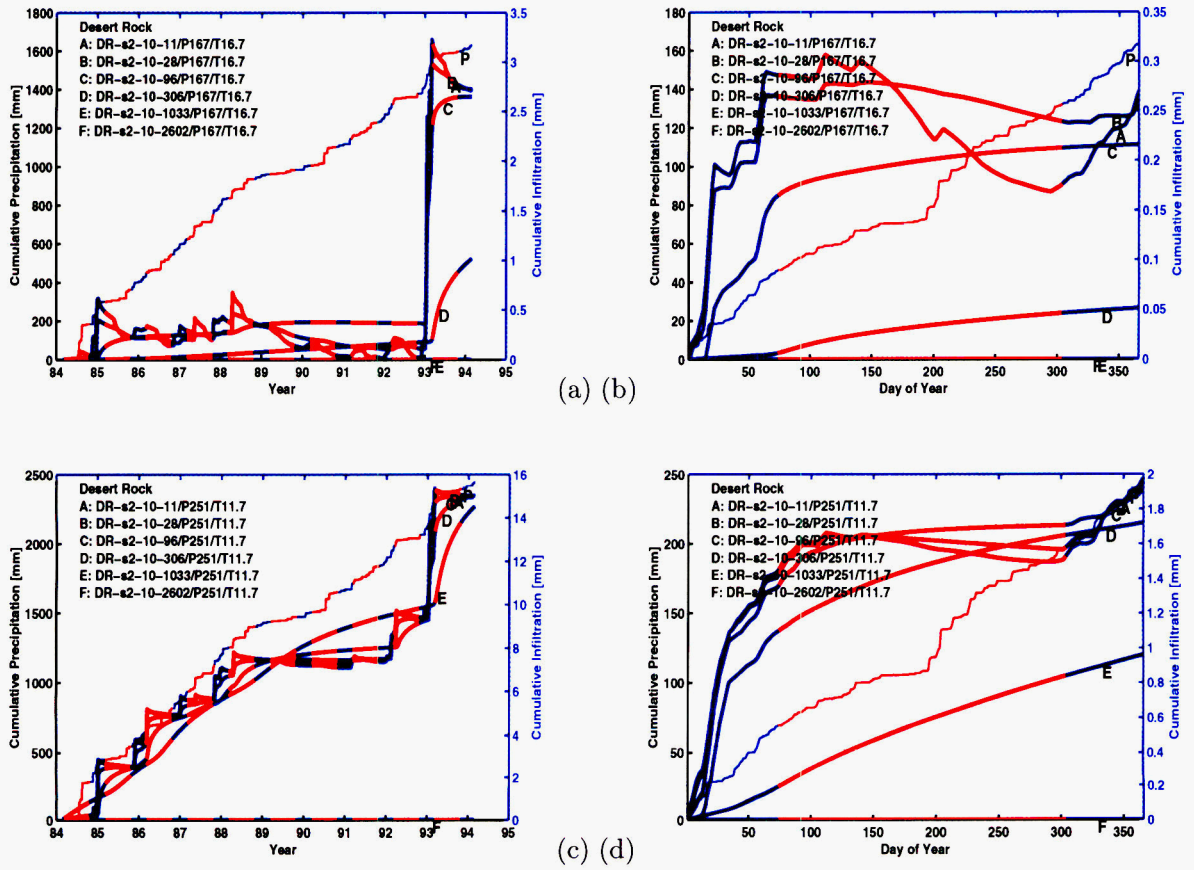

Figure 2-26: 8/11/00. Precipitation and moisture fluxes at 6 depths for 10 cm thickness of soil 2 using the Desert Rock meteorology. (a,c) Cumulative precipitation and moisture flux for different MAP and MAT scalings. (b,d) Corresponding mean daily values for the same simulations.

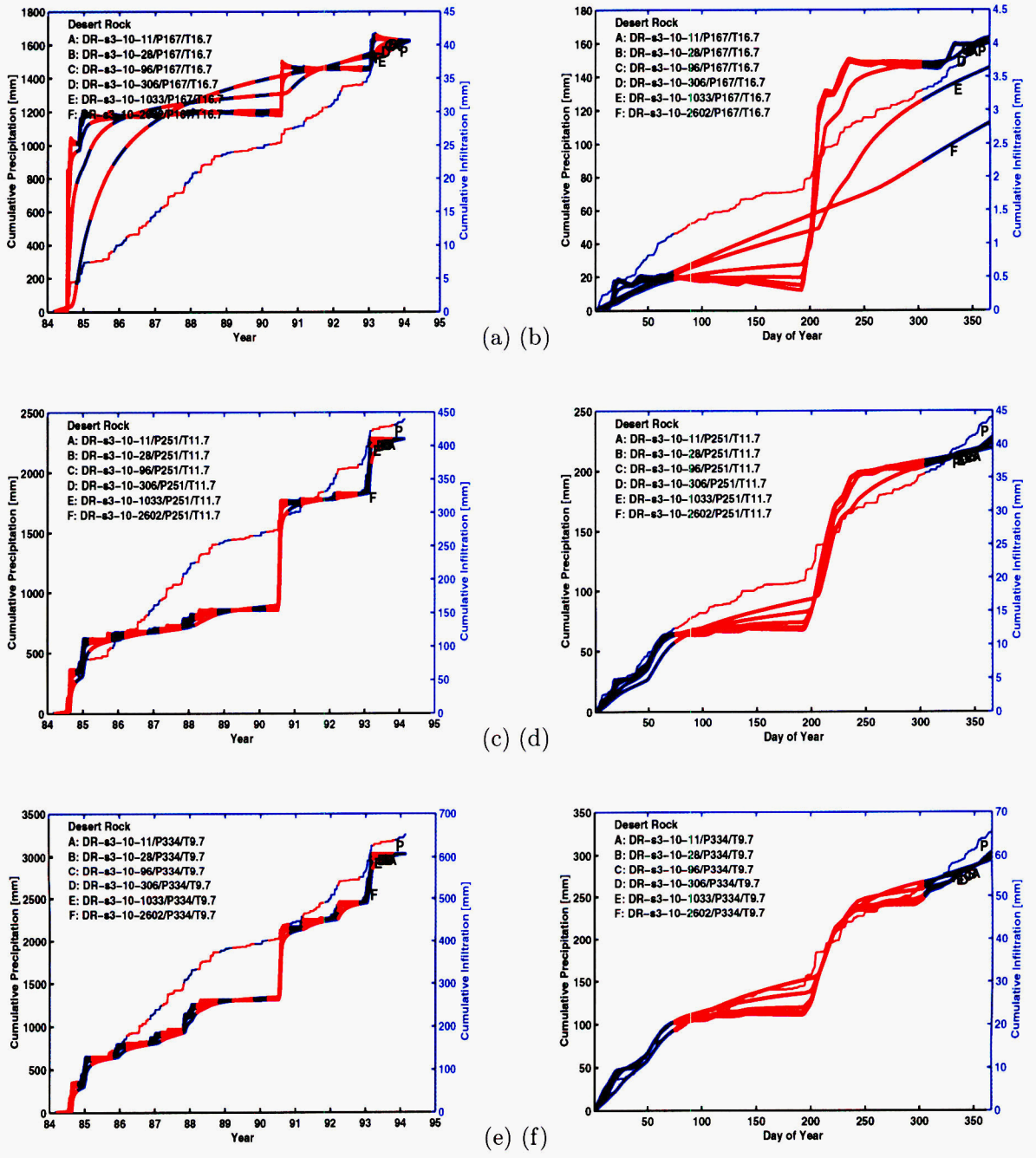

Figure 2-27: 8/11/00. Precipitation and moisture fluxes at 6 depths for 10 cm thickness of soil 3 using the Desert Rock meteorology. (a,c,e) Cumulative precipitation and moisture flux for different MAP and MAT scalings. (b,d,f) Corresponding mean daily values for the same simulations.

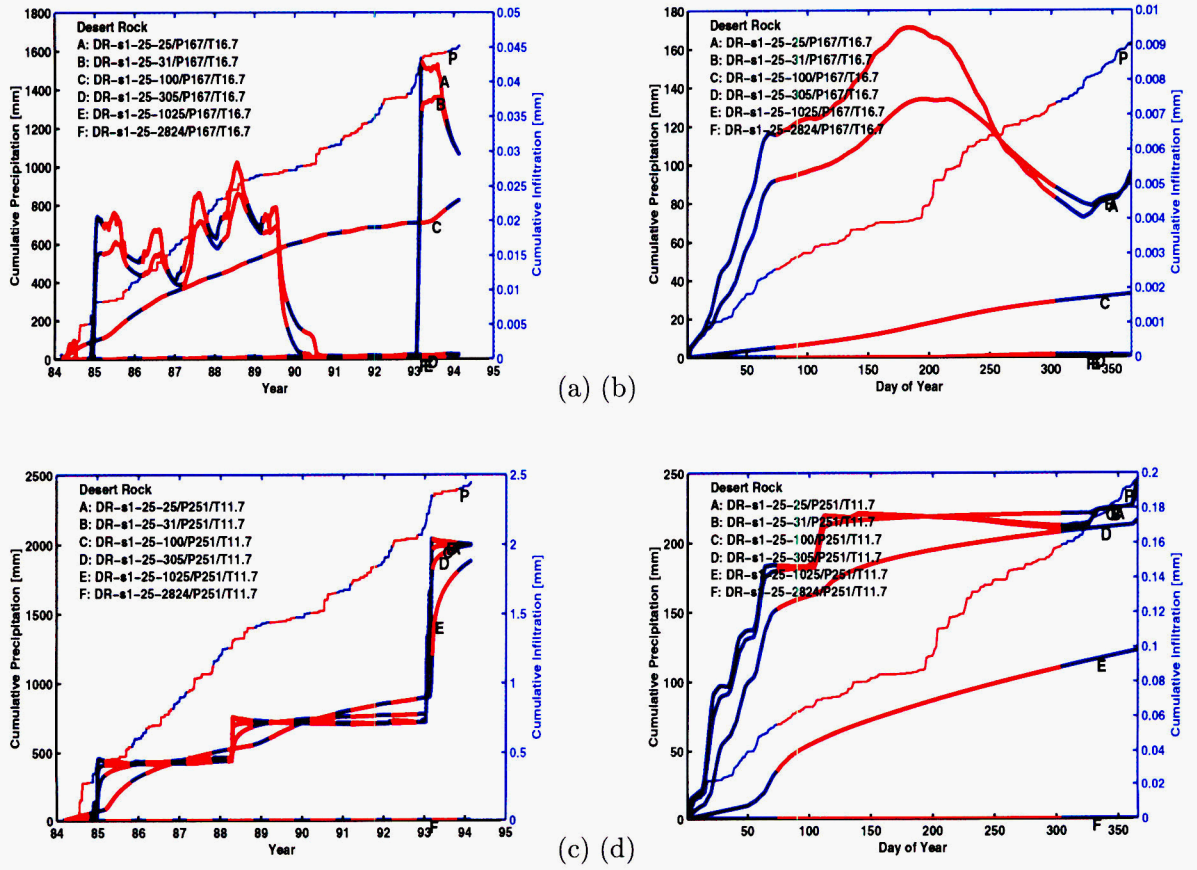

Figure 2-28: 8/11/00. Precipitation and moisture fluxes at 6 depths for 25 cm thickness of soil 1 using the Desert Rock meteorology. (a,c) Cumulative precipitation and moisture flux for different MAP and MAT scalings. (b,d) Corresponding mean daily values for the same simulations.

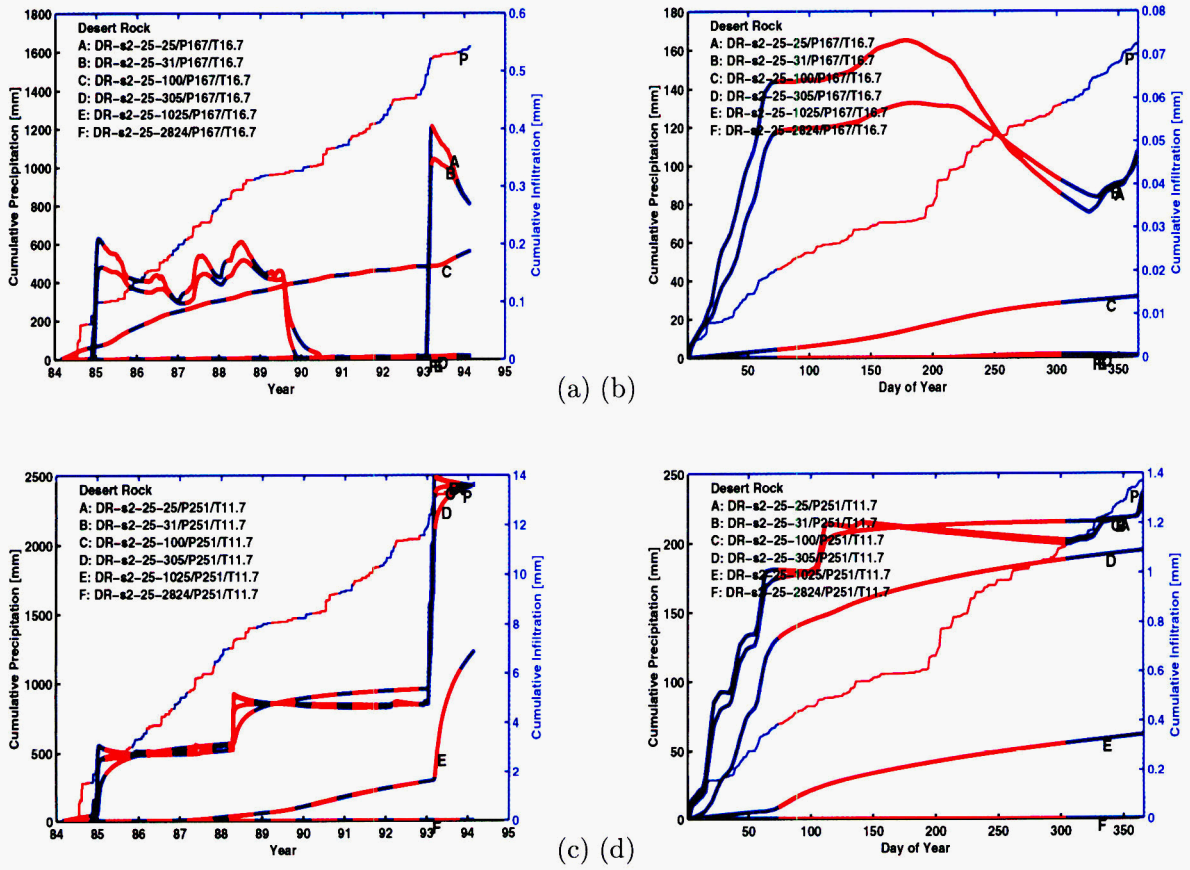

Figure 2-29: 8/11/00. Precipitation and moisture fluxes at 6 depths for 25 cm thickness of soil 2 using the Desert Rock meteorology. (a,c) Cumulative precipitation and moisture flux for different MAP and MAT scalings. (b,d) Corresponding mean daily values for the same simulations.

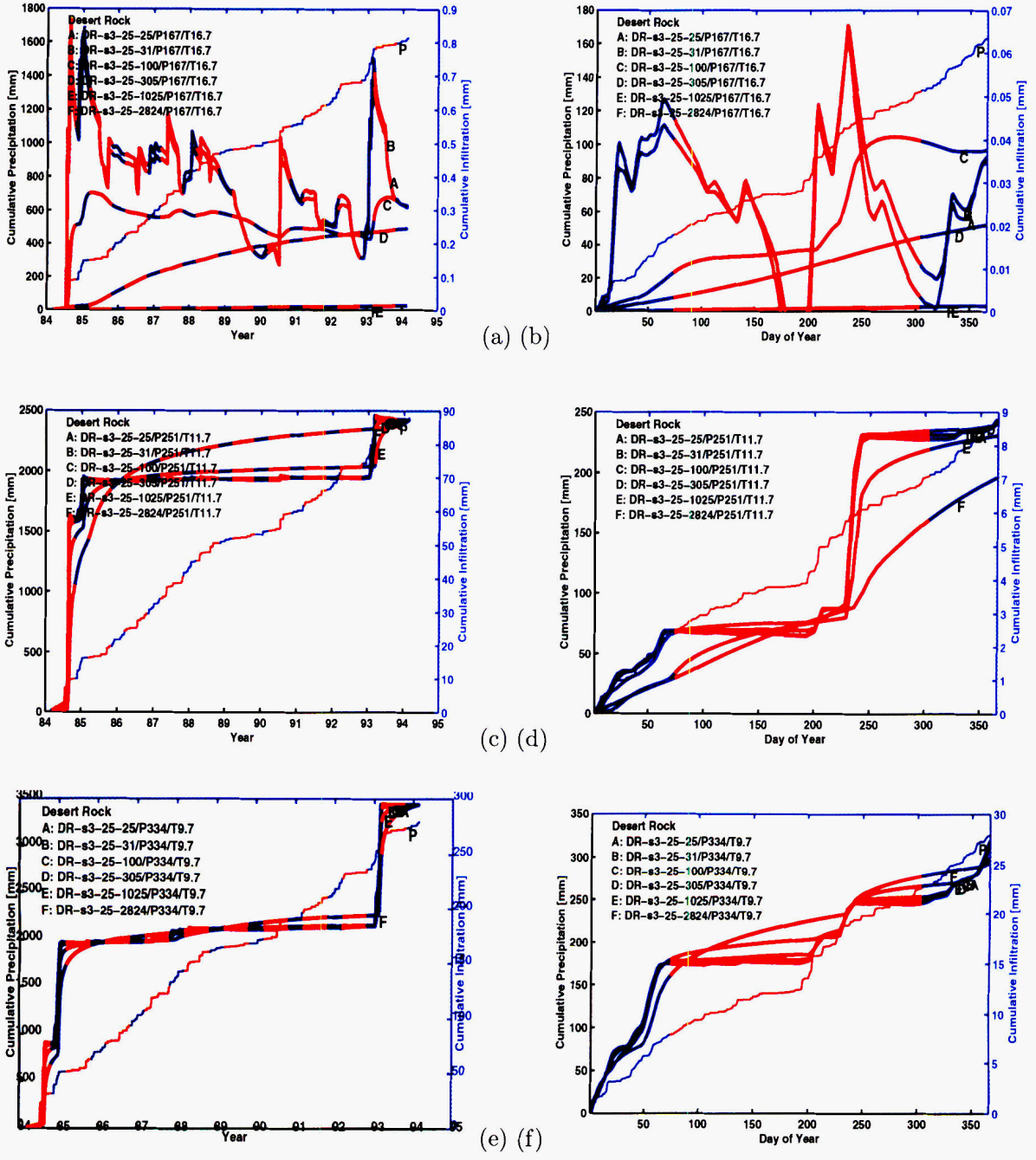

Figure 2-30: 8/11/00. Precipitation and moisture fluxes at 6 depths for 25 cm thickness of soil 3 using the Desert Rock meteorology. (a,c,e) Cumulative precipitation and moisture flux for different MAP and MAT scalings. (b,d,f) Corresponding mean daily values for the same simulations.

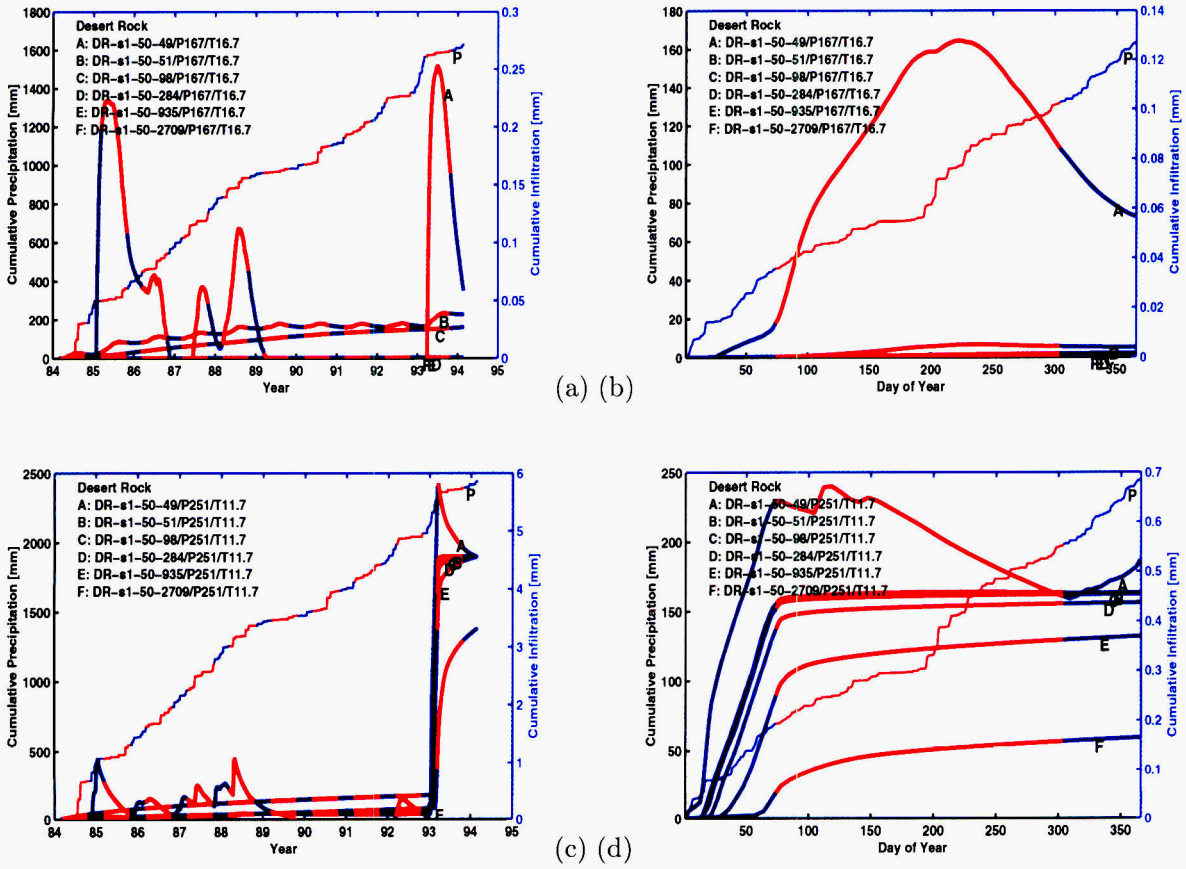

Figure 2-31: 8/11/00. Precipitation and moisture fluxes at 6 depths for 50 cm thickness of soil 1 using the Desert Rock meteorology. (a,c) Cumulative precipitation and moisture flux for different MAP and MAT scalings. (b,d) Corresponding mean daily values for the same simulations.

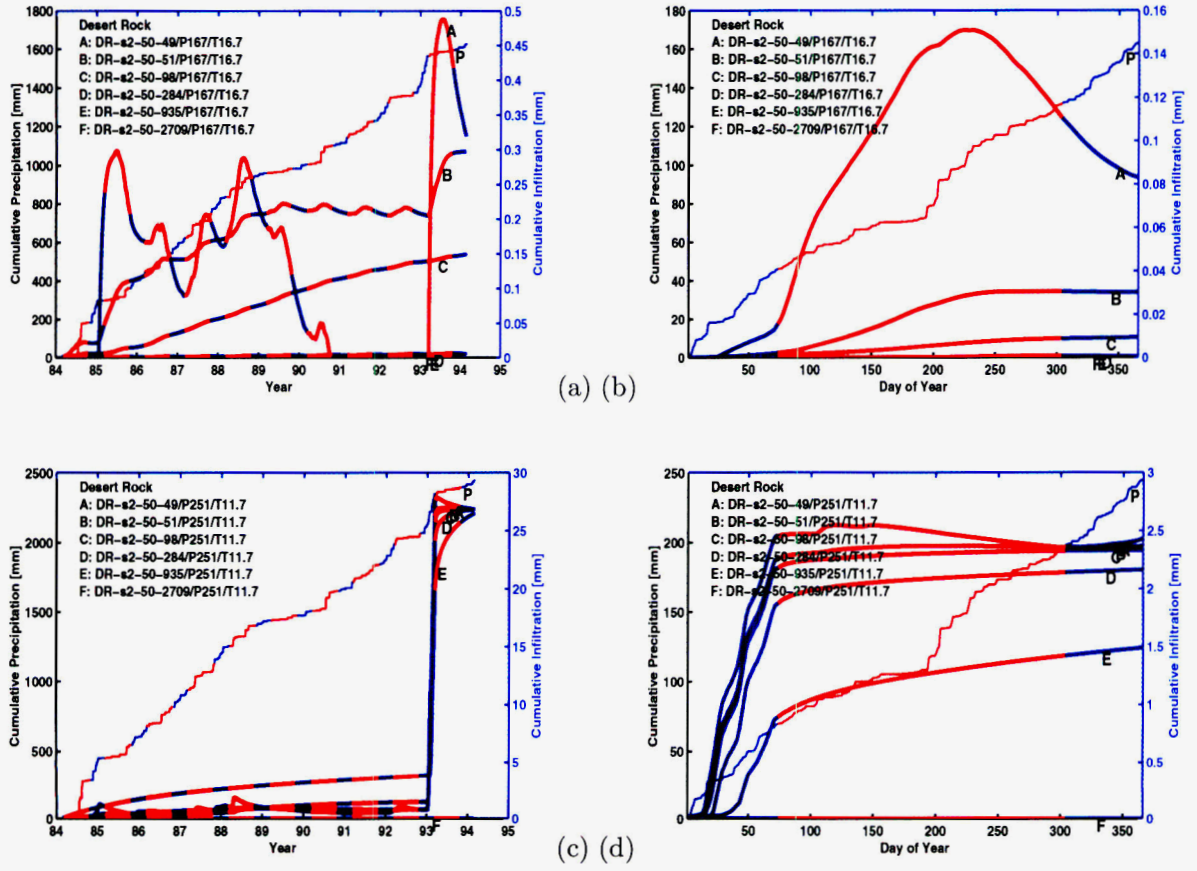

Figure 2-32: 8/11/00. Precipitation and moisture fluxes at 6 depths for 50 cm thickness of soil 2 using the Desert Rock meteorology. (a,c) Cumulative precipitation and moisture flux for different MAP and MAT scalings. (b,d) Corresponding mean daily values for the same simulations.

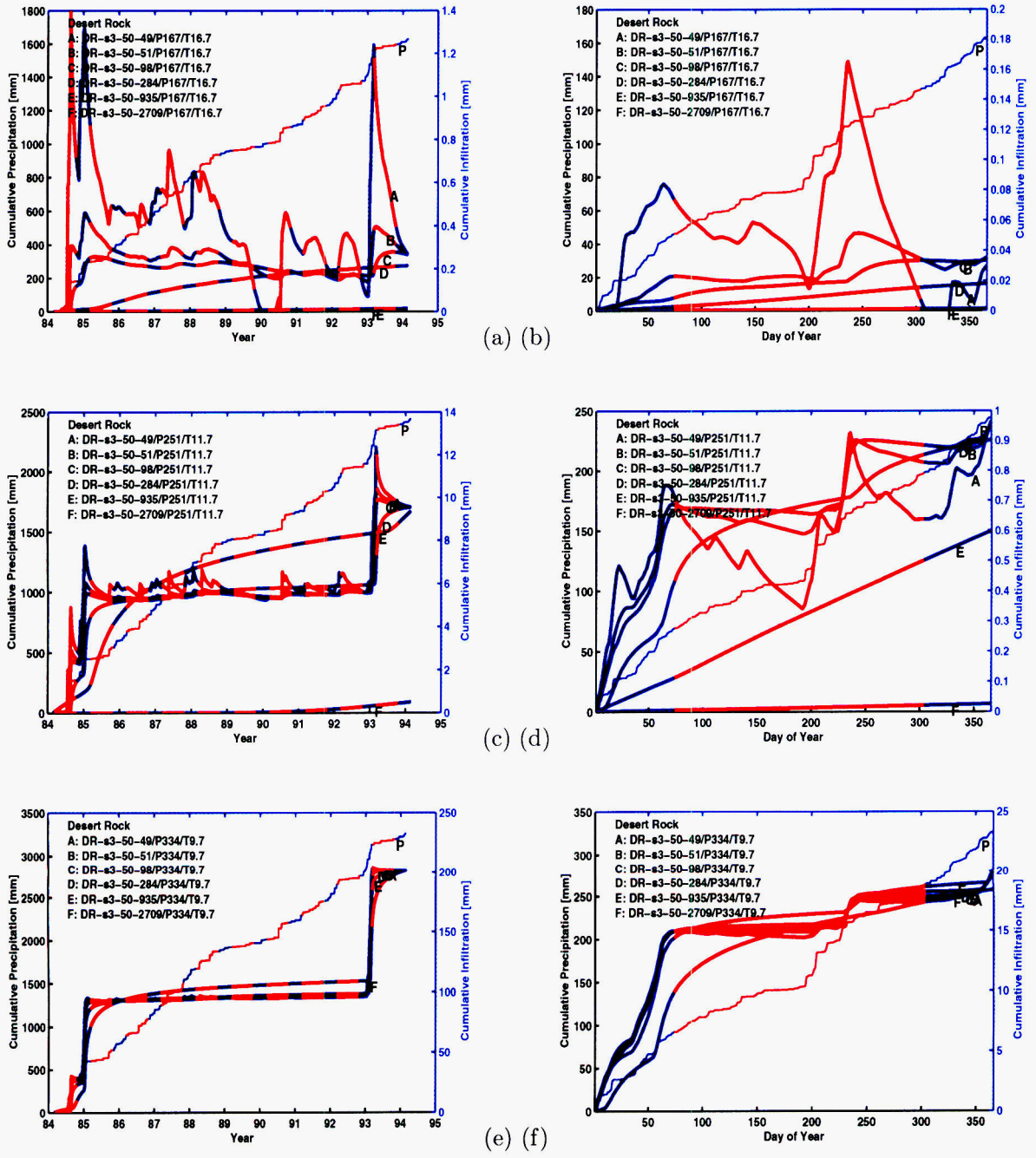

Figure 2-33: 8/11/00. Precipitation and moisture fluxes at 6 depths for 50 cm thickness of soil 3 using the Desert Rock meteorology. (a,c,e) Cumulative precipitation and moisture flux for different MAP and MAT scalings. (b,d,f) Corresponding mean daily values for the same simulations.

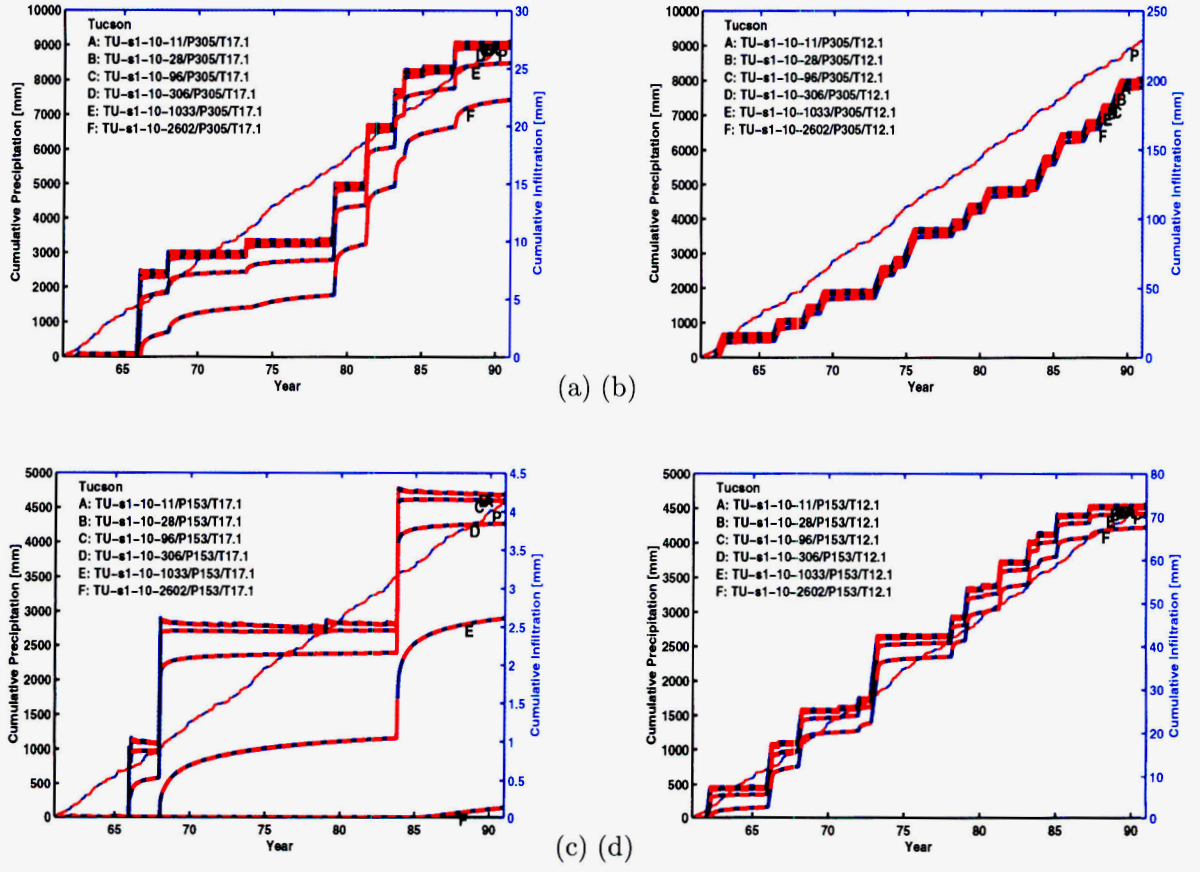

Figure 2-34: 8/11/00. Precipitation and moisture fluxes at 6 depths for 10 cm thickness of soil 1 using the Tucson meteorology. (a) Unscaled MAP with MAT like YM, (b) unscaled MAP with MAT 5 °C cooler than YM, (c) half MAP with MAT at YM values, (d) half MAP with MAT 5 °C cooler than YM.

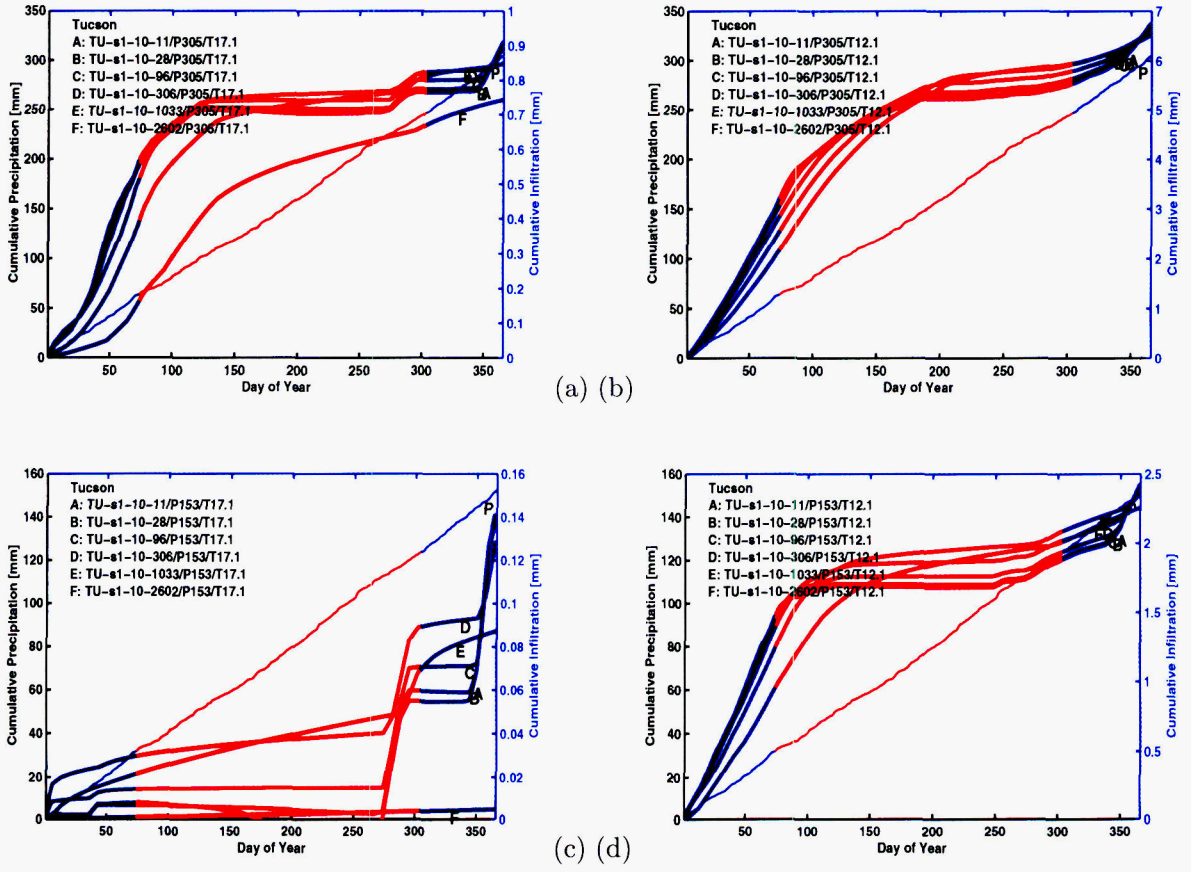

Figure 2-35: 8/11/00. Mean daily precipitation and moisture fluxes at 6 depths for 10 cm thickness of soil 1 using the Tucson meteorology. (a) Unscaled MAP with MAT like YM, (b) unscaled MAP with MAT 5 °C cooler than YM, (c) half MAP with MAT at YM values, (d) half MAP with MAT 5 °C cooler than YM.

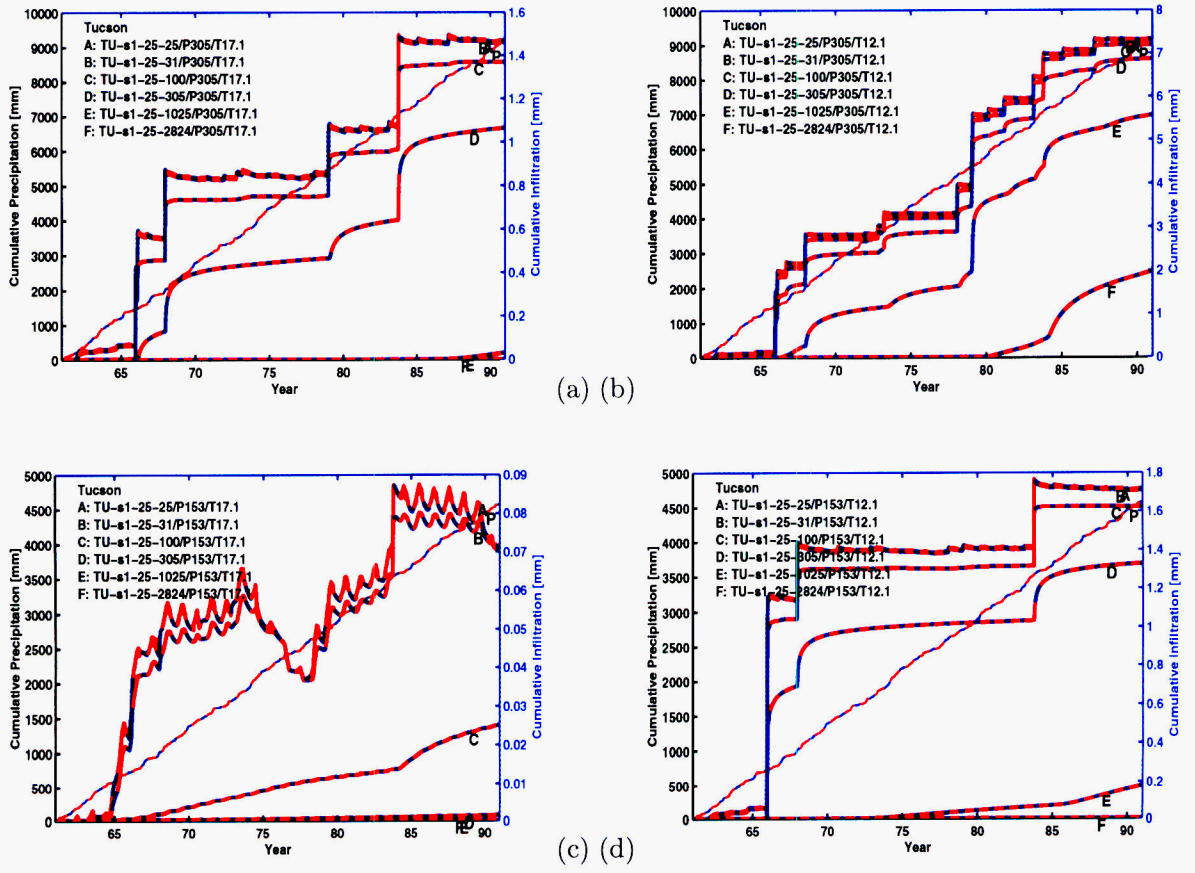

Figure 2-36: 8/11/00. Precipitation and moisture fluxes at 6 depths for 25 cm thickness of soil 1 using the Tucson meteorology. (a) Unscaled MAP with MAT like YM, (b) unscaled MAP with MAT 5 °C cooler than YM, (c) half MAP with MAT at YM values, (d) half MAP with MAT 5 °C cooler than YM.

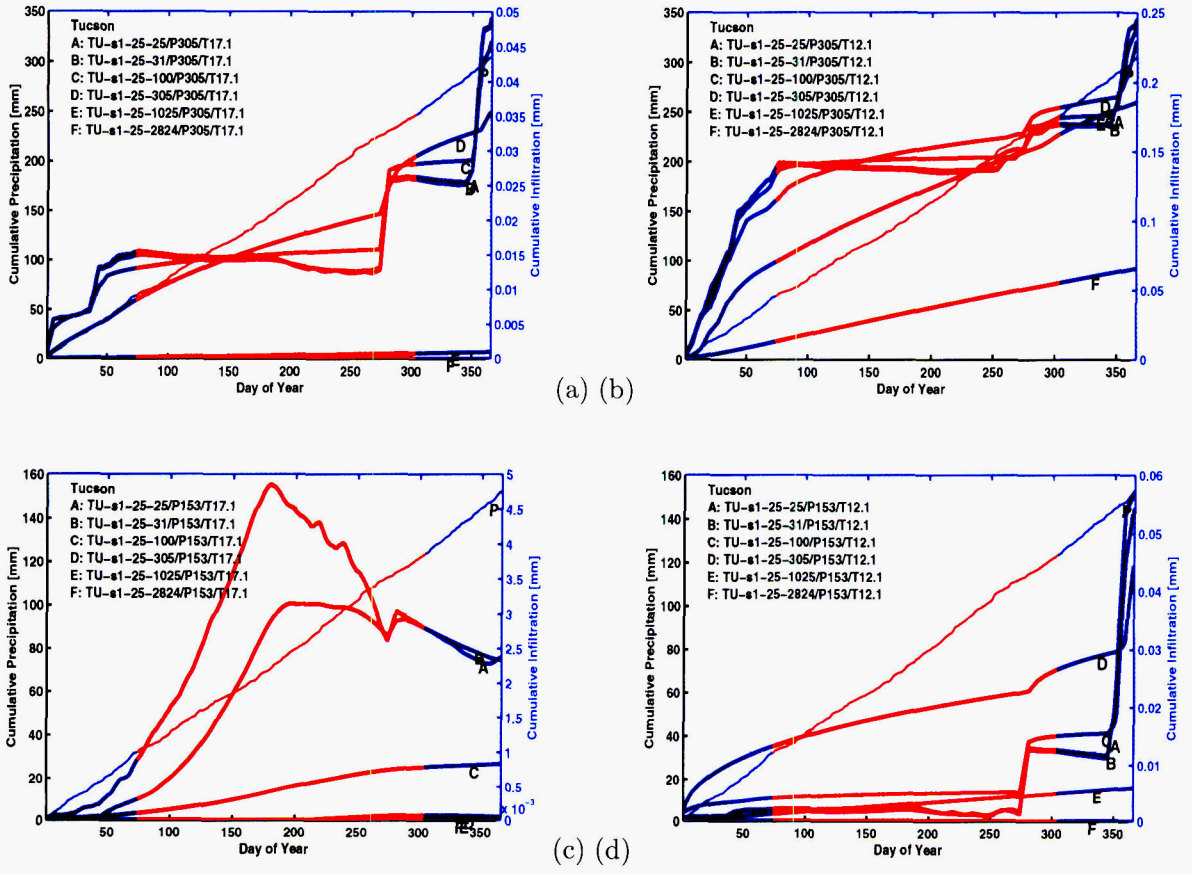

Figure 2-37: 8/11/00. Mean daily precipitation and moisture fluxes at 6 depths for 25 cm thickness of soil 1 using the Tucson meteorology. (a) Unscaled MAP with MAT like YM, (b) unscaled MAP with MAT 5 °C cooler than YM, (c) half MAP with MAT at YM values, (d) half MAP with MAT 5 °C cooler than YM.

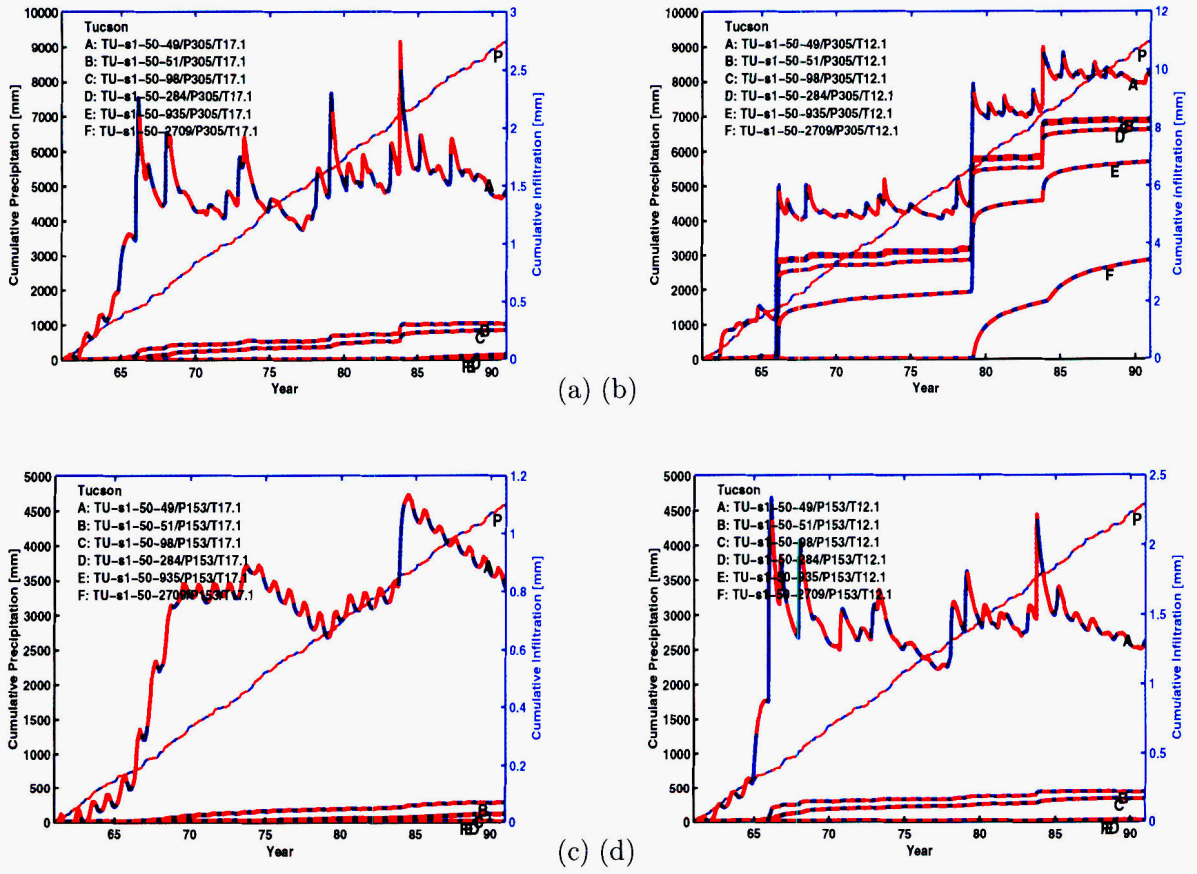

Figure 2-38: 8/11/00. Precipitation and moisture fluxes at 6 depths for 50 cm thickness of soil 1 using the Tucson meteorology. (a) Unscaled MAP with MAT like YM, (b) unscaled MAP with MAT 5 °C cooler than YM, (c) half MAP with MAT at YM values, (d) half MAP with MAT 5 °C cooler than YM.

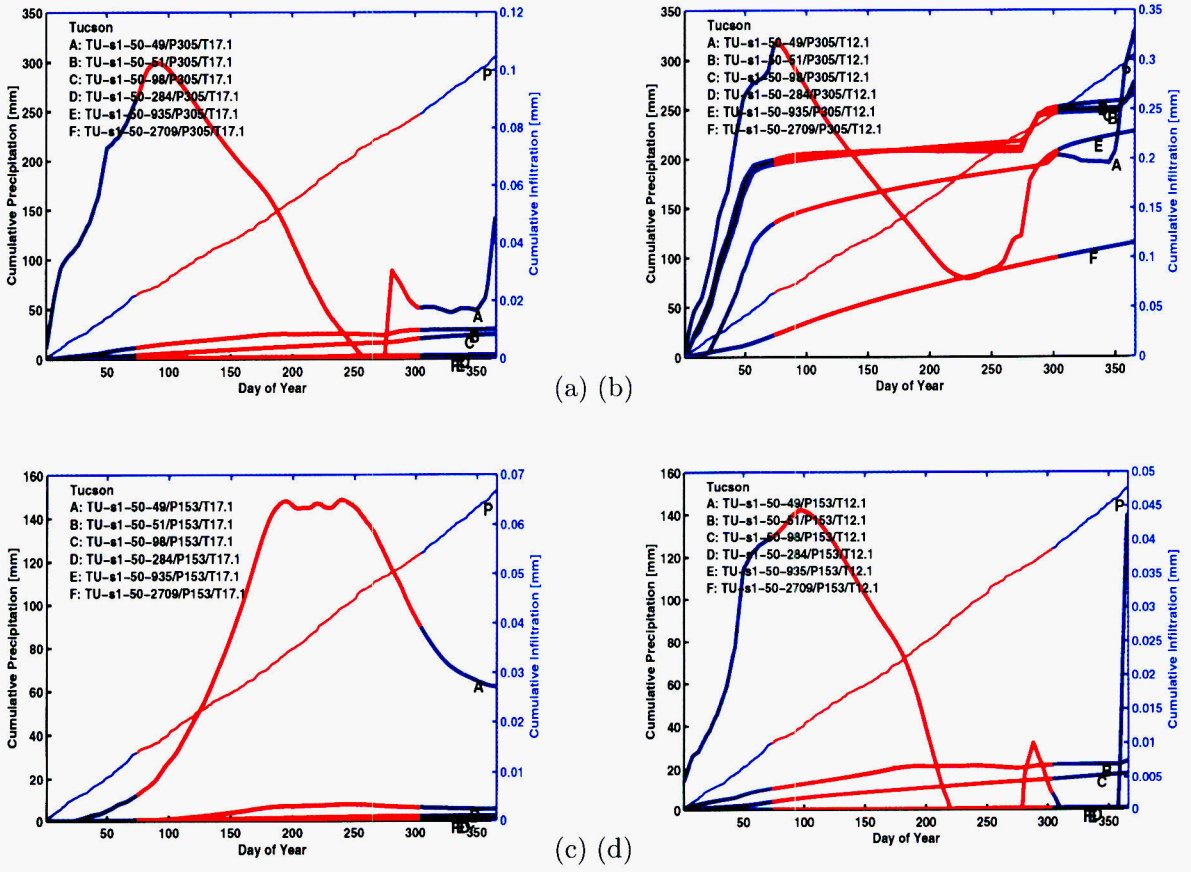

Figure 2-39: 8/11/00. Mean daily precipitation and moisture fluxes at 6 depths for 50 cm thickness of soil 1 using the Tucson meteorology. (a) Unscaled MAP with MAT like YM, (b) unscaled MAP with MAT 5 °C cooler than YM, (c) half MAP with MAT at YM values, (d) half MAP with MAT 5 °C cooler than YM.

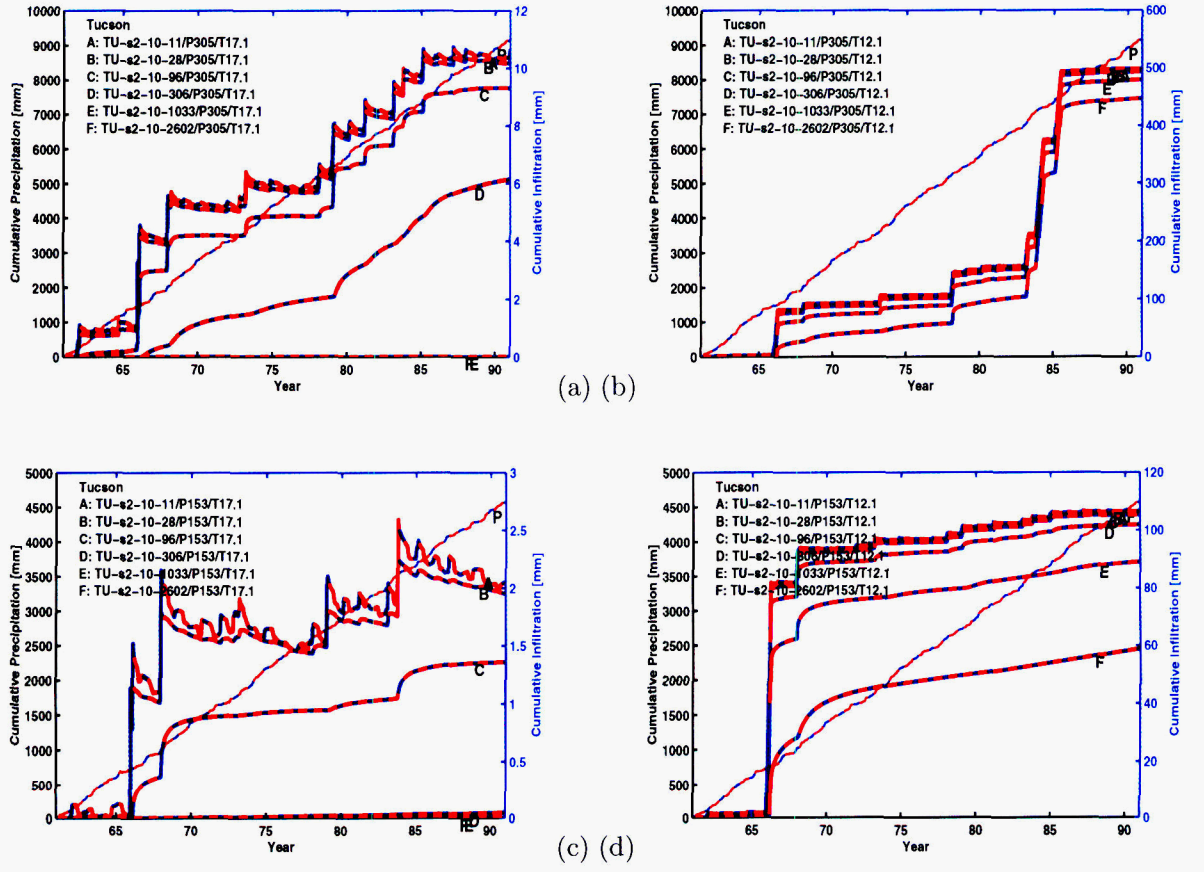

Figure 2-40: 8/11/00. Precipitation and moisture fluxes at 6 depths for 10 cm thickness of soil 2 using the Tucson meteorology. (a) Unscaled MAP with MAT like YM, (b) unscaled MAP with MAT 5 °C cooler than YM, (c) half MAP with MAT at YM values, (d) half MAP with MAT 5 °C cooler than YM.

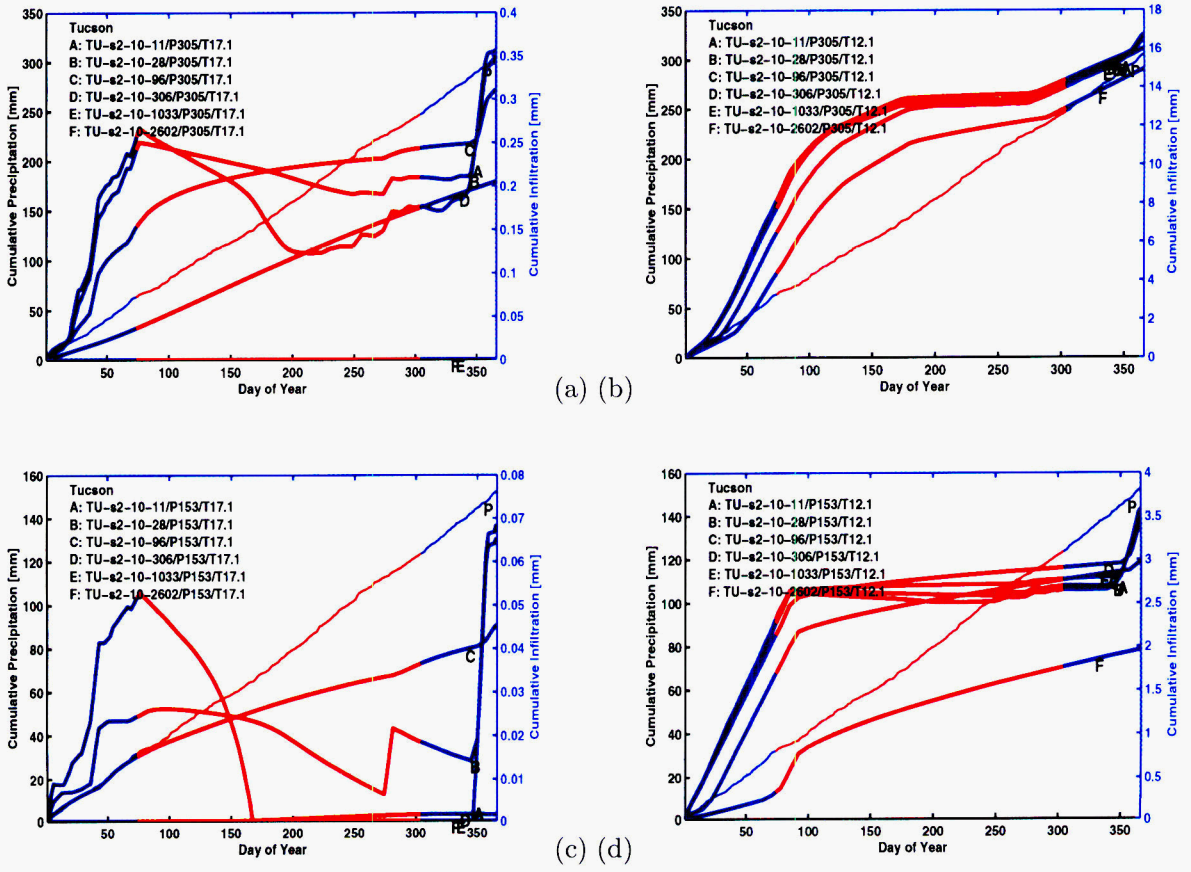

Figure 2-41: 8/11/00. Mean daily precipitation and moisture fluxes at 6 depths for 10 cm thickness of soil 2 using the Tucson meteorology. (a) Unscaled MAP with MAT like YM, (b) unscaled MAP with MAT 5 °C cooler than YM, (c) half MAP with MAT at YM values, (d) half MAP with MAT 5 °C cooler than YM.

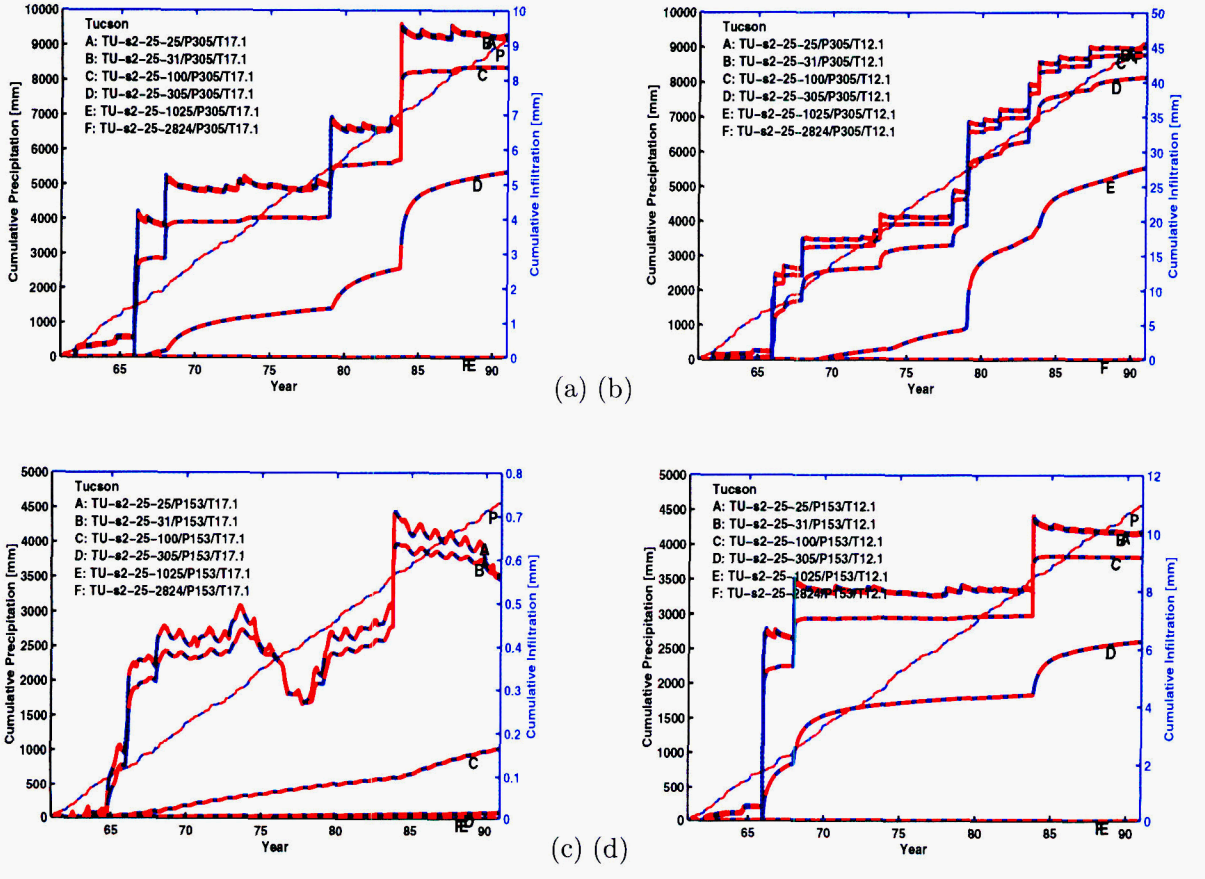

Figure 2-42: 8/11/00. Precipitation and moisture fluxes at 6 depths for 25 cm thickness of soil 2 using the Tucson meteorology. (a) Unscaled MAP with MAT like YM, (b) unscaled MAP with MAT 5 °C cooler than YM, (c) half MAP with MAT at YM values, (d) half MAP with MAT 5 °C cooler than YM.

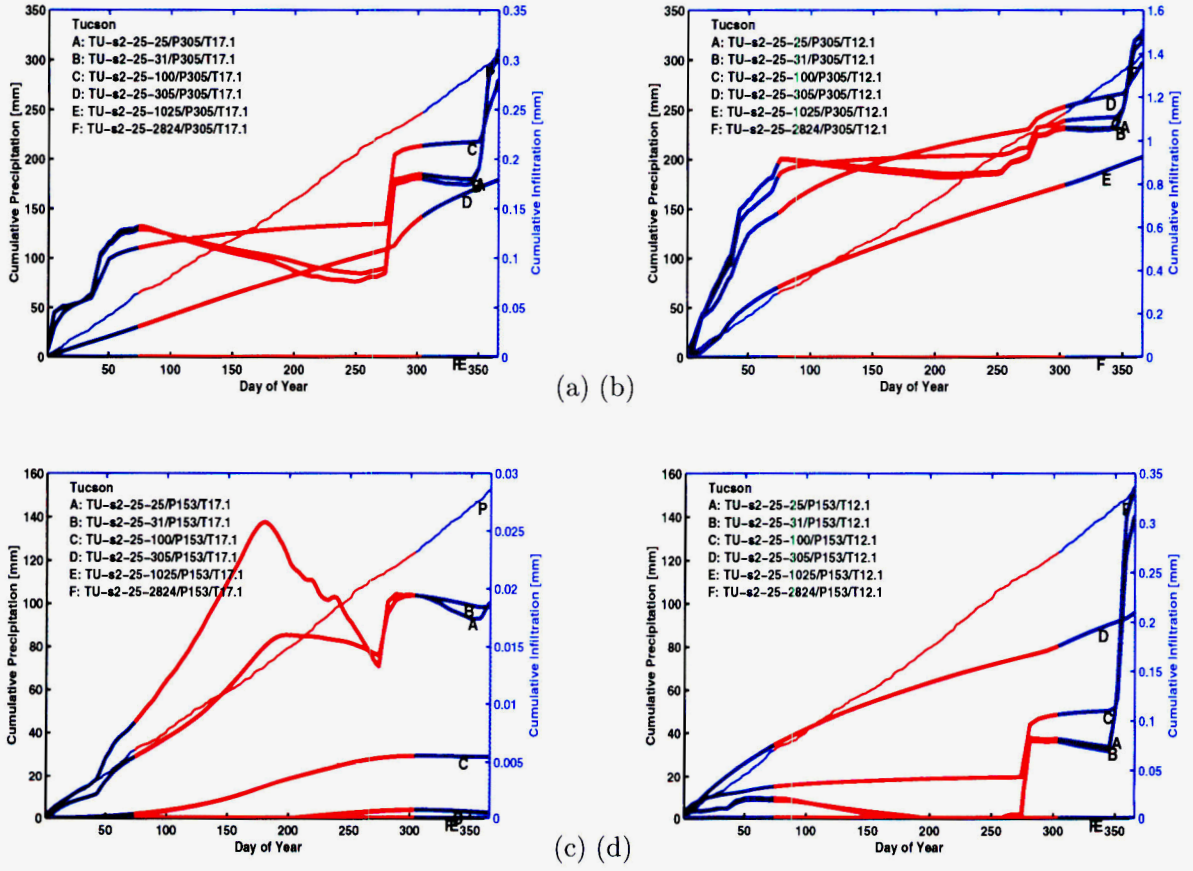

Figure 2-43: 8/11/00. Mean daily precipitation and moisture fluxes at 6 depths for 25 cm thickness of soil 2 using the Tucson meteorology. (a) Unscaled MAP with MAT like YM, (b) unscaled MAP with MAT 5 °C cooler than YM, (c) half MAP with MAT at YM values, (d) half MAP with MAT 5 °C cooler than YM.

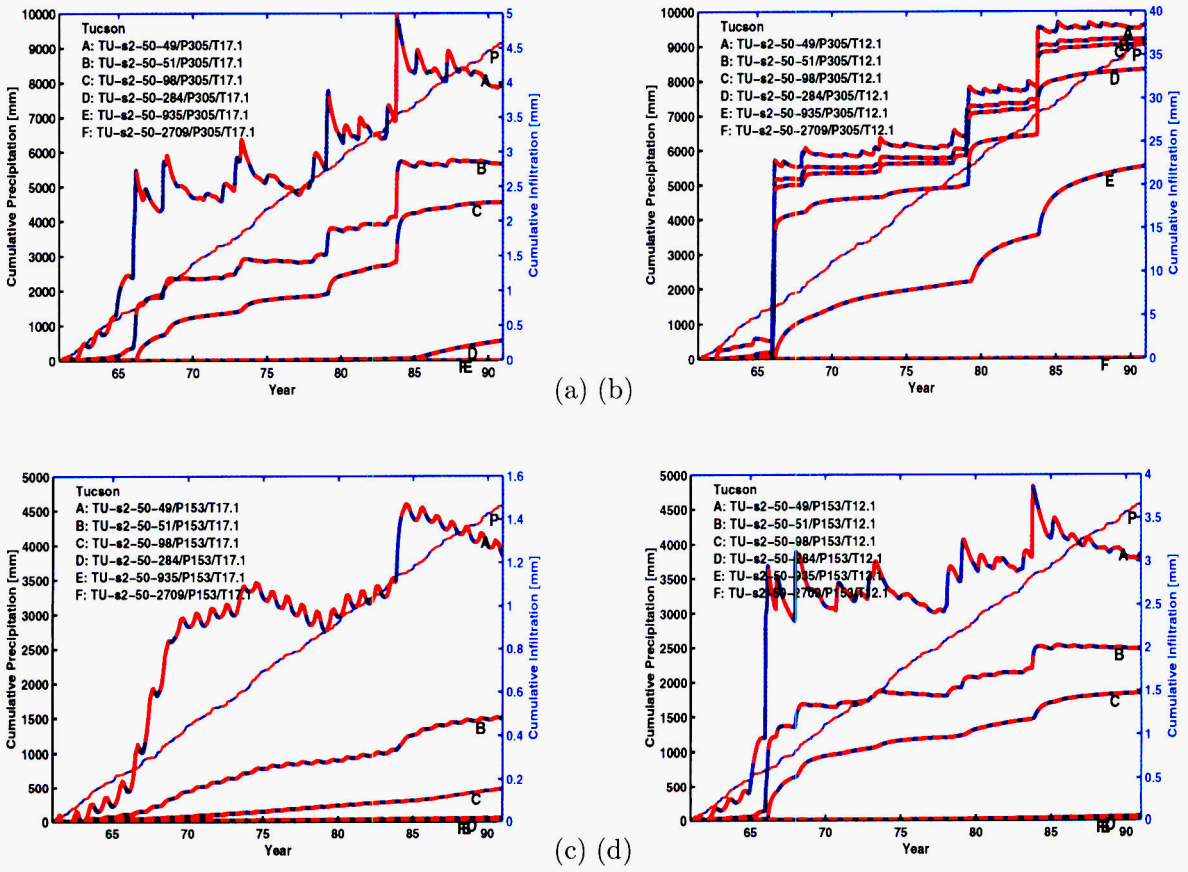

Figure 2-44: 8/11/00. Precipitation and moisture fluxes at 6 depths for 50 cm thickness of soil 2 using the Tucson meteorology. (a) Unscaled MAP with MAT like YM, (b) unscaled MAP with MAT 5 °C cooler than YM, (c) half MAP with MAT at YM values, (d) half MAP with MAT 5 °C cooler than YM.

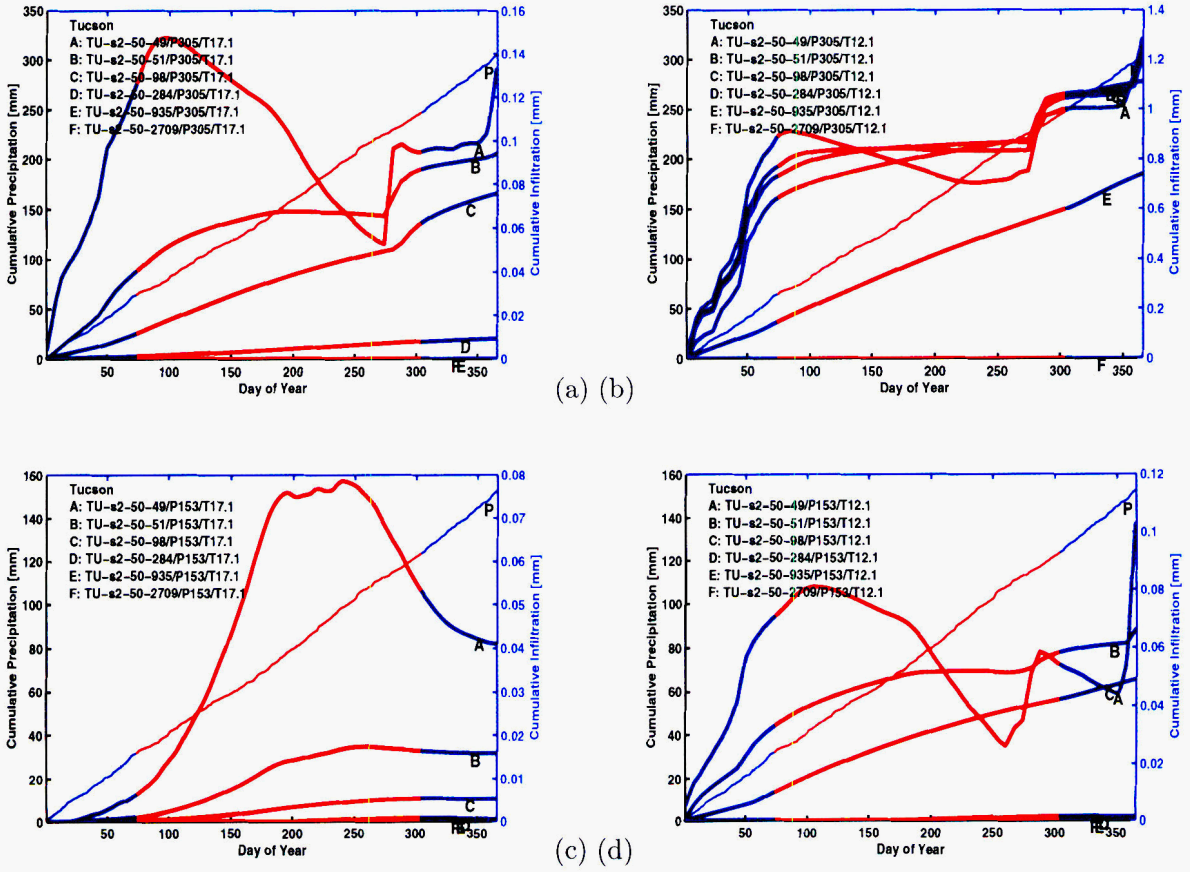

Figure 2-45: 8/11/00. Mean daily precipitation and moisture fluxes at 6 depths for 50 cm thickness of soil 2 using the Tucson meteorology. (a) Unscaled MAP with MAT like YM, (b) unscaled MAP with MAT 5 °C cooler than YM, (c) half MAP with MAT at YM values, (d) half MAP with MAT 5 °C cooler than YM.

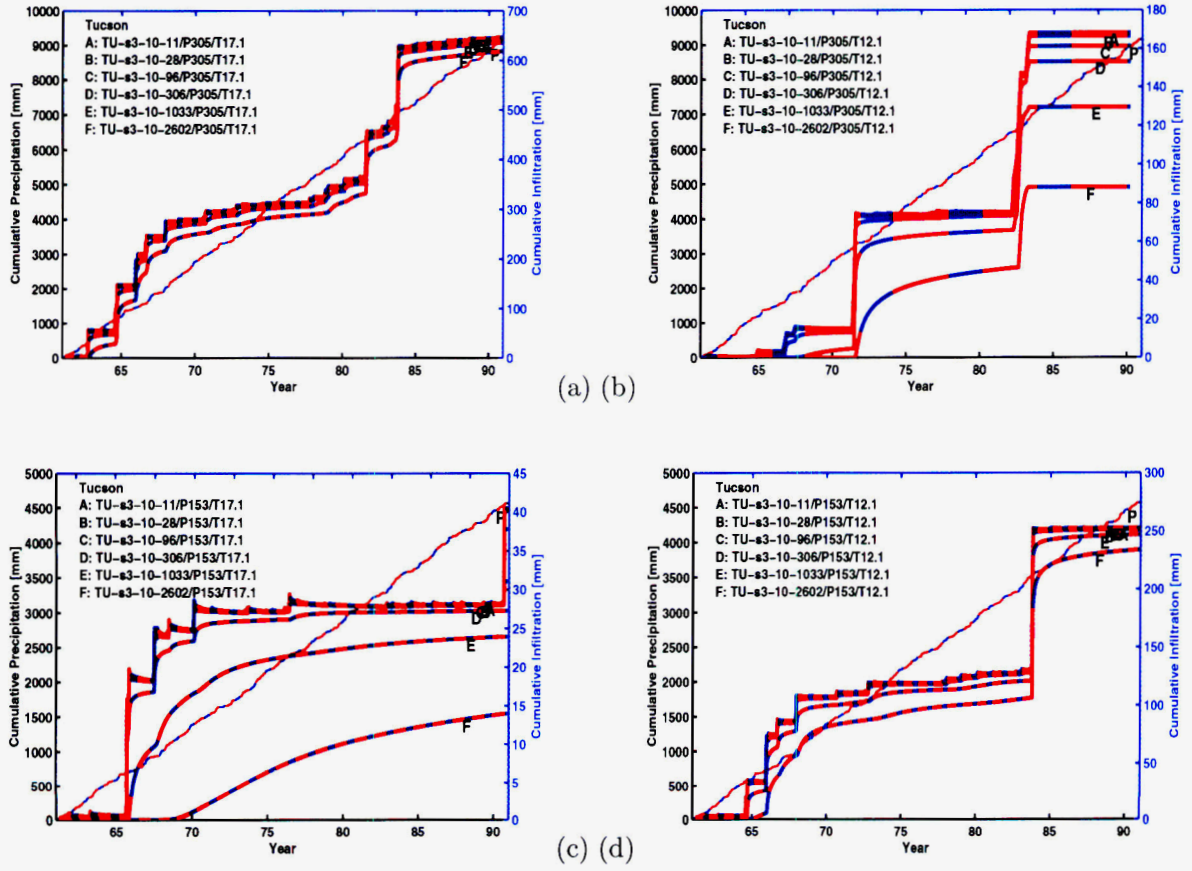

Figure 2-46: 8/11/00. Precipitation and moisture fluxes at 6 depths for 10 cm thickness of soil 3 using the Tucson meteorology. (a) Unscaled MAP with MAT like YM, (b) unscaled MAP with MAT 5 °C cooler than YM, (c) half MAP with MAT at YM values, (d) half MAP with MAT 5 °C cooler than YM.

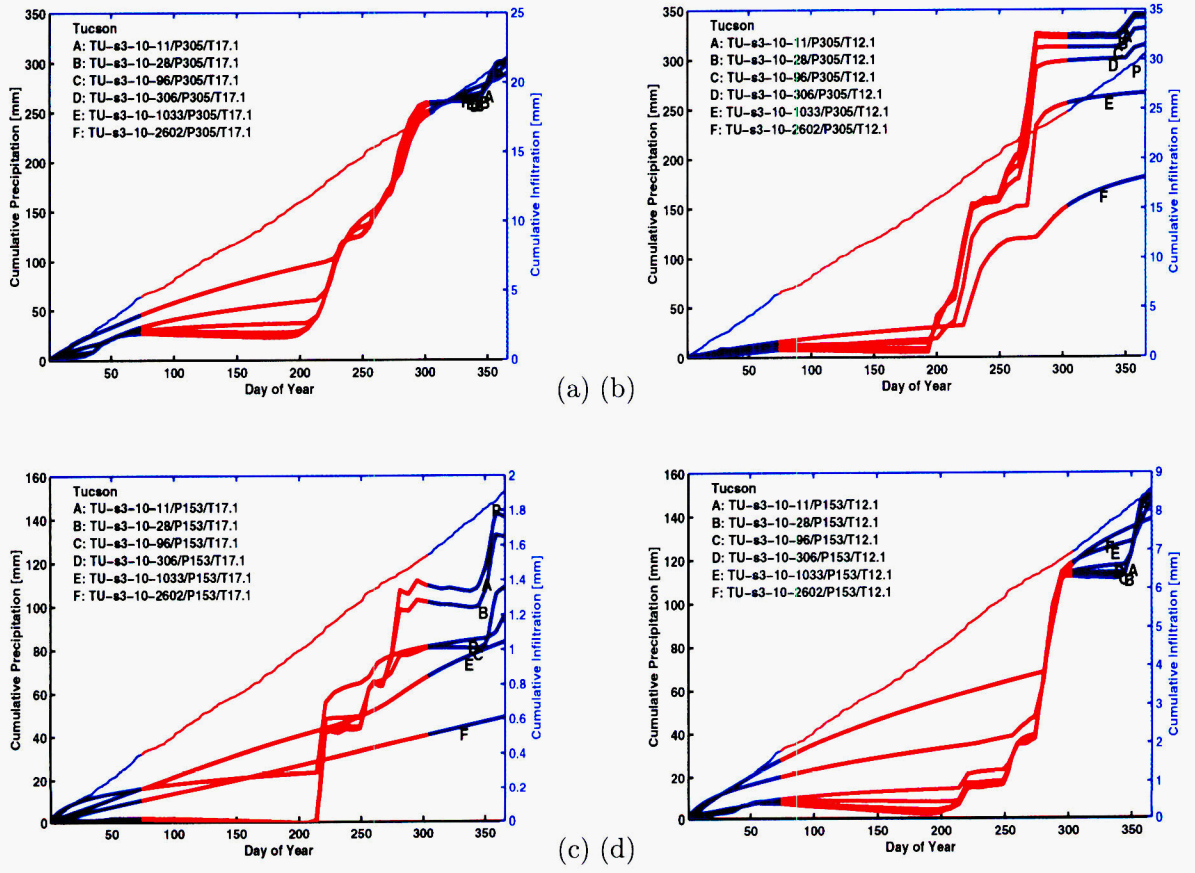

Figure 2-47: 8/11/00. Mean daily precipitation and moisture fluxes at 6 depths for 10 cm thickness of soil 3 using the Tucson meteorology. (a) Unscaled MAP with MAT like YM, (b) unscaled MAP with MAT 5 °C cooler than YM, (c) half MAP with MAT at YM values, (d) half MAP with MAT 5 °C cooler than YM.

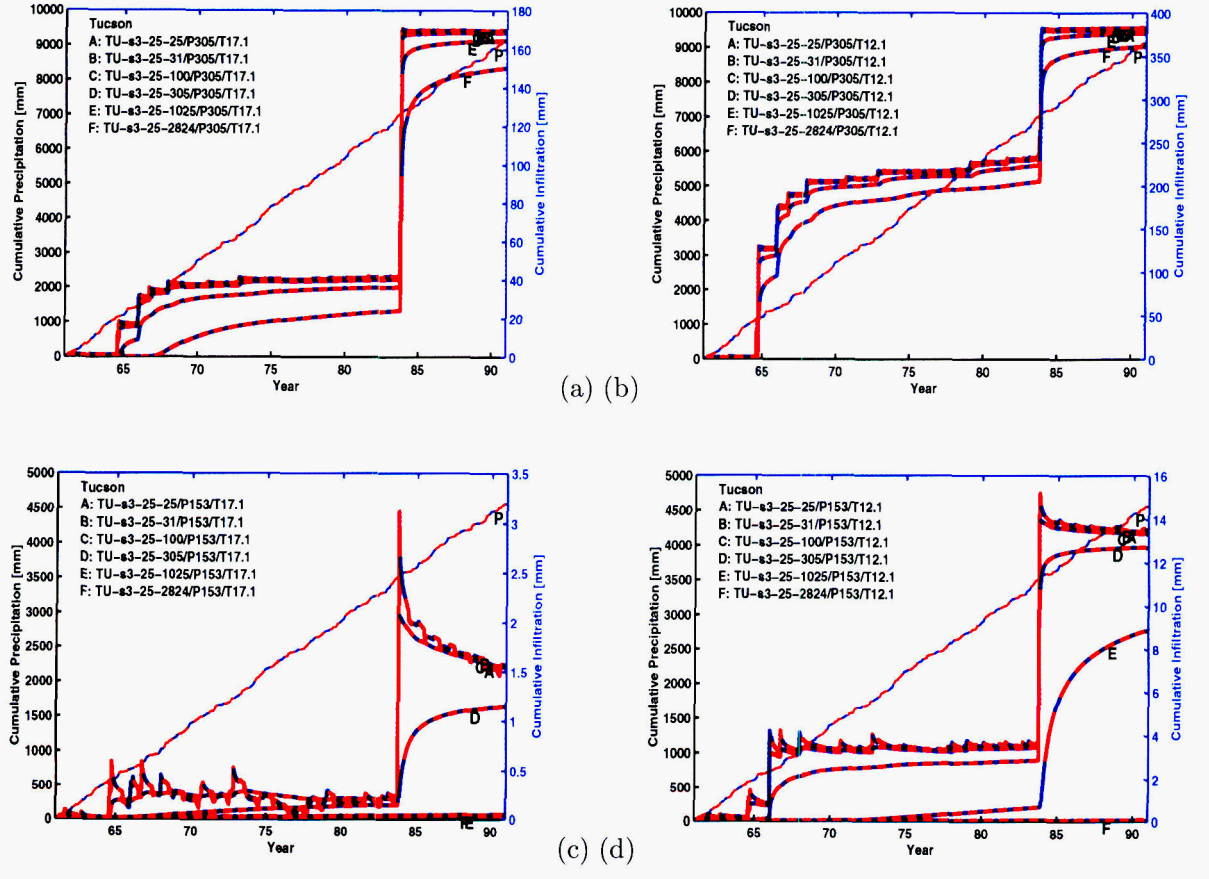

Figure 2-48: 8/11/00. Precipitation and moisture fluxes at 6 depths for 25 cm thickness of soil 3 using the Tucson meteorology. (a) Unscaled MAP with MAT like YM, (b) unscaled MAP with MAT 5 °C cooler than YM, (c) half MAP with MAT at YM values, (d) half MAP with MAT 5 °C cooler than YM.

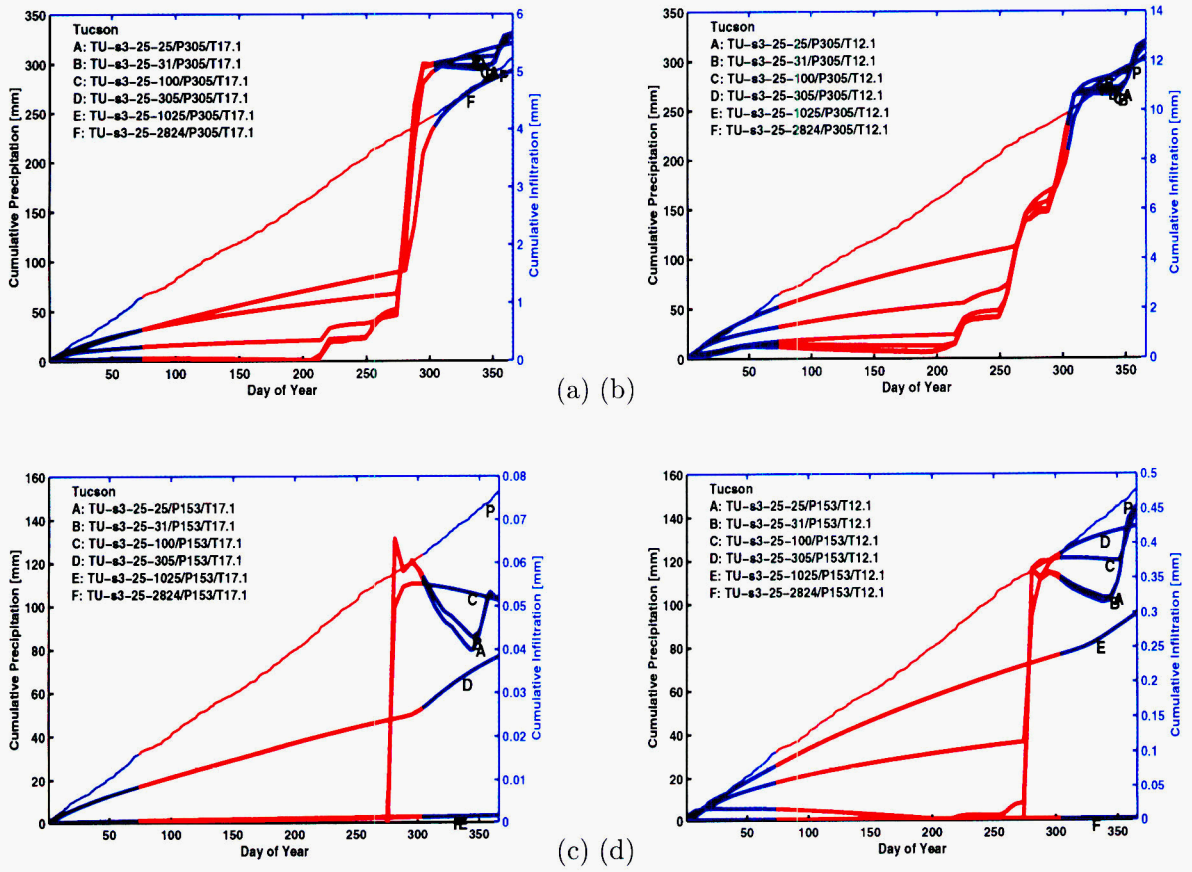

Figure 2-49: 8/11/00. Mean daily precipitation and moisture fluxes at 6 depths for 25 cm thickness of soil 3 using the Tucson meteorology. (a) Unscaled MAP with MAT like YM, (b) unscaled MAP with MAT 5 °C cooler than YM, (c) half MAP with MAT at YM values, (d) half MAP with MAT 5 °C cooler than YM.

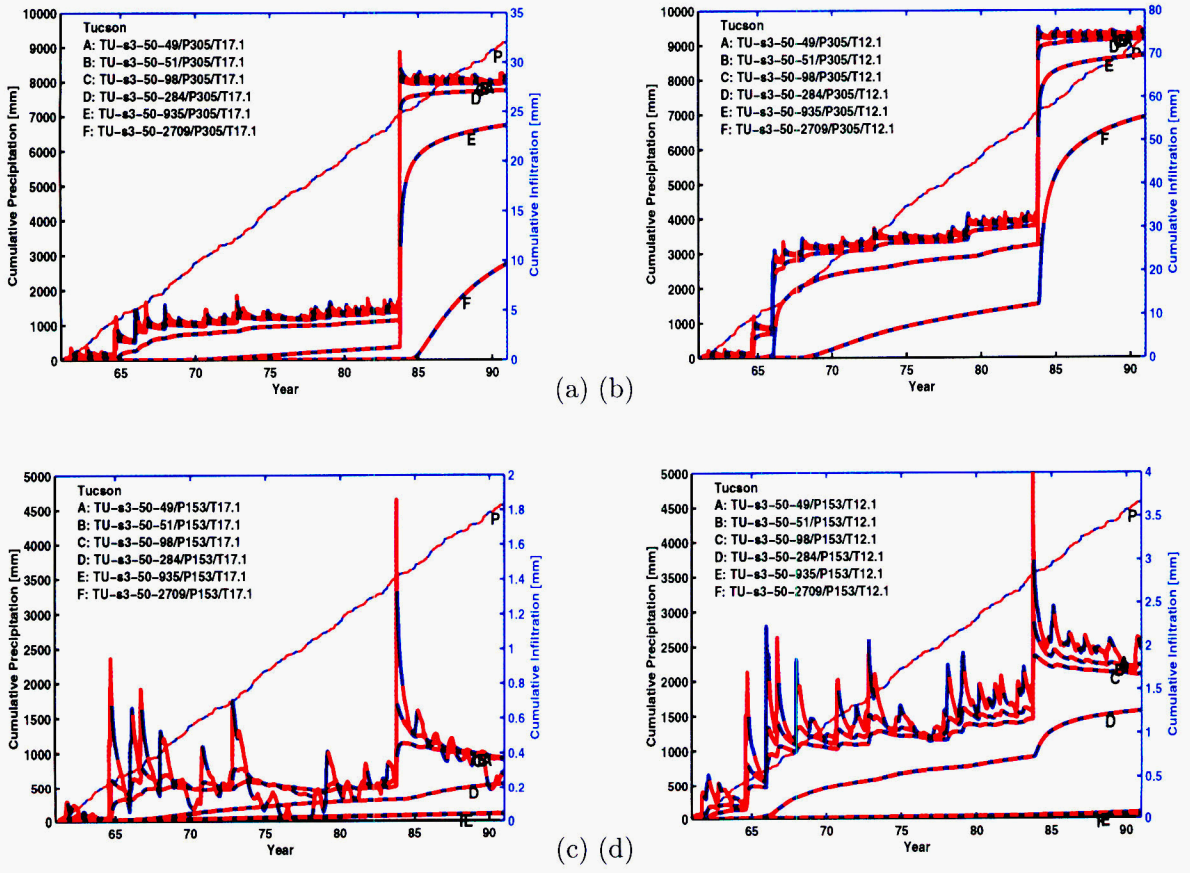

Figure 2-50: 8/11/00. Precipitation and moisture fluxes at 6 depths for 50 cm thickness of soil 3 using the Tucson meteorology. (a) Unscaled MAP with MAT like YM, (b) unscaled MAP with MAT 5 °C cooler than YM, (c) half MAP with MAT at YM values, (d) half MAP with MAT 5 °C cooler than YM.

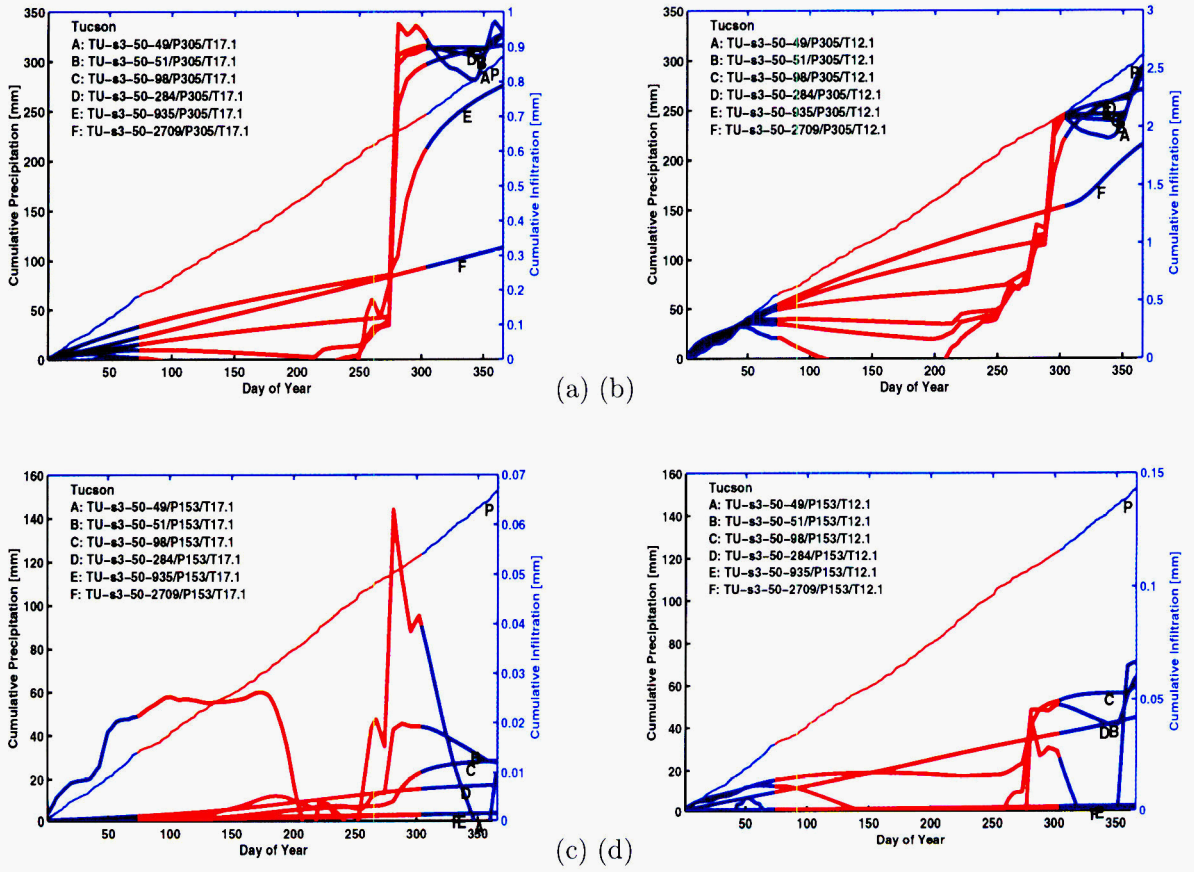

Figure 2-51: 8/11/00. Mean daily precipitation and moisture fluxes at 6 depths for 50 cm thickness of soil 3 using the Tucson meteorology. (a) Unscaled MAP with MAT like YM, (b) unscaled MAP with MAT 5 °C cooler than YM, (c) half MAP with MAT at YM values, (d) half MAP with MAT 5 °C cooler than YM.

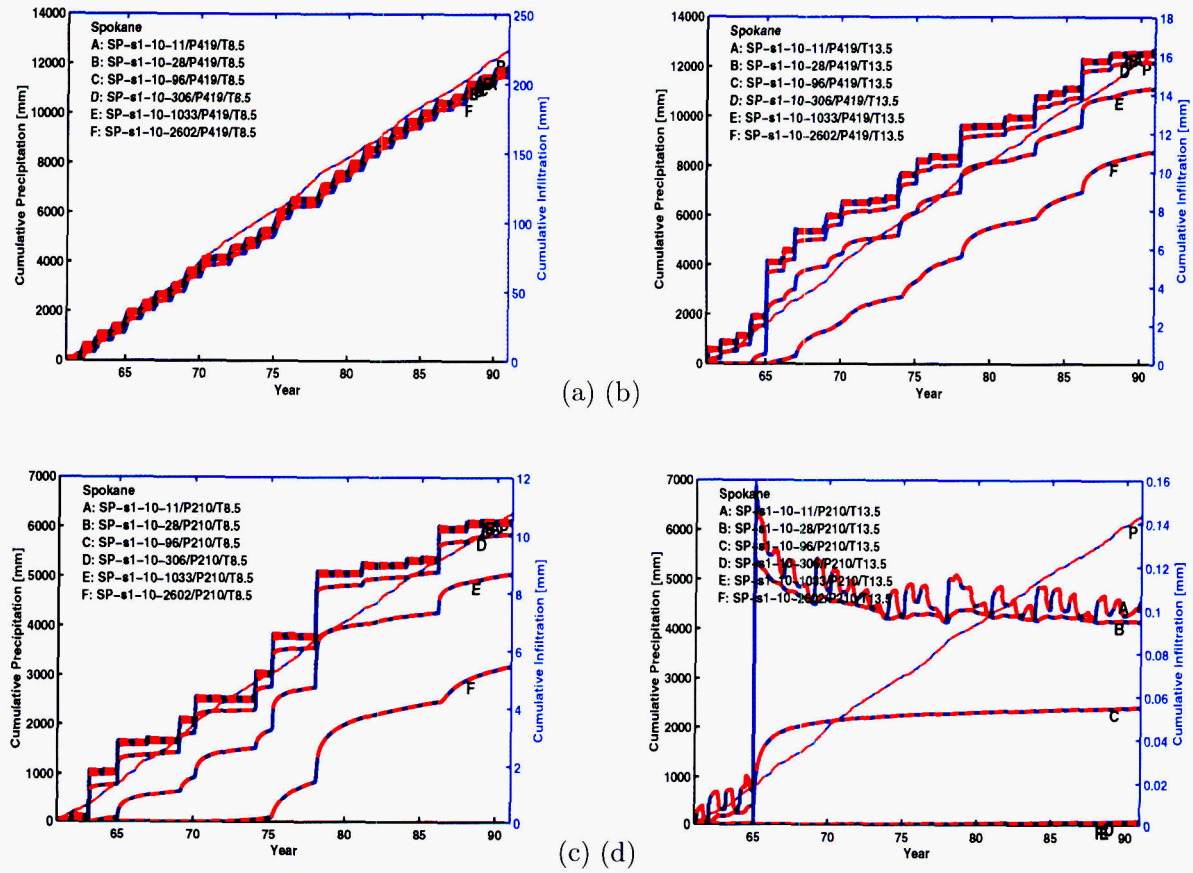

Figure 2-52: 8/11/00. Precipitation and moisture fluxes at 6 depths for 10 cm thickness of soil 1 using the Spokane meteorology. (a) Unscaled MAP with MAT at present values, (b) unscaled MAP with MAT 5 °C warmer than present, (c) half MAP with MAT at present values, (d) half MAP with MAT 5 °C warmer than present.

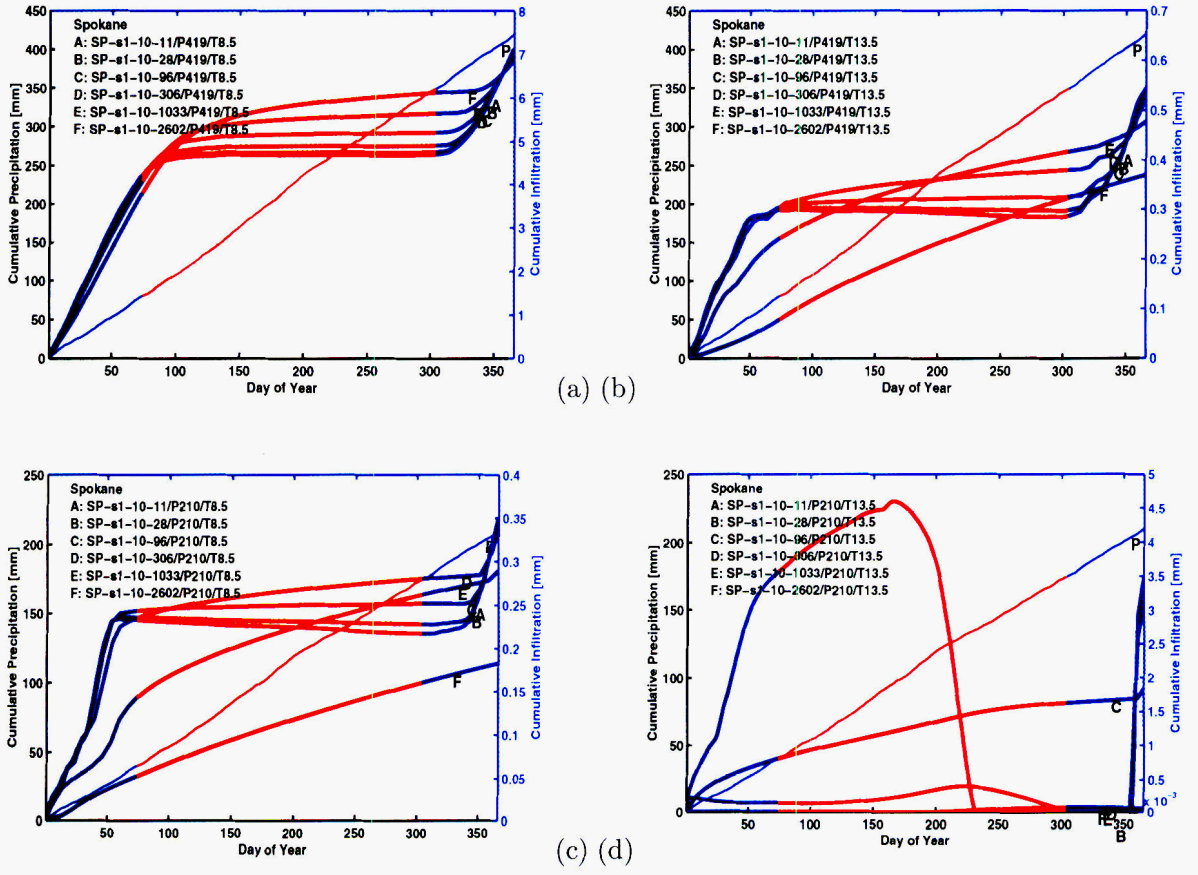

Figure 2-53: 8/11/00. Mean daily precipitation and moisture fluxes at 6 depths for 10 cm thickness of soil 1 using the Spokane meteorology. (a) Unscaled MAP with MAT at present values, (b) unscaled MAP with MAT 5 °C warmer than present, (c) half MAP with MAT at present values, (d) half MAP with MAT 5 °C warmer than present.

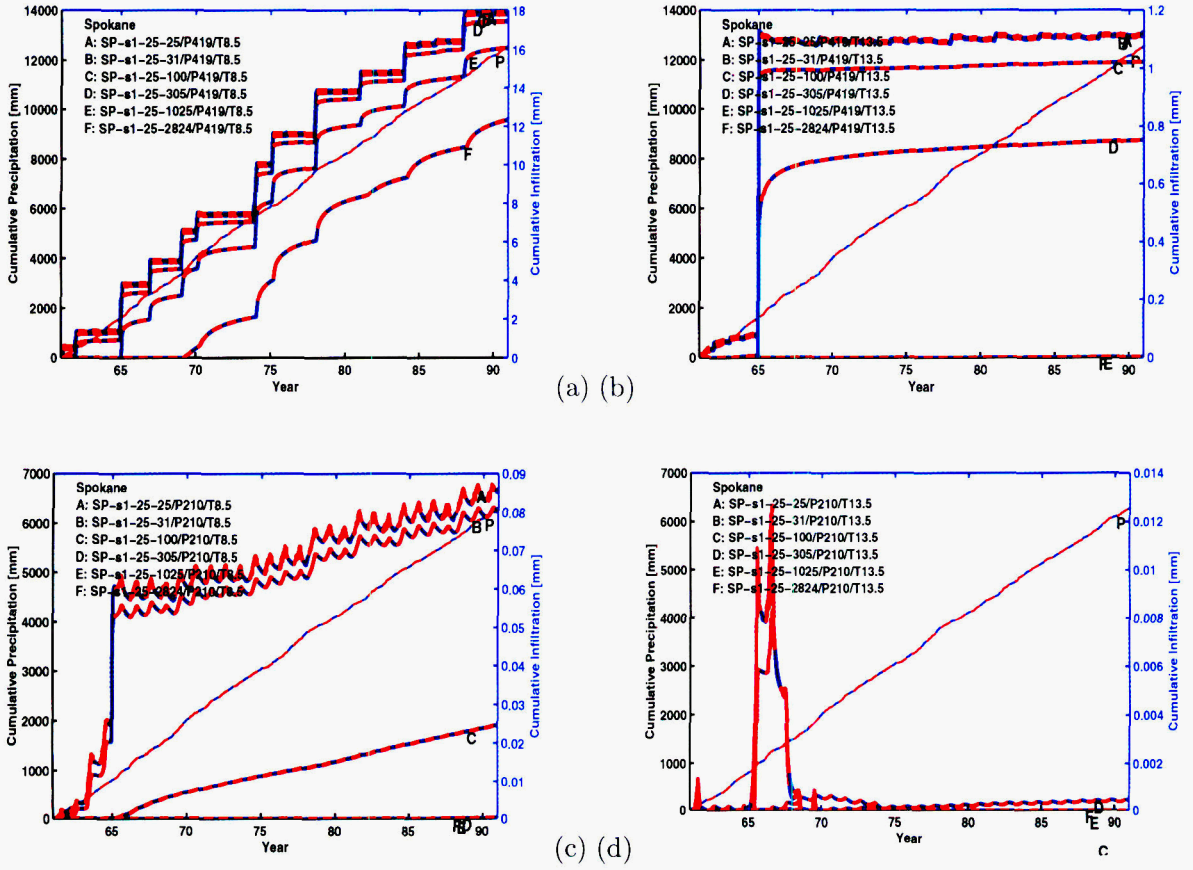

Figure 2-54: 8/11/00. Precipitation and moisture fluxes at 6 depths for 25 cm thickness of soil 1 using the Spokane meteorology. (a) Unscaled MAP with MAT at present values, (b) unscaled MAP with MAT 5 °C warmer than present, (c) half MAP with MAT at present values, (d) half MAP with MAT 5 °C warmer than present.

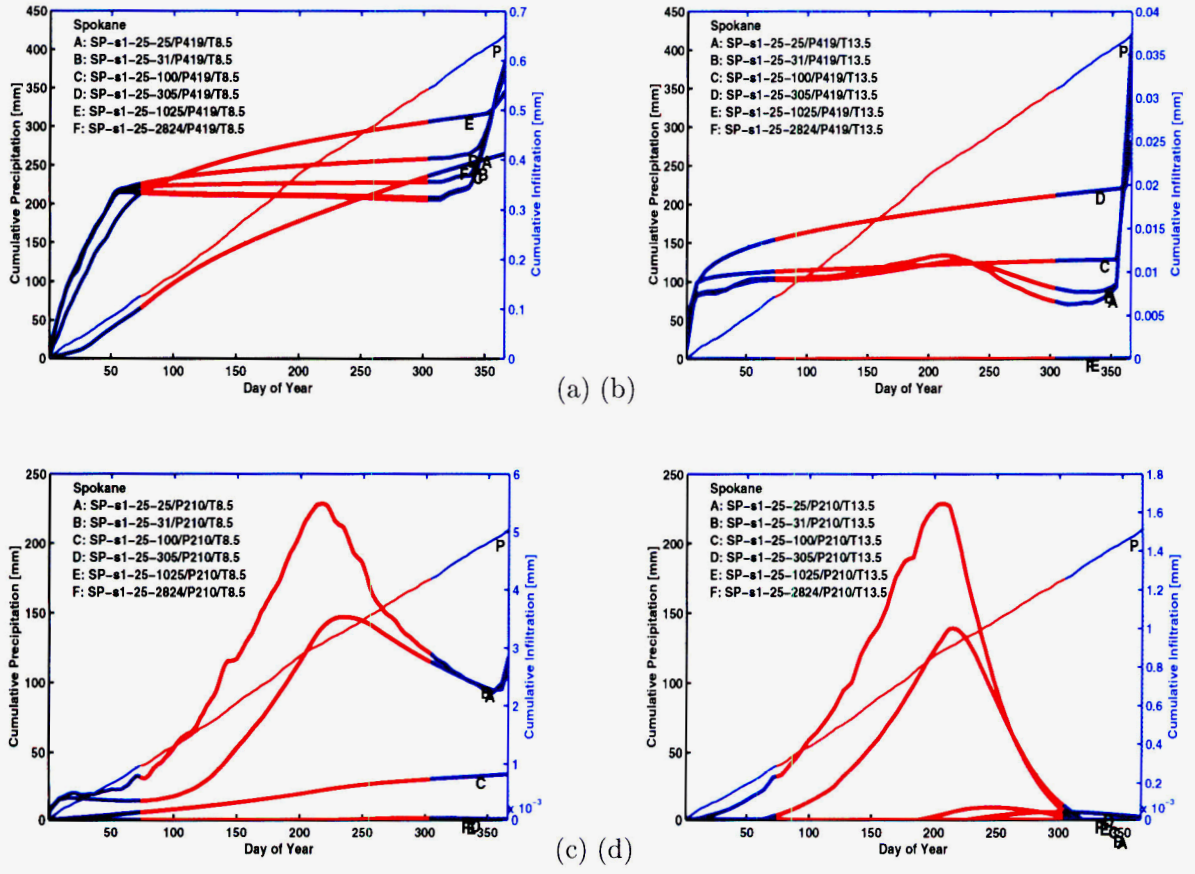

Figure 2-55: 8/11/00. Mean daily precipitation and moisture fluxes at 6 depths for 25 cm thickness of soil 1 using the Spokane meteorology. (a) Unscaled MAP with MAT at present values, (b) unscaled MAP with MAT 5 °C warmer than present, (c) half MAP with MAT at present values, (d) half MAP with MAT 5 °C warmer than present.

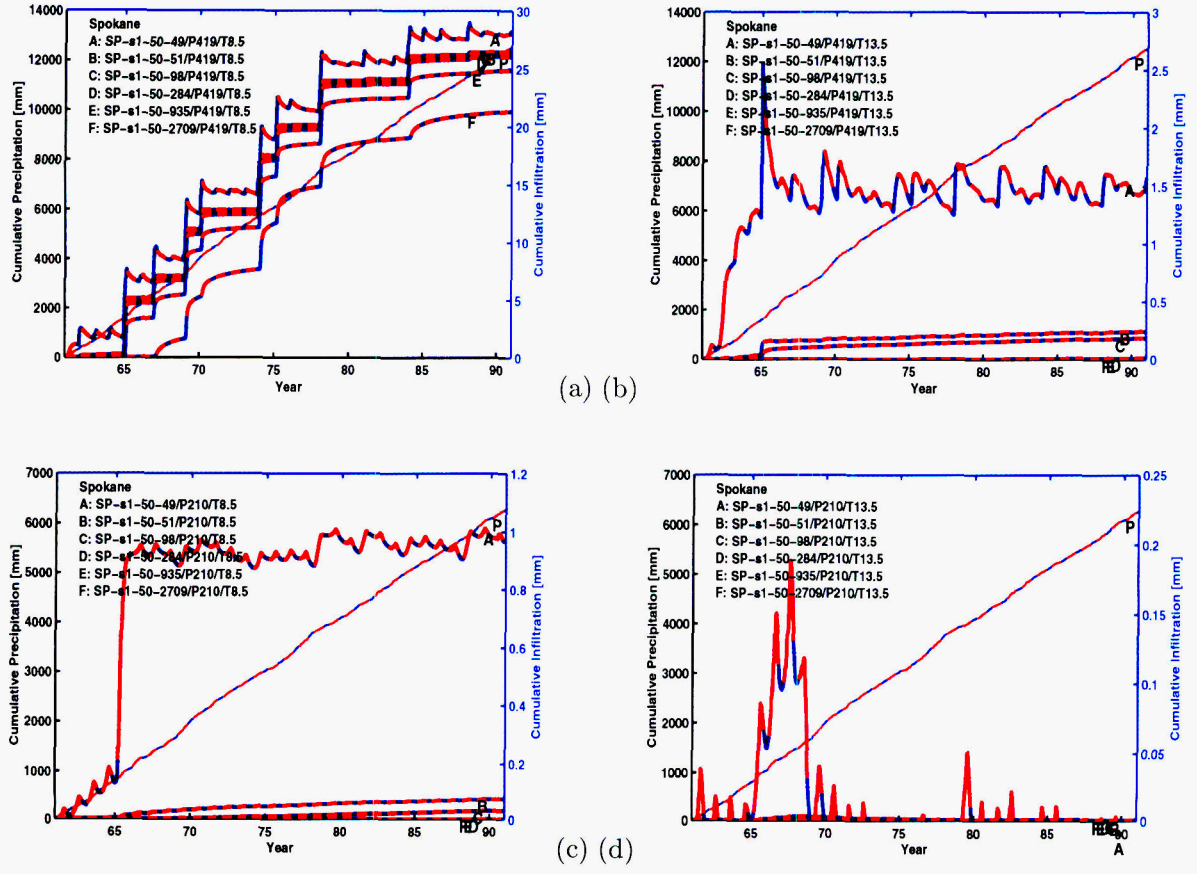

Figure 2-56: 8/11/00. Precipitation and moisture fluxes at 6 depths for 50 cm thickness of soil 1 using the Spokane meteorology. (a) Unscaled MAP with MAT at present values, (b) unscaled MAP with MAT 5 °C warmer than present, (c) half MAP with MAT at present values, (d) half MAP with MAT 5 °C warmer than present.

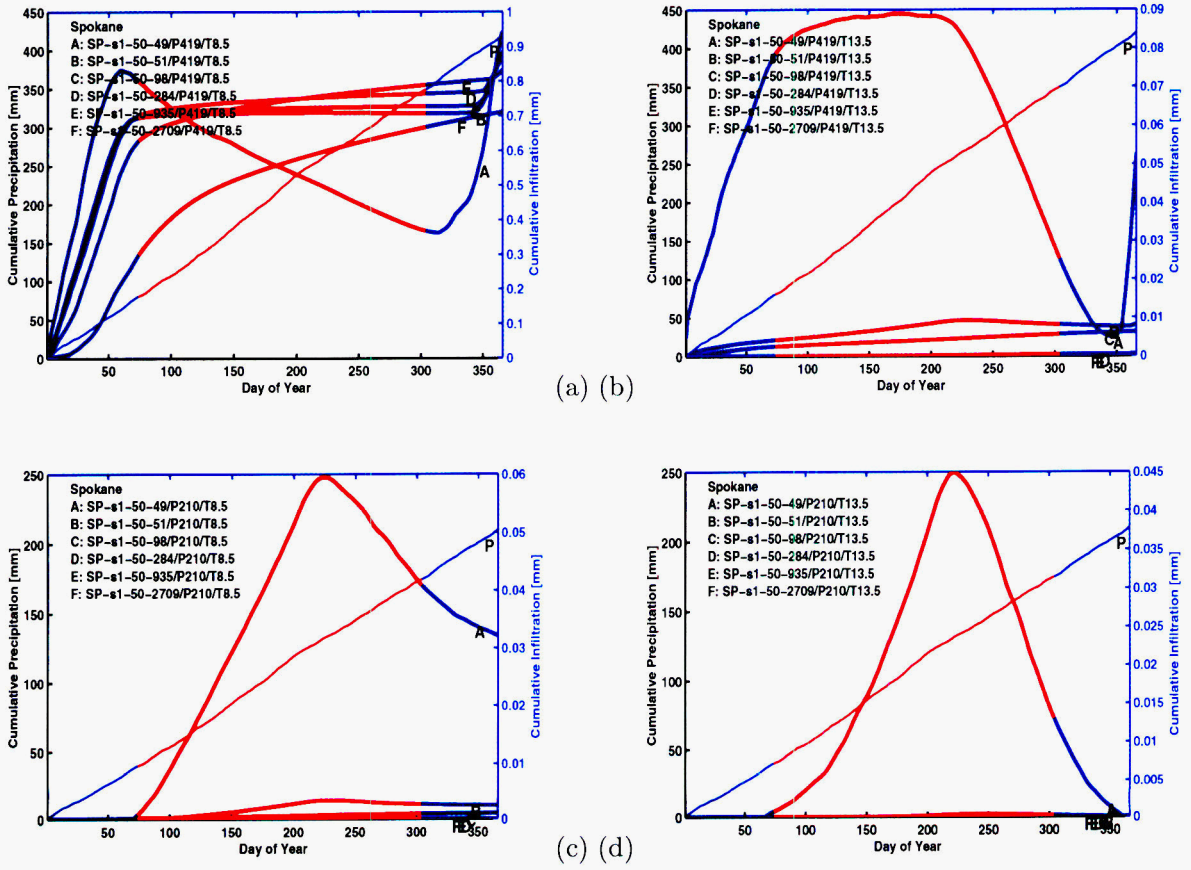

Figure 2-57: 8/11/00. Mean daily precipitation and moisture fluxes at 6 depths for 50 cm thickness of soil 1 using the Spokane meteorology. (a) Unscaled MAP with MAT at present values, (b) unscaled MAP with MAT 5 °C warmer than present, (c) half MAP with MAT at present values, (d) half MAP with MAT 5 °C warmer than present.

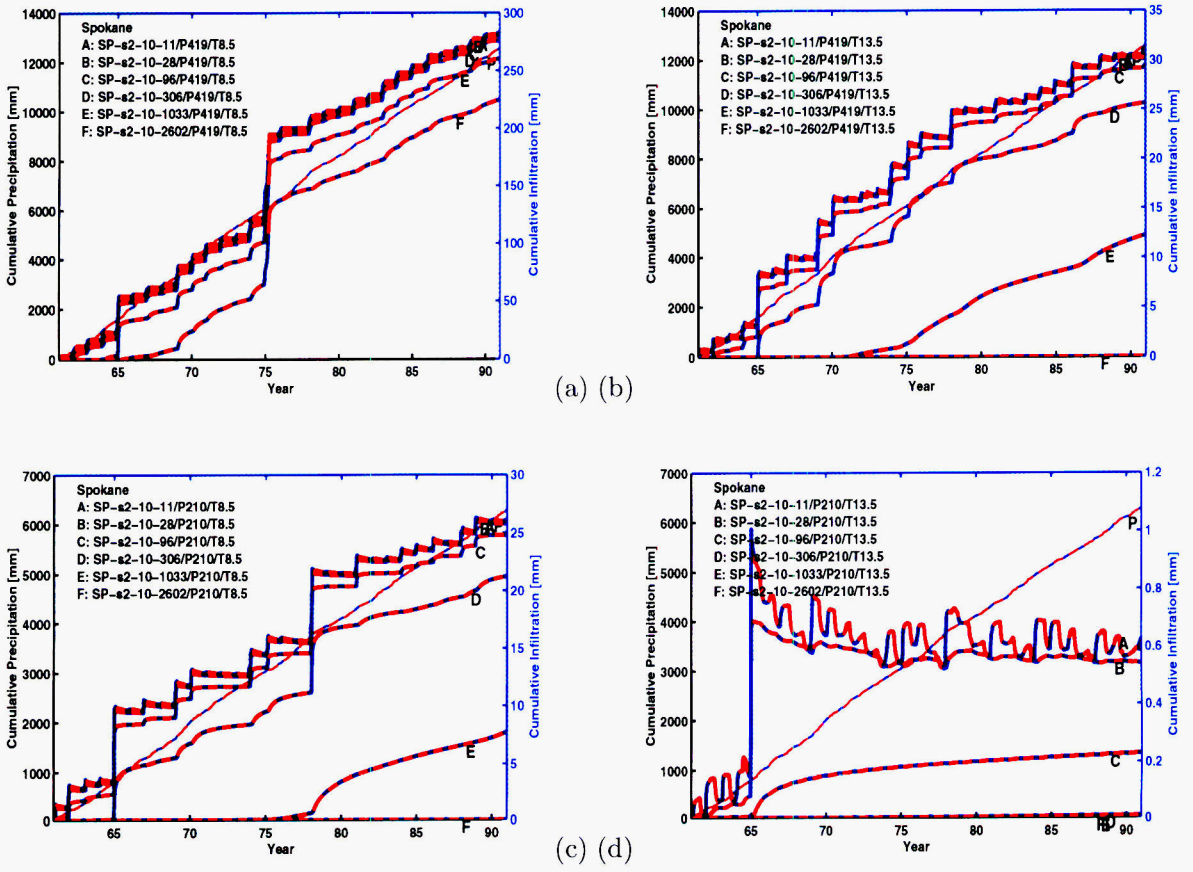

Figure 2-58: 8/11/00. Precipitation and moisture fluxes at 6 depths for 10 cm thickness of soil 2 using the Spokane meteorology. (a) Unscaled MAP with MAT at present values, (b) unscaled MAP with MAT 5 °C warmer than present, (c) half MAP with MAT at present values, (d) half MAP with MAT 5 °C warmer than present.

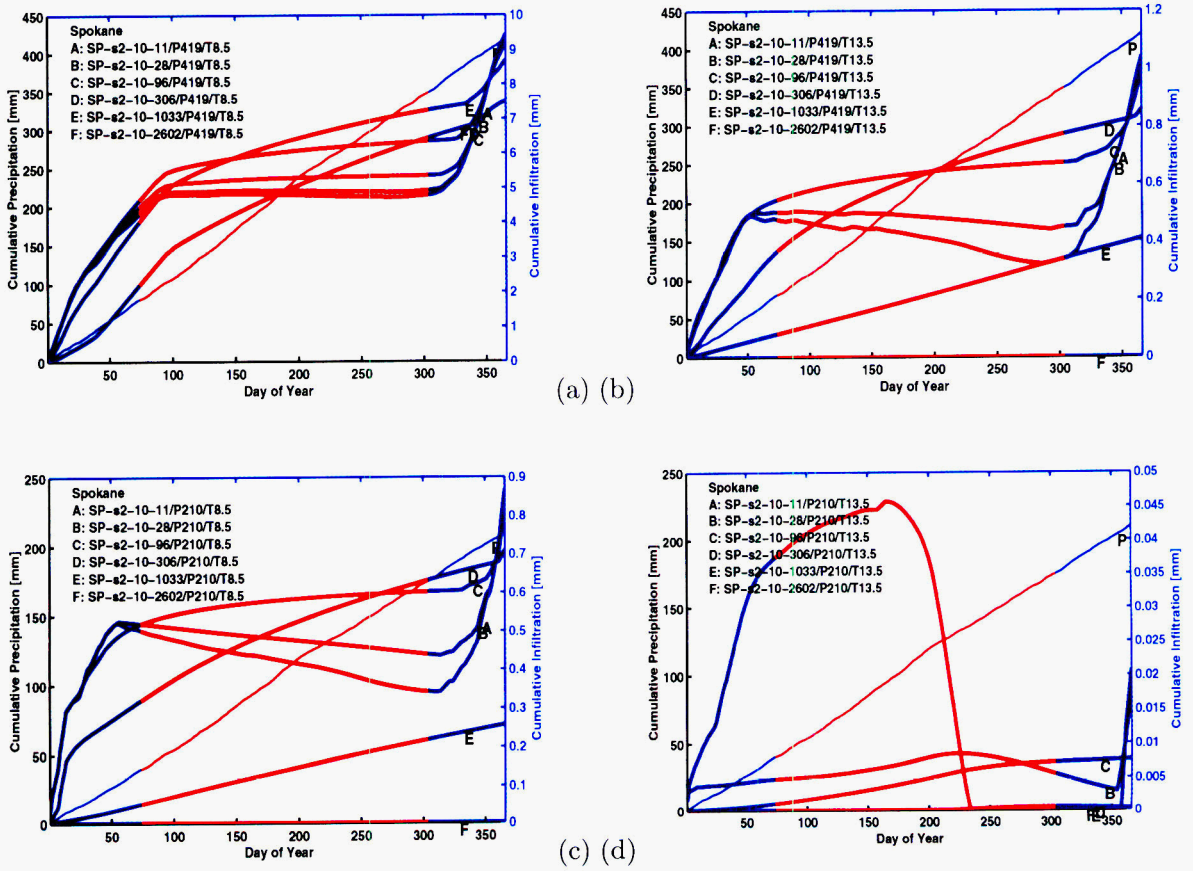

Figure 2-59: 8/11/00. Mean daily precipitation and moisture fluxes at 6 depths for 10 cm thickness of soil 2 using the Spokane meteorology. (a) Unscaled MAP with MAT at present values, (b) unscaled MAP with MAT 5 °C warmer than present, (c) half MAP with MAT at present values, (d) half MAP with MAT 5 °C warmer than present.

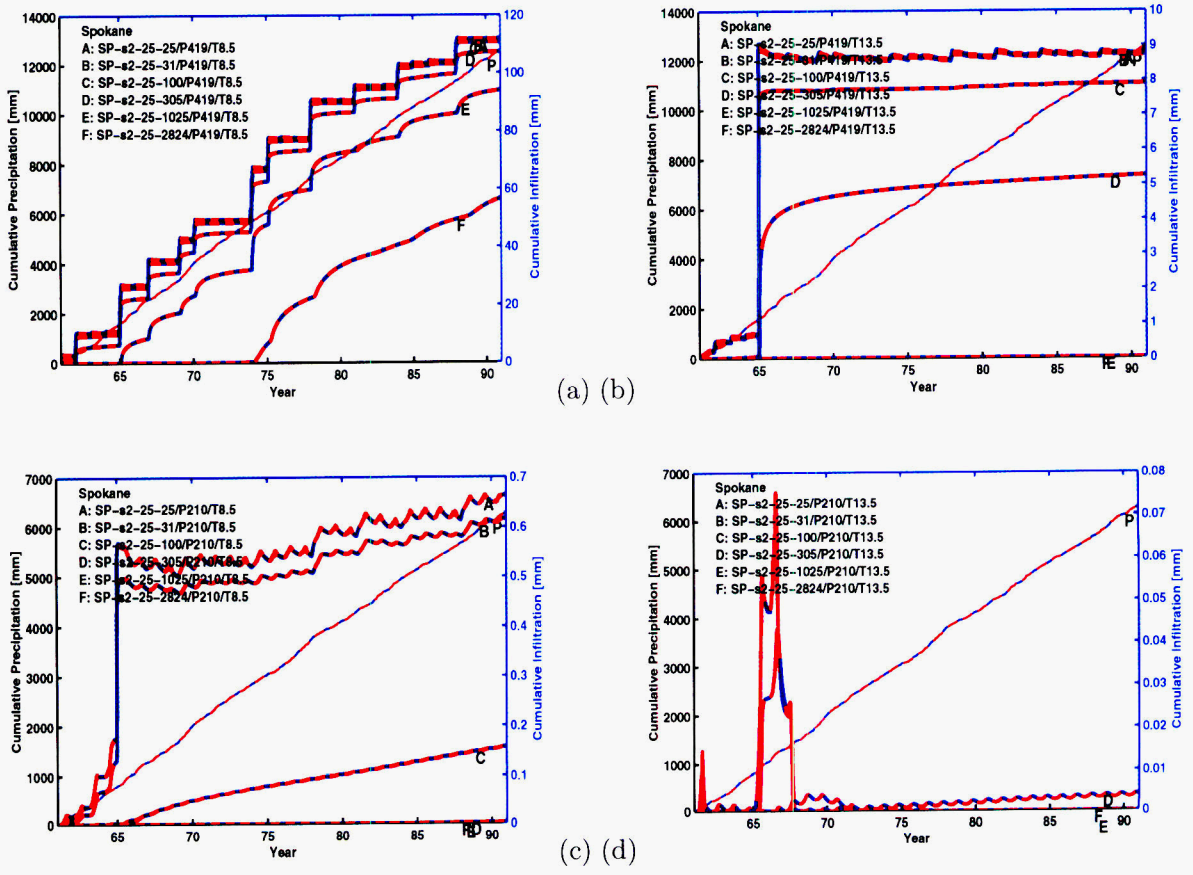

Figure 2-60: 8/11/00. Precipitation and moisture fluxes at 6 depths for 25 cm thickness of soil 2 using the Spokane meteorology. (a) Unscaled MAP with MAT at present values, (b) unscaled MAP with MAT 5 °C warmer than present, (c) half MAP with MAT at present values, (d) half MAP with MAT 5 °C warmer than present.

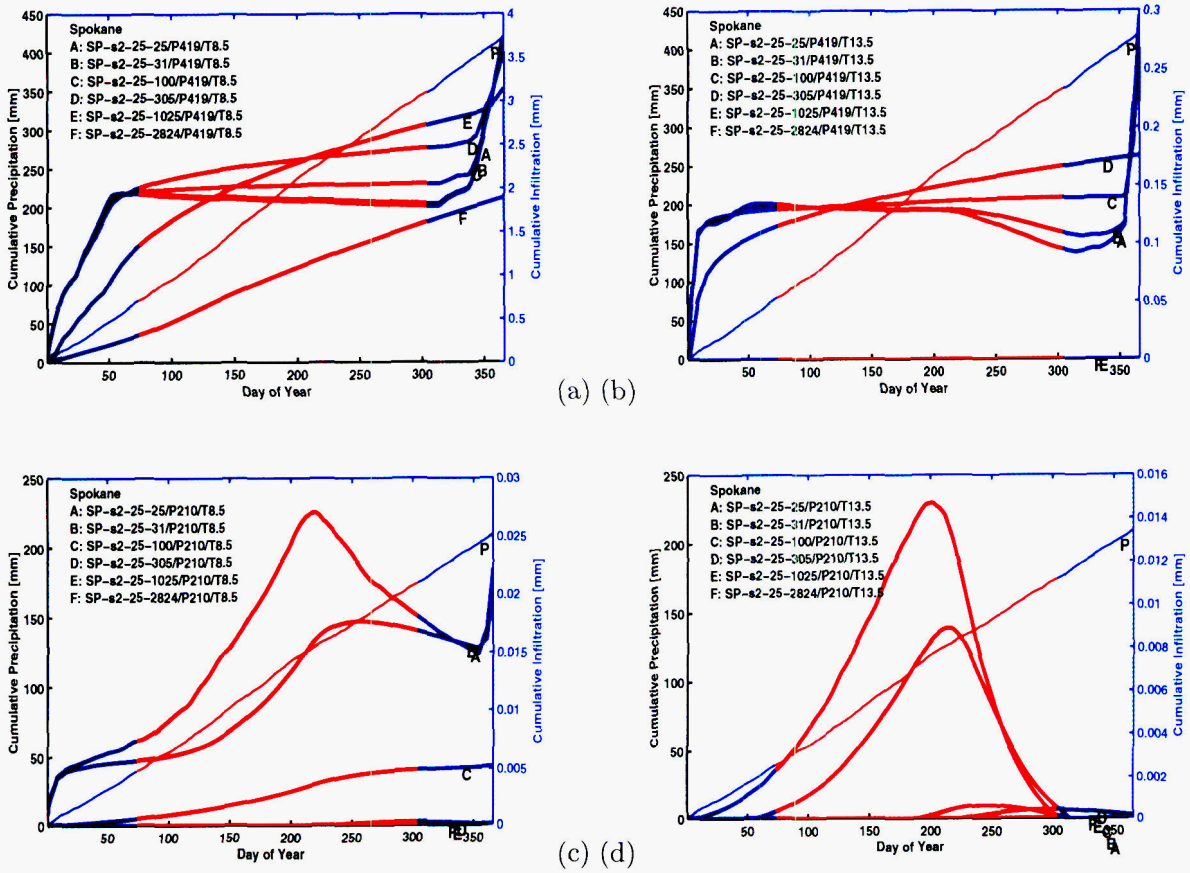

Figure 2-61: 8/11/00. Mean daily precipitation and moisture fluxes at 6 depths for 25 cm thickness of soil 2 using the Spokane meteorology. (a) Unscaled MAP with MAT at present values, (b) unscaled MAP with MAT 5 °C warmer than present, (c) half MAP with MAT at present values, (d) half MAP with MAT 5 °C warmer than present.

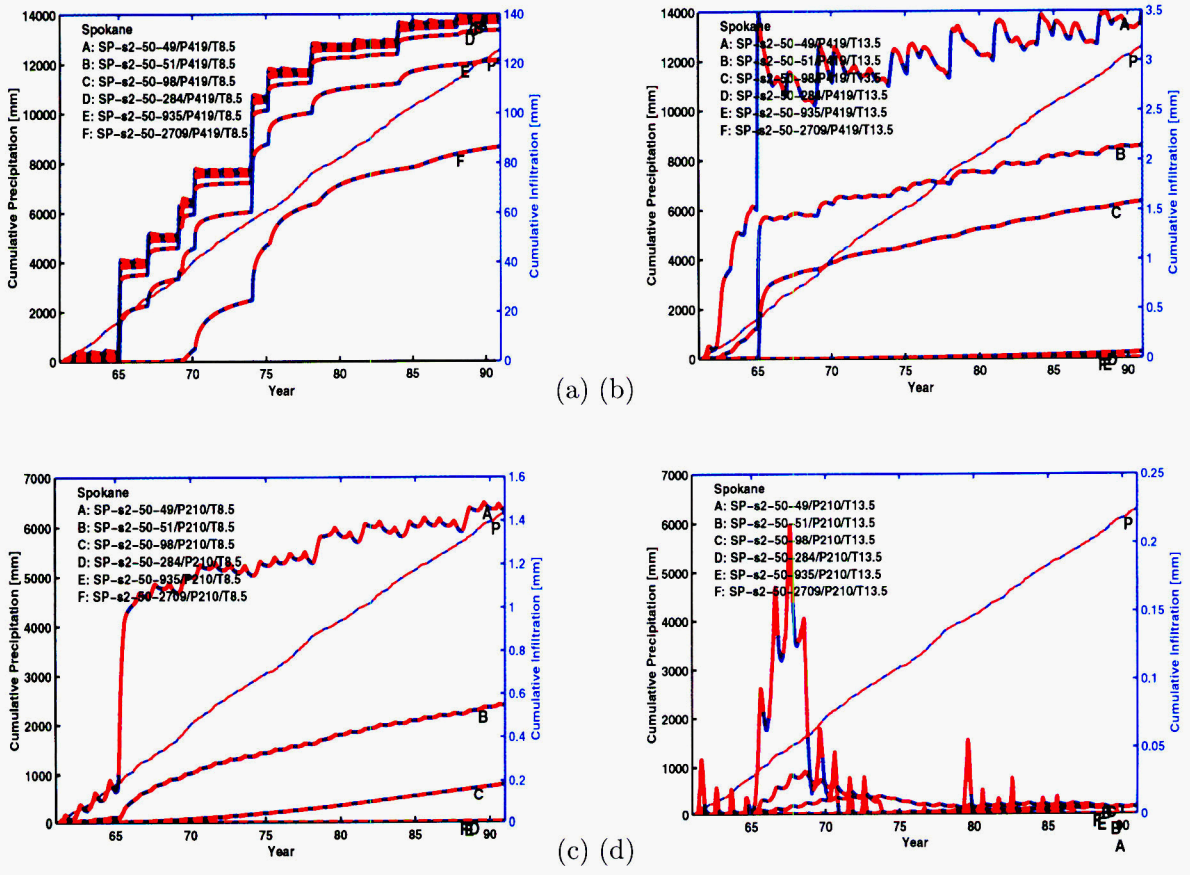

Figure 2-62: 8/11/00. Precipitation and moisture fluxes at 6 depths for 50 cm thickness of soil 2 using the Spokane meteorology. (a) Unscaled MAP with MAT at present values, (b) unscaled MAP with MAT 5 °C warmer than present, (c) half MAP with MAT at present values, (d) half MAP with MAT 5 °C warmer than present.

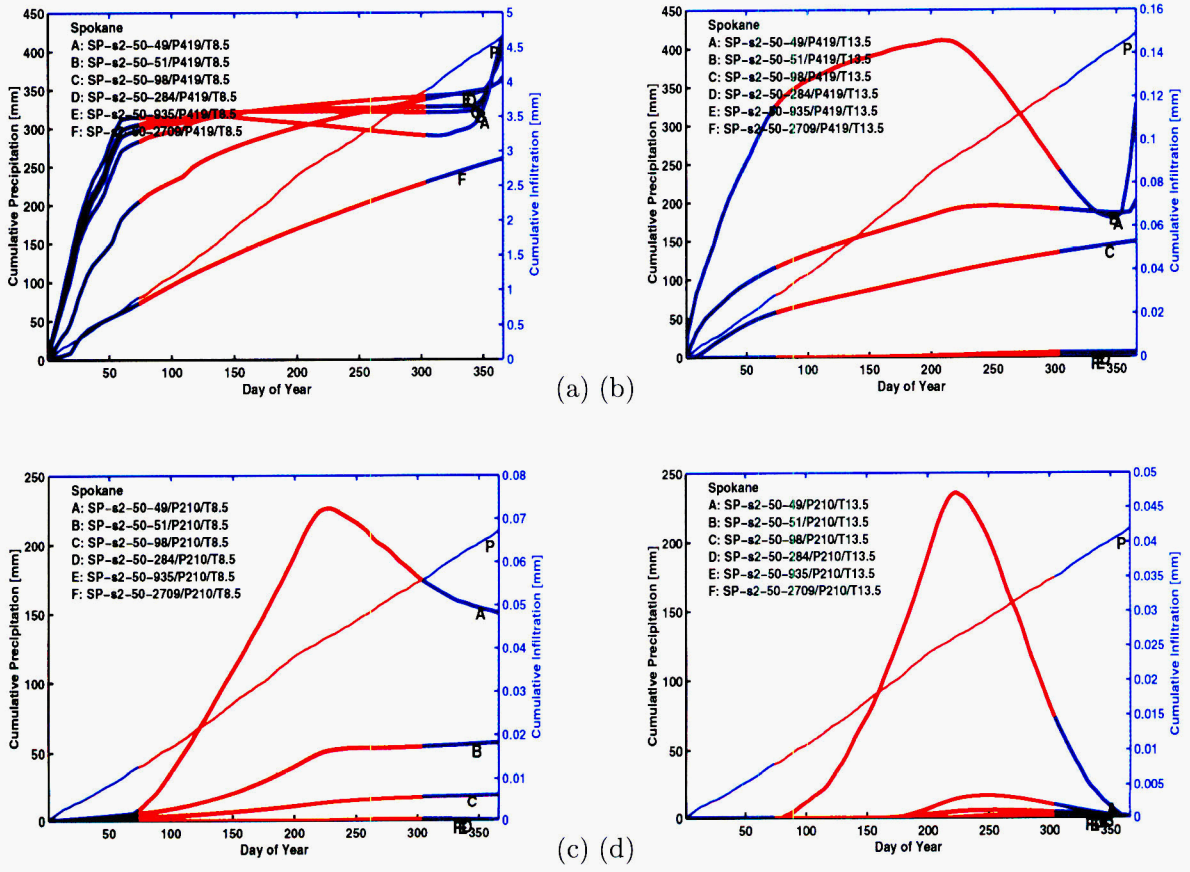

Figure 2-63: 8/11/00. Mean daily precipitation and moisture fluxes at 6 depths for 50 cm thickness of soil 2 using the Spokane meteorology. (a) Unscaled MAP with MAT at present values, (b) unscaled MAP with MAT 5 °C warmer than present, (c) half MAP with MAT at present values, (d) half MAP with MAT 5 °C warmer than present.

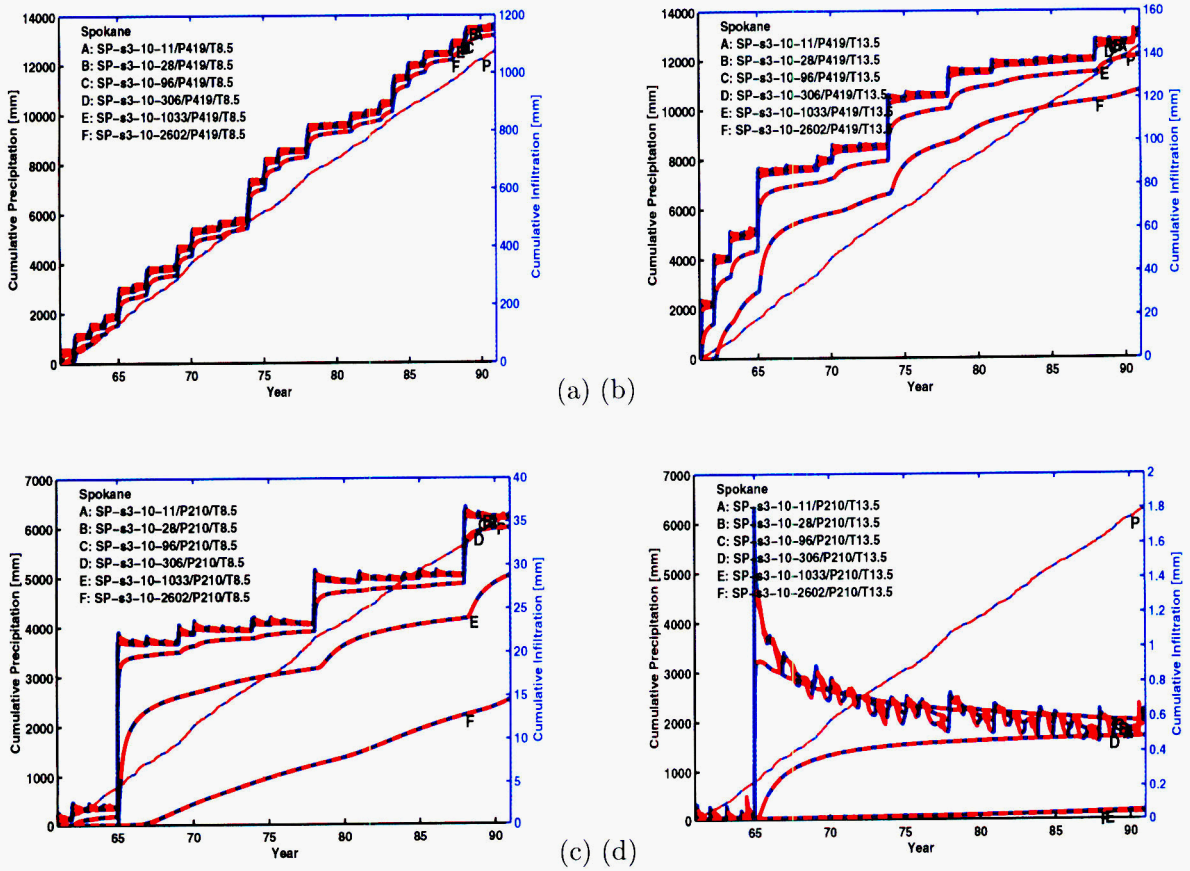

Figure 2-64: 8/11/00. Precipitation and moisture fluxes at 6 depths for 10 cm thickness of soil 3 using the Spokane meteorology. (a) Unscaled MAP with MAT at present values, (b) unscaled MAP with MAT 5 °C warmer than present, (c) half MAP with MAT at present values, (d) half MAP with MAT 5 °C warmer than present.

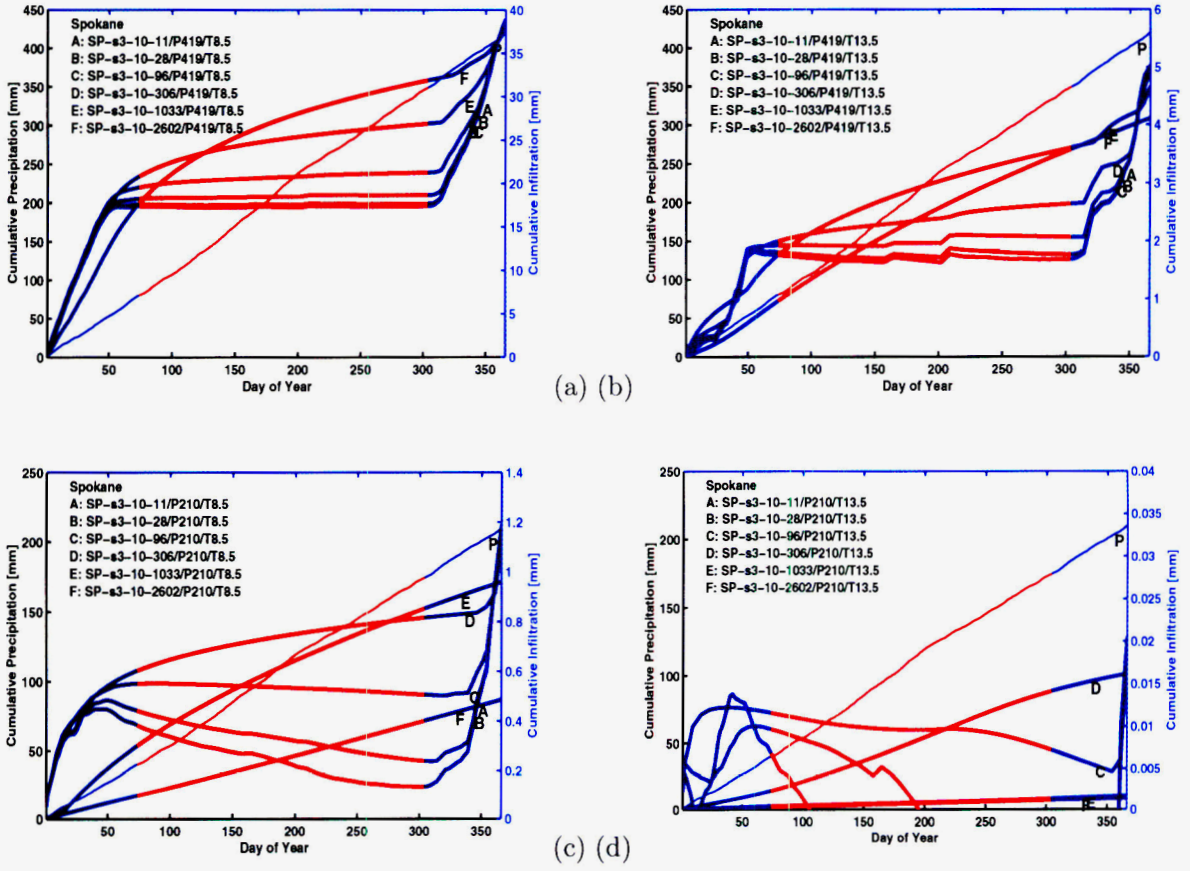

Figure 2-65: 8/11/00. Mean daily precipitation and moisture fluxes at 6 depths for 10 cm thickness of soil 3 using the Spokane meteorology. (a) Unscaled MAP with MAT at present values, (b) unscaled MAP with MAT 5 °C warmer than present, (c) half MAP with MAT at present values, (d) half MAP with MAT 5 °C warmer than present.

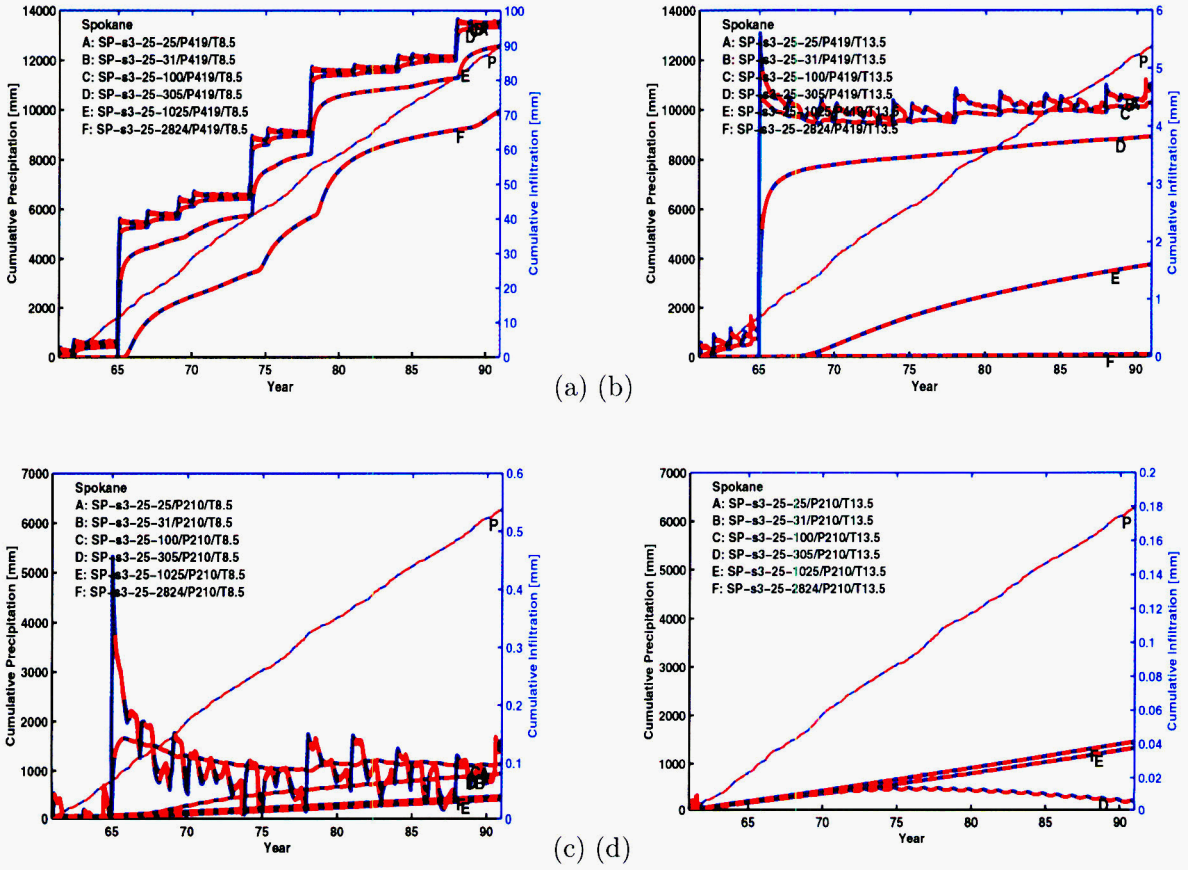

Figure 2-66: 8/11/00. Precipitation and moisture fluxes at 6 depths for 25 cm thickness of soil 3 using the Spokane meteorology. (a) Unscaled MAP with MAT at present values, (b) unscaled MAP with MAT 5 °C warmer than present, (c) half MAP with MAT at present values, (d) half MAP with MAT 5 °C warmer than present.

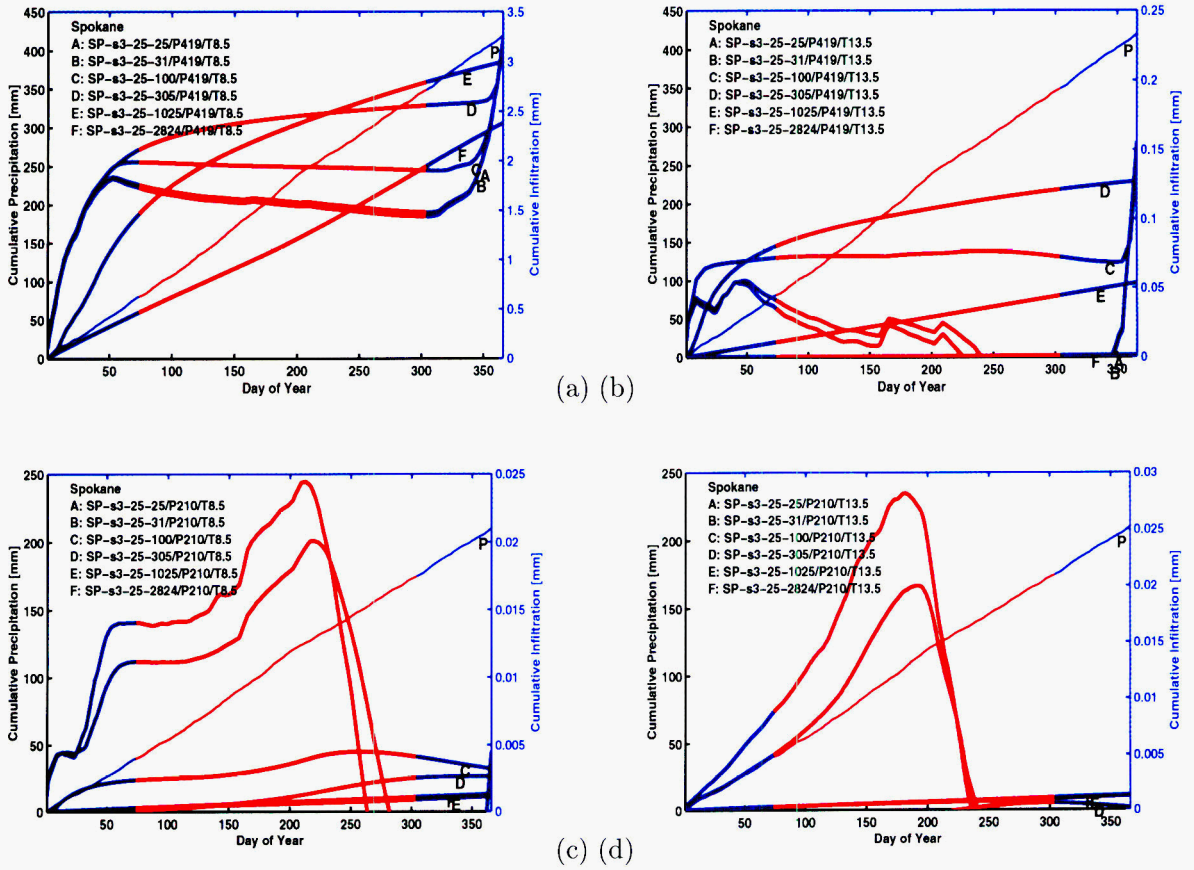

Figure 2-67: 8/11/00. Mean daily precipitation and moisture fluxes at 6 depths for 25 cm thickness of soil 3 using the Spokane meteorology. (a) Unscaled MAP with MAT at present values, (b) unscaled MAP with MAT 5 °C warmer than present, (c) half MAP with MAT at present values, (d) half MAP with MAT 5 °C warmer than present.

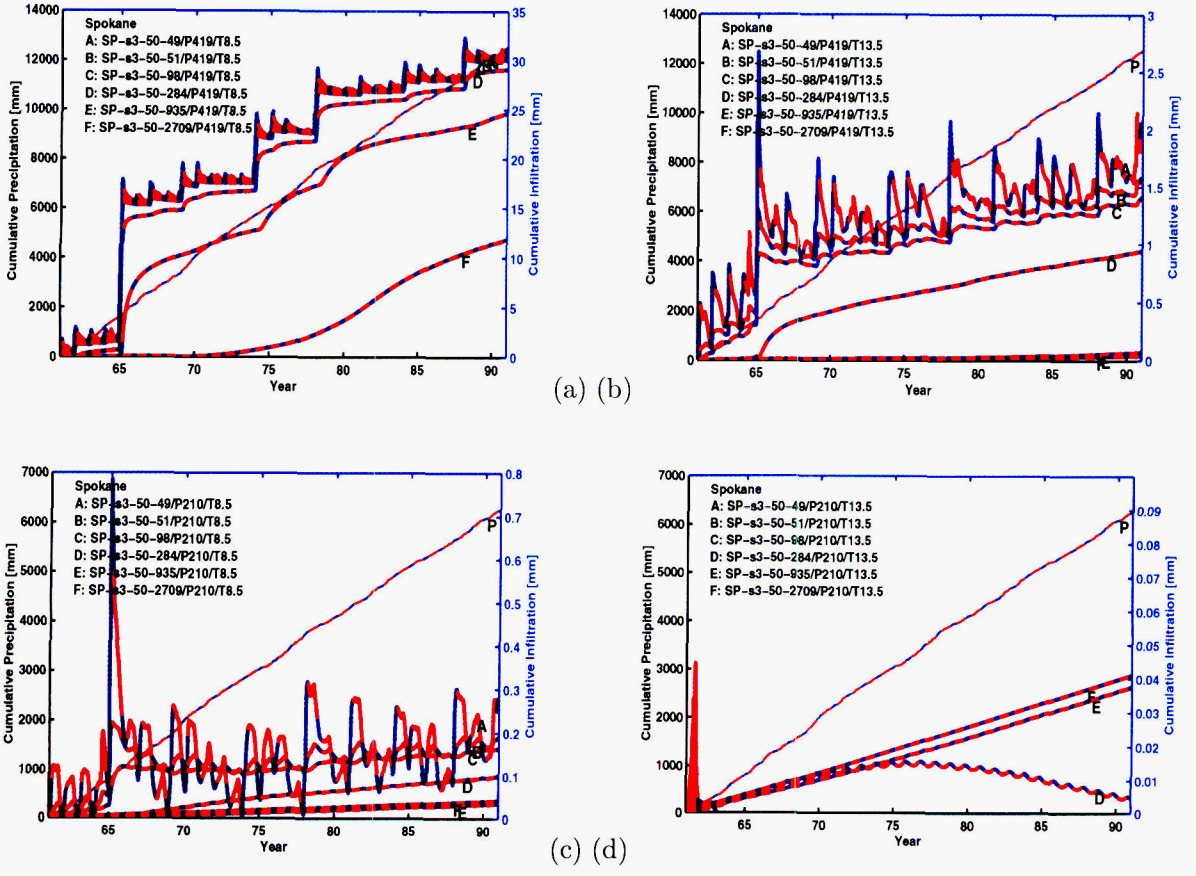

Figure 2-68: 8/11/00. Precipitation and moisture fluxes at 6 depths for 50 cm thickness of soil 3 using the Spokane meteorology. (a) Unscaled MAP with MAT at present values, (b) unscaled MAP with MAT 5 °C warmer than present, (c) half MAP with MAT at present values, (d) half MAP with MAT 5 °C warmer than present.

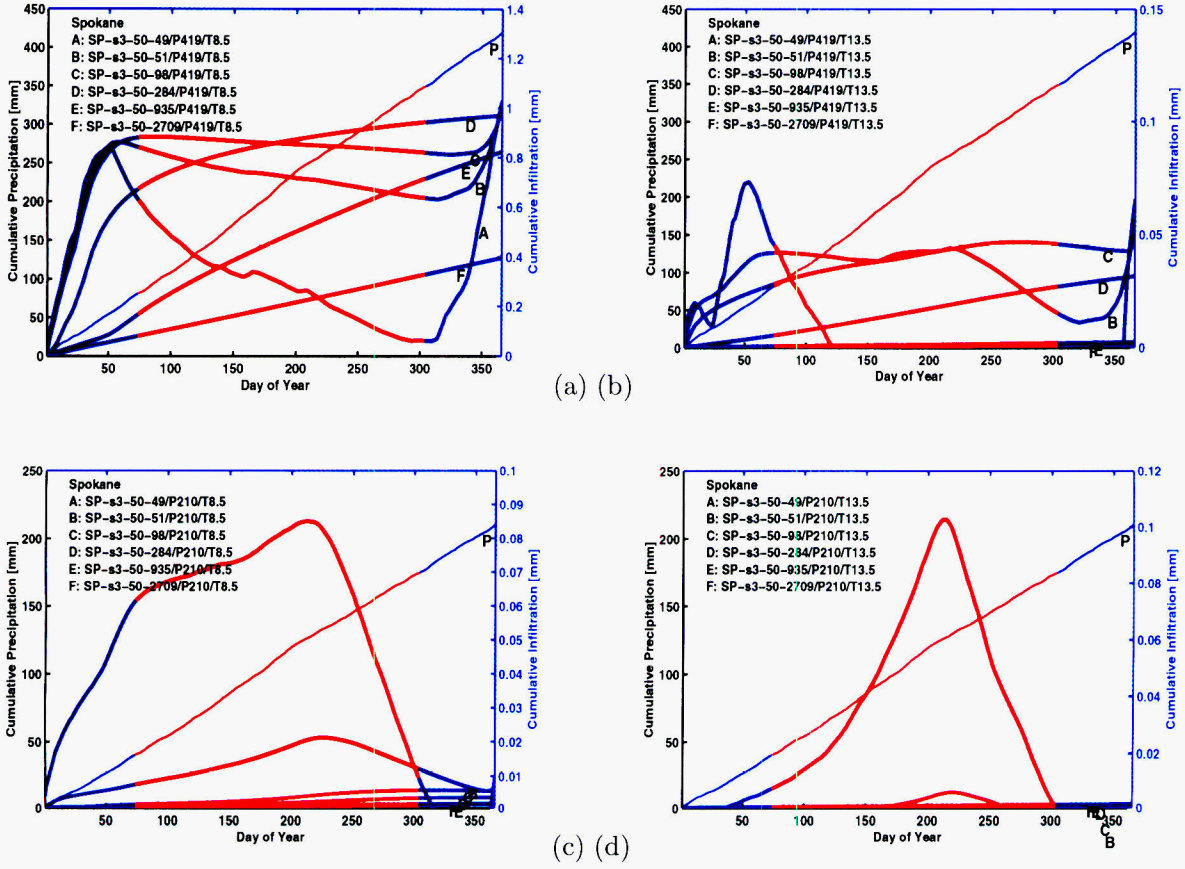

Figure 2-69: 8/11/00. Mean daily precipitation and moisture fluxes at 6 depths for 50 cm thickness of soil 3 using the Spokane meteorology. (a) Unscaled MAP with MAT at present values, (b) unscaled MAP with MAT 5 °C warmer than present, (c) half MAP with MAT at present values, (d) half MAP with MAT 5 °C warmer than present.

References

Allison, G. B., G. W. Gee, and S. W. Tyler. 1994. Vadose-Zone Techniques for Estimating Groundwater Recharge in Arid and Semiarid Regions. *Soil Science Society of America Journal 58*(1), 6–14.

Allison, G. B. and M. W. Hughes. 1978. The Use of Environmental Chloride and Tritium to Estimate Total Recharge to an Unconfined Aquifer. *Australian Journal of Soil Research 16*, 181–195.

Andrews, R. W., T. F. Dale, and J. A. McNeish. 1994. *Total System Performance Assessment–1993: An Evaluation of the Potential Yucca Mountain Repository.* B00000000-01717-2200-00099-Rev.01, Intera, Inc., Las Vegas, NV.

Bagtzoglou, A. C., N. M. Coleman, E. C. Pearcy, S. A. Stothoff, and G. W. Wittmeyer. 1997. Unsaturated and Saturated Flow Under Isothermal Conditions. In B. Sagar (Ed.), *NRC High-Level Radioactive Waste Program FY96 Annual Progress Report*, Volume NUREG/CR-6513, No. 1, Washington, DC, pp. 10–1–10–28. Nuclear Regulatory Commission.

Bagtzoglou, A. C., S. A. Stothoff, and M. A. Muller. 1995. *Progress Towards Estimating Infiltration and Deep Percolation at the Yucca Mountain Site.* , Center for Nuclear Waste Regulatory Analyses, San Antonio, TX.

Barnes, C. J., G. Jacobson, and G. D. Smith. 1994. The Distributed Recharge Mechanism in the Australian Arid Zone. *Soil Science Society of America Journal 58*(1), 31–40.

Brown, T., S. Conrad, S. Wirth, J. Cochran, and J. Emery. 1997. *Plausible Future Climate States at the Area 5 Radioactive Waste Management Site, Nevada Test Site.* SNL-?, Sandia National Laboratories, Albuquerque, NM.

Buesch, D. C., R. W. Spengler, T. C. Moyer, and J. K. Geslin. 1996. *Proposed Stratigraphic Nomenclature and Macroscopic Identification of Lithostratigraphic Units of the Paintbrush Group Exposed at Yucca Mountain, Nevada.* Open-File Report 94-469, United States Geological Survey, Denver, CO.

Campbell, G. S. 1985. *Soil Physics with BASIC.* Amsterdam, The Netherlands: Elsevier Science Publishers B.V.

Carsel, R. F. and R. S. Parrish. 1988. Developing Joint Probability Distributions of Soil Water Retention Characteristics. *Water Resources Research 24*(5), 755–769.

Clausnitzer, V. and J. W. Hopmans. 1993. *An Algorithm for Three-Dimensional, Simultaneous Modeling of Root Growth and Transient Soil Water Flow, V 1.0.* LAWR Paper No. 100022, Department of Land, Air, and Water Resources, University of California, Davis, CA.

Clausnitzer, V. and J. W. Hopmans. 1994. Simultaneous modeling of transient three-dimensional root growth and soil water flow adaptation. *Plant and Soil 164*, 299–314.

Conrad, S. H. 1993. Using Environmental Tracers to Estimate Recharge Through an Arid Basin. In *Proceedings of the Fourth Annual International Conference on High Level Radioactive Waste Management*, La Grange Park, IL, pp. 132–137. American Nuclear Society.

Curtis, D. C. and P. S. Eagleson. 1982. *Constrained Stochastic Climate Simulation.* Ralph Parsons Laboratory Report No. 274, Massachusetts Institute of Technology, Cambridge, MA.

Day, W. C., C. J. Potter, D. S. Sweetkind, and C. A. S. Juan. 1998. *Bedrock geologic map of the central block area, Yucca Mountain, Nye County, Nevada.* Miscellaneous Investigations Series I-2601, United States Geological Survey, Denver, CO.

du Bray, E. A., D. O. Hurtubise, and C. A. Bannister. 1987. *Geologic Map of the Weepah Spring Wilderness Study Area, Lincoln and Nye Counties, Nevada 1:50,000.* Miscellaneous Field Studies Map MF-1922, United States Geological Survey, Denver, CO.

Electric Power Research Institute. 1990. *Demonstration of a Risk-Based Approach to High-Level Waste Repository Evaluation.* EPRI NP-7057, Electric Power Research Institute, Palo Alto, CA.

Electric Power Research Institute. 1992. *Demonstration of a Risk-Based Approach to High-Level Waste Repository Evaluation: Phase 2.* EPRI TR-100384, Electric Power Research Institute, Palo Alto, CA.

Electric Power Research Institute. 1996. *Yucca Mountain Total System Performance Assessment, Phase 3.* EPRI TR-107191, Electric Power Research Institute, Palo Alto, CA.

Eslinger, P. W., L. A. Doremus, D. W. Engel, T. B. Miley, M. T. Murphy, W. E. Nichols, M. D. White, D. W. Langford, and S. J. Ouderkirk. 1993. *Preliminary Total-System Analysis of a Potential High-Level Nuclear Waste Repository at Yucca Mountain.* PNL-8444, Pacific Northwest Laboratory, Richland, WA.

Evans, D. D., T. W. Sammis, and D. R. Cable. 1981. Actual Evapotranspiration under Desert Conditions. In D. D. Evans and J. L. Thames (Eds.), *Water in Desert Ecosystems*, pp. 195–218. Stroudsburg, PA: Dowden, Hutchinson, and Ross, Inc.

Fabryka-Martin, J. T., P. R. Dixon, S. Levy, B. Liu, H. J. Turin, and A. V. Wolfsberg. 1996a. *Systematic Sampling for Chlorine-36 in the Exploratory Studies Facility.* LA-CST-TIP-96-001, Los Alamos National Laboratory, Los Alamos, NM.

Fabryka-Martin, J. T., H. J. Turin, A. V. Wolfsberg, D. Brenner, P. R. Dixon, and J. A. Musgrave. 1996b. *Summary Report of Chlorine-36 Studies.* LA-CST-TIP-96-003, Los Alamos National Laboratory, Los Alamos, NM.

Fayer, M. J. and T. L. Jones. 1990. *UNSAT-H Version 2.0: Unsaturated Soil Water and Heat Flow Manual.* PNL-6779, Pacific Northwest Laboratory, Richland, WA.

Fernandez, J. A., J. B. Case, C. A. Givens, and B. C. Carney. 1994. *A Strategy to Seal Exploratory Boreholes in Unsaturated Tuff.* SAND93-1184, Sandia National Laboratories, Albuquerque, NM.

Flint, A. L., J. A. Hevesi, and L. E. Flint. 1996a. *Conceptual and Numerical Model of Infiltration for the Yucca Mountain Area, Nevada.* Milestone 3GUI623M, Department of Energy, Las Vegas, NV.

Flint, L. E. 1996. *Matrix Properties of Hydrogeologic Units at Yucca Mountain, Nevada.* Milestone 3GUP604M, Department of Energy, Las Vegas, NV.

Flint, L. E. and A. L. Flint. 1990. *Preliminary Permeability and Water-Retention Data for Nonwelded and Bedded Tuff Samples, Yucca Mountain Area, Nye County, Nevada.* Open-File Report 90-569, United States Geological Survey, Denver, CO.

Flint, L. E. and A. L. Flint. 1995. *Shallow Infiltration Processes at Yucca Mountain, Nevada–Neutron Logging Data 1984-93.* Water-Resources Investigations Report 95-4035, United States Geological Survey, Denver, CO.

Flint, L. E., A. L. Flint, and J. A. Hevesi. 1994. Shallow Infiltration Processes in Arid Watersheds at Yucca Mountain, Nevada. In *Proceedings of the Fifth Annual International Conference on High Level Radioactive Waste Management*, La Grange Park, IL, pp. 2315–2322. American Nuclear Society.

Flint, L. E., A. L. Flint, C. A. Rautman, and J. D. Istok. 1996b. *Physical and Hydrologic Properties of Rock Outcrop Samples at Yucca Mountain, Nevada.* Open-File Report 95-280, United States Geological Survey, Denver, CO.

Fonteyn, P. J. and B. E. Mahall. 1981. An experimental analysis of structure in a desert plant community. *Journal of Ecology 69*, 883–896.

Gee, G. W., P. J. Wierenga, B. J. Andraski, M. H. Young, M. J. Fayer, and M. L. Rockhold. 1994. Variations in Water Balance and Recharge Potential at Three Western Desert Sites. *Soil Science Society of America Journal 58*(1), 63–72.

Gerwitz, A. and E. R. Page. 1974. An Empirical Mathematical Model to Describe Plant Root Systems. *Journal of Applied Ecology 11*, 773–782.

Goodall, D. W. 1952. Some considerations in the use of point quadrats for the analysis of vegetation. *Australian Journal of Scientific Research 5*, 1–41.

Groeneveld, D. P. 1997. Vertical point quadrat sampling and an extinction factor to calculate leaf area index. *Journal of Arid Environments 36*(3), 475–485.

Heady, J. F., R. P. Gibbens, and R. W. Powell. 1959. A comparison of the charting, line intercept and line-point methods of sampling shrub types of vegetation. *Journal of Range Management 12*, 180–188.

Herwitz, S. R. and L. Olsvig-Whittaker. 1989. Preferential upslope growth of *Zygophyllum dumosum* Boiss. (Zygophyllaceae) roots into bedrock fissures in the northern Negev desert. *Journal of Biogeography 16*, 457–460.

Hevesi, J. A., J. D. Istok, and A. L. Flint. 1992. Precipitation Estimation in Mountainous Terrain Using Multivariate Geostatistics. Part I: Structural Analysis. *Journal of Applied Meteorology 31*(7), 661–676.

Hickman, J. C. 1995. *The Jepson manual of higher plants of California.* Berkeley, CA: University of California Press.

Lachenbruch, A. H. and J. H. Sass. 1977. Heat Flow in the United States and the Thermal Regime of the Crust. In H. G. Heacock (Ed.), *The Earth's Crust*, Volume Geophysical Monograph 20, pp. 626–675. Washington, DC: American Geophysical Union.

Leary, K. D. 1990. *Analysis of Techniques for Estimating Potential Recharge and Shallow Unsaturated Zone Water Balance Near Yucca Mountain, Nevada.* Ph. D. thesis, University of Nevada, Reno, NV.

Lichty, R. W. and P. W. McKinley. 1995. *Estimates of Ground-Water Recharge Rates for Two Small Basins in Central Nevada.* Water-Resources Investigations Report 94-4104, United States Geological Survey, Denver, CO.

Long, A. and S. W. Childs. 1993. Rainfall and Net Infiltration Probabilities for Future Climate Conditions at Yucca Mountain. In *Proceedings of the Fourth Annual International Conference on High Level Radioactive Waste Management*, La Grange Park, IL, pp. 112–121. American Nuclear Society.

Matalas, N. C. 1967. Mathematical Assessment of Synthetic Hydrology. *Water Resources Research 3*(4), 937–945.

McKenna, S. A. and C. A. Rautman. 1995. *Summary Evaluation of Yucca Mountain Surface Transects with Implications for Downhole Sampling.* SAND94-2038, Sandia National Laboratories, Albuquerque, NM.

McKinley, P. and T. Oliver. 1994. *Meteorological, Stream-Discharge, and Water-Quality Data for 1986 through 1991 from Two Small Basins in Central Nevada.* Open-File Report 93-651, United States Geological Survey, Denver, CO.

McKinley, P. and T. Oliver. 1995. *Meteorological, Stream-Discharge, and Water-Quality Data*

for Water Year 1992 from Two Basins in Central Nevada. Open-File Report 94-456, United States Geological Survey, Denver, CO.

Nichols, W. D. 1987. *Geohydrology of the Unsaturated Zone at the Burial Site for Low-Level Radioactive Waste Near Beatty, Nye County, Nevada.* Water-Supply Paper 2312, United States Geological Survey, Denver, CO.

Noy-Meir, I. 1973. Desert ecosystems: environment and producers. *Annual Review of Ecological Systems 4*, 25–52.

Nuclear Regulatory Commission. 1992. *Initial Demonstration of the NRC's Capability to Conduct a Performance Assessment for a High-Level Waste Repository.* NUREG-1327, Nuclear Regulatory Commission, Washington, DC.

Nuclear Regulatory Commission. 1995. *NRC Iterative Performance Assessment Phase 2: Development of Capabilities for Review of a Performance Assessment for a High-Level Waste Repository.* NUREG-1464, Nuclear Regulatory Commission, Washington, DC.

Phillips, F. M. 1994. Environmental Tracers for Water Movement in Desert Soils of the American Southwest. *Soil Science Society of America Journal 58*(1), 15–24.

Quade, J. and T. E. Cerling. 1990. Stable Isotopic Evidence for a Pedogenic Origin of Carbonates in Trench 14 near Yucca Mountain, Nevada. *Science 250*, 1549–1552.

Ratliff, L. F., J. T. Ritchie, and D. K. Cassel. 1983. Field-Measured Limits of Soil Water Availability as Related to Laboratory-Measured Properties. *Soil Science Society of America Journal 47*, 770–775.

Rautman, C. A., L. E. Flint, A. L. Flint, and J. D. Istok. 1995. *Physical and Hydrologic Properties of Rock Outcrop Samples From a Nonwelded to Welded Tuff Transition, Yucca Mountain, Nevada.* Water-Resources Investigations Report 95-4061, United States Geological Survey, Denver, CO.

Richardson, C. W. and D. A. Wright. 1984. *WGEN: A Model for Generating Daily Weather Variables.* ARS-8, United States Department of Agriculture, Agricultural Research Service.

Rousseau, J. P., E. M. Kwicklis, and D. C. Gillies (Eds.). 1996. *Hydrogeology of the Unsaturated Zone, North Ramp Area of the Exploratory Studies Facility, Yucca Mountain, Nevada*, Water-Resources Investigations Report 96-????, Denver, CO. United States Geological Survey. Draft dated 8/29/96.

Sandia National Laboratories. 1992. *TSPA 1991: An Initial Total-System Performance Assessment for Yucca Mountain.* SAND91-2795, Sandia National Laboratories, Albuquerque, NM.

Sandia National Laboratories. 1994. *Total-System Performance Assessment for Yucca Mountain–SNL Second Iteration (TSPA-1993).* SAND93-2675, Sandia National Laboratories, Albuquerque, NM.

Sass, J. H. and A. H. Lachenbruch. 1982. *Preliminary Interpretations of Thermal Data from the Nevada Test Site.* Open-File Report 82-973, United States Geological Survey, Reston, VA.

Sass, J. H., A. H. Lachenbruch, W. W. Dudley, Jr., S. S. Priest, and R. J. Munroe. 1988. *Temperature, thermal conductivity, and heat flow near Yucca Mountain, Nevada: Some tectonic and hydrologic implications.* Open-File Report 87-649, United States Geological Survey, Denver, CO.

Sass, J. H., A. H. Lachenbruch, and C. W. Mase. 1980. *Analysis of Thermal Data From Drill Holes UE25a-3 and UE25a-1, Calico Hills and Yucca Mountain, Nevada Test Site.* Open-File Report 80-826, United States Geological Survey, Menlo Park, CA.

Scanlon, B. R. 1991. Evaluation of moisture flux from chloride data in desert soils. *Journal of Hydrology 128*, 137–156.

Scanlon, B. R. 1992. Evaluation of Liquid and Vapor Water Flow in Desert Soils Based on Chlorine 36 and Tritium Tracers and Nonisothermal Flow Simulations. *Water Resources Research 28*(1), 285–297.

Schenker, A. R., D. C. Guerin, T. H. Robey, C. A. Rautman, and R. W. Barnard. 1995. *Stochastic Hydrogeologic Units and Hydrogeologic Properties Development for Total-System Performance Assessments.* SAND94-0244, Sandia National Laboratories, Albuquerque, NM.

Schmidt, M. R. 1989. Classification of Upland Soils by Geomorphic and Physical Properties Affecting Infiltration at Yucca Mountain, Nevada. Master's thesis, Colorado School of Mines, Golden, CO.

Scott, R. B. and J. Bonk. 1984. *Preliminary Geologic Map (1:12,000 scale) of Yucca Mountain, Nye County, Nevada, with Geologic Cross Sections.* Open-File Report 84-494, United States Geological Survey, Denver, CO.

Šimůnek, J., T. Vogel, and M. T. van Genuchten. 1992. *The SWMS_2D code for simulating water flow and solute transport in two-dimensional variably saturated media V. 1.1.* Research Report No. 126, U. S. Salinity Laboratory, ARS USDA, Riverside, CA.

Somma, F., V. Clausnitzer, and J. W. Hopmans. 1997. *An Algorithm For Three-Dimensional, Simultaneous Modeling Of Root Growth, Transient Soil Water Flow, And Solute Transport And Uptake, Version 2.1.* LAWR Paper No. 100034, Department of Land, Air, and Water Resources, University of California, Davis, CA.

Stephenson, N. L. 1990. Climate control of vegetation distribution: The role of the water balance. *The American Naturalist 135*, 649–670.

Sternberg, P. D., M. A. Anderson, R. C. Graham, J. L. Beyers, and K. R. Rice. 1996. Root distribution and seasonal water status in weathered granitic bedrock under chapparal. *Geoderma 72*, 89–98.

Stothoff, S. A. 1997. Sensitivity of long-term bare soil infiltration simulations to hydraulic properties in an arid environment. *Water Resources Research 33*(4), 547–558.

Stothoff, S. A. and A. C. Bagtzoglou. 1995. Estimation of Recharge at Yucca Mountain, Nevada. *Supplement to Eos, Transactions 76*(46), F242.

Stothoff, S. A. and A. C. Bagtzoglou. 1996. Subregional Hydrogeologic Flow and Transport Processes. In B. Sagar (Ed.), *NRC High-Level Radioactive Waste Research at CNWRA, July–December 1995*, Volume CNWRA 95-02S, San Antonio, TX, pp. 9–1–9–20. Center for Nuclear Waste Regulatory Analyses.

Stothoff, S. A., A. C. Bagtzoglou, and H. Castellaw. 1996. Estimation of Spatial Distribution of Recharge Factors at Yucca Mountain, NV. In *Proceedings of the International Conference on Application of Geographic Information Systems in Hydrology and Water Resources Management*, Vienna, Austria. International Association of Hydrological Sciences.

Stothoff, S. A., H. M. Castellaw, and A. C. Bagtzoglou. 1995. Estimation of Spatial Distribution of Recharge Factors at Yucca Mountain. In B. Sagar (Ed.), *NRC High-Level Radioactive Waste Research at CNWRA, January–June 1995*, Volume CNWRA 95-01S, San Antonio, TX, pp. 9–5–9–12. Center for Nuclear Waste Regulatory Analyses.

Sykes, J. F., J. L. Wilson, and R. W. Andrews. 1985. Sensitivity Analysis for Steady State Groundwater Flow Using Adjoint Operators. *Water Resources Research 21*(3), 359–371.

TRW. 1995. *Total System Performance Assessment–1995: An Evaluation of the Potential Yucca Mountain Repository.* B00000000-01717-2200-00136, TRW Environmental Safety Systems Inc., Las Vegas, NV.

Tyler, S. W. and G. R. Walker. 1994. Root Zone Effects on Tracer Migration in Arid Zones. *Soil Science Society of America Journal 58*(1), 25–31.

van Genuchten, M. T. 1980. A Closed-form Equation for Predicting the Hydraulic Conductivity of Unsaturated Soils. *Soil Science Society of America Journal 44*, 892–898.

Yang, I. C., G. W. Rattray, and P. Yu. 1996. *Interpretations of Chemical and Isotopic Data From Boreholes in the Unsaturated Zone at Yucca Mountain, Nevada.* Water-Resources Investigations Report 96-4058, United States Geological Survey, Denver, CO.

Zwieniecki, M. A. and M. Newton. 1995. Roots growing into rock fissures: Their morphological adaptation. *Plant and Soil 172*, 181–187.